THE EFFECT OF FABRIC ON THE BEHAVIOUR OF GOLD TAILINGS

HSIN-PEI NICOL CHANG

A Thesis submitted in partial fulfillment of the requirements for the degree

PHILOSOPHIAE DOCTOR (CIVIL ENGINEERING)

In the

FACULTY OF ENGINEERING, BUILT ENVIRONMENT AND INFORMATION TECHNOLOGY

UNIVERSITY OF PRETORIA

PRETORIA

April 2009

THESIS SUMMARY

THE EFFECT OF FABRIC ON THE BEHAVIOUR OF GOLD TAILINGS

By H.N. Chang

Supervisor:	Professor G. Heymann (University of Pretoria)
Co- supervisor:	Professor C.R.I Clayton (University of Southampton)
Department:	Civil Engineering
University:	University of Pretoria
Degree:	Philosophiae Doctor (Civil Engineering)

The behaviour of cohesionless soils is known to be influenced by the method of reconstitution. It is generally accepted in the literature that different reconstitution methods produce samples of varying fabric and thus samples of varying behaviour. Very little evidence has been presented to validate this statement. The main aim of this is thesis is firstly to observe the fabric of in situ and reconstituted gold tailings samples and secondly to investigate the difference in behaviour between these samples at the same state.

The investigation focused on testing in situ and reconstituted gold tailings samples obtained from 3 positions on a tailings dam; pond, middle beach and upper beach. Laboratory reconstitution methods included moist tamping and slurry deposition. Fabric analysis involved the use of SEM images to classify the observed differences in the fabric of the undisturbed and reconstituted gold tailings samples. A particle interaction model based on the observed fabric was postulated to explain the differences or similarities in behaviour. The scope of behaviour investigated included sedimentation, collapse and swell, consolidation and compressibility, creep, stiffness and shear behaviour.

The fabric analysis indicates that differences in the fabric of undisturbed and reconstituted gold tailings samples are visible. Moist tamping produces an aggregated fabric while slurry deposition yields a homogeneous fabric similar to that of the

undisturbed samples. Comparison of behaviour indicates that neither moist tamping nor slurry deposition can replicate the behaviour of the undisturbed sample fully. Consolidation and compression is a function of the fabric while friction angle is independent of the fabric. Available shear strength and liquifaction potential is also affected by the preparation method and the resulting fabric.

Keywords: Tailings, gold, fabric, behaviour, aggregated, liquefaction, strain-
softening, sample preparation, moist tamping, slurry deposition .

Acknowledgement

Table of Contents

Appendixes

List of Figures

List of Tables

List of Symbols

Roman symbols

A	Area of electrodes, cross-sectional area of sample
a	Constant
A_0	Initial sample area
b	Constant
c'	Effective cohesion
C_α	Secondary compression index
CC	Clay content (% of material <0.002mm)
C_c	Compression index
CR	Creep rate
C_u	Coefficient of Uniformity = D_{60}/D_{10}
C_v	Coefficient of consolidation
C_z	Coefficient of Curvature = $D_{30}^2/(D_{10}D_{60})$
D_{10}	Effective size in mm where 10% of the material passes
D_{15}	Effective size in mm where 15% of the material passes
D_{30}	Effective size in mm where 30% of the material passes
D_{50}	Effective size in mm where 50% of the material passes
D_{60}	Effective size in mm where 60% of the material passes
D_{90}	Effective size in mm where 90% of the material passes
d	Drainage path length
E	Young's modulus
e	Void ratio
e_0	Initial void ratio

e_{max}, e_{min}	Maximum and minimum void ratio determined from limiting density test
FC	Fines content (percentage of material <0.075mm)
G_{max}	Small strain shear stiffness
Gs	Specific gravity of soil particles
H	Horizontal distance down the beach of a tailings dam.
I_B	Brittleness index
I_D	Relative density
K	Bulk modulus
k	Permeability
L	Distance between electrodes (Electrical conductivity), length of particle
LL	Liquid limit
M	Slope of the critical state line
m_v	Coefficient of compressibility
N	Intercept of the normal compression line at $p' = 1kPa$.
P	Applied pressure
p'	Mean normal effective stress
PI	Plasticity index
PL	Plastic limit
q'	Effective deviatoric stress
q_0'	Initial deviatoric stress (defining origin)
R	Resistance (Electrical conductivity)
r	Entrance pore radius
S	Wood's stability ratio
s'	$(\sigma_1'+\sigma_3')/2$
SR	Shear rate
t'	$(\sigma_1'-\sigma_3')/2$
t_{90}	Time for 90% consolidation
Ue	Excess pore pressure
W	Width of particle

Greek symbols

ε	Strain, normally in percent
ε_a	Axial strain
ε_v	Volumetric strain
ε_{a0}	Initial point defining origin
θ	Contact angle (MIP), stress path direction
λ	Slope of the normal compression line
σ	Surface tension of intruding liquid, Specimen conductivity, stress
σ_f	Conductivity of pore fluid (Electrical conductivity)
σ_v, σ_h	Vertical and horizontal conductivity (Electrical conductivity)
σ_{dp}, σ_{dr}	Peak and residual undrained shear strength
φ'	Effective angle of internal friction

Chapter 1

Introduction

1.1 BACKGROUND

The behaviour of soils in general can be modelled using two types of approach, namely the phenomenological approach and the structural approach (Feda, 1982). The former is considered on the basis of continuum theories, such as elasticity and plasticity, in which a material is replaced by a mathematical model of a structure-less continuum. Numerous models have been derived from studies involving remoulded and reconstituted soils. According to a model such as critical state soil mechanics, soil behaviour is described by the initial void ratio and its subsequent modification due to stress history (Vaughan, 1985; Vaughan et al., 1988). It is assumed that the soil deforms homogeneously during shear, reaching a critical state at large strains, regardless of the initial testing conditions.

An alternative approach is the structural approach. The behaviour of the soil is modelled on the basis of interactions between discreet particles, and any structural features would influence the behaviour of the soil. If every single particle is modelled with its own load conditions, the exact results can be obtained. This is however not possible with current technology and the solution must be estimated from a balance of the two approaches.

There have been differences in the definition of the terms 'structure' and 'fabric'. According to Terzaghi and Peck (1948), the term 'structure' is defined as 'the pattern in which soil particles are arranged in the aggregate' and according to Mitchell (1956), 'fabric' is defined as 'the appearance of

patterns produced by shapes and arrangement of the mineral grains'. Rowe (1972) defined 'fabric' as the size, shape and arrangement of solid particles, the organic inclusions and the associated voids while 'structure' is associated with arrangement of a particular size range. According to Lambe and Whitman (1969) and Mitchell (1976), 'structure' is defined as a combination of particle arrangement (fabric) and bonding (inter-particular forces, including cementation, electrostatic, electromagnetic or any other force which keeps the particles together). In the context of this thesis, this latter definition is adopted. 'Fabric' defines the arrangement of particles and associated pores while 'structure' defines the combination of fabric and bonding.

In the past two decades, researchers such as Mulilis et al. (1977), Keurbis et al. (1988), Vaid et al. (1990), Ishihara (1993), Zlatovic and Ishihara (1997), Chillarige et al. (1997), Dyvik and Hoeg (1999) and Vaid et al. (1999) have shown that the behaviour of a non-plastic, cohesionless soil produced using different reconstituted methods, but tested at the same state and loading conditions may be significantly different. They speculate that this difference in behaviour is a result of the different fabric which ensues upon sample preparation. This is in direct conflict with models such as the critical state model, which suggests that the behaviour of a soil is only dependent upon its current void ratio, mean effective stress and deviatoric stress. Natural soils differ from reconstituted soils on both micro and macro scales owing to the fabric. It is therefore important that fabric effects be understood and incorporated in the interpretation of laboratory test results.

Although tailings dams have been constructed for over a century in South Africa, relatively little is known about their behaviour. Predictions are often based on empirical observations or simple calculations from limited information. Tailings dams pose a potential threat to the environment in the event of a failure e.g. the failures at Bafokeng in 1974 and Merriespruit in 1994. Although failures of this magnitude are rare, they nevertheless impose significant potential risk to both the public and mining companies. Unless the understanding of tailings behaviour is advanced, these threats will remain in existence. Due to the complexity of undisturbed sampling of tailings,

predictions of the behaviour of tailings are generally based on controlled laboratory tests on reconstituted samples. Although many sample reconstitution methods are available, it is not clear which reconstitution method, if any, will present behaviour representative of in situ conditions.

1.2   OBJECTIVE

The objective of this research is to examine the behaviour of undisturbed and reconstituted gold tailings samples at the same state (void ratio and effective stress). It is postulated that samples constructed by different laboratory preparation methods will produce different particle arrangement (fabric) and will behave differently at the same state. Undisturbed samples will be compared to laboratory reconstituted samples to evaluate the similarities and differences in behaviour and fabric.

1.3   SCOPE

The extent of this study was limited due to the complex nature of tailings and soils in general. The limitations can be summarized as follows:

- The material was limited to gold tailings from ERPM dam 4.
- All samples were surface samples obtained within a depth of 1 metre.
- The research was laboratory based.
- Investigation of behaviour included sedimentation, collapse and swell, isotropic consolidation, creep, undrained shear and stiffness.
- Only saturated conditions were considered. Although in situ samples near the surface may have been de-saturated during desiccation, all triaxial tests were conducted on saturated in situ or laboratory reconstituted samples.
- The study concentrated on the physical properties of gold tailings particles and their influence on the mechanical behaviour of gold tailings. Mechanical behaviour is defined by Olson and Mesri (1970) as mechanical

bending, compressing and rupture of the particles coupled with shearing displacement at particle contacts. Although it is recognized that pore fluid chemistry plays an important role, all triaxial tests were conducted using de-aired tap water. Distilled water was used for sample preparation of slurry and moist tamped samples. In some cases, dispersant or flocculants were used to obtain the required void ratio. For these cases, an additional flushing process was incorporated to eliminate as much of the dispersant as possible. An assumption was made that the dispersant or flocculants had an effect only on the resulting fabric, and not on the mechanical behaviour of the tailings.

- The main aim of the research was to investigate the effect of particle arrangement (fabric) on the mechanical behaviour of gold tailings. Effects of factors such as fines content and particle shape which are known to influence the behaviour, were not controlled, but assumed to be constant for a particular sampling position.

1.4   METHODOLOGY

A hypothesis was proposed as a guideline for this study. The hypothesis states that: **Accurate simulation of the behaviour of gold tailings under laboratory conditions requires appropriate replication of the material fabric.** In order to validate the hypothesis, the tailings samples were subjected to a number of controlled laboratory tests. Testing can be summarized as follows:

- Indicator tests included particle size distribution, specific gravity and Atterberg limits.
- Maximum and minimum void ratio tests to establish void ratio limits for the tailings.
- Sedimentation tests with dispersant and flocculants
- Triaxial consolidation.

- Undrained triaxial tests on in situ and laboratory samples. Instrumentation included external displacement transducer, internal submersible load cell and LVDTs to measure local axial strain.

- Image analysis of in situ and laboratory prepared samples. This included the use of scanning electron microscopy (SEM) on naturally desiccated samples.

A method of fabric differentiation, based on SEM images, will be established. The method could be qualitative or quantitative. This allows some conclusions to be drawn about fabric and behaviour of gold tailings.

1.5   ORGANIZATION OF THESIS

The thesis consists of the following chapters:

- Chapter 1 serves as the introduction to the thesis.
- Chapter 2 presents the existing knowledge on gold tailings and reviews current methods and relevant information on fabric analysis.
- Chapter 3 discusses all experimental work including testing strategy, processes and procedures.
- Chapter 4 presents the fabric of gold tailings and methods of classification relevant to the behaviour of gold tailings.
- Chapter 5 discusses the analysed data in terms of the effect of particle arrangement (fabric) on the mechanical behaviour of in situ and laboratory prepared gold tailings.
- Chapter 6 closes the thesis with a summary of the main conclusions, recommendations for laboratory testing in industry and suggestions for further research based on the results of this thesis.
- Chapter 7 lists all references used in the thesis.
- Appendix A includes the preliminary SEM imagess.
- Appendix B consists of all instrumentation data as well as calibration graphs.

- Appendix C describes all sample preparation procedures.

- Appendix D includes all SEM images used for fabric classification.

- Appendix E presents all results obtained for the experimental programme. This includes the preliminary tests and the consolidation and shear tests.

Chapter 2

Literature Review

2.1 INTRODUCTION

The objective of the literature review is to present the available literature on the research topic. This provides the basis from which the experimental programme was developed. The first sections are dedicated to the description of gold tailings in general. The geology and mineralogy of the Witwatersrand gold reef, which is the primary source of the tailings used in this research, is discussed. This is followed by a brief discussion of the processes involved in gold extraction and general design and construction of tailings dams in South Africa. The engineering properties of gold tailings from documented literature are also presented. Discussion of soil fabric is introduced with documented differences in behaviour, followed by detailed literature on available methods of fabric measurement and analysis. As laboratory sample preparation is a significant part of this research, a detailed discussion on available methods of laboratory sample preparation is included. This is followed by a brief discussion on sampling and sample disturbance. The chapter is concluded with a summary of the literature review.

2.2 GEOLOGY AND MINERALOGY OF THE WITWATERSRAND GOLD REEF

The Witwatersrand goldfields were laid down between 2.7 and 3 billion years ago, in an oval area approximately 42 000km², in the Gauteng, North-West and Free State provinces of South Africa. Sediments originating from the

surrounding Archian granite-greenstone terrains were deposited in a large basin and through compression and chemical processes formed the gold-bearing rock body (Stanley, 1987). Detrital particles in the deposit underwent low-grade metamorphism which led to re-crystallization, thus forming gold. Gold ores in the Witwatersrand goldfields exist in sheets or reefs originally deposited horizontally under water (Vermeulen, 2001). Subsequent overburden and geological movements transformed the reefs into tilted or faulted strata with an average thickness of 300 mm. Generally the reefs exist in the form of coarse conglomerates, or less often, as greyish metamorphosed sedimentary rock. The conglomerates are composed of rock pebbles derived from vein quartz, quartzite, chert jasper or quartz porphyry cemented in a silicate matrix. In *Table 2-1*, Stanley (1987) summarizes the mineralogical composition of a typical gold reef in the Witwatersrand area.

Mineral	Abundance
Quartz (SiO_2), primary and secondary	70 – 90%
Muscovite and other phyllosilicates	10 – 30%
Pyrites	3 – 4%
Other sulphides	1 – 2%
Grains of primary minerals	1 – 2%
Uraniferous Kerogen	1%
Gold	~ 45 ppm in the Vaal reef

Table 2-1. Mineral composition of a typical Witwatersrand gold reef (Stanley, 1987)

2.3   THE GOLD EXTRACTION PROCESS

Tailings can be defined as the by-product of the mining process, consisting of finely ground and chemically treated rock flour (Vermeulen, 2001). In order to understand how tailings behave, it is important to understand how tailings are produced. The extraction of gold from the gold-bearing rock requires many

stages. The ore is first removed from the gold-bearing reef by drilling and blasting, which is known as the ore-winning process. This is followed by the process of ore-dressing, which is the mechanical preparation of ore rocks by crushing and grinding to liberate and expose the concentrated valuable minerals for metallurgical extraction (Ritcey, 1989). The main objective of ore-dressing is to increase the surface area available for metallurgical extraction by reducing the size of the ore. The size of the resulting rock flour has a significant influence on the behaviour of the tailings. Ore-dressing is followed by metallurgical extraction in which ore-minerals are extracted chemically through the processes of amalgamation or cyanidation (Stanley, 1987). Finally, the extracted gold is upgraded at the refinery to at least 99.5% pure by either the miller chlorination process or electrolytic refining. A detailed description of the gold extraction process is presented by Vermeulen (2001).

According to Vermeulen (2001), the Witwatersrand gold reef has an average grade of 8.74g/t. This implies that 1 tonne of rock flour is produced for every 8.74g of gold produced. Ripley et al. (1982) suggested that approximately 5 tonnes of solid and liquid waste is produced for every 10g of gold produced. The amount of tailings produced in the world was approximately 5 billion tonnes per year in 1994 (Vermeulen, 2001), and according to Penman (1994), this amount exceeds the amount of fill in the construction of embankment dams, motorway embankments and all other earthworks in the same period. In 1987, South African mines were producing in excess of 250 million tonnes of mine tailings annually. With such an amount of waste produced, it is not surprising that tailings impoundments were described by Smith (1972) as 'massive manhills'. These massive structures pose great risk to the public and the environment in the event of a failure.

2.4   TAILINGS DISPOSAL

As a significant amount of tailings are produced, the environmental impact of this waste material can be of great concern. The disposal site and method is

dependent on factors such as capital and operating costs, experience and preference, site topography and climate conditions (Vermeulen, 2001). Mining waste was traditionally dumped into the nearest water body. Such disposal methods have been eliminated due to an increase in environmental awareness. Tailings nowadays are generally disposed of into impoundments specially designed for storage and containment of the solid and liquid waste.

2.4.1 Tailings deposition methods

Deposition of tailings into an impoundment can either be dry, sub-aqueous or sub-aerial slurry, or in a dewatered slurry state. However, due to the financial implications of transportation and placement, initially dry tailings are usually slurried prior to disposal. Tailings slurry is usually pumped at the highest concentration feasible to reduce the cost of transportation and placement. The following section briefly describes the depositional methods that are commonly used in practice.

Dry deposition

As the name suggests, tailings in a dry state are deposited without the addition of water. This is usually in the form of ash produced from thermal coal-fired power stations, or the coarse rejects from some coal, metal or mineral recovery process (Robertson, 1987). Placement and handling of dry tailings is essentially similar to any other earth or overburden moving exercises. Essentially, dry tailings differ from slurried tailings in two fundamental aspects. Firstly, interim stability is usually of less concern and a retaining embankment is usually not required. Secondly, the tailings are usually of sufficient strength for compaction equipment to be used during placement.

Dewatered tailings

Tailings within this category may range from a sloppy semi-slurry to a product which behaves essentially as a dry granular material (Robertson, 1987). The 'handleability', 'trafficability' and stability of the deposit are essentially dependent on the degree of dewatering achieved. Sloppy semi-slurry cannot provide a trafficable surface and deposition requires specialized placement

equipment such as conveyors while 'dry' dewatered tailings can be deposited and compacted by conventional earth-moving equipment.

The only significant difference between sloppy dewatered tailings and slurry placed tailings is the uniformity (lack of segregation) that results from dewatered deposits. 'Dry' tailings are placed in a partially saturated state and can be compacted to achieve the desired densities, consolidation or shear strength characteristics (Robertson, 1987).

Due to the financial implications of tailings transportation, it is common practice to pump tailings as slurry to the disposal site. This might not be feasible in areas where evaporation occurs at a fast rate or the use of water needs to be minimized for cost implications. In such cases, tailings can be placed dry or in a dewatered state. Although these methods can be implemented at reduced water consumptions, other equipments are required for the facility, which increases the capital and operational costs.

Sub-aqueous deposition

Sub-aqueous deposition usually involves deposition of slurry in an uncontrolled manner into a body of water. Tailings settle out as soft-bottom sediment, or are transported and dispersed over a large area under water (Vermeulen, 2001). The resulting low density material is generally very soft and may require special construction techniques and reclamation procedures.

Sub-aqueous deposition generally results in tailings with fairly uniform grading. Deposition under water results in a low density material that is generally normally or under-consolidated. These deposits can generally be characterized by a high void ratio, high compressibility and a low permeability (Robertson, 1987).

Sub-aerial deposition

Sub-aerial deposition generally involves deposition of slurry in an aerial manner, usually in the form of open-ended pipe discharge, spigotting or cycloning.

- *Open-ended pipe discharge*: This method is often used as an inexpensive delivery system, typically accomplished by discharging the slurry from one or more open-ended pipe outlets around the perimeter of a dam. Discharge sequence is cycled around the dam perimeter to allow the recently deposited slurry sufficient time to dry and gain strength before the next layer is placed. The slurry exiting the pipe outlet forms a plunge pool from which it breaches and flows towards the central semi-permanent pond. Flow is fast and concentrated on the beach (sloped area above water level) before fanning out in a delta towards the pond area. Ideally, segregation should take place on the beach, leaving coarse particles closer to the daywall and finer material in the central area. Although there is a general trend of fineness towards the pond, flow on the beach tends to concentrate in meandering streams of high velocity, passing most of the material directly into the pond, leaving little opportunity for segregation (Penman, 1994).

- *Spigotting*: Very similar to open-ended pipe discharge, but with the objective of reducing the velocity of the deposited stream and encouraging sheet-like flow across the beach to aid segregation (Vermeulen, 2001). This is accomplished by partially covering the delivery pipe outlet with a faceplate, leaving only a half moon opening. The slurry is sprayed over a large area on the beach with more uniform sheet-like flow. This form of deposition effectively separates the coarse fractions from the fines by gravitational segregation on the beach, and is generally used for tailings that have a wide grading and a high percentage of clay-sized particles. Deposition is achieved by groups of 20 to 40 spigots, placed at 1 to 5 metre intervals, which have to be raised periodically as the dam rises.

- *Cycloning:* The slurry can be cycloned to mechanically separate the slurry into the coarse fractions (cyclone underflow) and the finer material (cyclone overflow). The relatively free-draining characteristic of the coarse fraction makes it a suitable construction material, as it is relatively uniform in terms of particle size, consolidates rapidly, and produces a low water

table (Robertson, 1987). The finer overflow fraction is deposited by conventional spigotting techniques at a low slurry density. Operation of a cycloning system requires planning and management in order for the dam to function properly. It is only practical when the tailings have a wide grading and sufficient coarse fraction for daywall construction (Vermeulen, 2001).

2.4.2 Tailings dam construction methods

There are essentially three primary types of disposal facilities. Disposal of tailings can be done in natural basins such as under-sea or in-lake disposal as practiced in Canada and New Guinea (Robertson, 1987) or in-pit disposal. Although these methods minimize financial implications, environmental damage from under-sea or in-lake disposal can potentially be catastrophic.

Disposal can also be done as a central discharge cone deposit, commonly known as thickened discharge method (Robrinski, 1975). No embankments are required and deposition is achieved from a central discharge point onto the surface of the ground. The most critical factor is the angle of beach slope, as this determines the area and volume of the deposition cone (Robertson, 1987). The slurry is often thickened to increase the beach angles and thus the storage capacity of the cone.

The third method, which is the most common method of tailings disposal, involves construction of an embankment. Construction can be done in a valley such as conventional earth or rock filled dam construction methods or as freestanding raised embankments. Raised embankments are frequently used for tailings dam construction due to the flat terrain. There are three methods of construction for raised embankments, namely upstream, downstream or centreline construction.

Upstream construction

This method involves advancing the impoundment crest upstream by periodically constructing small dykes on the tailings deposit immediately

upstream from the previous deposition. The upstream method is shown in *Figure 2-1*. The main concern with upstream construction is that the successive dykes are constructed on previously deposited material and this requires that the deposited tailings have sufficient shear strength for stability. This method of construction should be avoided in regions of seismic activity.
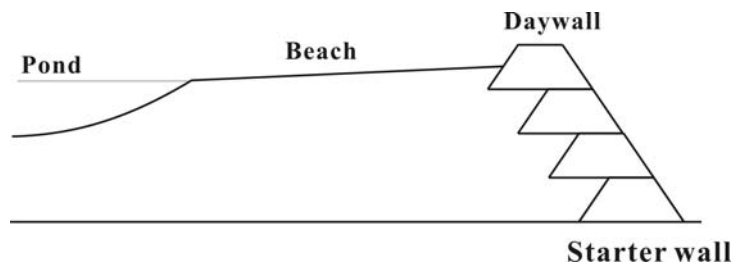
Figure 2-1. Upstream method of tailings dam construction

Downstream construction

Downstream construction is achieved by advancing the crest downstream as the smaller dykes are constructed. This is illustrated in *Figure 2-2*. The method is only required when the tailings are extremely weak, where the pool is impounded against the embankment, or in areas of severe climatic, seismic or toxic conditions. Additional area and thus cost are required for this type of construction (Robertson, 1987).
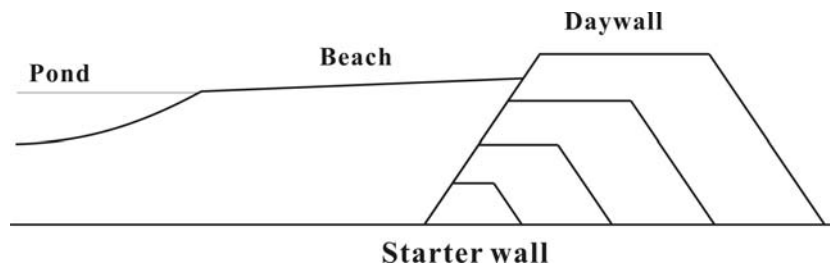
Figure 2-2. Downstream method of tailings dam construction

Centreline construction

With this method the crest is raised vertically upward as illustrated in *Figure 2-3*. Successive smaller dykes are constructed on the upstream side on previously deposited material and on the downstream side on borrowed or cycloned material over which some control can be exercised. The method is a balance between upstream and downstream construction methods.
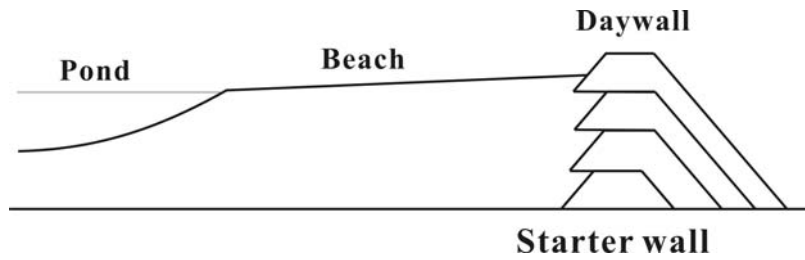
Figure 2-3. Centreline method of tailings dam construction

Daywall-Nightpan Paddock system

The method can be used in conjunction with upstream, downstream or centreline construction aforementioned. The periphery, also known as the daywall, is sectioned into paddocks in which tailings are poured from the midpoint. The fill is then compacted, either by tractor plough, or by labour intensive shovel packing. Excess water is decanted into the interior of the dam known as the nightpan. The daywall is left to dry, consolidate and crack for up to three weeks before the next lift, improving the mechanical properties of the material as a result of densification (Blight and Steffen, 1979). The construction of the daywall is entirely done during the day, due to the required supervision and close control, and hence the name. During the night, tailings are discharged into the interior or nightpan.

Paddock systems are successful when the tailings of fairly uniform grading remain well in suspension at a constant density until placed, and when the rate of rise matches the drying time of the tailings (Gowen and Williamson, 1987). The method results in a reasonably firm and well consolidated daywall, while the material in the nightpan, especially in the pond area, are usually significantly less consolidated and soft (Wagener and Jacobsz, 1999).

The choice of deposition and construction method depends on site availability and type of material available for construction. The most common method of tailings disposal in South Africa is the construction of raised embankments in which tailings, generally in the form of slurry, can be stored. These impoundments are often high and pose great threat to the environment in the event of failure. The gradation, and thus permeability of the tailings, is largely a function of the method of deposition into the impoundment. The stability of

these impoundments is largely dependent on the position of the phreatic surface which is a function of the permeability of the tailings.

2.5   ENGINEERING PROPERTIES OF GOLD TAILINGS

The construction of tailings impoundments resembles that of a natural deposit. Transportation of sediments is followed by deposition, sedimentation and eventually consolidation due to self-weight or external loading (Imai, 1981; Schiffman et al., 1988). Tailings, however, have a very recent stress history compared with natural deposits (Vermeulen, 2001). The following sections deal with the formation and state of tailings in general and briefly discuss the fundamental particle properties, index parameters, particle size distribution and beach profile. Engineering properties such as permeability, compressibility and consolidation, stiffness, shear strength and void ratio are also considered. For a more detailed discussion on the state and composition of gold tailings, refer to Vermeulen (2001).

2.5.1   Tailings in general

After deposition, the slurry flows along the beach towards the pond, during which tailings particles are deposited. Coarse particles are deposited first, closer to the discharge point, while finer particles are deposited further away from the point of discharge. This is known as segregation or hydraulic sorting of tailings. The result is a decrease in particle size towards the pond and a beach sloping down towards the centre of the dam (Papageorgiou, 2004). Hydraulic sorting is one of the main factors influencing the in situ properties of gold tailings. The particle size distribution determines geotechnical parameters such as density, permeability and shear strength. These in turn influence the rate of drainage, consolidation characteristics, acceptable rate of construction, safe slope angle of daywall and maximum height (volume) of the tailings dam (Papageorgiou, 2004). One of the design objectives for a tailings dam is to promote hydraulic sorting, as coarser material deposited near the edge has higher shear strength and permeability.

Another consistent feature of tailings impoundments is the highly layered nature of the profile. Deposition generally takes place cyclically around the dam to allow sufficient time for the newly deposited material to desiccate and consolidate. This significantly increases the strength and storage capacity of the impoundment. Layers can vary between 10 to 200mm in thickness, and often take the form of alternating coarse and fine deposits, with up to 50% variation in fineness (Vermeulen, 2001).

2.5.2 Fundamental properties and index parameters

Unless any significant chemically reactions have taken place during chemical extraction, tailings solids basically has the same mineralogy as the parent rock from which mining took place. Energy dispersive X-ray spectrometry in the SEM showed that tailings consist mainly of silicon with varying amounts of sodium, aluminium, potassium, iron and sulphur. Mineralogy of typical tailings from the Witwatersrand gold reef can be summarized as 75% quartz, 10% muscovite, 5% pyrophyllite, 5% illite and small percentages of clinochlore, kaolinite and pyrite (Vermeulen, 2001). Gold tailings have been classified as fine, hard and angular rock flour, with 0 to 15% fine sand, 80 percent silt and 0 to 10% clay-sized particles slurried with process water (Vick, 1983; McPhail and Wagner, 1989). Specific gravity of gold tailings from the literature can be summarized in *Table 2-2*.

Reference	G_s
Pettibone and Kealy (1971)	2.5 – 3.5
Hamel and Gunderson (1973)	3.1
East et al. (1988)	3.02
Vermeulen (2001)	2.75

Table 2-2. Specific gravity, G_s, of gold tailings

In terms of particle shape, gold tailings generally range from highly angular to sub-round to flat. Coarse tailings are composed of highly-angular to sub-

rounded particles with sharp edges and some rough surfaces (Mittle and Morgenstern, 1975; Lucia et al., 1981; Garga and McKay, 1984; Vermeulen, 2001). Fines consist mainly of flat plate-like particles and small amounts of bulky silt-sized particles (Vermeulen, 2001; Chang, 2004). Undispersed samples (*Figure 2-4*) show an aggregation of the finer plate-like particles around the bulky, coarse particles.
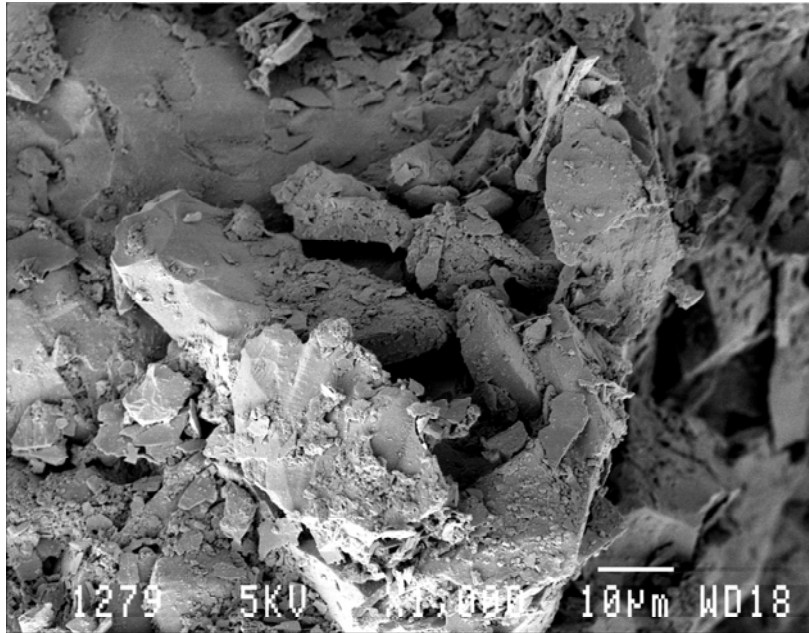
Figure 2-4. Scanning electron micrograph of gold tailings (After Chang, 2004)

Gold tailings generally exhibit little plasticity and no cohesion (McPhail and Wagner, 1989). Based on their Atterberg limits, gold tailings can be classified as low to high plasticity silts. The Atterberg limits of typical gold tailings from the Witwatersrand Gold reef are given in *Table 2-3* (Vermeulen, 2001):

Sample	Liquid limit	Plastic limit	Plasticity index
	(%)	(%)	(%)
Whole tailings	29	22	7
Coarse (> 0.075mm)	28	22	6
Fines (< 0.075mm)	43 – 56	32 – 39	11 – 17

Table 2-3. Atterberg limits of typical gold tailings (Vermeulen, 2001).

2.5.3   Particle size distribution

The grading or particle size distribution of gold tailings is a function of factors, such as, the effectiveness of the size reduction process, and the solid content of the slurry. Due to hydraulic sorting, the sampling position also has an effect on the grading of the gold tailings. Pettibone and Kealy (1971) and van Zyl (1993) described the grading of typical gold tailings as uniformly distributed in the silt size range with small percentages, in the order of 10 percent, in the sand and clay size ranges. *Figure 2-5* shows the grading envelope for typical South African gold tailings published by Blight and Steffen (1979).
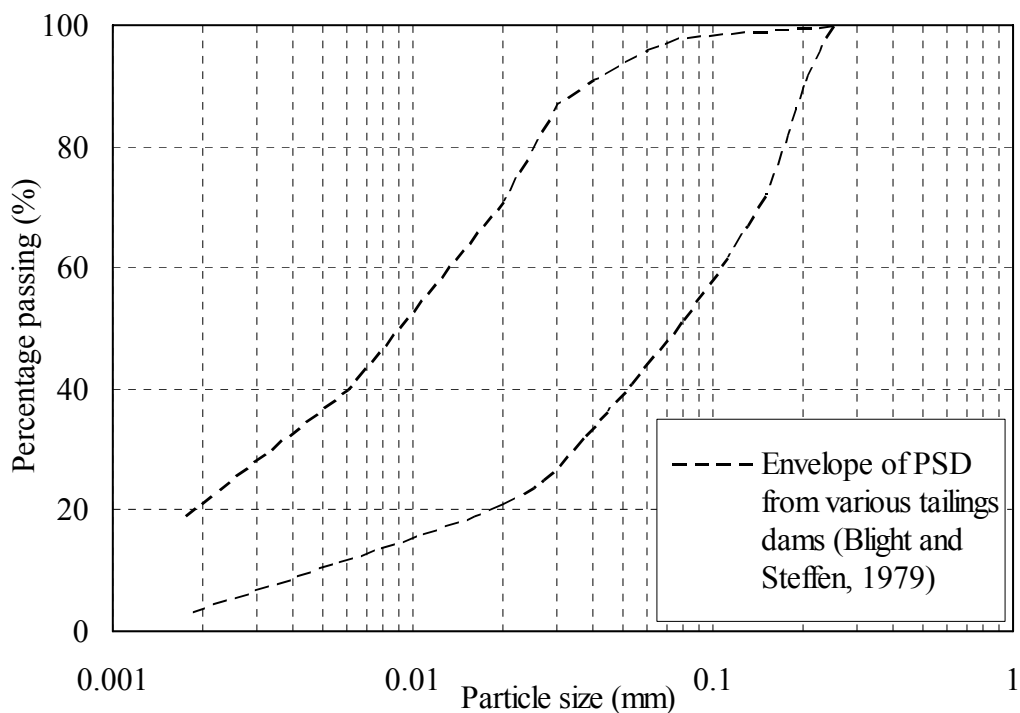
Figure 2-5. Particle size distribution envelope of South African gold tailings (After Blight and Steffen, 1979)

Vermeulen (2001) showed that after chemical treatment, which included removal of organic material and calcareous content and dispersion, grading properties could be summarized as in *Table 2-4*.

Description	D_{10}	D_{30}	D_{60}	D_{90}	C_U[*]	C_Z[**]
	(μm)	(μm)	(μm)	(μm)		
Whole tailings	2	10	55	125	27.5	0.91
Coarse (>0.075mm)	2–3	9-25	43-75	115-145	21.5-25	0.94-2.78
Fine (<0.075mm)	1.5-1.7	3.2-4.5	8.3-16	41-55	4.9-10.7	0.75-0.84

[*]C_U = Coefficient of Uniformity = D_{60}/ D_{10}

[**] C_Z = Coefficient of Curvature = $D_{30}^2/(D_{10}D_{60})$

Table 2-4. Summary of grading properties of dispersed gold tailings (Vermeulen, 2001)

2.5.4 Permeability

The permeability of soil is a function of the particle characteristics, density and particle arrangement of the soil (Pettibone and Kealy, 1971). As a result of hydraulic sorting, tailings differ in grading, and thus permeability, from the peripheral wall to the pond. According to Kealy and Busch (1979), this variation in permeability is by far the most significant factor in determining the position of the phreatic surface. Anisotropy in permeability due to deposition cycles has significantly lesser effects on the location of the phreatic surface (Vermeulen, 2001). Quoted values for the permeability of gold tailings are summarized in *Table 2-5*.

Reference	Description	Permeability (m/yr)
Blight (1980)	Range	1 – 50
Blight (1981)	General	3
Vermeulen (2001)	Whole tailings	10
	Fines	1.5 – 5
	Coarse	2.5 – 15

Table 2-5. Summary of permeability of gold tailings

The permeability of the tailings material at any point down a slurry deposited beach can also be estimated by equations of the type:

$$k = ae^{-bH} \qquad \qquad \textit{Equation 2-1}$$

where k is the permeability at a distance H down the beach and a and b are constants of a particular beach and tailings. Blight et al. (1985) showed, using model beaches, that for a particular active gold tailings beach, $a = 2.72 \times 10^{-5}$ m/s and $b = 0.0315$ /m. The permeability can also be estimated via the well-known Hazen expression or by the expression given more recently by Sherard et al. (1984):

$$k = 0.35(D_{15})^2 \qquad \qquad \textit{Equation 2-2}$$

2.5.5   Compressibility and consolidation characteristics

Consolidation can generally be classified into primary and secondary consolidation. Primary consolidation deals with the gradual reduction in volume of a fully saturated soil as the excess pore water pressure, built up by an increase in total stress, dissipates. Secondary compression or creep, however, is thought to be due to the gradual realignment of particles into a more stable configuration with time under constant stress conditions. Primary consolidation can be expressed in terms of the *compression index C_c*, a measure of the stiffness of the material and in terms of the *coefficient of consolidation C_v*, which is an indication of the rate of consolidation. The value of C_v can be determined using Casagrande's log-time method or Taylor's root-time method and the compression index C_c is the slope of the linear portion of the e-log$p$' plot.

Tailings are generally more compressible than similar natural soils due mainly to their grading characteristics, high angularity and loose depositional state (Vick, 1983). Matyas et al. (1984) conducted oedometer tests on uranium tailings and found that fine tailings appear more compressible than coarse

tailings. Similar results were reported by Vermeulen (2001). Interestingly, Matyas et al. (1984) also concluded that the compressibility of undisturbed samples was higher than its reconstituted counterparts. *Table 2-6* shows typical values of C_c for gold tailings as quoted in the literature.

Reference	Compression Index, C_c	
	Coarse	Fine
Blight and Steffen (1979)		0.35
Vick (1990)	0.05 – 0.1	0.23 – 0.3
Stone et al. (1994)		0.75 (centrifuge)
		0.35 (Rowe cell)
Qiu and Sego (2001)		0.083 – 0.156

Table 2-6. Quoted values of Compression Index, C_c, for gold tailings

The coefficient of consolidation for gold tailings reported in the literature is summarized in *Table 2-7*.

Reference	Coefficient of consolidation, C_v (m²/yr)	
	Coarse	Fine
Blight and Steffen (1979)		198
Vick (1990)	$1.6 \times 10^3 - 0.6 \times 10^6$	0.3 – 30
Stone et al. (1994)		15 – 26
Vermeulen (2001)	800 – 6900	210 – 1200
Qiu and Sego (2001)		13.58 – 80.07

Table 2-7. Coefficient of consolidation, Cv, for gold tailings.

Very little literature was found dealing with creep of gold tailings, but according to Vick (1983), secondary consolidation in gold tailings is relatively insignificant compared to primary consolidation.

2.5.6 Stiffness

The bulk stiffness of a soil can be expressed by the *Bulk modulus, K*, as in *Equation 2-3*:

$$\frac{1}{K} = \frac{\delta p'}{\delta \varepsilon v}$$

Equation 2-3

where $\delta p'$ is the change in normal effective stress and $\delta \varepsilon_v$ is the change in volumetric strain. Isotropic compression tests data (Vermeulen, 2001) on reconstituted and undisturbed gold tailings samples is plotted in terms of the bulk modulus K and shown in *Figure 2-6*.
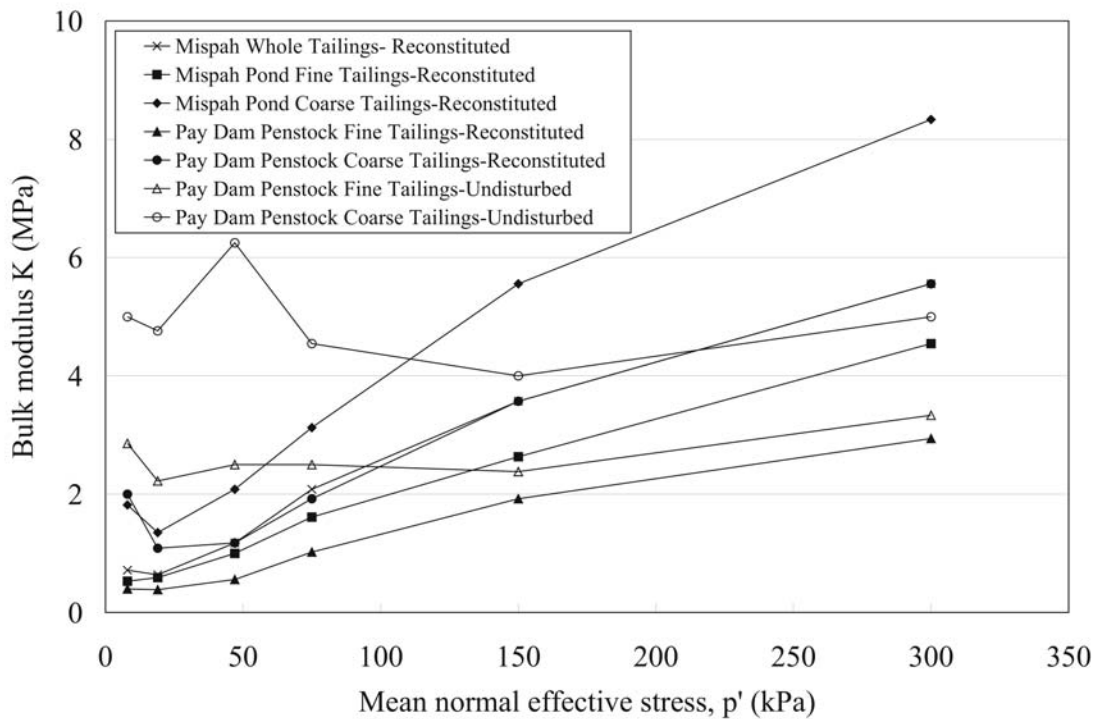
Figure 2-6. Bulk modulus of undisturbed and reconstituted gold tailings samples.

It is evident that fine tailings generally have a lower bulk modulus than coarse tailings. Furthermore, it is interesting to note that undisturbed samples have higher K values than their reconstituted counterparts.

The small strain stiffness of soils depends on the void ratio and the effective confining stress. G_{max} for gold tailings was estimated from the bender element results (Chang, 2004) to be in the range of 20 to 200MPa for effective confining stresses of up to 400kPa. Höeg et al. (2000) assessed the small strain stiffness, G_{max}, of fine tailings of the Polish Zelazny dam, and found that the recorded G_{max} of undisturbed samples were 20 to 30 percent higher than their reconstituted counterparts at the same state. The difference was attributed to soil fabric, as no evidence of cementation was found. Furthermore, G_{max} seemed to decrease with increasing fines content.

2.5.7   Shear behaviour

The static shear strength of saturated soil can be expressed in terms of the effective angle of internal friction, φ', and cohesion, c'. Gold tailings can be described as cohesionless in most cases, and having an effective angle of internal friction in the range of 30º to 37 º (Vick, 1983). According to Vick (1983), factors such as grading, density and over-consolidation ratio have a relatively small effect on φ'. The effective angle of internal friction is mainly dependent upon the effective stress level, with the strength envelope curved at high stresses due to particle crushing. The shear strength parameters of gold tailings in the literature are summarized in *Table 2-8*.

Reference	Material	Test	c' (kPa)	φ' (º)
Hamel and Gunderson (1973)	Dense air-dry	Direct shear	79	38
	Loose air-dry		0	39
	Loose wet		100	28
	Dense, saturated		11	24
Mittal and Morgenstern (1975)	Peak, loose	Direct shear	0	34
Blight and Steffen (1979)	Slimes		0	28-41
Blight (1981)	General		0	35
Vick (1983)	General			30-37

Table continued…				
Sully (1985)	Average	Direct shear	5	33
Van Zyl (1993)	Sand/slimes		0	35
Blight (1997)	Sand/slimes	Triaxial/ Direct shear	0	29-35
Vermeulen (2001)	Average	Triaxial	0	34

Table 2-8. Summary of static shear strength parameters of gold tailings quoted in the literature

Vermeulen (2001) demonstrated, using both tube samples and moist tamped samples, that the stress paths generally show some phase transformation, and are seldom purely contractive or dilative. Theron (2004) reproduced the behaviour of gold tailings with a sand-mica mixture, and postulated that the mechanical behaviour of gold tailings is governed by the platy particles.

2.5.8 Liquefaction potential

According to Castro and Poulos (1977) and Sladen et al. (1985), liquefaction is defined as *a phenomenon wherein a saturated material loses a large percentage of its shear resistance (due to monotonic or cyclic loading) and flows in a manner resembling a liquid until the shear stresses acting on the mass are as low as its reduced shear resistance*.

The behaviour of soils may be described as strain-hardening or strain-softening and as contractive or dilative.

- *Strain-hardening*: plastic straining beyond the yield point is accompanied by increase in stress.

- *Strain-softening*: plastic straining beyond the yield point is accompanied by a decrease in stress.
- *Contraction*: loading of loosely packed particles results in a tendency for a decrease in void space. Under undrained conditions, this leads to an increase in pore pressure and a resultant decrease in effective stress. Contraction is demonstrated using the marble analogy in *Figure 2-7a*.
- *Dilation*: loading of densely packed particles results in a tendency for an increase in void space. The resultant decrease in pore pressure leads to an increase in the effective stress. This is demonstrated in *Figure 2-7b*.

a) Contraction   b) Dilation
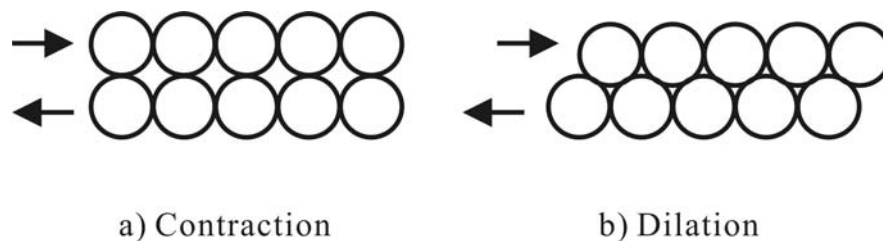
Figure 2-7. Marble analogy demonstrating contractive and dilative behaviour.

Saturated cohesionless soils may display one of three possible types of behaviour as displayed in *Figure 2-8* when subjected to undrained loading (Papageorgiou, 2004):

- *Contractive/liquefaction/strain-softening behaviour:* displays an increase in pore pressure to a constant value accompanied by a peak in the deviatoric stress within a few percent of loading followed by a sudden decrease to a constant residual value. The stress path moves to the left during the entire shear process, initially up (increase in q') and then down after the peak has been reached. This is demonstrated in *Figure 2-8* curve *(a)*.
- *Dilative/strain hardening behaviour*: displays an initial increase followed by a continuous decrease in pore pressure. The deviatoric stress increases continuously throughout the shear process. This is demonstrated in *Figure 2-8* curve *(b)*.

- *Limited liquefaction*: defined as a soil which exhibits a temporary decrease followed by an increase in the shear strength as strain increases. Limited liquefaction is demonstrated by curve *(c)* in *Figure 2-8*.
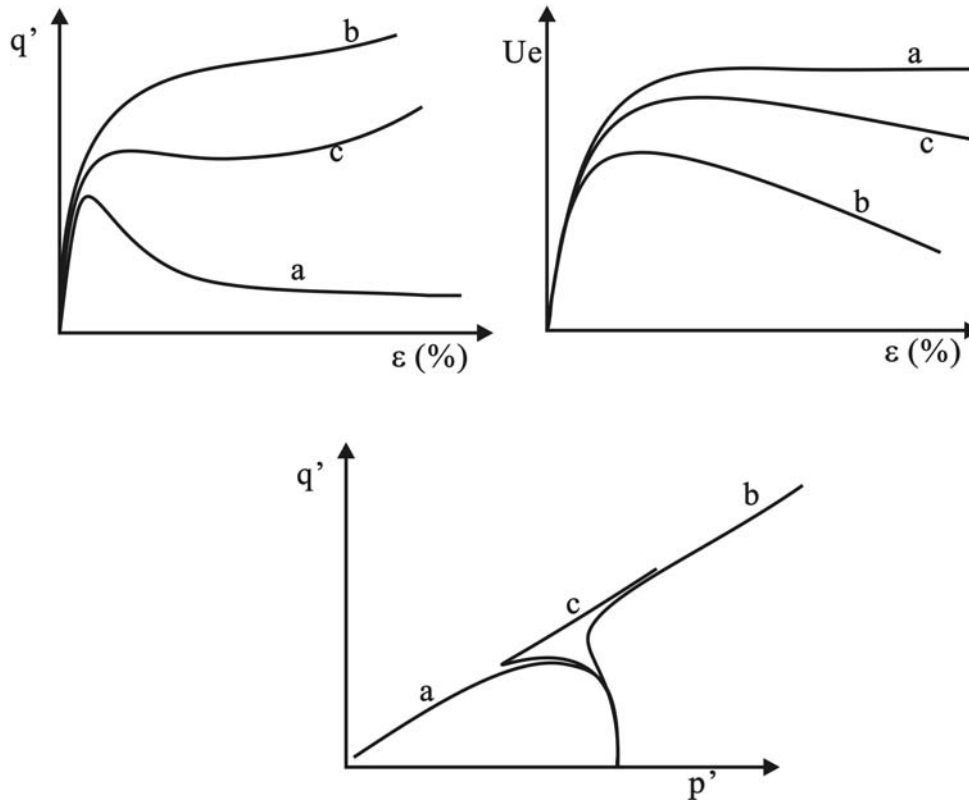
Figure 2-8. Possible behaviours for saturated cohesionless soils.

It has been shown by researchers such as Vaid et al. (1990) and Vaid and Sivathalayalan (2000) that moist tamping generally produces strain-softening behaviour while samples produced using water pluviation techniques generally dilate. It has also been concluded by the Canadian Liquefaction Experiment (CANLEX) that samples produced using water pluviation techniques generally show better agreement with undisturbed samples of Syncrude sands.

The reduction in undrained strength of a strain-softening material may be expressed in terms of the brittleness index, I_B (Bishop, 1967):

$$I_B = \frac{\sigma_{dp} - \sigma_{dr}}{\sigma_{dp}}$$

Equation 2-4

where σ_{dp} is the peak undrained shear strength and σ_{dr} is the residual undrained shear strength. The brittleness index ranges between 0 and 1, with a higher I_B associated with a higher reduction in shear strength.

2.5.9 Density and void ratio

The density or void ratio of most natural deposits can be estimated by acquiring undisturbed samples. The difficulty in estimating the density state of mine tailings arises from the inability to obtain undisturbed samples, especially in the pond area. Vermeulen (2001) suggested that, depending on

Reference	Description	Density (kg/m³)	Void ratio
Blight (1969)	After deposition		1.7
	After evaporation		1.25
	After sun drying		0.5
Blight and Steffen (1979)	General		1.1-1.2
Blight (1981)	In situ dry density	1835	
Vick (1983)	Tailings sand		0.6-0.9
	Low plasticity slimes		0.7-1.3
	High plasticity slimes		5-10
East et al. (1988)	In situ dry density	1340-1740	
	Average dry density	1650	
van Zyl (1993)	In situ dry density	1000-1450	
Vermeulen (2001)	Delivery pulp dry density	300-750	
	In situ dry density (sands)	1250-1650	
	In situ dry density (slimes)	1000	
	In situ void ratio (coarse)		0.77-0.87
	In situ void ratio (fine)		1.39-1.49

Table 2-9. In situ densities and void ratios for gold tailings

the specific gravity, pond tailings settle to a dry density of approximately 1000kg/m³ with a moisture content of 60 percent while on the beach tailings generally settle to a density of approximately 1450kg/m³ with a moisture content of 20 to 50 percent. Furthermore, density increases with depth as consolidation takes place. Vick (1983), however, suggests that the in situ void ratio of tailings is a better indication of the density state than dry density, as void ratio excludes the effects of specific gravity and is only a function of tailings particle properties and stress level. In situ densities and void ratios are summarized in *Table 2-9*. In situ void ratio is also dependent upon the grading of the tailings. Coarse particles close to the daywall settle to a lower void ratio than finer material further down the beach or in the pond (Vermeulen, 2001).

2.6   SOIL FABRIC

The effect of particle arrangement has long been recognized, even in the early days of soil mechanics development, with little or no substantial evidence. In the mid-1950s, with the development of suitable optical, X-ray and electron microscopes, direct observations became possible. Interest was mainly centred around clay particle arrangement and their effects on mechanical properties. In the late 1960s, improved techniques of sample preparation and the development of the scanning electron microscope (SEM) greatly facilitated the expansion of the science. In the early 1970s research interest expanded to include cohesionless soils and this led to the realization that soil characterization cannot be done in terms of density or relative density alone. Soil behaviour is also dependent upon stress history and the soil structure (Mitchell, 1993).

2.6.1   Observed difference in behaviour of soils

It is generally agreed that the fabric of clays may affect the behaviour of the clay (e.g. Seed et al., 1962; Mitchell, 1993). Various researchers have also demonstrated that cohesionless soils prepared using different reconstitution methods display different behaviour:

- Based on results of cyclic triaxial tests performed by Mulilis et al. (1977), Ishihara (1993) showed that the resistance to liquefaction of samples from the same type of sand prepared at the same relative density can vary over a wide range depending on the nature of the fabric created by different methods of sample preparation.

- Seed and de Alba (1986) and Yoshimi et al. (1989) showed that both the shear strength and liquefaction resistance of soils in its natural, undisturbed state are found to be significantly larger than measured in the laboratory.

- Zlatovic and Ishihara (1997) demonstrated that sand prepared using different reconstitution methods to similar void ratios (0.799 and 0.802) behaves differently under the same stress conditions. Water pluviated samples show strain-hardening behaviour while moist tamped and dry deposited samples show temporary strain-softening.

- Vaid et al. (1999) showed that the undrained response of uniform medium-grained sand could exhibit different undrained response at the same void ratio and effective stress conditions. Loose sand, when moist tamped, is contractive and susceptible to liquefaction while water pluviated specimens show dilative behaviour. This contractive, strain-softening response is due to the loose, collapsible structure that ensues upon moist tamping. They further concluded that characterizing in situ fluvial deposit and hydraulic fill sands using moist tamping will unjustifiably condemn it as being liquefiable.

- Wood (1999) showed that the specimen reconstitution method could influence the liquefaction behaviour of the silty sand. Dense and loose specimens formed from various reconstitution methods show similar behaviour: dense silty sand exhibits dilative behaviour and loose material shows contractive behaviour. The undrained response of medium silty sand can, however, be profoundly influenced by the reconstitution method. In general, wet methods are more resistant to liquefaction.

Although it is commonly believed that the difference in observed behaviour is a result of different fabric, there has however been a lack of substantiating evidence. Researchers have generally observed differences in behaviour

between in situ samples and samples reconstituted using various methods and speculated that the difference in behaviour is a result of fabric differences. In the past two decades, with the aid of improved image analysis methods and availability of microscopy equipment, fabric analysis is becoming increasingly feasible. If the fabric does indeed affect the behaviour of cohesionless soils then it is important to incorporate the effect of fabric in the soil models.

2.6.2 Description of soil fabric and fabric elements

Fabric description has traditionally been used by soil scientists to facilitate their understanding of root growth and fluid movement. It is, however, becoming increasingly used in the description of soils for geotechnical research. The fabric of soils can, in general, be described as comprising three distinct elements (Collins and McGown, 1974). This is demonstrated in *Figure 2-9*. Natural soils are generally composed of one or some of these fabric features:
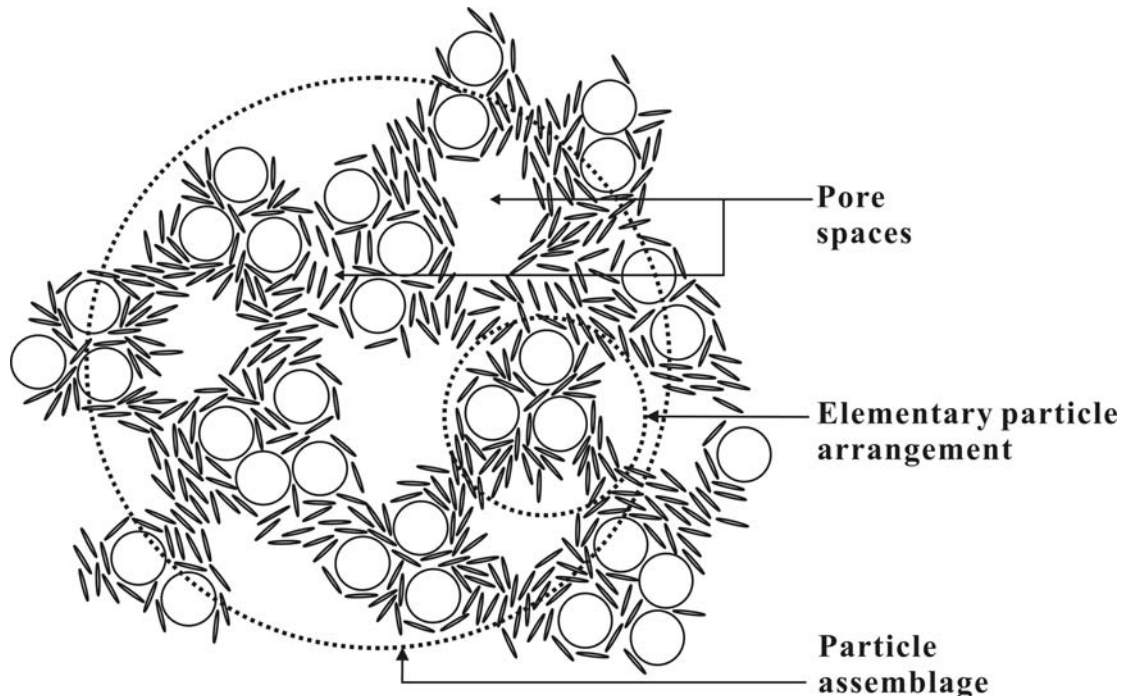
Figure 2-9. Three distinct elements of soil fabric.

- *Elementary particle arrangements:* single forms of particle interaction at the level of individual clay silt or sand particles.
- *Particle assemblages*: units of particle organization having definable physical boundaries and a specific mechanical function, which consist of one or more forms of the elementary particle arrangement.
- *Pore spaces*.

The fabric of a soil may also be considered, based on the level of scale (Mitchell and Soga, 2005):

- *Micro-fabric*: consists of the regular aggregation of particle and the very small pores between them. Typical fabric units are up to a few tens of micrometres across.
- *Mini-fabric*: contains the aggregation of the micro-fabric and the inter-assemblage pores between them. Mini-fabric units may be a few hundred micrometres in size.
- *Macro-fabric*: contains cracks, fissures, root-holes, laminations etc that correspond to the trans-assemblage pores.

Mechanical and flow properties of soils depend, to a varying degree, on these three levels of fabric. Hydraulic conductivity will be a function of the macro- and mini-fabrics while creep will be dependent on mini- and micro-fabrics (Mitchell, 1993).

2.6.3 Methods of fabric measurement

Various methods have been used to analyse the fabric of soils. These techniques range from visually observing the fabric under a microscope to measuring the electrical conductivity (Anandarajah and Kuganenthira, 1995) of the soil. The methods give insight into the observed behaviour of the soil through the fabric. These methods can be categorized into indirect and visual methods, which are summarized with example references in *Table 2-10*.

METHOD	REFERENCE
Indirect methods	
Mercury intrusion porosimetry (MIP)	Lefebvre and Delage (1983)
Hydraulic conductivity	Dewhurst et al. (1996)
Wave velocity	Pan and Dong (1999), Santamarina and Cascanta (1996)
Electrical conductivity	Anandarajah and Kuganenthira (1995)
Visual methods	
Optical Microscopy	Oda and Kazama (1998)
Thin sections	Oda and Kazama (1998)
Scanning Electron Microscopy (SEM)	Cafaro and Cotecchia (2001), Cotecchia and Chandler (1997), Fearon and Coop (2000)
X-ray computed tomography	Oda et al. (2004)
Laser scanning confocal microscopy	Fredrich et al. (1995)

Table 2-10. Indirect and visual methods for fabric analysis

Visual methods involve collecting and analyzing image data while indirect methods involve measuring some physical quantity and relating them to the fabric of the material. Other available visual methods used in soil testing that have not been referenced are x-ray scattering, neutron scattering and nuclear magnetic resonance. These methods require investigation regarding their suitability for soil fabric analysis, but provide potential possibilities.

This section deals with the various methods available for measurement and analysis of fabric, and includes the basic principles, benefit and limitations of each method.

Indirect methods

These methods are used to give an idea of the arrangement of the particles without visually observing the particles. Indirect methods measure various

properties of the material and relate the properties to the arrangement of the particles. Indirect methods (except for MIP) are generally used to assess fabric anisotropy.

- *Mercury intrusion porosimetry (MIP)*: This method is based on the principle that a non-wetting fluid, like mercury, does not enter a porous medium unless sufficient pressure is applied to force the liquid into the pores. Assuming pores to be cylindrical capillaries, the pressure, *P*, is related to the entrance pore radius, *r*, by Laplace's Law:

$$P = \frac{2\sigma \cos\theta}{r}$$
<div align="right">*Equation 2-4*</div>

  where σ is the surface tension of the intruding liquid and θ is the contact angle (for mercury, $\sigma = 0.484$ N/m and $\theta = 141°$). By increasing *P*, increasingly smaller pores are filled and the results can be plotted on a cumulative curve giving the pore-size distribution of the porous medium. The benefit of this method is that it is non-destructive (Lawrence, 1978) and does not cause damage the soil. There are a few limitations to the method. Firstly, the soil needs to be dehydrated before mercury intrusion can take place. However, air or oven drying may cause significant shrinkage of clays with high water content. Secondly, mercury intrusion porosimetry does not indicate the exact size of the pores, but rather the size of the entrance of the pores. Finally, the use of the method requires special care, since mercury is a poisonous substance.

- *Hydraulic conductivity*: The hydraulic conductivity of a material is a function of its fabric, thus development of an anisotropic fabric (Morgenstern and Tchalenko, 1967) may result in anisotropy in hydraulic conductivity (Arch and Maltman, 1990). Field and laboratory studies have suggested that shear zones in clays may enhance or retard fluid flow (Lupini et al., 1981). The behaviour of large strain shear zones is governed by the residual fabric of the sheared soil, which is dependent on the clay content and composition (Dewhurst et al., 1996). Hydraulic conductivity

may be used as a relative measure of fabric. By comparison of the hydraulic conductivity in two directions, the material anisotropy can be determined. The method, however, cannot yield a unique measure of fabric.

- Wave velocity: Particulate mechanics suggest that the mechanical behaviour of a particulate material is dependent on the distribution and orientation of the particles and the contact forces. Elastic wave velocity (including compression and shear waves) can be related to the fabric of granular material and its evolution during shearing (Santamarina and Cascanta, 1996; Pan and Dong, 1999). The fabric of a natural granular assembly can be evaluated from wave velocity measurements via an analytical procedure. This procedure involves a stress-dependent micromechanics-based elastic model, a theory of elastic-wave propagation for anisotropic material, and an optimization procedure (Pan and Dong, 1999). The analytical procedure is illustrated in *Figure 2-10.*
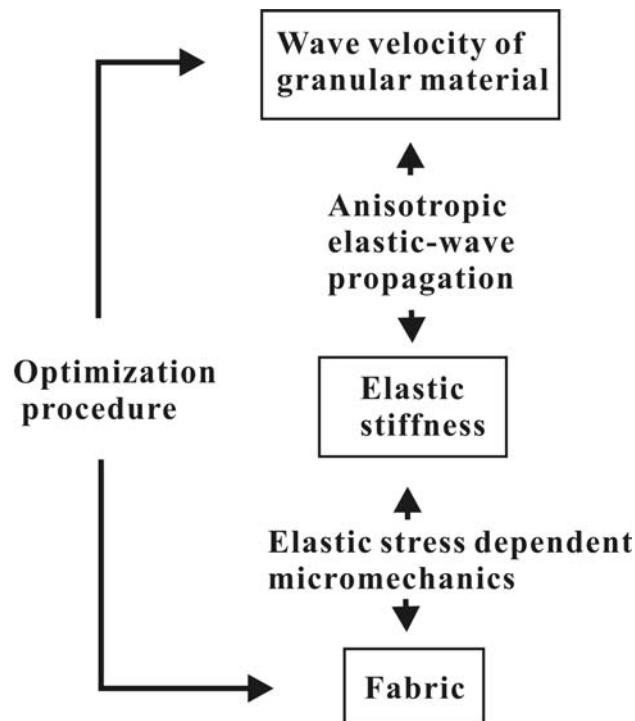
Figure 2-10. Analytical procedure for determining the relationship between fabric and measured wave velocity (Pan and Dong, 1999).

The analytical procedure relates wave velocity anisotropy to the anisotropic distribution of fabric and contact forces. The results indicate that an assembly shows a concentration of contact normals in the major principle direction and a residual fabric after subsequent loading/unloading sequences (Pan and Dong, 1999).

- Electrical conductivity: Electrical conductivity can be measured between two electrodes on either side of a saturated soil specimen, as shown in *Figure 2-11*. The soil skeleton is non-conductive, and thus electricity flows through the interstitial fluid. The conductivity of the specimen σ, can be defined as:

$$\sigma = L / RA \qquad\qquad\qquad Equation\ 2\text{-}5$$

where L is the length of the distance between the electrodes, A is the area of each electrode and R is the measured resistance. σ is a function of the conductivity of the pore fluid σ_f, the void ratio, and the orientation of soil particles. The vertical path shown in *Figure 2-11* is more tortuous than the horizontal path, and so σ_v will be less than σ_h. The magnitude of σ_v and σ_h will also depend on the value of σ_f.
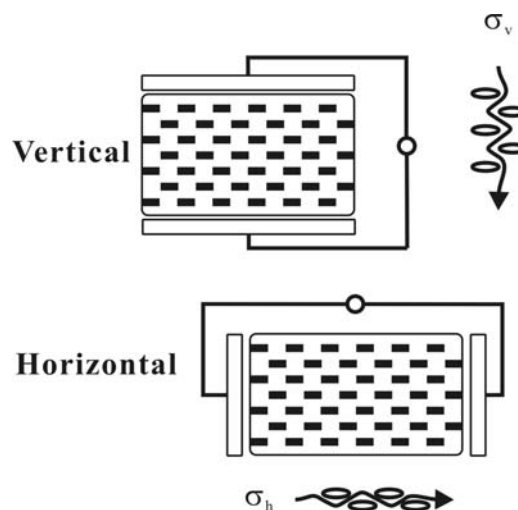
Figure 2-11. Electrical conduction in clay specimen in vertical and horizontal directions (After Anandarajah and Kuganenthira, 1995).

The major problem with most indirect methods is that the fabric is not visually observed and verified. The fabric is often related to the measured property by mathematical expressions or empirical relationships. The advantages are that firstly, the methods are usually non-destructive, and secondly, the measured properties can be expressed quantitatively as opposed to qualitatively. Measurements are also averages over the entire specimen and the possibility of measuring only the property of a specific structural feature is thus minimized.

Visual methods

The principles of all visual techniques involve bombarding the sample with particles, and monitoring the ejected particles. The methods are differentiated in terms of the types of incident and ejected particles. The ejected particles are then analysed and presented as an image from which the fabric can be visually observed and analysed.

- Optical microscopy: An object becomes visible when light is reflected off the object to an image capturing device, such as the human eye. When a lens is placed in between the object and the image capturing device, the refractive property of the lens changes the focal point of the light-rays, and the image can be magnified. The applications of optical microscopy are somewhat limited in geotechnical engineering. Firstly, the magnification that can be achieved with an optical microscope is limited due to properties of light (usually to a few hundred times magnification), and secondly, the clarity of images is restricted to the depth of focus of the lens. Other positions which do not fall within the depth of focus will seem blurred.

- Thin sections: Different elements can be identified by making use of the difference in refractive index between various crystal lattices which exist in different elements. The section must be sufficiently thin to allow passage of light-rays. Thin sections can be produced from soil specimens by impregnation with a suitable resin. Impregnated specimens are

sectioned and polished before they can be viewed. This method is an excellent way of observing grain orientations within a soil specimen.

- Scanning Electron Microscopy (SEM): This method has been used extensively in the geotechnical field for topographical imaging purposes (eg. Cotecchia and Chandler, 1997; Fearon and Coop, 2000; Cafaro and Cotecchia, 2001). The principle of SEM is to bombard the specimen with an incident electron beam, and to detect the emitted electrons. Two main types of electrons are emitted, namely secondary electrons and back-scattered electrons.

Secondary electrons are emitted when incident electrons knock loosely bound conduction electrons out of the sample. The intensity of the signal is dependent upon the angle between the incident beam and the specimen surface. A strong signal (large amounts of emitted electrons) will produce a bright spot, and a weaker signal (small amounts of emitted electrons) will produce a darker spot. Back-scattered electrons may be emitted when an electron beam passes close to a positively charged atomic nucleus and is attracted by its positive charge. Depending on the electron energy and the distance away from the nucleus, the angle of electron deflection may vary between 0 to 180°. These deflected electrons are collected by the detector and an image is produced from these back-scattered electrons. Similar to secondary electron images, the brightness of the image is dependent on the amount of electrons detected at a particular position.

The electron beam, typically with a radius of 5nm scans the specimen and an image is produced with bright or dark spots at the corresponding position. The images produced are three-dimensional topographical images with a shallow depth of view, because electrons cannot be detected from deep inside the specimen. The main difference between a back-scattered electron image and a secondary electron image is that a back-scattered electron image is a function of the atomic number while a secondary electron image is dependent upon the topography of the specimen.

Non-conductive specimens, like soil, need to be coated with a conductive coating to reduce electrical charging of the specimen, which creates image defects. This is usually accomplished with sputter-coating of gold or gold/palladium alloy. The use of a metal coating also yields a stronger signal and can aid in conducting heat and excess electrons away from the specimen.

SEM usually produces excellently clear images at very high magnifications. By varying the type of emitted electrons topographical or compositional images can be produced. There are a few limitations to SEM. Firstly the image is a three-dimensional surface image. When internal images of soil are required, it is necessary to open up the specimen which causes disturbance. Furthermore, the soil needs to be dry, as the sample is placed under high vacuum and any volatile material will cause contamination of the vacuum chamber leading to a reduced resolution.

Another benefit of SEM is its ability to produce x-rays which can be used to provide compositional information about the specimen. When an electron beam interacts with an element, an electron in the element may be removed, causing a vacancy. If the vacancy is at a higher energy, an electron from the outer shell (at lower energy) will fall into the vacancy. Energy is released in this process in the form of a photon of electromagnetic radiation. If the ejected electron was from an inner shell, then the photon is an x-ray. The released energy varies with the atomic number and can therefore be used to identify various elements.

- X-ray microscopy: X-radiation occurs when electrons, highly accelerated under high voltage, reduce speed when collided against a target made of a heavy metal such as tungsten. When an x-ray passes through an object, it attenuates at different rates, depending on the distribution of its electron density, if the x-ray energy level is kept constant (Johns et al., 1993). The attenuation of the x-ray is recorded on a detector and from the attenuation data, an image is created by means of a numerical technique known as *filter-back projection.* If the attenuation properties change sharply across

the material, it is possible to identify the boundaries of the material. The target, which corresponds to the x-ray source, must be small enough to minimize the scattering zones of the x-ray detector. A microfocus x-ray system uses a target as small as 5μm, and therefore the resolution of the image is greatly improved.

Oda et al. (2004) successfully imaged a sample of Toyoura sand (D_{50} = 0.206mm) using a microfocus x-ray system to investigate the microstructure in the shear band of the sample after shear. Although the sand was impregnated with a resin before imaging, the procedure was not necessary. The advantage of microfocus x-ray computed tomography is that sample preparation and imaging is simple, and the images obtained are three-dimensional images. The problem is that the x-ray apparatus with a microfocus target is extremely expensive and scarce, and the clarity of the image is not as good as SEM images.

- Laser scanning confocal microscopy: Laser scanning confocal microscopy (LSCM) has been used extensively in the biological sciences, but has only limited applications with geological material such as soils and rocks. Light (laser) particles are used as incident particles and imaging is achieved from the reflected light particles. LSCM involves saturating the specimen with an epoxy mixed with a suitable fluorochrome. The natural weak fluorescence of minerals allows a contrast between the epoxy-filled voids and the solid minerals. Specimen preparation techniques are similar to thin sectioning, where the sample is immersed in epoxy and later sectioned to a thickness of 0.5 to 1mm. The section is then polished by means of standard abrasive techniques. Both illumination and detection are confined to a single location on the specimen, and the resolution to 100nm is typically achieved. The use of single location illumination and detection also eliminates the problem of depth-of-field associated with optical microscopy. Penetration of the laser into geological samples is limited by the opacity of the minerals. This can be compensated for because geological samples can, if necessary, be illuminated at full laser intensity, unlike delicate biological samples which usually require a filter to reduce

laser intensity to a few percent of the original laser power. Using LSCM, Fredrich et al. (1995) successfully imaged the pore structure of rocks with various porosities. The method creates a three-dimensional image of the specimen, which is an advantage over surface techniques which only yield a two-dimensional image.

2.6.4 Methods of fabric characterization

Fabric can be classified according to the methods of measurement. Indirect methods of fabric measurement will classify fabric according to the physical property that is measured. These physical measurements can be related to a certain fabric, and this needs to be verified by visual means. There has been very little research on the relationship between physical properties and fabric, due mainly to the difficulty and the complexity of the factors involved in visual classification of fabric.

Qualitative characterization of soil fabric has been investigated extensively in the field of soil science, and thus geotechnical engineers tend to utilize the terms and definitions which have been applied by soil scientists (eg. Brewer and Sleeman, 1988). However, when describing fabric, geotechnical engineers generally prefer quantitative methods as these methods are unbiased and have some relevance to mechanical behaviour of soils.

Fabric of natural soils can be described as either single-grain or multi-grain fabrics. Single-grain fabrics are generally found in cohesionless soils while fine-grained soils are commonly found as multi-particle aggregates. Characterization of single grain fabrics can be done in terms of grain shape factor, grain orientation and inter-particle contact orientations (Ingles and Lafeber, 1966; Oda, 1972; Mahmood and Mitchell, 1974; Mitchell et al., 1976). The grain shape factor is the length to width ratio (*L/W*) of particles and can be presented in a histogram. Orientation of soil particles can be expressed in terms of the inclination of the particle axes to a set of reference axes (Mitchell, 1993). Thin sections are generally used to simplify the result to a single angle (the angle between the particle long axis to a reference axis). In

this case, the spatial orientations of the thin section are relative to the sample or deposit should also be considered as part of the description. Particle orientations are generally expressed by histogram or rose diagram. Examples of the rose diagrams are given in *Figure 2-12* (Cetin, 2004). The diagram illustrates change in pore orientation of a clay-mica sand mix during consolidation.
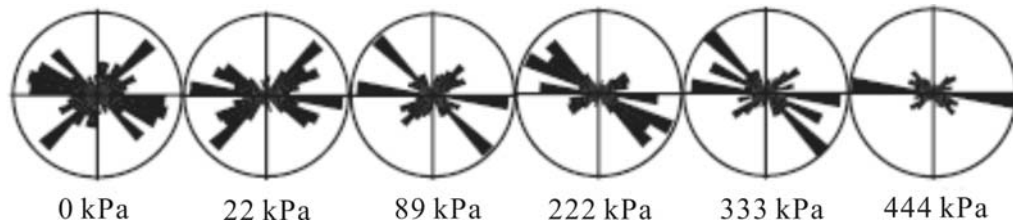
Figure 2-12. Rose diagram of pore orientation during various stages of consolidation for a clay-mica sand mix (After Cetin, 2004)

Single grain fabrics are rare in soils containing silt- and clay-sized particles because the particles are sufficiently small to be influenced by surface forces. In these cases, fabric is generally of a multi-grain nature. Mitchell (1993) also mentioned that silt-sized particles form multi-grain arrangements during slow sedimentation. This is reminiscent of the processes which take place in a tailings impoundment.

As pores are essential fabric elements, the characterization of pore size, shape and distribution is also an important part the soil fabric. Pore size, shape and distribution influence the conductive property, deformation behaviour and anisotropy of a soil (Mitchell, 1993). Pore shape and distribution can be characterized using image-processing techniques such as SEM. Volumetric pore size distribution can also be estimated using mercury intrusion.

The multi-grain nature of tailings makes characterizing fabric difficult. Characterization may require a combination of methods reviewed in this section. Statistical methods may also be an important tool.

To the best of the author's knowledge, the only research which included observation of soil behaviour as well as a direct measurement of fabric for the same material was presented by Wood (1999), who demonstrated that the difference in observed behaviour for samples prepared using different reconstitution methods was a result of grain contact as proposed by Yamamuro and Lade (1997). The theory proposes that three types of grain contacts exist in a sand-silt mixture. This is illustrated in *Figure 2-13*.
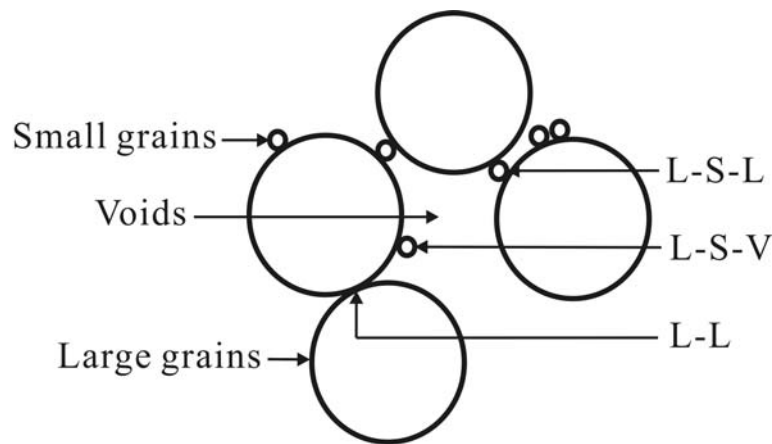
Figure 2-13. Grain contact structure as proposed by Yamamuro and Lade (1997)

Yamamuro and Lade (1997) postulated that stable contacts exist between large grains (L-L) while unstable contacts exist when large grains are bridged by small grains (L-S-L). Passive contacts occur when small grains rest on large grains without being part of the force chain. It is theorized that stable (strain hardening) behaviour is due in part to the presence of stable contacts (L-L) while significant presence of unstable contacts (L-S-L) results in unstable (strain-softening) behaviour.

Wood (1999) showed that for the same silt content of 10 percent, water sedimented samples, which showed strain hardening behaviour, contained significantly more stable contacts and less unstable contacts than the dry funnel deposited samples, which showed strain softening behaviour. A stability ratio, *S*, was also introduced which is expressed as the ratio of

percentage of stable to unstable contacts. If S is less than unity, an unstable response is expected either in the form of temporary or complete liquefaction, as illustrated in *Figure 2-14*.
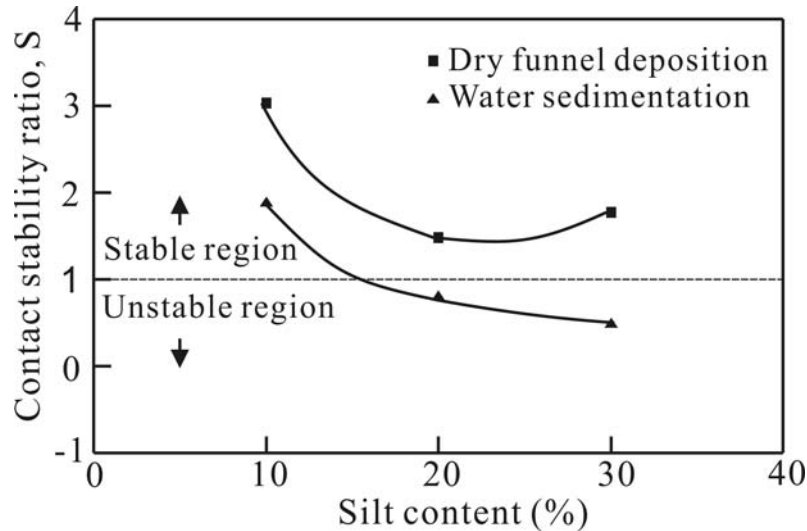
Figure 2-14. Contact stability ratio, S, versus silt content for reconstituted sand-silt mix (After Wood, 1999).

2.6.5 Concluding remarks regarding soil fabric

Although fabric and fabric effects is recognized as an important soil characteristic, methods of fabric classification is still insufficient, mainly due to the complexity of soils in general. As pointed out by Mitchell and Soga (2005), the variety of particle size, shape and distribution implies that the potential number of soil fabric is almost limitless. The method of fabric analysis will thus need to be adapted according to the observed fabric.

2.7 SAMPLE PREPARATION

The behaviour of a soil can be observed by soil testing, which can be divided into two main categories, namely in situ tests and laboratory tests. In situ tests have the advantages of testing in situ conditions such as structural features, pore water conditions and environmental effects, while laboratory testing can

be done under controlled conditions. Furthermore, laboratory specimens can be either undisturbed or reconstituted. Undisturbed specimens are brought into the laboratory in its in situ intact state, while reconstituted or remoulded specimens are prepared by remoulding natural material to break down particle associations, destroy shear planes or any structural features, eliminate large pores and create a more homogeneous specimen (Fearon and Coop, 2000). High quality undisturbed specimens are extremely difficult to obtain, as the natural structure of the soil can be altered during the processes of drilling, sampling, transportation, storage or specimen preparation for testing, due to changes in stress conditions, mechanical deformations, changes in water content or void ratio, or chemical changes (Clayton et al., 1995). In some cases, as is the case for tailings or some cohesionless sands, obtaining undisturbed specimens are difficult and sometimes impossible. Reconstituted specimens, on the other hand, can be easily obtained and re-constructed, but to obtain meaningful results, the specimen must replicate the in situ conditions as closely as possible. Burland (1990) suggested that a reconstituted sample should be made from a natural sample, mixed with water to form slurry, without drying the soil prior to mixing. The slurry should have moisture content between the liquid limit (*LL*) and 1.5*LL*. It is then consolidated, preferably under one-dimensional consolidation. Ideally, the water used should have similar chemistry to the pore fluid.

Laboratory specimen reconstitution methods have some influence on the fabric and shear behaviour of the soil. Many researchers have shown that the behaviour of sands can be profoundly influenced by the sample reconstitution technique (Oda, 1972; Mulilis et al., 1977; Ladd, 1974, 1977; Vaid et al., 1999; Wood and Yamamuro, 1999). The energy used in reconstitution may also have an influence on the soil. Rippa and Picarelli (1977) showed that the Atterberg limits of a structurally complex soil were highly dependent on the preparation method. They believed that this was due to the breaking down of silt sized clay aggregates with increased remoulding energy. Fearon and Coop (2000) showed that the energy used in reconstitution of a specimen can alter the structure of scaly clay. They suggested that hand-mixing generally used for constructing laboratory test specimens produces a fabric similar to that of

natural clay while more vigorous methods of mixing may destroy the natural fabric of the clay.

2.7.1 Specimen reconstitution methods

Reconstituted specimens can be constructed using different preparation techniques depending on, among other factors, the soil type, moisture content, void ratio required and in situ fabric. Tamping and pluviation techniques are most commonly used in current practice (Vaid et al., 1999), while other techniques such as slurry deposition, mixed dry deposition, dry funnel deposition and wet sedimentation are used to better simulate field depositional conditions. For triaxial testing, specimens generally have a length to diameter ratio of 2, with diameters of 38, 50, 75 or 100 millimetres.

Reconstituted test specimens should be of high uniformity to reduce complexities in characterizing the soil. This is however not possible. As shown by Frost et al. (1998), even highly controlled air pluviated specimens show some degree of non-homogeneity of void ratio distribution. These authors suggest that global void ratio values may lead to errors in the results of liquefaction tests.

2.7.2 Tamping methods

Tamping techniques are also known as rodding techniques. The method involves compacting soil of known mass into a mould of known volume. The soil can be compacted dry, known as dry tamping, or the specimen can be constructed with certain moisture content, known as moist tamping. Compaction is generally done in layers for better uniformity. The method has a few advantages over other reconstitution methods. Firstly, the method is simple and can be completed in a relatively short time. Furthermore, there is greater control over the initial density of the specimen, because a required mass of soil is compacted into a volume, yielding the required void ratio or density. Finally, the range of void ratios that can be achieved is wider compared with other reconstitution methods due to capillary effects between

grains. There are contradicting views in the literature about the uniformity of tamped specimens. Researchers such as Mulilis et al., (1977), Vaid and Negussey (1988) and Vaid and Sivathayalan (2000) suggest that moist tamped sand specimens tend to be less uniform, while others like Sladen et al., (1985) and Chen and van Zyl (1988) found moist tamping to yield highly homogeneous samples.

2.7.3 Dry funnel deposition and water sedimentation

Dry funnel deposition involves deposition of dry material via a funnel into the bottom of a split mould. The material is then placed in the funnel, which is raised along its axis of symmetry. Sedimentation specimens are formed by placing the soil in a low energy state without any drop height. The method, shown in *Figure 2-15a*, is commonly used for testing silty sands (Ishihara, 1993; Lade and Yamamuro, 1997; Yamamuro and Lade, 1997; Zlatovic and Ishihara, 1997). In order to achieve higher densities, the split mould can be tapped periodically. This is known as tapped funnel deposition. Dense specimens can also be produced by raising the funnel rapidly (although still without any fall height) prior to tapping. This method of specimen preparation is known as the fast funnel deposition.

Water sedimentation, which is also known as water pluviation, is essentially similar to funnel deposition, but differs in that the soil, either dry soil (Tatsuoka et al., 1986; Ishihara, 1993; Zlatovic and Ishihara, 1998) or saturated soil (Wood, 1999), is deposited via a volumetric flask into water. The volumetric flask is filled with soil and water. As the soil flows out of the flask, equal volumes of water flow into the flask due to the suction within the flask as soil is displaced. The method is shown schematically in *Figure 2-15b*. The nature of the water into which the solid particles are deposited may also have an effect on the response of the soil. Vaughan (1997) reported on tests in which a fine silty sand was pluviated into water containing various amounts of colloid clay particles. He concluded that the colloid clay particles can significantly influence the relative density of the water pluviated specimens.

The deposition of tailings into a stationary pond may be similar to water sedimentation and thus results in a saturated, low density deposit.
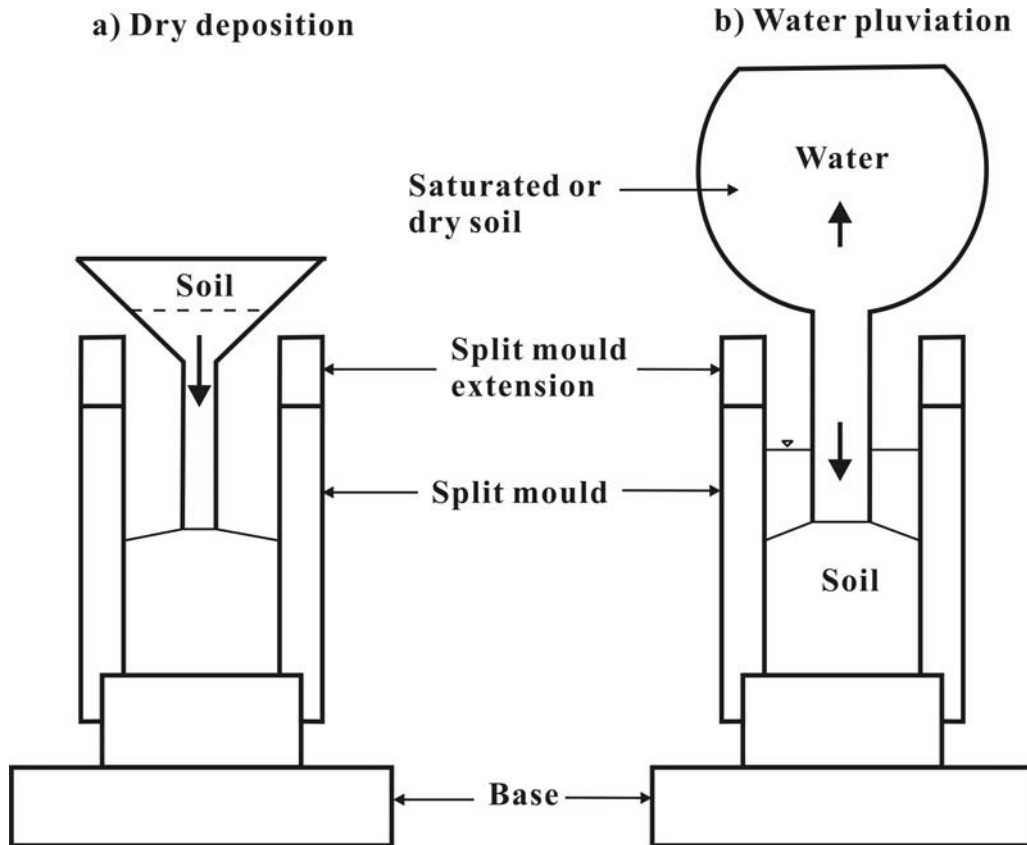
Figure 2-15. Schematic representation of dry deposition and water pluviation (After Wood, 1999).

Wood (1999) showed that dry funnel deposition and wet sedimentation produced silty sands specimens that exhibited a core and a shell structure. Silts reside more towards the periphery of the sample, and this is more apparent for the water-sedimented specimen. Furthermore, the silt content of the water-sedimented specimen increased from the bottom to the top of the specimen height. This is due to segregation of the different sized particles. Vaid et al. (1999) showed that in situ ground frozen specimens of sand behave very similarly to water pluviated specimens under triaxial and simple shear tests. They concluded that water pluviation can thus be used as an inexpensive and simple way of characterizing in situ fluvial and hydraulic fill sands. The in situ

void ratio of various sands were obtained from ground freezing techniques and compared with the loosest possible void ratio of water pluviated specimens (Vaid and Pillai, 1992; Vaid and Sivathayalan, 2000). They found that in situ sands deposited in water are unlikely to exist in states looser than the loosest achievable water pluviation specimens.

2.7.4 Slurry deposition and mixed dry deposition

The slurry deposition method was used by Kuerbis and Vaid (1988) and Kuerbis (1989), and was modified by Wood (1999). The method entails the use of slurry in a mixing tube, rotated for a certain amount of time. The mixing tube is then extracted slowly, leaving the slurry in the split mould. The mixed dry deposition is similar to slurry deposition, except that the soil is placed in a dry state. A schematic presentation is shown in *Figure 2-16*.
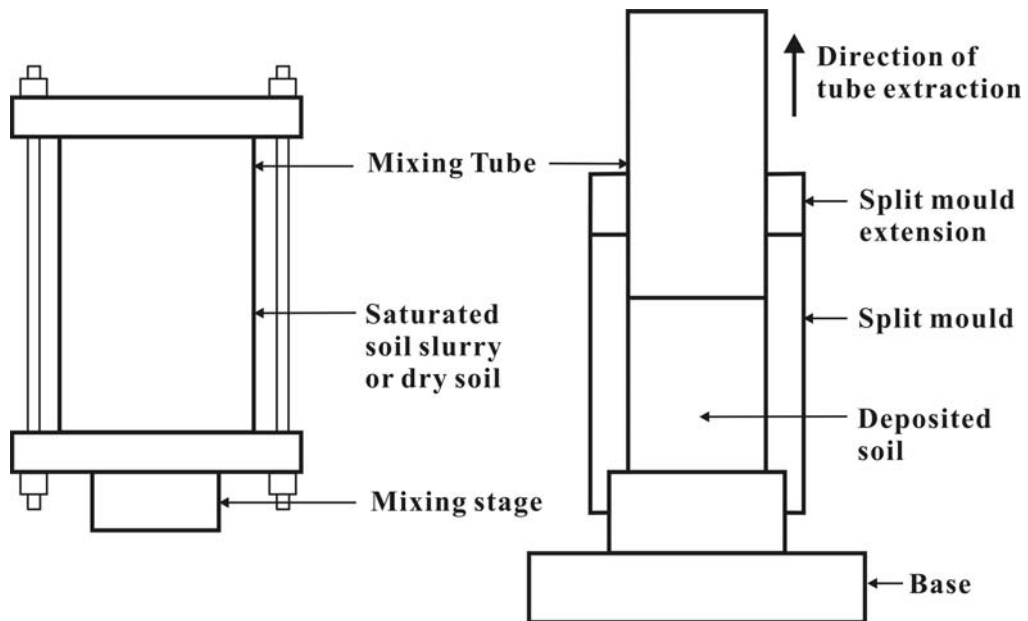
Figure 2-16. Mixed dry deposition and slurry deposition (After Wood, 1999).

Using silty sand, Wood (1999) showed that both slurry deposition and mixed dry deposition produce homogeneous specimens. Theron (2004) prepared a slurry sample using a mixture of fine platy particles and rotund sand. A three-

part split mould was installed on the triaxial pedestal and the sample was built on the pedestal. To prevent segregation, a layered approach was used. Slurry was deposited in thin layers and each layer was stirred before the new layer was deposited. This method allows slurry samples to be built for soils such as gold tailings, where segregation is possible.

2.7.5 Air pluviation method

Pluviation essentially involves raining dry soil from a fixed height through a long tube into the split mould. A variation in fall height and pouring rate is often used to create specimens of different densities (Miura and Toki, 1982; Vaid and Negussey, 1984, 1988; Rad and Tumay, 1987). A higher fall height creates denser specimens while a higher pouring rate decreases the density. In order to construct uniform specimens, Vaid and Negussey (1984) suggested that the fall height should remain constant with the top surface of the sample as it is formed.

Air-pluviated sand specimens were shown to contain alternating thin layers of loose and dense sand (Mulilis, 1977). Wood (1999) found that air-pluviated silty sand specimens show distinct thin horizontal silt layers, although the silt content was homogeneous throughout the specimen.

2.8 SAMPLING AND SAMPLING DISTURBANCE

In order to obtain reasonable engineering parameters for geotechnical design, carefully executed testing is required. Testing may either be in situ or laboratory tests, and in both cases, sample disturbance must be minimized. The mechanisms of disturbance can be classified as follows (Clayton et al., 1995):

- Changes in stress conditions
- Mechanical deformation

- Changes in water content and void ratio
- Chemical changes

These mechanisms can occur at various stages during the process of the investigation and at different rates. Although some disturbance is unavoidable, it can nevertheless be minimized by understanding the mechanisms involved and by careful design and execution of the testing procedures. There are three types of laboratory sampling techniques, namely (Clayton et al., 1995):

- Disturbed sampling: There is no attempt to retain the structural features of the soil and is adequate for classification tests.
- Tube sampling: The soil sample is obtained by pushing a tube into the soil. The soil is sheared, but integrity and structural features remain intact to some degree. Sampling disturbance from tube sampling can be minimized by careful design of the sampler. Samples obtained from tube sampling are considered 'undisturbed'.
- Block sampling: Samples are cut from the base or the side of a trail pit, or as part of a rotary drilling process. Block samples undergo stress relief and swell, but should not be subjected to shear distortion as with tube sampling.

In general, block sampling produces the highest quality undisturbed samples when compared with other sampling techniques (Heymann and Clayton, 1999).

2.9   SUMMARY

The state, composition and engineering behaviour of gold tailings have been presented. Tailings could be described as a low plasticity rock flour with coarse angular and fine platy particles (Vermeulen, 2001). The behaviour of gold tailings is recognized as somewhere between that of clay and sand, with fines dominating the mass (Pettibone and Kealy, 2971; Mittle and Morgenstern, 1975; Vick, 1990; Theron, 2004).

The method of reconstitution of tailings and soils in general has been shown to influence the mechanical behaviour. Investigations have generally concentrated on the liquefaction behaviour of granular materials. Questions such as consolidation, creep and small strain stiffness have seldom been mentioned. Furthermore, very little evidence has been presented to demonstrate that these observed differences in behaviour are in fact as a result of the different fabric.

With these questions in mind, an experimental methodology will be set up to evaluate the hypothesis: **Accurate simulation of the behaviour of gold tailings under laboratory conditions requires appropriate replication of the material fabric.**

Chapter 3

Experimental Methodology

3.1   BACKGROUND

The objective of this chapter is to present in detail the experimental work conducted during this project. This includes the reasoning behind the choice of tests and parameters used, descriptions of the experimental methods as well as of the equipment and instrumentation used in the testing.

3.2   EXPERIMENTAL STRATEGY

As mentioned in the opening chapter, material was sampled from a single tailings dam which had the same source. To ensure that the entire spectrum of gold tailings was investigated, material was sampled from three different positions on the tailings dam to represent typical gold tailings gradings. A few dams were considered, and finally it was decided that ERPM 4 would be the source of all gold tailings used in this research. The reasons for choosing ERPM 4 were that, firstly, the dam has been decommissioned for about 10 years, making sampling of pond material possible. Secondly, ERPM 4 had been constructed using the daywall-nightpan paddock system, typical of South African tailings dams.

The choice of a decommissioned dam, however, implied that oxidation may have occurred on the pyrite particles as a result of exposure to air (oxygen) and water (Blight and du Preez, 1997). Pyritic oxidation results in a reduction in pH (to acidic) near the surface of the dam and leaching of soluble salts of

approximately 0.1% by dry mass of tailings (Blight, 1976). Although fluid chemistry may have some influence on behaviour of gold tailings and on the fine platy particles in particular, it was assumed, as stated in section 1.3, that fluid chemistry only had an influence on the initial fabric, and not on the mechanical behaviour of the tailings.

The coarsest material (named upper beach) was sampled from the beach near the daywall while the finest material (named pond) was sampled near the penstock. Material with an intermediate grading (named middle beach) was also tested. The objective was to get some variation in the grading and particle shape characteristics of the material and to observe how this variation relates to fabric.

The main aim of the research was to compare mechanical behaviour of undisturbed and laboratory prepared (by moist tamping and slurry) gold tailings samples at the same state. Material from each position was tested at two effective confining stresses, 200 and 400kPa, to investigate the effect of confining stress. Desiccation suctions for general beach tailings were estimated to be in the range of 150kPa (Westraad, 2004). It can thus be assumed that undisturbed samples will be normally consolidated above 200kPa as to eliminate the effect of over-consolidation. The testing included triaxial consolidation and shear, and as samples needed to be tested at the same state, consolidation and shear samples were tested separately. Details of the testing will be discussed in the following section. Coding for the test samples are summarized in *Table 3-1* and *Table 3-2*.

Consolidation samples

	Undisturbed	Moist tamped	Slurry
Upper beach	UB-U-con	UB-MT-con	UB-S-con
Middle beach	MB-U-con	MB-MT-con	MB-S-con
Pond	P-U-con	P-MT-con	P-S-con

Table 3-1. Sample coding for consolidation samples.

Shear samples

	Undisturbed	Moist tamped	Slurry
Upper beach			
200kPa	UB-U-200	UB-MT-200	UB-S-200
400kPa	UB-U-400	UB-MT-400	UB-S-400
Middle beach			
200kPa	MB-U-200	MB-MT-200	MB-S-200
400kPa	MB-U-400	MB-MT-400	MB-S-400
Pond			
200kPa	P-U-200	P-MT-200	P-S-200
400kPa	P-U-400	P-MT-400	P-S-400

Table 3-2. Sample coding for shear samples.

Abbreviations used in sample coding are summarized below:

- UB - Upper beach sample
- MB - Middle beach sample
- P - Pond sample
- U - Undisturbed sample
- MT - Laboratory prepared by moist tamping
- S - Laboratory prepared by the slurry method
- 200, 400 - Isotropic consolidation stress (in kPa) before shear
- con - Consolidation to 1000kPa effective stress

Test sample names are given as *material type-fabric type-confining stress*. P-U-200 would indicate an undisturbed pond sample sheared at an initial effective confining stress of 200kPa.

Undisturbed triaxial samples were cut from undisturbed blocks, which also provided information about the in situ void ratio and moisture content of the tailings. The moisture content used for preparing moist tamped samples was

determined from limiting density tests while that for slurry samples was established for all three material types by trial and error.

To compare the effect of fabric on the samples, it was important that samples were tested at the same initial state. Consolidation samples were at the same state prior to consolidation while shear samples were at the same state before and after consolidation and therefore throughout the shear processes, as the tests were undrained. The accuracy of the void ratio was within 2% of the target void ratio for all tests. The target void ratio was taken as the void ratio of the undisturbed sample, i.e. consolidation samples were at the same void ratios as the undisturbed sample after saturation. Shear samples were prepared to the same void ratios as the undisturbed sample after consolidation and creep.

For each test sample, a corresponding fabric sample was produced for fabric analysis. The fabric sample underwent the same triaxial processes as the test sample, without the final testing stage, to avoid modifications of the fabric. Consolidation fabric samples were removed after saturation while shear fabric samples were removed after creep at the corresponding effective stresses. This allowed the fabric to be compared immediately before the test phase (consolidation or shear). The void ratio of fabric samples was within 5% of its test sample counterparts. Fabric samples were given an extension '- f' added to the name of the corresponding test sample. MB-S-con-f therefore indicates a middle beach consolidation sample removed after saturation for fabric analysis. The triaxial testing scheme is summarized in *Table 3-3*.

Preliminary testing included indicator tests such as grading, specific gravity and Atterberg limits which gave some indication of the index properties of the gold tailings. Maximum and minimum density tests were also be performed on all three material types, at varying moisture content to aid in selecting appropriate moisture content for moist tamped samples. Sedimentation tests were performed with dispersant and flocculent to investigate the possible void ratios that could be obtained for slurry samples.

	Test samples		Fabric samples	
	Cons.	Shear	Cons.	Shear
Sample preparation	√	√	√	√
Flushing	√	√	√	√
Saturation against back pressure	√	√	√	√
Consolidation	√	√		√
Creep		√		√
Shear		√		

Table 3-3. Triaxial testing scheme for the experimental work.

Observation of the fabric was based on SEM images. SEMs were chosen over other indirect methods because, as a first step, the fabric difference must be observable to be comparable. A limitation with the use of SEM was that samples had to be dry before they could be examined in the SEM. This implied that samples had to undergo desiccation, which would induce some change in void ratio. As the samples were at the same void ratio, it is assumed that any changes in void ratio during desiccation would be similar, and would not significantly change the existing fabric.

3.3   SAMPLING

Pond samples were taken directly next to the penstock while the upper and middle beach samples were taken at approximately 20m and 45m away from the penstock respectively. The distance between the penstock and the daywall was approximately 50m. The three sampling positions are shown in the satellite image in *Figure 3-1*.

At each position, a hole of approximately one metre deep was dug in attempting to obtain a layer in excess of 100mm. The three sampled layers are shown in *Figure 3-2*. It should be noted from *Figure 3-2* that the gold yellow colour of the middle and upper beach material indicate pyritic oxidation.
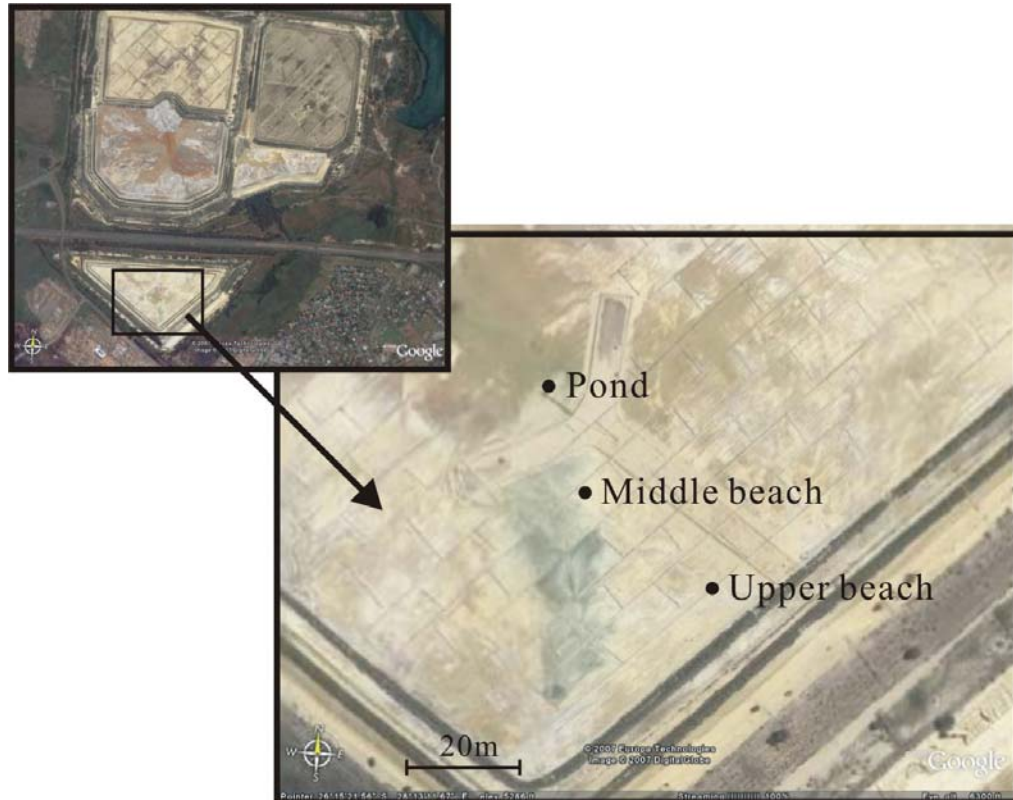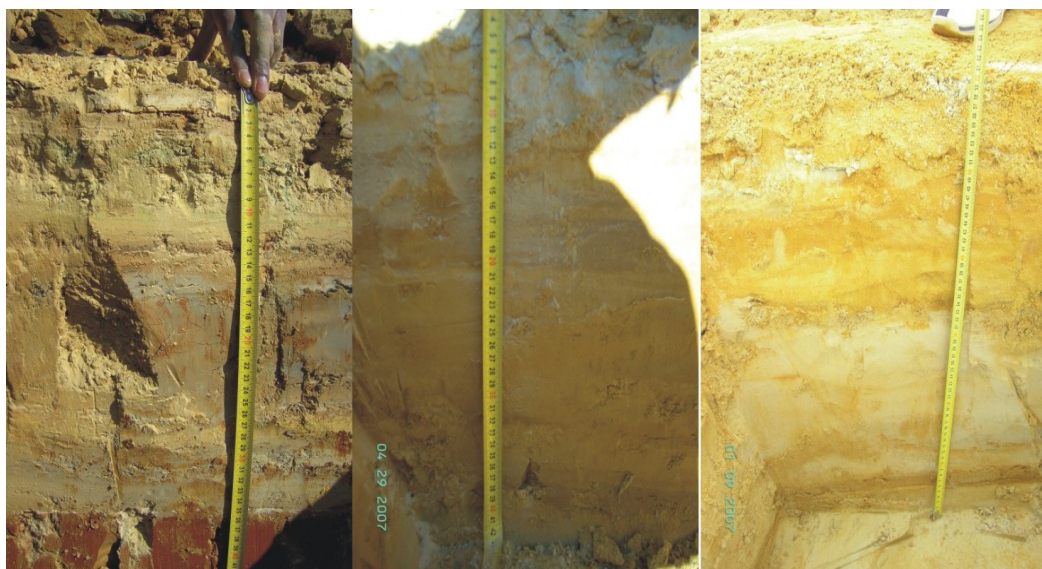
Figure 3-1. Satellite view of sampling positions.

Pond   Middle beach   Upper beach

Figure 3-2. In situ depth profile of block samples.

Sample layer depth and layer thickness for the three materials are shown in *Table 3-4*. The table also includes visual descriptions of the three materials.

	Layer depth	Layer thickness	Visual description
Pond	150mm	150mm	Grey fine clayey silt
Middle beach	200mm	200mm	Light brown sandy silt
Upper beach	100mm	170mm	Yellow sandy silt

Table 3-4. Position and visual description of undisturbed block samples.

After a suitable layer had been targeted, the targeted block was exposed by removing the material above and around it, as shown in *Figure 3-3*. The block was then cut from the bottom and removed from its original position. The method is described by Clayton et al. (1995).

Figure 3-3. Exposing a suitable block by excavating around the block.

All samples were wrapped in plastic wrap and aluminium foil and finally another layer of plastic wrap to prevent moisture loss. This is demonstrated in *Figure 3-4*. The use of a plastic wrap/aluminium foil combination was shown

by Heymann and Clayton (1999) to be effective in minimizing moisture loss in undisturbed samples. The samples were then marked (top), hand-carried down the tailings dam and placed on foam mattresses for transportation back to the lab.

Figure 3-4. Wrapping the block sample to prevent moisture loss.

Average weather conditions for 30 days prior to sampling were obtained from 'Weather Underground' and are presented in *Table 3-5*.

	Date sampled	Average temperature (°C)	Total precipitation (mm)	Wind speed (km/h)	Humidity (%)
Upper beach	9/1/07	20.8	148.6	4.2	61.7
Middle beach	30/4/07	17.0	45.0	3.3	58.6
Pond	1/9/06	11.4	28.4	0.3	53.3

Table 3-5. Average weather conditions for 30 days before sampling

Average weather conditions were included for reference purposes as the in situ moisture content may be affected by these factors.

3.4 PRELIMINARY TESTING

Preliminary tests were conducted to classify the material and to give some indication as to the behaviour that can be expected. The contents of preliminary testing mentioned in section 3.2 can be summarized as follows:

- Grading
- Specific gravity
- Atterberg limit
- Maximum and minimum density tests
- Sedimentation test using dispersant and flocculent
- Image analysis

Preliminary testing was done using the remaining disturbed material from the undisturbed blocks. All disturbed material (excluding that used for the Atterberg limit tests) was oven-dried at 50°C for 48 hours and passed through a 1mm sieve. The objective was to break down all existing fabric to present a truly 'disturbed' material. The methodology of the preliminary tests are discussed in the following sections.

3.4.1 Grading

Particle size distribution of the pond, MB and UB material was determined using procedures for wet sieving of fine non-cohesive material (BS1377: Part2:1990:9.3) followed by the hydrometer sedimentation test (BS 1377: Part 2:1990:9.5).

Wet sieving was done using 100g of dry material (as specified by BS for material smaller than 2mm) with sieves of 0.3, 0.15 and 0.075mm. Grading was done on both dispersed and undispersed material. The dispersed material was pre-treated with 100g of standard dispersant (35g sodium hexametaphosphate, 7g sodium carbonate and distilled water to make a one litre solution) because tailings are known to flocculate (Vermeulen, 2001,

Chang, 2004). Material passing the 75μm sieve was transferred directly to a measuring cylinder for hydrometer sedimentation test. Sieves were weighed before and weighed again with retained material after oven-drying. Sieving for each material was repeated twice.

Hydrometer analysis was done in four 1000ml cylinders (two for each material type and two for reference with distilled water and distilled water with dispersant). Cylinders were placed in a glass tank filled with water with a constant temperature of between 21 and 24°C. Corrections were made for the viscosity of water accordingly.

Test for calcareous matter was not performed, as carbonate bonding does not occur in tailings (Vermeulen, 2001). Organic pre-treatment on tailings was not used as hydrogen peroxide may also oxidize sulphide minerals such as pyrites (Vermeulen, 2001).

Vermeulen (2001) also suggested that sieve and hydrometer grading results were slightly finer when compared with the actual particle size as observed under the SEM. This is due to the fact that tailings contain flat and elongated particles which may pass through the square aperture of the tests sieves. Flat and elongated particles also do not adhere to Stoke's Law, which assumes spheres.

3.4.2   Specific gravity

The particle density or specific gravity of the tailings was determined for all three materials, although it is recognized that all tailings particles from the same source should have the same density (Vermeulen, 2001). Particle density was determined using the density bottle method specified by BS 1377: Part 2:1990:8.3. The density bottle test is suitable for soils consisting of particles finer than 2mm, as tailings particles generally are. The density bottles were washed, dried, cooled to room temperature and weighed to within 0.01g. Distilled, de-aired water was used for all density tests. As only one constant temperature bath was available, density bottles were placed in the same tank in

which the hydrometer analysis was done, and temperature correction for water density was made accordingly. The mass of density bottle only, density bottle and dry soil, density bottle and water, and density bottle with soil and water was determined and the particle density calculated.

3.4.3 Atterberg limit

Atterberg limits were determined for all three materials to allow classification of the tailings. For this, material was used at its natural moisture content (as specified by BS 1377:1990), as the plasticity properties of some soils may change due to drying. The liquid limit was determined using the cone penetrometer method (BS 1377: 1990:4.3). This method was chosen over the Casagrande method (BS 1377:1990:4.5) as it is less liable to experimental and operator errors (Sherwood and Ryley, 1968). The plastic limit was established using BS 1377: Part 2:1990:5.3. As tailings are not considered a cohesive material, determination of the plastic limit may not be possible, especially for the coarse material.

3.4.4 Maximum and minimum density test

Maximum and minimum density tests were performed to give an indication of the range of void ratios that can be expected for the tailings. Limiting densities can also be used as a guideline to minimize collapse and preserve the fabric for moist tamped samples during flushing. Maximum density was determined according to ASTM D4253-00 method 2A (maximum index density and unit weight of soils using a vibratory table), while minimum density was determined according to ASTM D4254-00. Both tests were modified to accommodate the testing of gold tailings. Both ASTM D4253-00 and D4254-00 require the material to be oven-dried and containing up to 15% particles by dry mass passing the 0.075mm sieve. Gold tailings contain mostly silt-size particles finer than 0.075mm, and the test was done at varying moisture content. The use of moist soil is contradictory to that specified in the standard test procedures and thus the results can only be used as a guide and not be compared with other standard limiting density results.

Material was compacted in a circular mould with an average internal diameter of 152.65mm and an average depth of 152mm. Surcharge load, including the base plate, was 25.63kg, which yielded a pressure of approximately 14kPa. The duration of the vibration was 8 minutes at 3600vpm at a peak-to-peak displacement of 0.33mm. Distilled water was used for all density tests. Moisture content ranges for different material types and the tests were terminated when the material liquefied and overflowed.

The minimum void ratio line (at various moisture content), together with visual uniformity assessment and practicality issues, were used as the basis on which the preparation moisture content for the moist tamped samples were determined. It is assumed that when the target void ratio lies on or below the minimum void ratio line, collapse during flushing can be minimized and the initial fabric can be preserved as best as possible. The choice of preparation moisture content is explained in detail in section 3.6.2.

3.4.5   Sedimentation test using dispersant and flocculent

Preparation of slurry samples may be a problem in that it is not always possible to prepare slurry or water sedimentation samples to the same void ratio as the undisturbed or moist tamped samples. There is less control over the void ratio for slurry samples compared with moist tamped samples and slurry or water sedimentation methods often yield denser samples. This was a difficulty for this project, as the void ratio at which the tests were started was important. Dispersant and flocculent were used to overcome this problem.

Sedimentation tests were done using dispersant and flocculent to observe the possible void ratios obtainable. Sedimentation tests were done for all three material types, with standard dispersant and flocculent concentrations of 0, 25, 50, 75 and 100% of the total fluid (mixed with tap water). Standard dispersant is defined as 35g sodium hexametaphosphate, 7g sodium carbonate and distilled water to make a one litre solution while standard flocculent is defined as 0.25g Magnafloc Mg 919 (supplied by Allied Colloids as a standard mining flocculent) diluted in one liter tap water. All samples were sedimented in

250ml cylinders with 100g dry material and 100g total fluid. Cylinders were shaken thoroughly and then shaken again for one minute immediately before the start of the test. Height readings were taken at 1, 2, 5, 10, 30, 60, 120, 240, 480, 1500 and 5000 minutes after commencement of sedimentation.

3.4.6 Image analysis

The objectives of the preliminary image analysis were, firstly, to observe if there were in fact any differences in the fabric of undisturbed and reconstituted tailings and, secondly, to evaluate the feasibility of different imaging techniques. Gold tailings used for the preliminary analysis originated in the Free State Goldfields, and was similar to that used by Chang (2004). Moist tamped and slurry samples were prepared at arbitrary void ratios for the preliminary test. Image analysis using raw intact samples and polished section samples showed that there was some observable difference in the fabric. Intact samples were viewed directly in the SEM and gave a three-dimensional image of the fabric while polished sections were prepared by immersing the intact samples with epoxy and polishing a section from the resultant epoxy block. The result was a binary image of either particle or epoxy (void). Two-dimensional (from polished sections) and three-dimensional (from raw intact samples) images are attached in *Appendix A* and summarized in *Table 3-6* below.

Image	Description
A-1	Moist tamped sample (raw intact)
A-2	Moist tamped sample (polished section)
A-3	Slurry sample (raw intact)
A-4	Slurry sample (polished section)
A-5	Undisturbed samples (raw intact)
A-6	Moist tamped samples (raw intact moist taken in ESEM)

Table 3-6. Summary of preliminary electron microscopy images.

From the preliminary images, it was decided that fabric analysis for this project would be based on SEM images of raw intact samples (similar to images *A-1* and *A-3* and *A-5*). The motivation was that, as a first step, the particle orientation should be observed physically and not be based on binary images or physical properties which cannot be directly observed. This would imply that classification of the fabric would be qualitative, as quantitative analysis of a three-dimensional was complex.

The reason for using image analysis was also to determine whether desiccation will alter the fabric of the samples. This was done by comparing images of raw intact samples using the conventional SEM and images from the ESEM (environmental SEM), which allows the use of moist samples. For this, moist tamped samples were prepared at various void ratios and imaged. The ESEM images show that moist tamped samples had similar fabric to that of naturally desiccated samples. This suggested that the initial fabric could be maintained after desiccation, and the use of SEM could be justified.

3.5   TRIAXIAL SETUP

The undrained shear behaviour of various samples was tested in a Wykeham Farrance 75mm triaxial cell. The base pedestal was modified to accommodate 50mm samples and local strain instrumentation. The cell was also modified to accommodate an internal submersible load cell. The experimental system is illustrated in *Figure 3-5*.

Pressure to the triaxial system was supplied by a compressor and converted to water pressure via an air-water interface. The cell pressure, however, was supplied by a digital pressure controller to allow a higher pressure to be applied to the cell fluid. Two lines led to the bottom of the sample while one line led to the top of the sample. Cell water was supplied through the cell valve. Pore pressure was measured at the bottom valve and volume changes measured through the top valve. The top valve was also modified to allow the

digital pressure controller to apply suction to slurry samples, and later during the test, to apply pressure to the cell fluid.
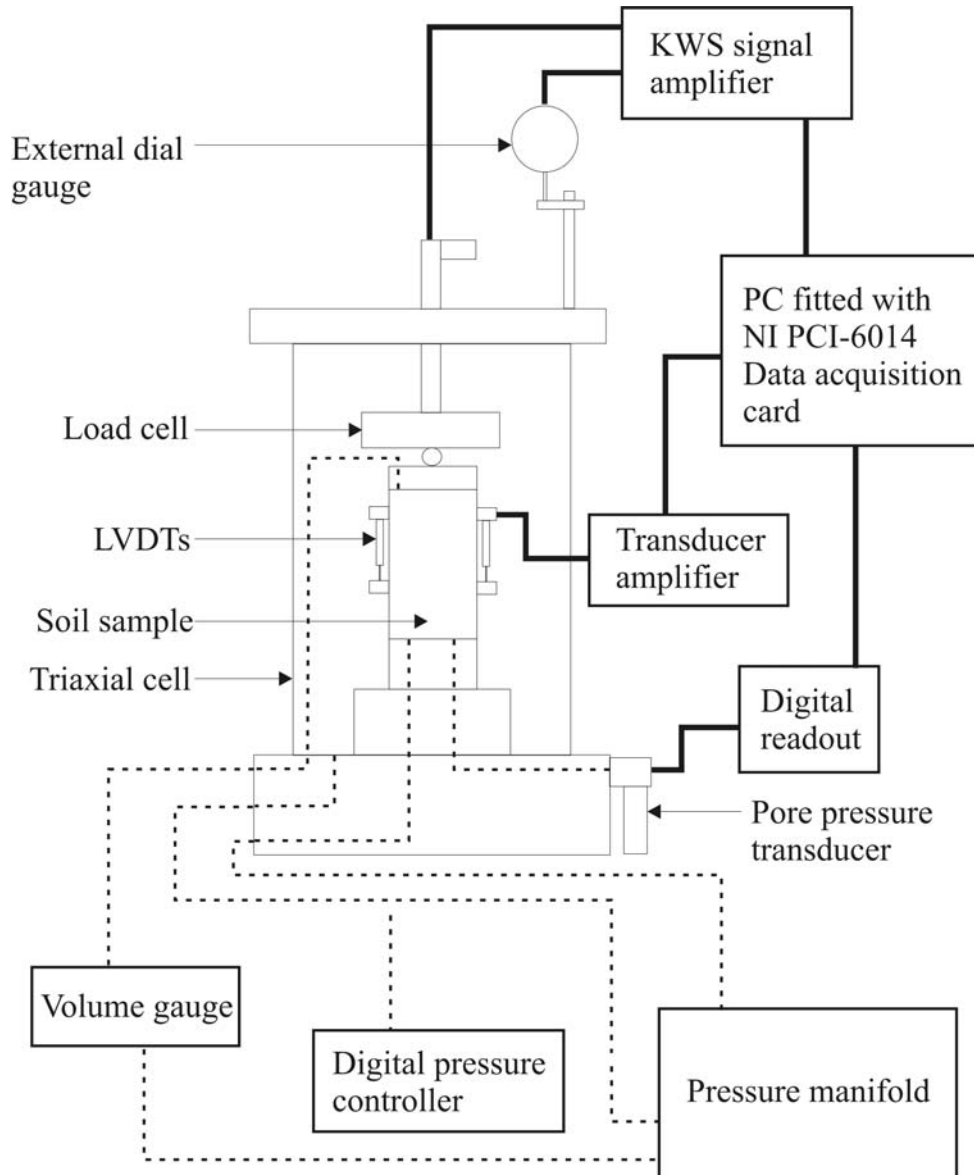

Figure 3-5. The triaxial system and instrumentation.

3.5.1 Instrumentation

Electronic instrumentation for the triaxial system included two LVDTs to measure local small strain deformation, a linear displacement transducer for large strain deformation, an Imperial College type internal submersible load

cell and an external pore pressure transducer. Output from these instrumentations were logged and stored on a computer via a NI PCI-6014 data acquisition card. The specifications of all electronic instrumentation as well as the data acquisition card are attached in *Appendix B*. Non-electronic instrumentations included a Budenberg Standard test pressure gauge and a Wykeham Farrance volume gauge. The instrumentation is discussed in detail in the following sections.

Linear variable differential transformer (LVDT)

The LVDTs used to measure local small strain deformation were obtained from RDP Electronics model D5/200 with a S7AC transducer amplifier. LVDTs were mounted onto the soil samples via brackets designed to fit 50mm samples. Calibration procedures for the LVDTs and other electronic instrumentation is discussed in the calibration section.

Linear displacement transducer

Large strain deformations were measured by a Kyowa linear displacement transducer (LDT) DT-20 D. Output signal was channeled through an HBM KWS 3073 signal amplifier, at a sensitivity of 1mV/V, and then logged by the computer.

Internal load cell

Deviatoric stress was measured via an Imperial College type internal submersible load cell (load capacity of 450kg) to eliminate ram friction from the measurements. The output signal was amplified via the same HBM KWS 3073 amplifier used for the external displacement transducer. The sensitivity setting for the internal load cell was set at 0.5mV/V.

Pore pressure transducer

Pore pressure was measured by a Genspec GS4200 pressure transducer which has a maximum output of 10V and a range of 1000kPa. Output was channeled through a custom made digital readout and finally recorded onto the computer.

Pressure gauge

With the exception of cell pressure (which was supplied by the digital pressure controller), all pressure used in the triaxial system were supplied by a traditional compressor which supplied constant air pressure of up to 550kPa. Air pressure was converted to water pressure via an air-water interface. Pressure was controlled using pressure regulators and read by a Budenberg standard test pressure gauge. The gauge had a capacity of 1700kPa and a resolution of 10kPa.

Volume gauge

Sample volume change measurements during saturation and consolidation were measured by a Wykeham Farrance burette type volume gauge, which has a 100 ml capacity and a resolution of 0.2ml.

3.5.2 Instrumentation calibration

All instrumentation was calibrated to evaluate the accuracy of the transducers. Transducers were calibrated against a suitable reference in order to establish the closeness of the outputs to the true values. According to authors such as Doebelin (1990), Collett and Hope (1983) and Sydenham (1982), the accuracy of the reference system should be 3 to 10 times that of the instrument being calibrated. A consistent calibration methodology (Heymann, 1998) was used to calibrate all instrumentation. The methodology included the following steps:

1. Calibration of the transducer (including signal conditioning unit and A/D converter) or apparatus against a suitably accurate reference.
2. A least squared linear transfer function was determined to describe the relationship between the measured quantity and the digital output.
3. Error was calculated for each calibration point as the difference between true value (engineering units) and the measured value converted to engineering units via the transfer function. Errors were plotted against true value to allow for visual assessment of measurement uncertainty.
4. The accuracy of each instrument was calculated as ±1.96 times the standard deviation of the errors. Assuming that errors are normally

distributed, this gave a confidence level of 95% that the difference between true values and measured values was within the specified accuracy.

Calibration data and graphs for all instrumentation are attached in *Appendix B*. The instrumentation was calibrated to ensure that the measurements were in an acceptable range. Factors such as accuracy, resolution, sensitivity, hysteresis and noise were quantified for each instrument. A brief description of these terms is given in *Table 3-7*.

Term	Description
Accuracy	The closeness of measured value to the true value.
Resolution	Smallest division on the readout scale. In this thesis, resolution of logged data is restricted by the resolution of the data acquisition card (65536 bit per full range).
Sensitivity	Amount of output response per input quantity.
Hysteresis	The difference between the loading and unloading curves.
Noise	Random measurement variation caused by external factors.

Table 3-7. Terms used in defining measurement uncertainty.

LVDT calibration

Before the calibration process, it is important to locate the electric zero of the instrument, as the sensitivity of the signal becomes non-linear further away from the electric zero. This was done by pressing the zero input button and adjusting the zero control to have a zero output. The LVDTs were calibrated over four gain (amplification) settings. Gain setting of 5 was used the measurement of all deformations prior to shearing. The gain was adjusted to 8 just prior to shearing commencing. During shear, the gain setting was gradually reduced from 8 through to 7, then 6 and finally back to 5 as axial strain increases.

Before calibration, the effects of armature position for the LVDTs were first evaluated. At a gain of 5 (coarse gain) it was found that for both LVDTs, a

linear relationship can be expected within a range of ±7mm of the electrical zero. At gains 6, 7 and 8, the output was linear throughout the entire physical range of the LVDT. The effects of armature position for both LVDTs are illustrated in *Figure B-1 to B-4* and *B-9 to B-12* in *Appendix B*. All measurements (irrespective of gain) were taken within the ±7mm range for this project to ensure that the linear transfer function was valid.

Two systems with contrasting benefits were used as a reference system. Firstly, YPG Tungsten Carbide gauge blocks with an accuracy of ±30nm at 20°C were used. The system, however, required the manual replacing of blocks during calibration. Potential errors from this calibration method occur as a result of the change in alignment of LVDT rods during placement and replacement of the gauge blocks. In addition, measurements could only be made at discrete intervals equal to the thickness of the gauge blocks. The second system was the use of a Mitutoyo micrometer. Calibration involves fixing the micrometer and the LVDT while adjusting the height of the lever arm via a height adjustment screw. This is demonstrated in *Figure 3-6*. The micrometer, however, had a lower accuracy of ±1.5μm in comparison with the gauge blocks. Measurements were also limited to the resolution of the micrometer of 1μm.
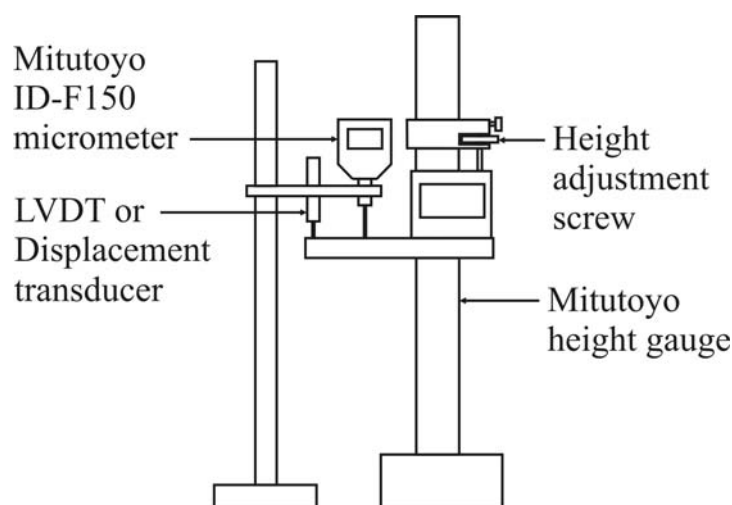
Figure 3-6. Calibration setup for the LVDTs.

It was originally decided that gain 8 would be used for small strain measurements. During trial tests, it was difficult keep the output within the range of the amplifier after the gain had been increased from 5 to 8. This requires that after deformation has taken place, the signal must be within the range of -0.9V to 0.45V on gain 5. This was sometimes not possible, as axial deformation would then require to be estimated with an accuracy of 1mm. This problem was solved by starting shearing at gains of either 6 or 7 when the armature position (after deformation) falls outside the range at gain 8. The use of gains 6 and 7, however, sacrificed output sensitivity and resolution for a larger workable range on gain 5. The workable ranges on coarse gain 5 for gains 6, 7 and 8 are summarized in *Table 3-8*.

Gain	6		7		8	
	Max	**Min**	**Max**	**Min**	**Max**	**Min**
LVDT 1	3.67V	-6.0V	1.24V	-2.54V	0.45V	-0.90V
LVDT 2	3.74V	-6.0V	1.25V	-2.53V	0.46V	-0.88V
Range	≈6.6mm		≈2.6mm		≈0.9mm	

Table 3-8. Working range for the two LVDTs at various gain levels.

From *Table 3-8*, it can be seen that when the gain was decreased, the range within which axial deformations needed to be estimated increased. The accuracy, sensitivity and resolution of both LVDTs on all gain positions are summarized in *Table 3-9*. The linear transfer function was calculated from the micrometer calibration data as a higher accuracy was obtained when compared with the gauge block calibration data.

Calibration data for both LVDT1 and LVDT2 at gains 5, 6, 7 and 8 are illustrated in *Figure B-5* and *B-13* respectively. Errors for both LVDTs are plotted in *Figure B-6* and *B-14*. Loading and unloading plots of the two LVDTs on both coarse and fine gain are illustrated in *Figure B-7, B-8, B-15* and *B-16*. Hysteresis for LVDT1 on gains 5 and 8 were 0.06V and 0.4V. Calibration data for LVDT2 yielded a hysteresis on gains 5 and 8 of 0.04V and

0.4V respectively. The hysteresis on gain 8 is result of an offset of the height gauge during change in the direction of movement, and is evident from the constant values in the hysteresis graph for both LVDTs on gain 8. Hysteresis for the LVDTs on gain 8 is estimated to be 0.2V.

Gain	Accuracy (µm)		Sensitivity (µm/V)		Resolution (µm)	
	LVDT 1	LVDT 2	LVDT 1	LVDT 2	LVDT 1	LVDT 2
5	12.6	13.6	676	683	0.206	0.208
6	2.2	3.5	219	224	0.067	0.068
7	1.8	3.0	74	75	0.023	0.023
8	2.8	1.4	27	27	0.008	0.008

Table 3-9. Accuracy, sensitivity and resolution for the two LVDTs at various gain levels.

LDT calibration

Calibration of the linear displacement transducer used for external displacement measurements followed the same process as the LVDT calibrations, using both gauge blocks and the micrometer. In this case, it was evident that the gauge blocks showed a better accuracy than the micrometer, and thus the transfer function was determined from the gauge block data was used. The calibration range was limited to the capacity of the LDT, which was 20mm. The calibration graph shown in *Figure B-17* shows a sensitivity of 1.9786mm/V. The accuracy of the transfer function was calculated as 44µm. Error and hysteresis graphs are shown in *Figure B-18* and *B-19*. From *Figure B-19*, it was evident that some hysteresis was shown by the LDT. This was not considered a problem as no load/unload cycles was done during the experimental work. Resolution of the LDT is again restricted by the data acquisition card to approximately 0.6µm.

Load cell calibration

Before calibration took place, the load cell was checked for possible faults such as oil leakages and wiring. Calibration was done in a Lloyds LRX Plus

single column test system to a load of 1000N. For a 50mm sample, this amounts to a deviatoric stress of approximately 500kPa, which is sufficient for tailings samples, as demonstrated by Vermeulen (2001). Calibration data yielded a sensitivity of 102N/V and an accuracy of 7N. Calibration and error graphs are shown in *Figure B-20* and *B-21* respectively. No hysteresis was found, as loading and unloading plots were identical. The load cell could thus be interpreted with a resolution of 0.03N.

Pressure instruments calibration

Pressure instruments included the GDS digital pressure controller (which supplied the cell pressure), the pore pressure transducer and the Budenberg standard test pressure gauge on the pressure manifold. All pressure instruments were calibrated with the pressure transducer, which in turn was calibrated using the Budenberg 3/500 dead-weight calibration device. The reason for this indirect calibration was that the Budenberg test gauge was not movable and nor was the Budenberg dead-weight system.

Calibration involved first establishing a relationship between the pressure transducer and the Budenberg dead weight system (assumed to be the true pressure). The output (recorded by a computer), digital pressure controller and Budenberg standard test gauge were then calibrated against the calibrations of the Budenberg dead-weight system (via the pressure transducer). The relationship between the pressure transducer and the Budenberg 3/500 is shown in *Figure B-22*. Calibration ranges for output and digital pressure controller were restricted to the capacity of the pressure transducer (1000kPa). The Budenberg standard test gauge was calibrated to the capacity of the compressor (around 550kPa) *Figure B-23* illustrates the relationship between output, digital pressure controller and Budenberg standard test gauge outputs, and the true pressure as defined by the Budenberg dead-weight system. The errors for the three apparatus are plotted in *Figure B-24*. From the figure, it is evident that at low pressures, the Budenberg standard test gauge yields higher errors than at higher pressures. Accuracies and sensitivities are summarized in *Table 3-10*.

Instrument	Accuracy	Sensitivity	Resolution
Output	1.5 kPa	100 kPa/V	0.03 kPa
Digital pressure controller	2 kPa	1 kPa/kPa	1 kPa
Standard test gauge	4 kPa	1 kPa/kPa	10 kPa

Table 3-10. Accuracy, sensitivity and resolution for GDS, Budenberg and PC output.

No hysteresis tests were conducted on any pressure apparatus.

Volume gauge calibration

Calibration of the volume gauge involved measurement of the weight of displaced de-aired water to a resolution of 0.1g (approximately 0.lml). The calibration method is similar to that used by Heymann (1998), and is demonstrated in *Figure 3-7*.

It is important that the volume gauge and all tubes are properly flushed and the de-aired water is of high quality. It is also important that the exit tube is submersed in water, as shown in *Figure 3-7*.
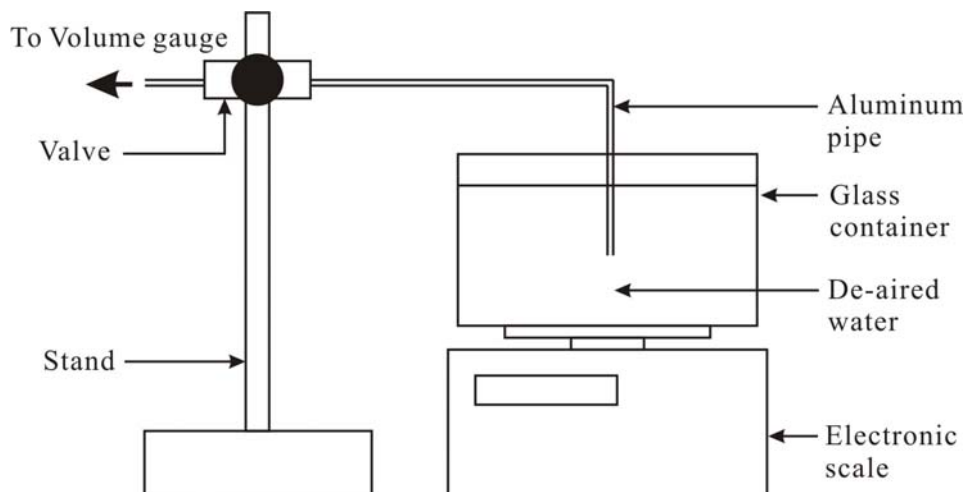
Figure 3-7. Calibration setup for the volume gauge.

The calibration range was restricted by the readability of the paraffin/water interface, and thus was calibrated in regions where the interface in the inner tube was clearly visible. The range was approximately 60ml. Calibration curve and error curve are shown in *Figure B-25 and B-26* respectively. Calibration data yielded accuracy for the volume gauge of approximately 0.2ml, with a resolution, also defined by the marking, of 0.2ml.

3.5.3 Measurement uncertainty

The calibration of the instrumentation aided in estimating the uncertainty of the computed parameters such as stress and strain. This section presents a brief discussion of the uncertainties in the analysis.

Uncertainties in void ratio measurements

The accuracy with which void ratios can be determined has been investigated by various authors (Vaid and Sivathayalan, 1996; Garga and Zhang, 1997 and Papageorgiou, 2004). They conclude that uncertainties in void ratio measurements can be caused by the following factors:

- Measurement technique
- Accuracy of the instrument and the precision of the operator
- Uncertainties in:
  - Sample height
  - Sample diameter
  - Sample weight
  - Specific gravity

Garga and Zhang (1997) investigated the uncertainty of void ratio measurements using aluminium dummies of known height and diameter, and concluded that the potential error in void ratio for a nominal 50mm x 100mm sample at a relative density of 30% using the calliper technique for height and diameter was 0.006 to 0.003. They further concluded that the uncertainty in

void ratio measurement as a result of the error in weight measurement is less than 0.01% and is thus negligible.

Papageorgiou (2004) investigated the uncertainties in void ratio measurements of gold tailings samples due to uncertainties in mass, height, diameter, volume and specific gravity at various initial void ratios and concluded that void ratio errors can be as high as ±0.08 for initial void ratios of up to 2. He further concluded that an increase in sample diameter and a decrease in initial void ratio can both reduce measurement uncertainties. It was also recommended that the void ratio of gold tailings samples measured using conventional measuring techniques (i.e. verniers, callipers, mass balances etc) can at best be quoted to 1 or 2 decimal places.

Taking into account the measuring instruments used, it was estimated that for the range of void ratios required for this thesis, the uncertainty of void ratio measurements were ±0.04.

Uncertainties in stress measurements

Stress is a measure of the intensity of force over a certain area, and thus both the uncertainties of area and force measurements must be taken into account. Force measurement errors are given by the load cell calibration data while area errors can be estimated from the accuracy of the measurement instrument, in this case, the Vernier calliper. Uncertainties in force measurements were estimated to be 6.4N while the error in area measurement is approximated to be 3.08mm², assuming a sample diameter of 50mm and a calliper accuracy of 0.01mm. This equates to uncertainties in stress measurements of approximately 6.5kPa in the calibrated load range.

During testing, changes in area could lead to changes in axial stress and thus area correction had to be considered in the stress calculations. The average cross-sectional area A of the sample was obtained from *Equation 3-1*:

$$A = A_0 \frac{1 - \varepsilon_v}{1 - \varepsilon_a}$$

Equation 3-1

where A_0 is the initial area and ε_v and ε_a are volumetric and axial strains respectively. Under isotropic conditions, the axial strain in three directions is constant and ε_v can be determined from *Equation 3-2*:

$$\varepsilon_v = (1 - \varepsilon_a)^3 - 1 \hspace{4cm} Equation\ 3\text{-}2$$

Stress redistributions due to barrelling effects produced by rough platens during shear were not considered.

Uncertainties in axial strain measurements

For this research, three axial strain measurements were made during shear, namely using two LVDTs and an external linear displacement transducer (LDT). Axial strain is determined as the ratio of the change in length and the original length, and is given as a percentage. The accuracy of the LVDTs were estimated from calibration data as 0.012mm and 0.0021mm for gain settings of 5 and 8 respectively while the error of gauge length measurement for the LVDTs was the calliper accuracy of 0.01mm. The uncertainty in axial strain measurements from the LVDTs were then determined to be 0.047% and 0.008% for amplifier gains of 5 and 8 respectively. The accuracy of the LDT measurements was determined as 0.042mm in the range of 20mm. Uncertainties in axial strain measurements were therefore determined to be 0.082%.

3.6   LABORATORY SAMPLE PREPARATION

As mentioned in section 3.2, all disturbed samples (excluding those used for the Atterberg limit) were oven-dried at 50°C for 48 hours and passed through a 1mm sieve. Laboratory samples were prepared using two reconstitution techniques, namely moist tamping and slurry. The moist tamped method is the most commonly used laboratory preparation method that is suitable for all soil types. It is a simple method and target void ratios can be achieved with relative ease. However, there has been some evidence that the behaviour of moist tamped samples does not reflect in situ conditions. The other method, slurry

preparation, closely resembles the deposition of tailings, but difficulty of attaining the required target void ratio has generally been recognized. The two methods are discussed in detail in the following sections.

Before commencement of any testing, it was important that the triaxial cell was checked and de-aired. Preparation of the triaxial cell included flushing the top, back and pore pressure valves with de-aired water, de-airing the GDS pump and testing the membrane for leakage.

3.6.1 Undisturbed samples

Undisturbed samples were obtained from the undisturbed blocks. Plastic wrap and aluminium foil were carefully removed to expose the block. The block was first trimmed to fit into a soil lathe and then trimmed to a 50mm diameter sample in the lathe. After the sample had been trimmed to the required diameter, it was removed and trimmed to the required height of 100mm. Moisture content for the specimen was obtained from the trimmings. Procedures of sample preparation of the undisturbed samples are attached in *Appendix C*.

3.6.2 Moist tamped samples

The method of moist tamping has been described in section 2.7. The moisture content used for moist tamped samples was dependent upon:

- The position of the target void ratio in relation to the minimum void ratio at the specific moisture content. The moisture content was chosen so that the minimum void ratio was as close to the target void ratio as possible. It was assumed that collapse or swell would thus be minimized and the initial fabric preserved.
- The appearance of the sample. The moisture content was chosen to prevent the formation of lumps visible to the naked eye.

- Practicality. Sufficiently high moisture content was chosen so that samples had some strength during sample preparation and handling.

Table 3-11 summarizes the preparation moisture content, minimum void ratio at the preparation moisture content, liquid limit and in situ void ratio.

	Preparation moisture content (%)	Liquid limit (%)	In situ void ratio	Minimum void ratio
Pond	25	51	1.42	1.68
MB	15	30	1.09	0.97
UB	7.5	25	0.61	0.62

Table 3-11. Summary of preparation moisture content, minimum void ratio at the preparation moisture content, liquid limit, in situ void ratio for the three materials.

Conventional moist tamping requires the material to be compacted using tamping rods. For this research, a hydraulic jack was used to compact all moist tamped samples in the mould. As the in situ void ratio lies on or close to the minimum void ratio, conventional compaction did not provide sufficient energy to compact samples to the target void ratio. Furthermore, at such a high density, moist tamped samples tend to crack when the mould is removed. Using a hydraulic jack allowed the compacted samples to be extruded from the mould.

Although all moist tamped samples were compacted using the hydraulic jack, the effort required to compact the samples to the target void ratio differed significantly with all three material types. Since measurements were available to quantify compaction effort, a comparative description is given. A significant effort was required to compact the moist tamped pond sample to the target void ratio. This may result in bending or breaking of the platy particles as well as disintegration of the flocks. Compaction of the moist tamped upper beach samples to the target void ratio required far less effort in

comparison with the pond samples. Moist tamped middle beach samples could easily be compacted using conventional moist tamping methods as described in section 2.7.2. An estimate of the force required at the handle of the hydraulic jack for compaction of moist tamped samples is given in *Table 3-12*.

Material type	Pond	Middle beach	Upper beach
Force required (N)	600	50	150

Table 3-12. Estimate of force required for moist tamping.

The procedures for preparing moist tamped samples are summarized below and illustrated in *Figure 3-8*. Photographs are included in *Appendix C*.
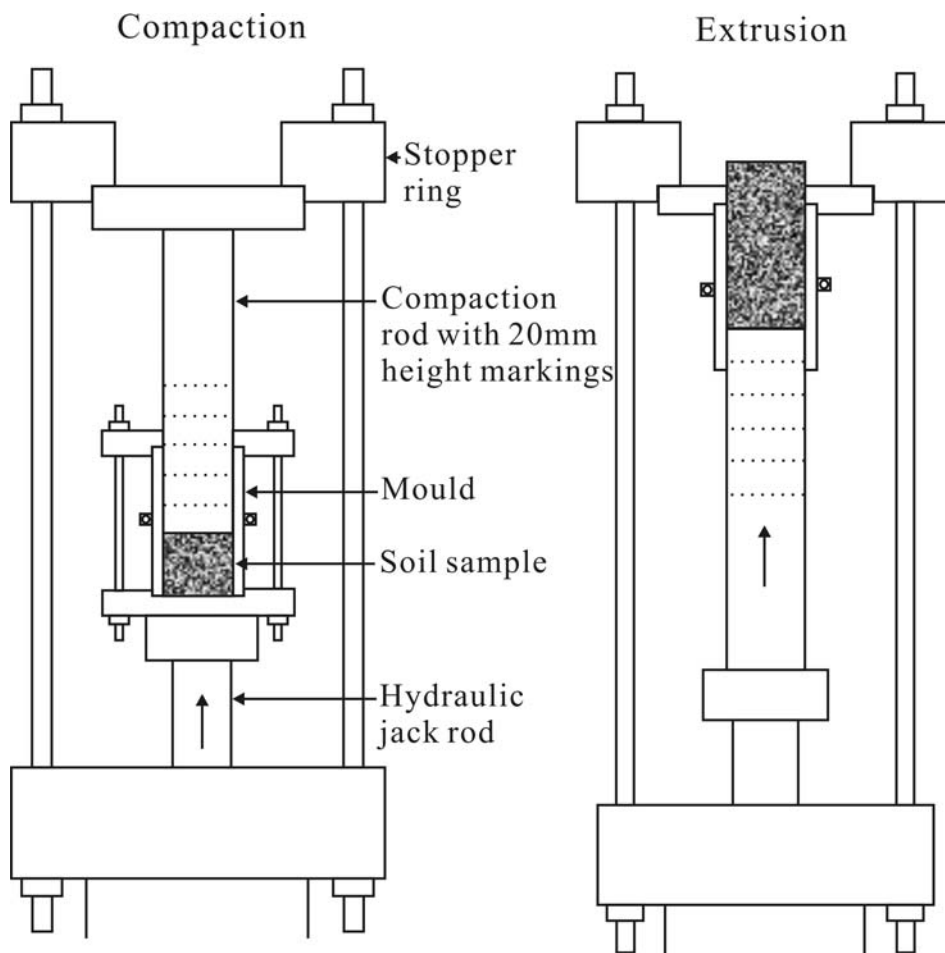
Figure 3-8. Illustration of compaction and extrusion of moist tamped samples using a hydraulic jack.

1. Dry tailings were weighed and mixed with the required moisture content (using tap water) and sealed in a closed container for 24 hours. This allowed the moisture to be distributed equally throughout the material. The material was mixed thoroughly again before use.

2. The total amount of moist soil for the target void ratio was determined. The amount of material to be deposited in each layer was then a fifth of the total amount.

3. The hydraulic jack and mould were setup.

4. The required amount of material was weighed and deposited into the mould. The material was compacted to the predetermined height marking (each layer is 20mm high). The surface of the previous layer was scratched before the next layer was placed. The procedure was repeated until the mould was full.

5. The sample was extruded from the mould.

6. Weight and dimensions of the sample were measured.

7. A moisture content sample was taken and weighed.

8. The bottom porous disk was placed on the base pedestal followed by the sample. The membrane was then stretched over the sample with a membrane stretcher. O-rings were then positioned over the base pedestal with an O-ring stretcher, holding the membrane tightly against the pedestal.

9. The top porous disk and the top cap were then placed over the sample, and the membrane was rolled over the top cap. Top O-rings were positioned over the top cap, holding the membrane over the top cap.

10. The brackets for LVDTs were then fixed onto the membrane using contact adhesive. The gauge length (distance between the top and bottom brackets) is approximately 50mm. Positions for the LVDT brackets were marked before the brackets were fixed. After the LVDTs had been positioned, the gauge length was measured again using a vernier calliper. The initial output for the LVDTs was also recorded.

11. The cell was then placed and fixed to the base, and the chamber filled with de-aired water.

3.6.3 Slurry preparation

For this research, slurry samples were prepared using a method similar to that described by Theron (2004). The decision on the appropriate preparation moisture content of slurry samples was not simple. Segregation can occur for slurries of high moisture content, resulting in alternating layers of coarse and fine material. On the other hand, slurries with low moisture content tend to trap air, resulting in cavities and a non-uniform sample. The initial idea was to prepare all slurry samples at moisture content just above the liquid limit to prevent segregation. This could be done with pond samples at a moisture content of 62% (1.2 times *LL*), but not with MB or UB samples. The void ratio for slurry samples prepared using MB and UB material were significantly lower than the in situ void ratio. For UB material, the highest void ratio achievable for a slurry samples was 0.5 while the in situ void ratio was around 0.6. MB slurry samples could be prepared at a void ratio of around 0.8 while the in situ void ratio was 1.1. Only a slight increase in void ratio could be achieved by increasing the moisture content of the slurry.

To solve this problem, dispersant and flocculent were added to the water used to prepare slurry samples. From the sedimentation tests, it was evident that the addition of dispersant or flocculent at specific concentrations can increase the void ratio. After some trial and error testing, it was decided that all UB slurry samples (including consolidation and shear) could be prepared to the required void ratio using 25% dispersant at a moisture content of 32% (just above the LL of 30%). MB slurry samples required a flocculent concentration of 50% for consolidation samples, 75% for shear samples consolidated to 200kPa, and 100% for shear samples consolidated to 400kPa. Moisture content was about 500%. This amounts to a moisture content/LL ratio of 17. Segregation was not a problem as the material settled in flocks and the excess water was removed using a syringe. An attempt was made to minimize the effects of the chemical additives by flushing out as much of these additives as possible. Once assembled in the triaxial cell, approximately three litres of water was flushed through each sample. This constitutes approximately 20 pore volumes of de-aired water. Flushing was done under a cell pressure of 25kPa and a back

pressure varying from 10kPa (at the deairator) and atmospheric (at the top drainage line).

The setup of the mould on the triaxial pedestal is demonstrated in *Figure 3-9*.

a) Sample preparation   b) 1-D consolidation
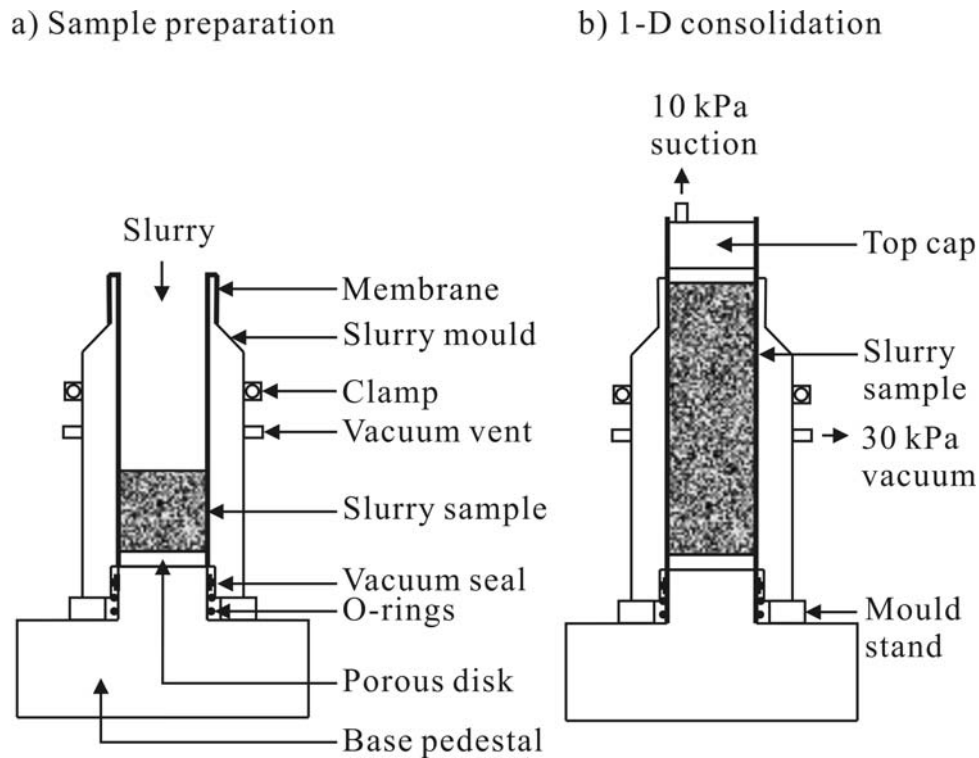
Figure 3-9 Illustration of slurry preparation method.

Procedures for the preparation of slurry samples are summarized below:

1. Tailings and tap water were first mixed in the required proportion to form enough slurry to fill the mould at the specific moisture content. The slurry mixture was de-aired in a desiccator for approximately 30 minutes.

2. The membrane was stretched over the triaxial base pedestal and O-rings were stretched over the membrane as shown in *Figure 3-9*. The bottom porous disk was then placed on the base pedestal. All porous disks were saturated before use.

3. The mould stand (two semi-circular parts) was placed on the pedestal followed by the sample mould (split mould). The mould was only placed when the vacuum seal for air suction was properly in place. The entire

mould was then clamped. The membrane was then stretched over the top of the mould and fastened in place via soft O-rings. This created an air-tight chamber between the membrane and the sample mould, and when the 30kPa vacuum was applied, the membrane was sucked tightly against the sample mould.

4. Slurry was then placed in the mould in thin layers. After each layer was placed, the top layer was stirred, without agitating the previous layer, to prevent segregation. Slurry was placed up to the top of the mould. The sample was approximately 100mm high.

5. After the slurry had been deposited, the top porous disk was placed, followed by the top cap. The membrane was then rolled over the top cap and O-rings were stretched over the top cap, holding the membrane tightly against the top cap.

6. 10kPa water suction was then applied through the top valve. This was done by adjusting -10kPa on the digital pressure controller. During the application of suction, the top cap was allowed to sink into the slurry mould, allowing some one-dimensional consolidation. This was required to maintain the cylindrical shape of the slurry sample. Once the pore pressure (measured at the bottom of the sample) had stabilized throughout the sample, the mould was removed.

7. Sample dimensions were then measured. Membrane thickness was deducted from diameter measurements. Sample weight was obtained by deducting the final mass from the original mass of the slurry.

8. A moisture content sample was taken and weighed.

9. Steps 10 and 11 for moist tamped samples were completed.

A detailed description with photographs for preparing slurry samples is attached in *Appendix C*

3.6.4 The effect of dispersant and flocculent

The use of laboratory preparation methods such as water pluviation or slurry deposition produces samples which duplicate the characteristic behaviour of natural soils and hydraulic fills (Oda et al., 1978; Vaid et al., 1999; Mao and

Fahey, 1999; Vaid and Sivathalayalan, 2000). It is well recognized by these researchers that these methods may produce samples of low void ratios.

Dispersant and flocculent were used in this research to achieve the target void ratios for slurry samples, after initial trials indicated that middle and upper beach slurry samples could not be prepared at the target void ratio using only tap water. The decision to use dispersant and flocculent was difficult as it was unclear what effects these chemical additives would have on the behaviour of gold tailings. It was decided that longer flushing times would be allowed to remove as much of the chemicals as possible and to minimize their effect on gold tailings behaviour. For these samples, approximately three litres of de-aired water, equivalent to approximately 20 pore volumes, was flushed through each sample.

Olson and Mesri (1970) conducted one-dimensional compression tests on various clays using different pore fluids. The concluded that the compression behaviour of clays such as muscovite, kaolinite and illite are dominated by mechanical bending, compressing and rupture of the particles coupled with shearing displacement at the contacts. Pore fluid chemistry influences the original soil structure of the clay, and thus has an indirect influence on th compression behaviour of the clay.

Mao and Fahey (1999) studied the effect of the flocculent Mg 919 on the behaviour of aragonite soil which is a silty calcareous soil obtained from below the seabed. According to Ruehrwein and Ward (1952), synthetic polymer flocculent such as Mg 919 are composed of long-chain molecules which adhere to the particles surfaces, binding them together physically to form stable flocs. The strength of these bonds is dependent on charge effects, dispersion forces or hydrogen bonding, and increases with molecular weight of the flocculent (Akers, 1975). Studies by Mao and Fahey (1999) indicate that the consolidation and shear behaviour are not affected by the addition of flocculent.

Anandarajah and Zhao (2000) investigated the stress-strain behaviour of kaolinite with various pore fluids. They concluded that pore fluids which decrease the repulsive barrier of particles may lead to an apparent over-consolidation in the specimen, and pore fluids which increase the net attraction of particles increase the cohesion of the specimen.

From the literature, it appears that the effect of dispersant and flocculent on the behaviour of gold tailings is minimal. Gold tailings consist of rotund and platy particles of quartz which is a stable mineral with no weakly bonded ions. Rotund particles are dominated by mechanical interaction due to the lower specific surface area. Platy particles in the clay size range may be affected by these surface forces, but it is assumed that the effect is only on the original fabric. Once the fabric is established, the behaviour of gold tailings is dominated by mechanical effects.

3.7   TRIAXIAL TESTING

The triaxial test was the standard consolidated undrained triaxial test. This included flushing, saturation under elevated back pressure, consolidation and shear. The triaxial testing procedure used in this research was performed according to the guidelines given in BS1377: Part 8:1990 and is summarized below.

1.   After the sample was in place and the cell filled, the cell pressure was raised to 25kPa. The sample was then flushed by allowing de-aired water to flow (under a head of approximately 15kPa) from the back value, first through the bottom line (where pore pressure was measured) and then through the top valve. The objective of flushing was to remove as much air trapped in the sample as possible. The flushing process took approximately 24 hours. LVDT outputs were recorded to monitor volume change of the sample during flushing.
2.   LVDT output was recorded at the end of each stage (flushing, saturation, consolidation and creep).

3. Saturation which followed the flushing process involved raising the pore pressure of the sample to dissolve trapped air into the water. To ensure saturation, samples must obtain a B-value of at least 0.95. B-value is determined as the ratio between the changes in pore pressure and changes in cell pressure. For this research, all samples were tested under a back pressure of either 300 or 400kPa.

4. Testing for this research required samples to be either consolidated or consolidated and sheared.

5. Consolidation samples were consolidated to an effective stress of 1000kPa. Consolidation samples were consolidated using a linear increase of cell pressure with time at a rate of 10 seconds per kPa.

6. Shear samples were first consolidated to an effective stresses of either 200 or 400kPa. 200kPa samples were consolidated following the standard consolidation procedure (by raising the cell pressure under undrained conditions and then opening the drainage to allow consolidation to take place) while 400kPa samples were consolidated using the same linear increase of 10 seconds per kPa as the consolidation samples.

7. Creep was allowed for 24 hours for all samples before shearing.

8. The creep rate was checked by closing the drainage for 10 minutes. It was expected that no excess pore pressure buildup should take place within the 10 minutes. If pressure build-up took place then the sample was left a further 24 hours to creep. No sample required a third 24 hour period to creep.

9. A constant rate of shear of 0.103mm/min was used for all tests. This was consistent with consolidation properties as determined from the shear-200 samples which were consolidated in the standard manner. The shear rate resulted to approximately 6% axial strain per hour.

10. Tests were terminated when a stresses have stabilized (at the critical state) or when further shearing could damage the LVDTs.

3.8   IMAGE ANALYSIS

Fabric of soils can be measured using various methods, each with its own benefits and limitations. As mentioned in section 2.6.3, methods of fabric measurement can generally be categorized into two main sections, namely visual methods and indirect methods. Visual methods are often based on image analysis of some image of the soil, while indirect methods, on the other hand, measure some physical property and relate the value to a certain fabric.

For this research, visual methods were chosen over indirect methods as a basis on which the fabric of tailings was compared. All samples were desiccated at room temperature. Fabric samples were constructed in the same manner as triaxial samples, but were removed before the test (consolidation or shear). Triaxial procedures for the fabric samples are summarized in *Table 3-3*.

It was further decided that raw intact samples would used for the SEM images. The reason for this was that three-dimensional images, although far more complex, give more detail and would aid in the understanding of gold tailings fabric.

3.8.1   Samples preparation for direct SEM

Fabric samples were viewed directly under the SEM. After desiccation, the samples taken from the triaxial were broken into smaller fragments to reveal the required surface. Care was taken to avoid the shear plane for the shear samples. Positions for SEM samples are shown in *Figure 3-10*.

Samples were mounted onto aluminium plates using conductive carbon paint. All samples were mounted with the orientation of the top noted. Care was taken to ensure that there was sufficient paint to hold the sample firmly. Extra carbon paint was used for MB and UB samples, as these samples were more brittle than the pond samples. The carbon paint was then allowed to oven-dry in a desiccator overnight. After the carbon paint had dried, the mounted sample was then further broken to reveal an undisturbed surface. Loose

material was gently blown away. The entire aluminium plate with the mounted samples was then coated with 5 layers (30nm) of gold (approximately 30 seconds per layer) using the sputter method. Coated samples could then be viewed in the SEM.
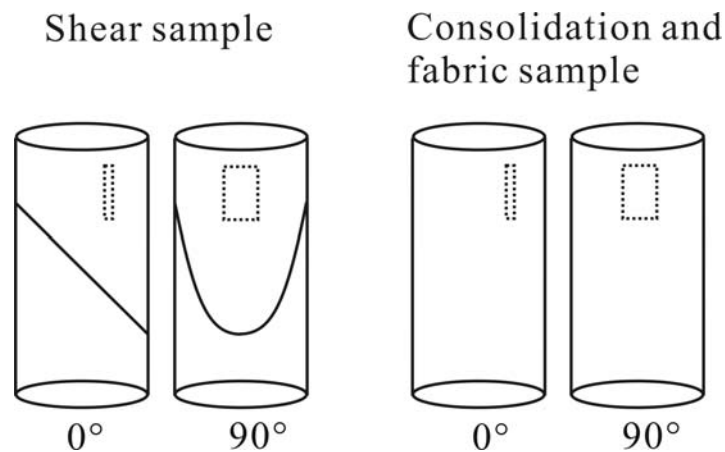
Figure 3-10. Sample positions for SEM samples.

3.8.2 SEM viewing

The SEM images were taken with a JOEL JSM-840 scanning microscope at a probe current of 3×10^{-11} amp, working distance of 12 mm and acceleration voltage of 5kV. Samples were placed in the vacuum chamber (1×10^{-5} torr) of the SEM. Two random positions were viewed at a magnification of 50, 200, 500, 1000 and 2000 times to examine the macro and micro fabric. Although random, positions were chosen where conduction was good to minimize charging effects. Charging effects (seen as bright lines or spots) could occur when electrons cannot drain through the carbon paint to the base. This was possible when the sample was too thick, or when the sample cracked or dislodged from the plate during desiccation or handling. Charging was generally a problem at higher magnifications as the entire electron beam is directed at a small area. Charged areas were avoided as far as possible.

3.9   CONCLUSION

An experimental programme was designed to investigate the effect of fabric on the consolidation, creep, shear and small strain behaviour of gold tailings. This included testing undisturbed and laboratory reconstituted gold tailings specimens obtained from various positions on ERPM 4 dam. The fabric was viewed under the SEM and these images form the basis of the fabric analysis.

Chapter 4

Fabric Analysis

4.1   BACKGROUND

The hypothesis for this thesis states that **accurate simulation of the behaviour of gold tailings under laboratory conditions requires appropriate replication of the material fabric.** The general understanding is that samples prepared using different laboratory preparation methods behave differently due to a difference in fabric which ensues upon reconstitution. This chapter presents the fabric of undisturbed, moist tamped and slurry deposited gold tailings samples at the same void ratio as observed under the SEM. Visual fabric analysis is the basis on which the sample fabric is compared. The implications of the observed fabric on the behaviour of gold tailings and possible modes of particle interaction are discussed.

4.2   VISUAL FABRIC ANALYSIS

As mentioned in Chapter 3, SEM was chosen over physical methods of fabric analysis because SEM images allowed interactions at a particulate level to be observed physically. Quantitative analysis of the observed fabric was complicated and was therefore not used.

SEM images were taken of all samples before testing at magnifications of 50, 200, 500, 1000 and 2000. SEM images of all samples at 50, 200 and 1000 times magnification are attached in *Appendix D.* SEM images of samples after testing were not used as no fabric differences could be observed between the

undisturbed and the reconstituted samples. As suggested by Zlatovic and Ishihara (1997), all fabric is destroyed when the samples reach the critical state.

Fabric comparison was made between each material type (ie pond, middle beach and upper beach) as particle properties and size distribution were different for each material type.

4.2.1 General fabric of gold tailings

The composition of gold tailings has been shown by authors such as Hamel and Gunderson (1973), Mittle and Morgenstern (1975) and Vermeulen (2001) to consist of coarse, rotund particles with finer, plate-like flat particles. This was further demonstrated by the SEM images obtained for this project. As exemplified by *Figure 4-1*, the MB sample at 1000 times magnification showed gold tailings consisting of rotund and platy particles.
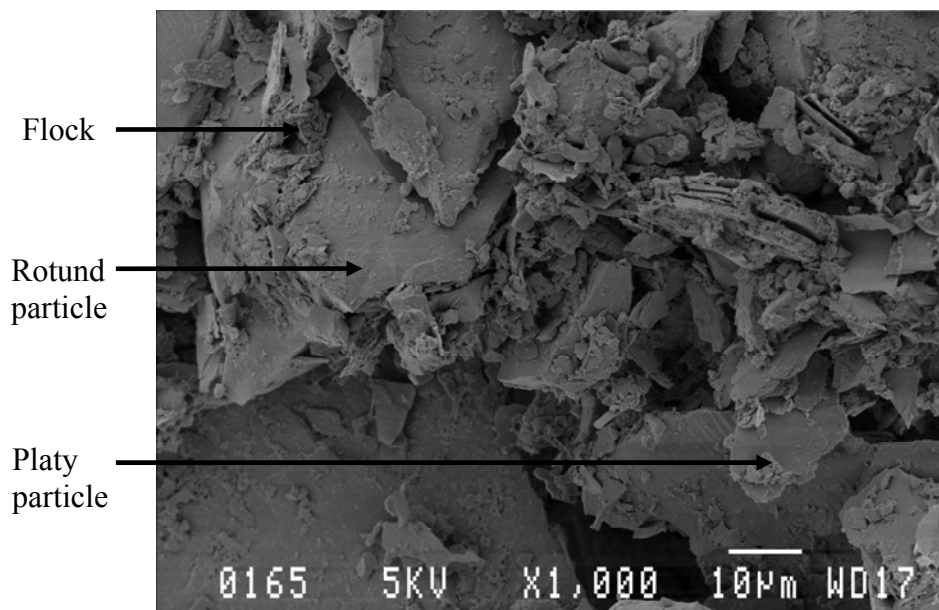
Figure 4-1. Physical constitution of gold tailings at 1000 times magnification

It was interesting to note that, besides the rotund and platy particles, flocks of particles also existed, as demonstrated in *Figure 4-1*. These flocks existed in various quantities (most abundant in pond samples) and sizes in the range of 5μm. The flocks consisted of fine platy and/or rotund particles, and were

probably a result of the addition of flocculent to facilitate settlement during deposition.

4.2.2 Pond samples

The SEM images showed that pond material consisted mainly of platy particles in the silt and clay-size range and only a few silt-sized rotund particles. The general trend of the fabric of pond samples at various magnifications was that the rotund particles were scarce and not in direct contact with each other, but were dispersed in a matrix of platy particles and flocks (*Figure 4-2a)*, similar to the partially or fully dispersed states proposed by Thevanayagam et al (2002) for sand-silt mixtures (*Figure 4-2b)*.

Rotund particle

Platy particle/flock matrix

Rotund particle

Silt matrix
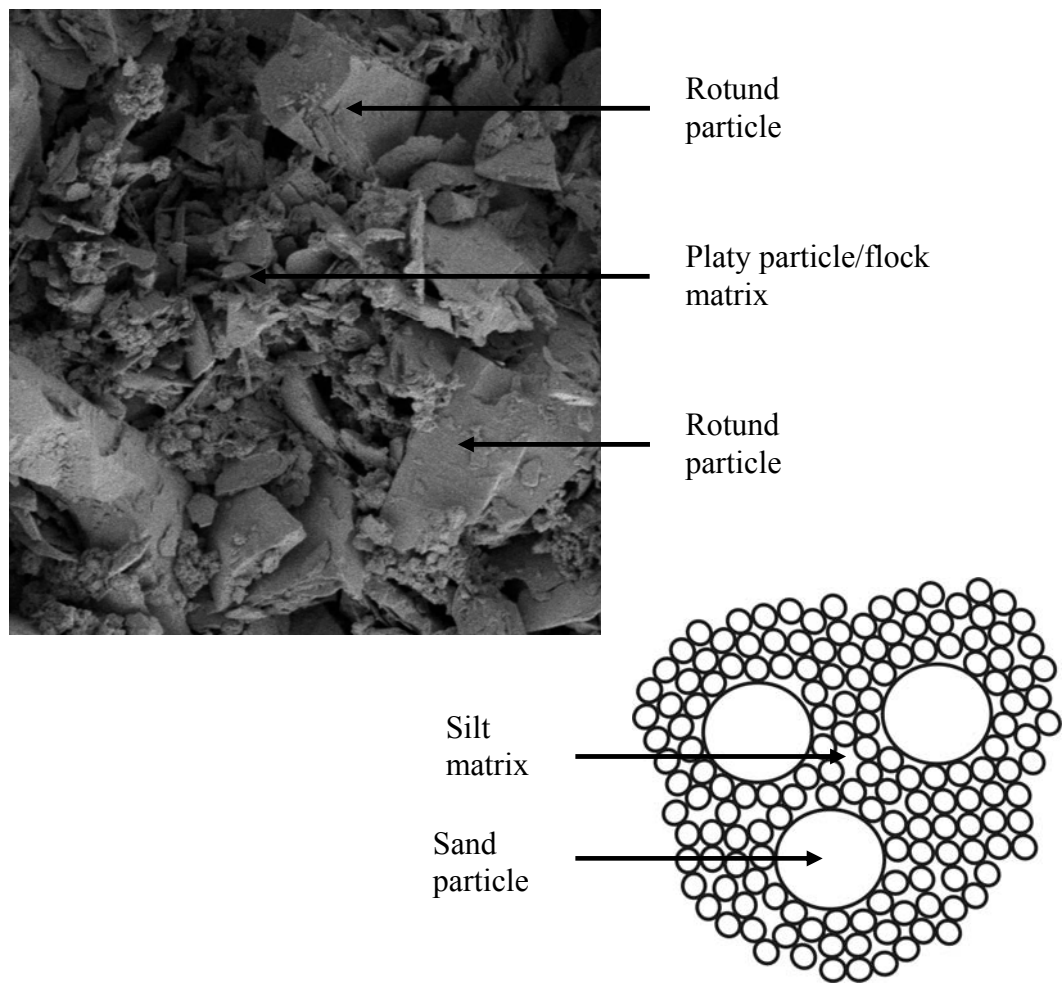
Sand particle

Figure 4-2. Dispersed state of rotund particles in gold tailings compared with sand-silt mixtures.

The SEM images also showed that there is no visible difference between the randomly orientated fabric of moist tamped and slurry samples (*Figure 4-3b* and *c*). It appears that the high compaction stresses required to prepare the moist tamped pond samples have erased any initial fabric which ensued upon sample preparation. The undisturbed consolidation samples (*Figure 4-3a*) however contained particles with some horizontal orientation. This could be expected in a depositional environment where platy particles settle in still water, analogous to that of a leaf falling through air. No specific particle orientation could be observed in any of the moist tamped or slurry shear samples. The horizontal particle orientation previously observed in undisturbed consolidation samples was also visible in the undisturbed shear samples. This indicated that the shear samples retained the horizontal particle orientation throughout the consolidation process.
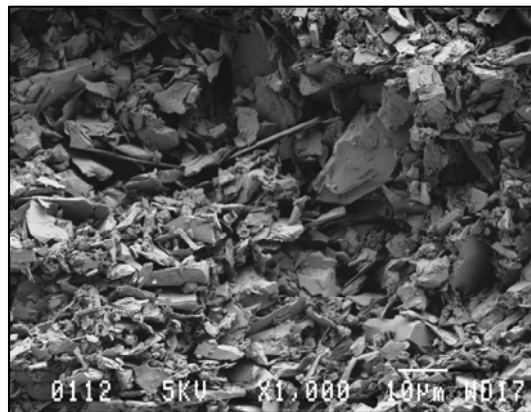
a) Undisturbed
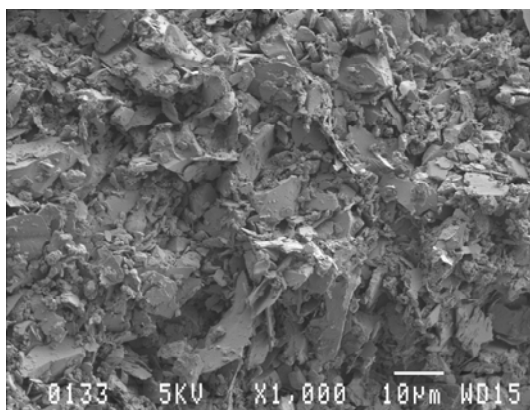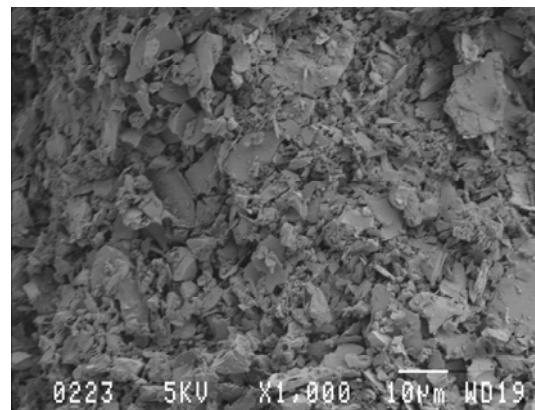
b) Moist tamped   c) Slurry

Figure 4-3. Particle orientation of pond consolidation samples.

4.2.3 Middle beach samples

The SEM images showed that the middle beach material was significantly coarser than the pond material, comprising both rotund and platy particles. This can be demonstrated by comparing undisturbed pond (*Figure b* page 191) and MB (*Figure b* page 196) images at 200 times magnification. The rotund particles in middle beach material were also significantly larger than those observed in pond material.

On examining the fabric of middle beach consolidation samples, one significant difference could be observed. At low magnifications, moist tamping created an aggregated fabric which was also visible, but to a lesser degree, in both the undisturbed or slurry samples. This is demonstrated in *Figure 4-4a*. At higher magnifications (*Figure 4-4b*), it was visible that these aggregates were composed of finer, rotund or platy particles, clinging closely to the coarse rotund particle. These platy particles generally appeared to be orientated parallel to the surface of the rotund particle, as demonstrated in *Figure 4-5*. Similar conclusions have been drawn by Theron (2004) on mica-sand mixtures. The aggregates originated during the process of moist tamping where capillary suctions are known to hold soil particles together. The aggregates were not visible to the naked eye during sample preparation, but are clearly visible from the SEM images.

It is interesting to note that although these aggregates originated from the capillary suction between the gold tailings particles, subsequent saturation did not disintegrate these them. The same distinct aggregation could be observed after consolidation and creep in the moist tamped shear 200 and 400 samples, but to a lesser degree. It appeared that although some aggregates may have been destroyed during consolidation, the general aggregated fabric was still visible. No specific particle orientation was identified in any of the consolidation or shear middle beach samples.

The aggregation observed in the moist tamped consolidation and shear samples may have some influence on the behaviour of the gold tailings.
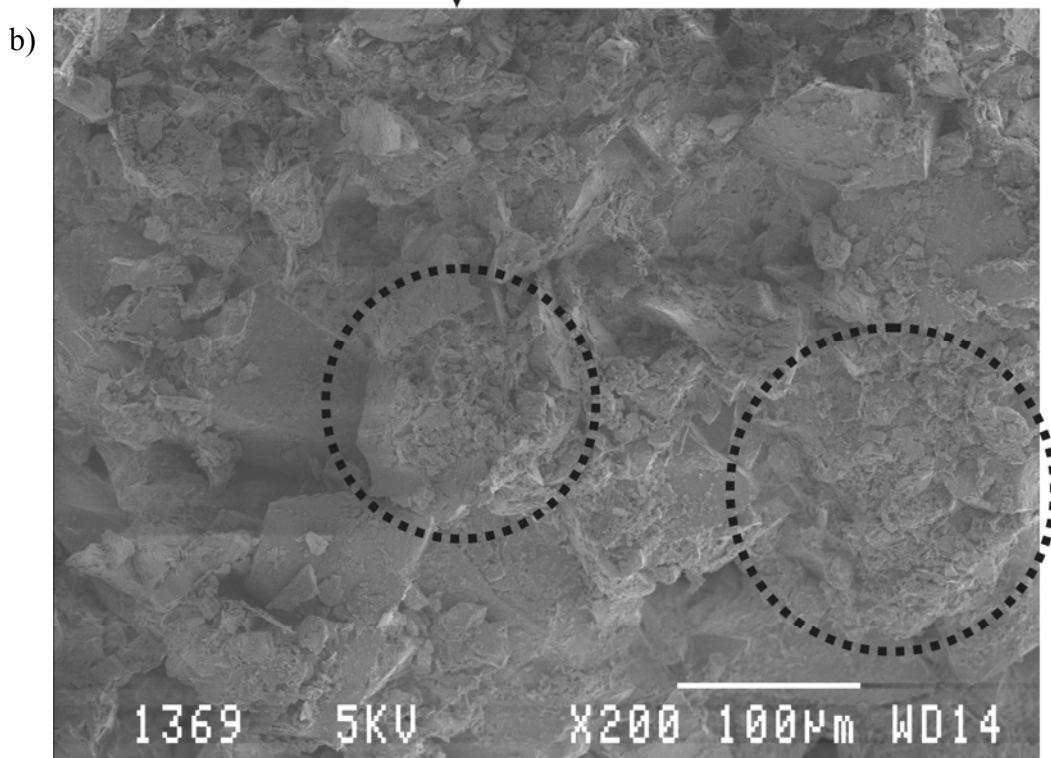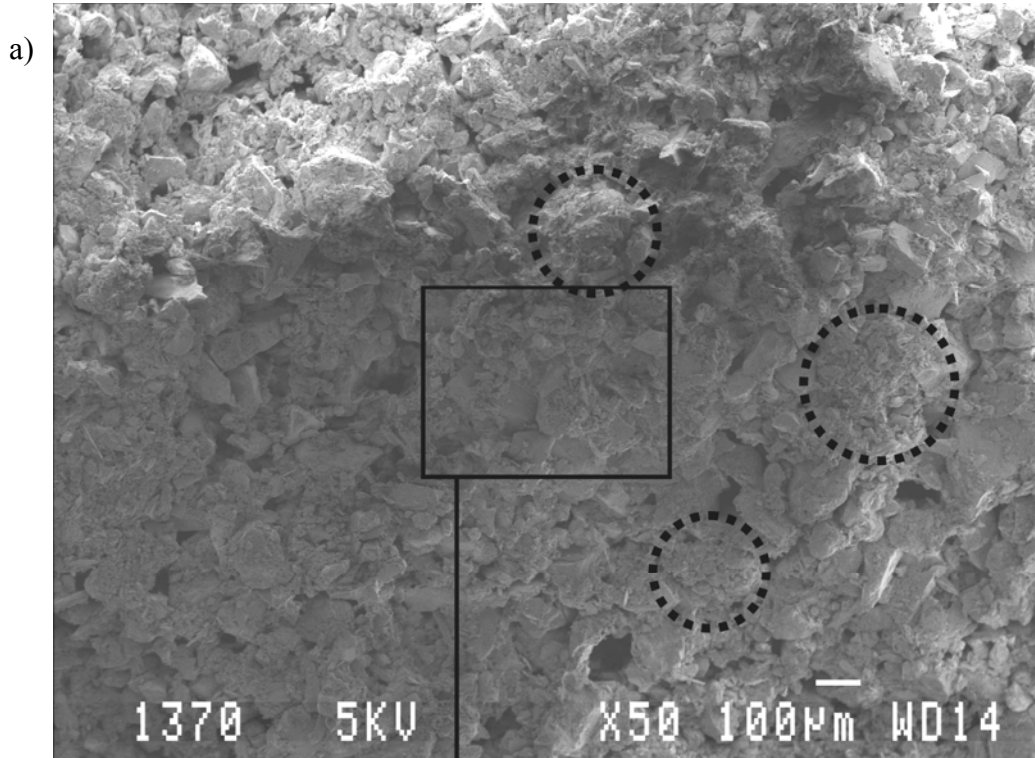
Figure 4-4. Aggregated fabric of moist tamped MB consolidation samples
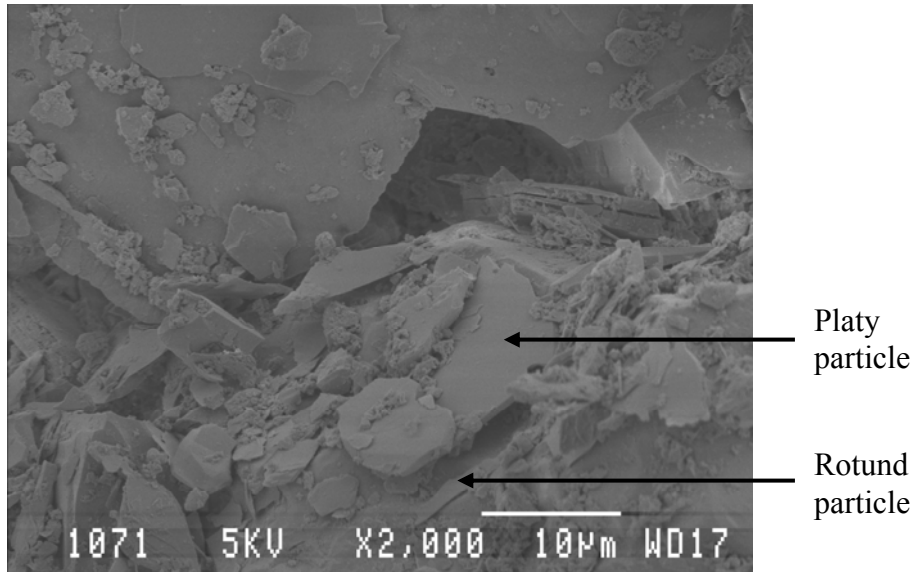
Figure 4-5. Platy particles aligned parallel to the rotund surface

4.2.4 Upper beach samples

Upper beach material consisted of rotund and platy particle similar in size to those of the middle beach material. Upper beach samples, however, existed in a denser state than middle beach samples. Fabric of upper beach samples was similar to that observed in middle beach samples. Moist tamped samples also showed a pronounced aggregated fabric (demonstrated by *Figure (a)* page 202 and *Figure (d)* page 203) which was less obvious in the undisturbed or slurry samples. Similar to the middle beach samples, these aggregates appeared to remain intact after consolidation. Particle orientation was not visible in any of the upper beach test samples.

4.2.5 Fabric classification

The fabric of gold tailings has been described in the previous section. It was, however, important that the fabric be classified systematically in order for comparisons to be made. The existence of aggregates could be considered an important fabric feature observed in gold tailings, and classification of fabric is thus based on the visibility of the aggregation. According to the Oxford English Dictionary, the word 'aggregation' indicates 'the action or process of

collecting particles into a mass, or particulars into a whole'. The American Heritage Dictionary describes aggregation as 'composed of a mixture of minerals separable by mechanical means'. For the purpose of this thesis, aggregation is defined as 'the collection of particles of various sizes and shapes into a mass which, under certain conditions, behaves as a single body.

Aggregates existed in various quantities in all samples. Two types or sizes of aggregates could be seen in the SEM images: small aggregates or flocks (as shown in *Figure 4-1*) in the order of 5 to 20μm and large aggregates in the order of 50 to 200μm. This is demonstrated in *Figure 4-6*. All samples contained small aggregates. These small aggregates were composed mainly of platy particles and had probably been formed as a result of the addition of flocculent to facilitate settlement of tailings in the dam. The large aggregates were composed of a collection of rotund particles, platy particles and flocks, and could be abundantly seen in the MB and UB samples. Undisturbed and slurry samples contained small quantities of these large aggregates, but moist tamped samples seemed to be dominated by these large aggregates.

Fabric classification was based on visual differences as described in the previous sections. Features which were common to all samples are not included in the classification. Two parameters were used to describe the fabric of gold tailings:

- *Aggregation*: refers to the collection of rotund particles, platy particles and flocks forming the large aggregates as demonstrated in *Figure 4-6*. Flocks as shown in *Figure 4*-1 were common to all samples and were not included in the classification. Samples were classified either as aggregated or non-aggregated based on visual assessment:

  o *Aggregated*: Platy particles and/or flocks adhere closely to rotund particles forming aggregates (*Figure 4-7)*.
  o *Non-aggregated*: Platy particles and flocks are loosely dispersed around and between rotund particles (*Figure 4-8*).

Examples of aggregates
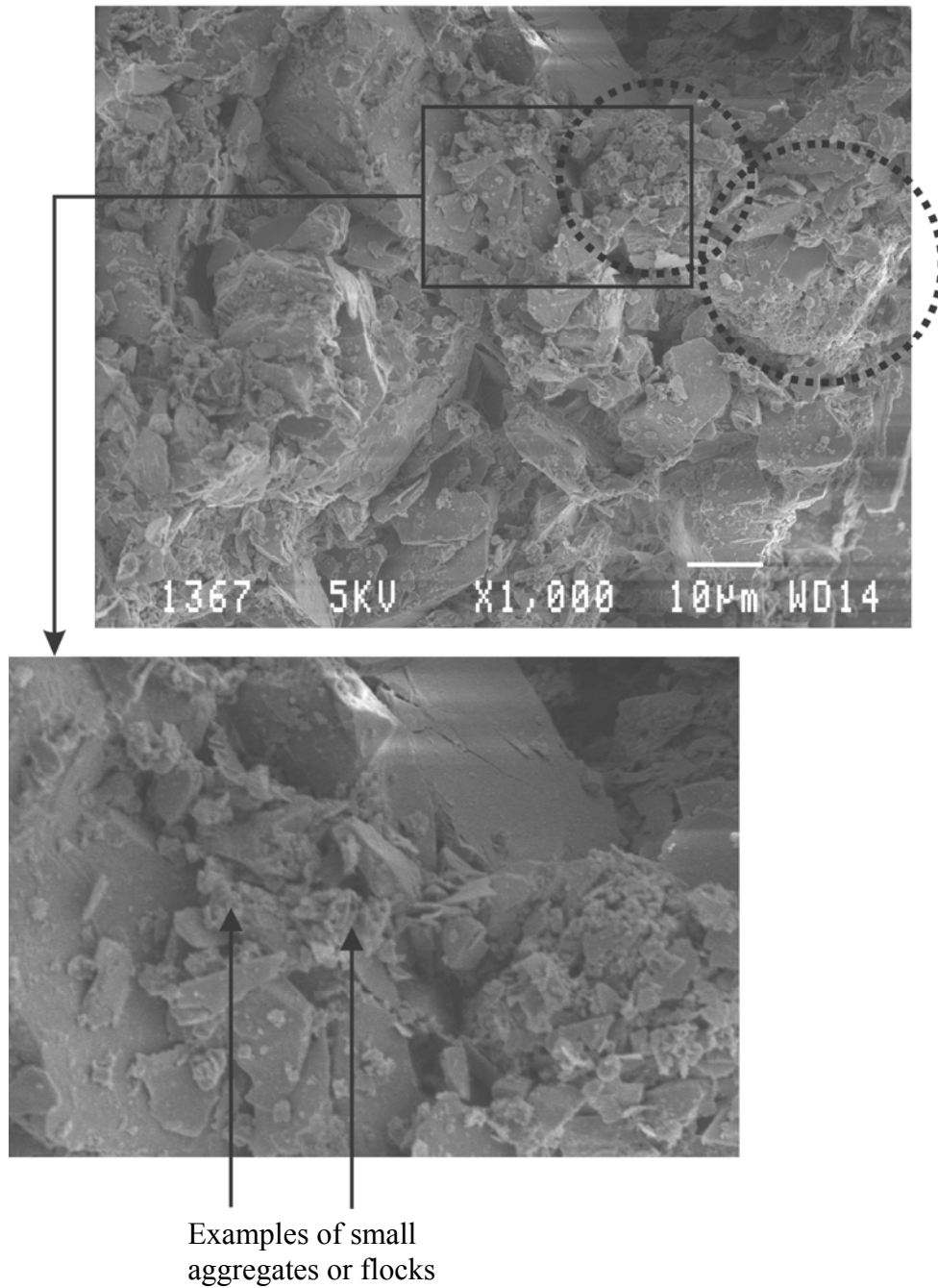
Figure 4-6. Illustration of small and large aggregates in gold tailings

Examples of small
aggregates or flocks

Classification as aggregated required that two criteria be met simultaneously:

1. At low magnifications (50X), sample must appear to constitute 'individual particles'.

2. At high magnifications (1000X), these 'individual particles' must be observed to constitute a collection of rotund and platy particles.

It should be noted that, with the two criteria, samples may have contained some aggregates, but may not have been classified as aggregated. Furthermore, zooming was always at the centre of the images and therefore at higher magnifications the image may not represent the majority of the sample.
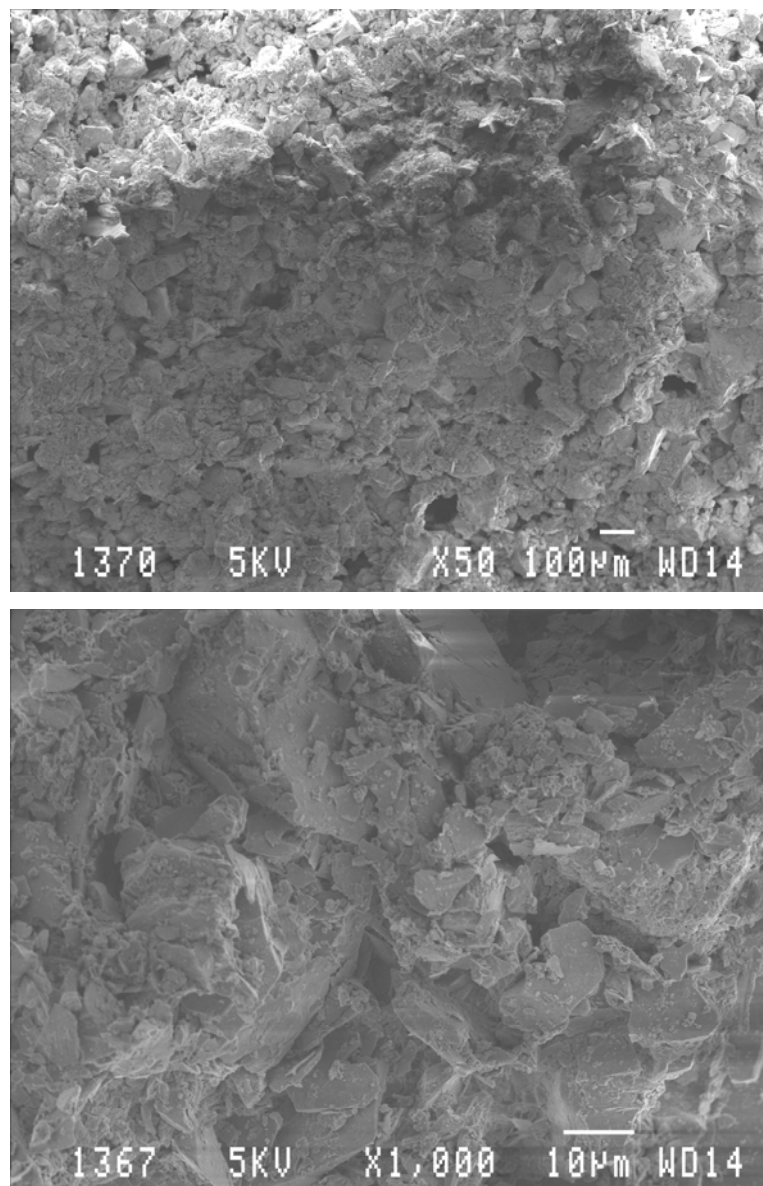
Figure 4-7. Aggregated fabric of gold tailings
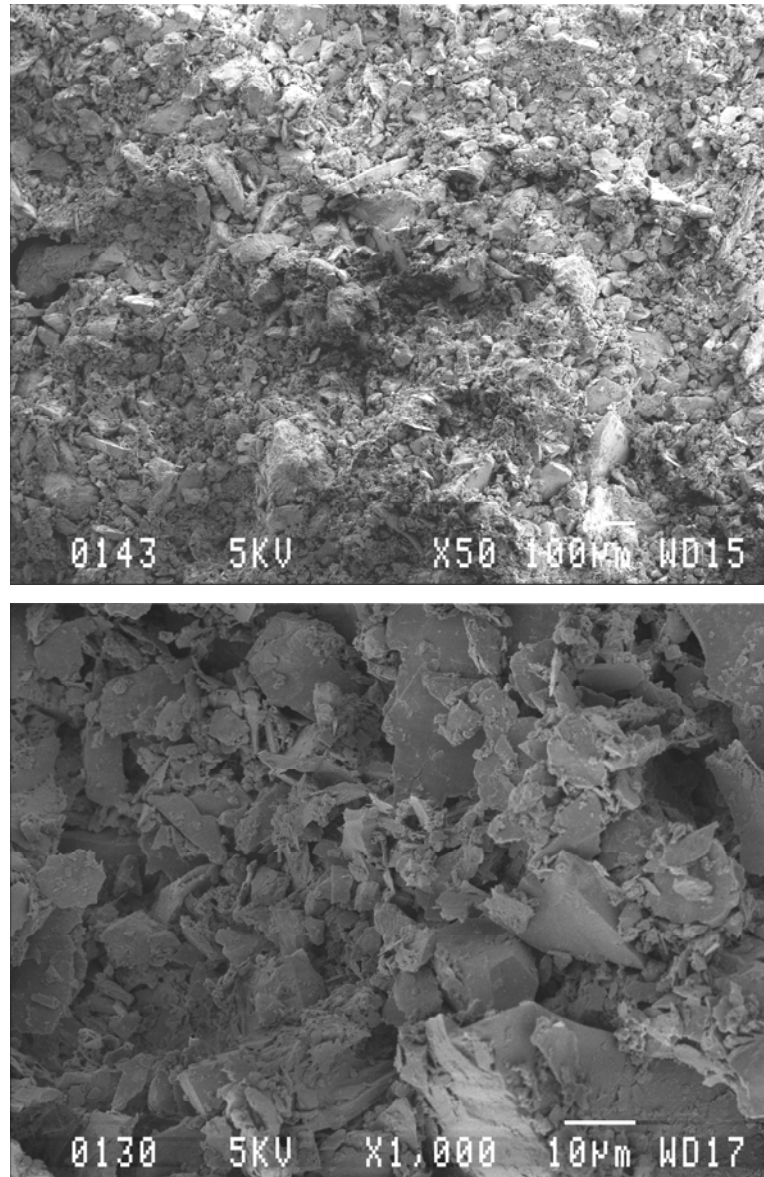
Figure 4-8. Non-aggregated fabric of gold tailings

- *Orientation*: describes the general spatial orientation of the particles and/or aggregates as observed in the SEM images:
    - o *Orientated*: Majority of particles and aggregates are orientated in the same axis (*Figure 4-9 (a)*).
    - o *Non-orientated*: Particles and aggregates are randomly orientated (*Figure 4-9 (b)*).

a)

b)
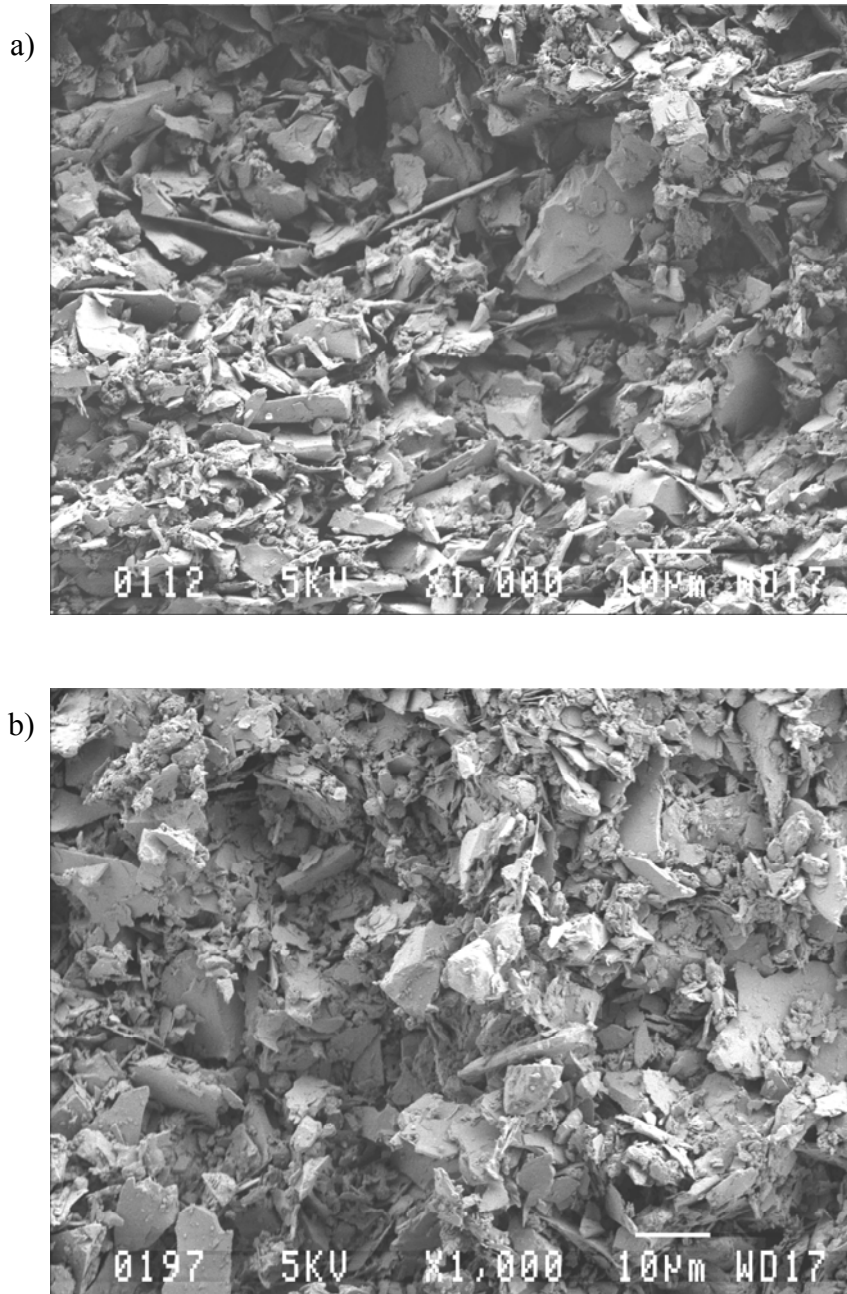
Figure 4-9. Orientated and non-orientated fabric for gold tailings.

To simplify the classification, the fabric was classified into four structural levels:

> Level 1: non-aggregated and non-orientated.
>
> Level 2: aggregated but non-orientated.
>
> Level 3: non-aggregated and orientated.
>
> Level 4: aggregated and orientated.

It should be emphasized that the classification is qualitatively assessed based on the overall appearance of the images as perceived by the author, and results may vary according to the observer. According to the classification described above, the fabric of gold tailings can be classified as shown in *Table 4-1*. A 'consolidation' sample demonstrates the fabric before consolidation and 'shear 200' or 'shear 400' samples show the fabric after consolidation (to 200kPa or 400kPa) and creep, and observed before shear.

Material	History	Undisturbed	Moist tamped	Slurry
Pond	Consolidation	3	1	1
	Shear 200	3	1	1
	Shear 400	3	1	1
Middle beach	Consolidation	1	2	1
	Shear 200	1	2	1
	Shear 400	1	2	1
Upper beach	Consolidation	1	2	1
	Shear 200	1	2	1
	Shear 400	1	2	1

Table 4-1. Levels of fabric observed in gold tailings.

Pond samples

Table 4-1 shows that the undisturbed pond samples have a non-aggregated and orientated fabric (level 3) while both the moist tamped and slurry samples have level 1 fabric which is non-aggregated and non-orientated. Comparison of results shown in *Table 4-1* indicates that all pond samples have similar non-aggregated fabric, irrespective of the sample preparation method or stress history. Upon close inspection, it was clear that flocks could be observed in all pond samples. According to the definition, pond samples are generally classified as 'non-aggregated', despite of the presence of these flocks.

The only difference observed in pond samples was that some horizontal orientation could be observed in undisturbed samples, but not in the moist

tamped and slurry samples. This may be a result of the depositional environment of the undisturbed pond material as described in section 4.2.2. This initial orientation was also observed in the shear fabric samples. This implies that consolidation does not destroy the initial orientation and the initial fabric was preserved after consolidation and creep.

In general it appears that neither laboratory reconstitution methods (moist tamping or slurry) could reproduce the orientated fabric observed. This may be a problem in terms of laboratory testing of pond tailings if the behaviour is sensitive to the sample fabric.

Middle and upper beach samples

Middle and upper beach samples show similar trends in terms of fabric and are thus discussed in the same section. The fabric of undisturbed and slurry middle beach and upper beach samples appear similar with a level 1, non-aggregated and non-orientated classification. This is similar to the conclusions reached by authors such as Vaid et al. (1990) and Vaid and Sivathalayalan (2000), that water pluviation produces a similar sand fabric to that of natural sands. Moist tamped middle beach and upper beach samples however, exhibit a level 2, aggregated and non-orientated fabric. The fabric of the middle and upper beach samples appear similar before and after consolidation, indicating that the initial fabric which ensued upon sample preparation remained intact after consolidation. This difference in fabric observed in gold tailings samples before shear commenced may affect the behaviour of gold tailings during shear.

Typical SEM images of all samples are collated in *Table 4-2*. It should be noted that the images of pond samples are at a magnification of 500 times whereas the middle and upper beach samples are at 50 times magnification.
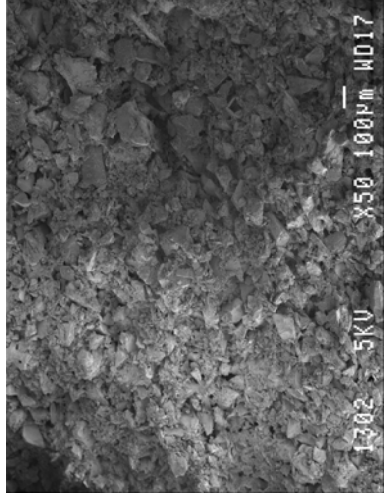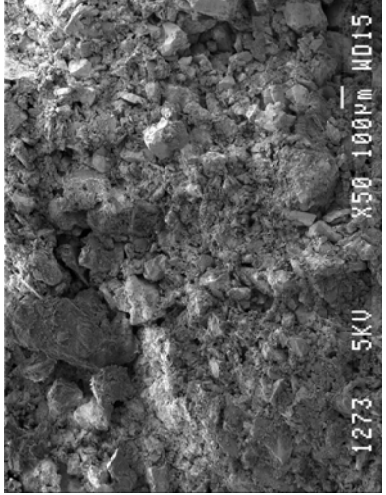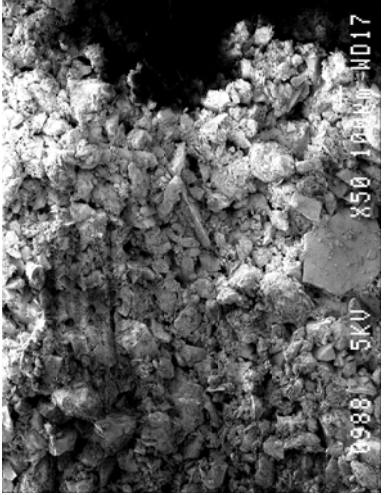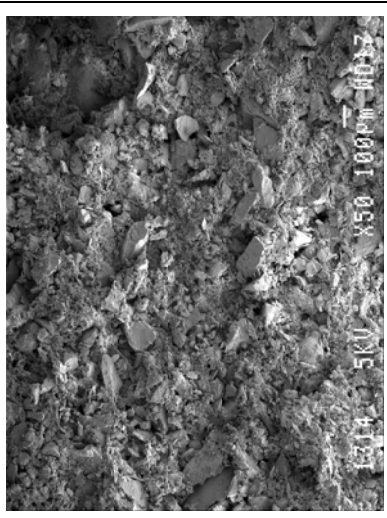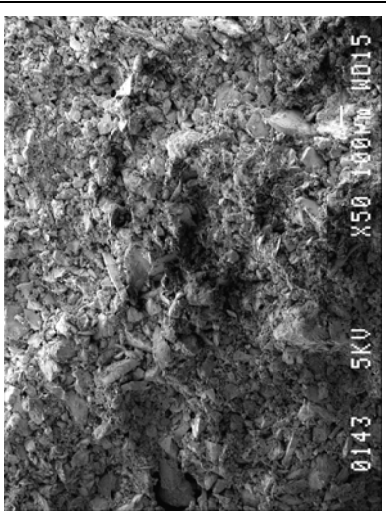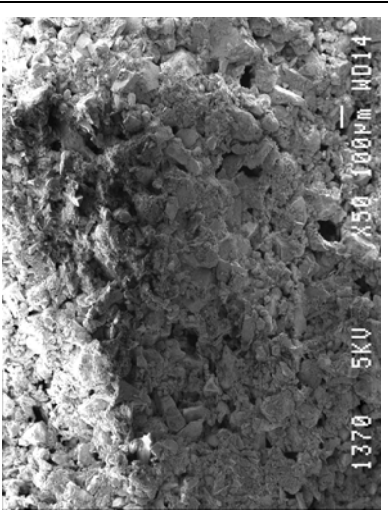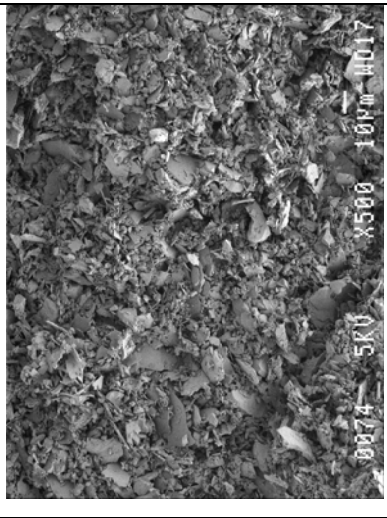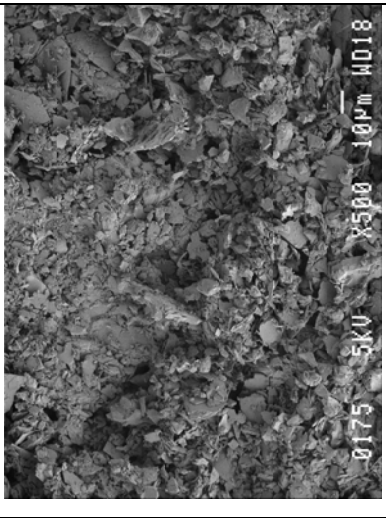
	Undisturbed	Slurry	Moist tamped
Upper beach			
Middle beach			
Pond			

Table 4-2. Typical SEM images of undisturbed and reconstituted gold tailings.

106

4.3   SIGNIFICANCE OF AGGREGATION IN GOLD TAILINGS

In this section, the significance of aggregation in gold tailings is discussed. Natural soils with an aggregated fabric show some difference in behaviour to homogeneous soils and thus the effects of aggregation may be responsible for any difference in behaviour observed in samples prepared using different laboratory preparation methods.

4.3.1   Origin of aggregation

Aggregation in natural soils occurs as a result of swelling and shrinkage as well as biological and chemical processes (Babel et al., 1995). Aggregate formation in natural soils is however, most frequently brought about by stress release and shear failure processes (Hartge and Rathe, 1983).

In a moist tamped specimen, soil particles are held together by suction in the pore fluid which exists between soil particles. The effect may be amplified in material such as gold tailings where a significant amount of fine platy particles are present. Aggregation in gold tailings therefore appears to be an artefact of moist tamping as it is not present in undisturbed or slurry samples.

4.3.2   Particle interaction of aggregated gold tailings

The difference in fabric between aggregated and non-aggregated middle and upper beach samples may be visualized at macro level as simply a difference in homogeneity and at micro scale as a difference in the mode of particle contact. Gold tailings are generally composed of rotund and platy, non-colloidal particles, and the behaviour of the material is dominated by mechanical particle contact. Following the definition of aggregation and non-aggregation, a model can be postulated with regard to particle interaction in aggregated and non-aggregated gold tailings samples. Aggregated samples are composed of platy particles and flocks clinging tightly around the rotund particles forming a stiff outer shell similar to that described in *Figure 4-10 (a)*. The orientation of these platy particles is generally parallel to the surface of

the rotund particle, similar to those observed by Theron (2004). On a macro scale, the aggregates system comprising rotund particles and a stiff platy shell is analogous to a particle with rough but brittle surface, as demonstrated in *Figure 4-10 (b)*. At a particulate scale, isotropic compression will induce forces normal to the orientation of the platy shell, resulting in higher bulk stiffness values for aggregated samples in comparison with undisturbed or slurry samples. Shear force transfer between aggregates will also occur through the platy contacts, but at an angle tangential to the orientation of the platy particles. This results in a reduced shear strength and stiffness in comparison with the undisturbed and slurry counterparts.

a) Idealized aggregated fabric

b) Analogy of aggregated fabric
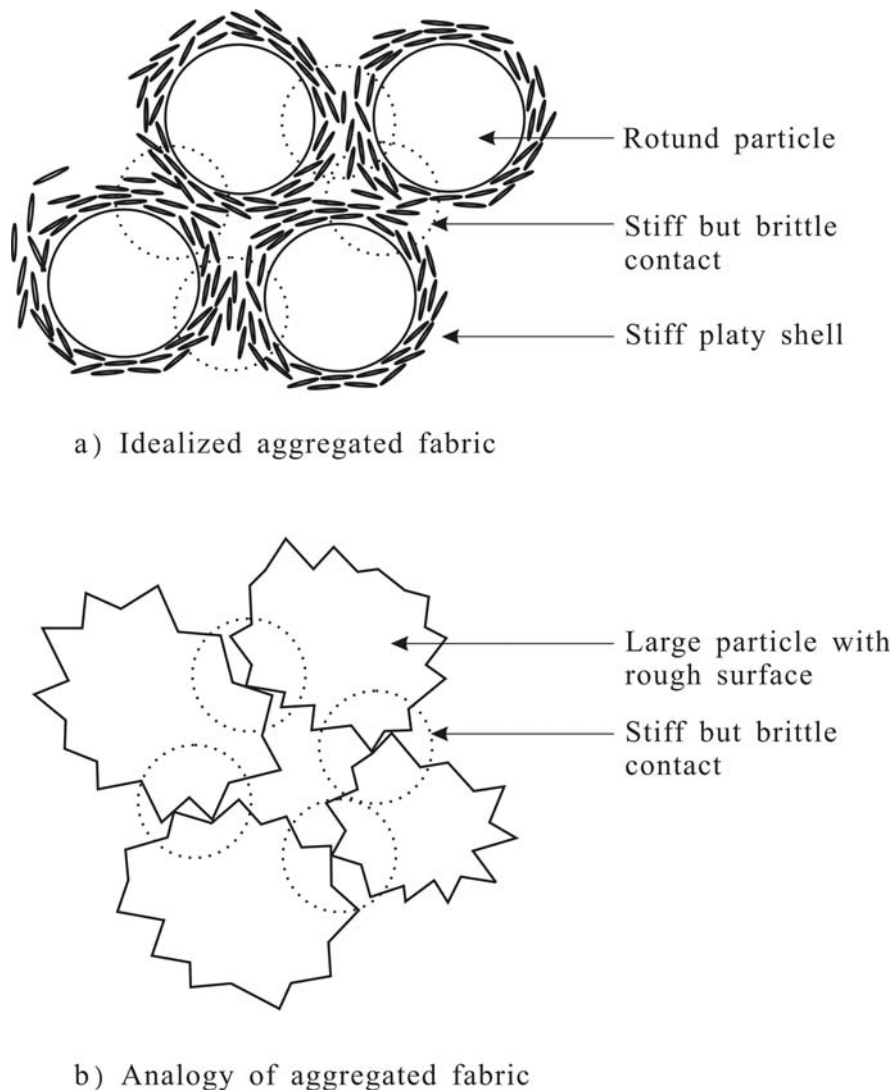
Figure 4-10. Idealized particle interaction in aggregated gold tailings.

The undisturbed and slurry deposited samples exhibit non-aggregated fabric and the mode of particle contact is dependent on the proportion of the platy particles/flocks in the sample. At low platy particle/flock content, rotund particles will be in direct contact with each other and the platy particles and flocks will only occupy the voids between the rotund particles, as shown in *Figure 4-11 (a)*. The behaviour of the sample will be dominated by the rotund particles, with the platy particles and flocks playing a secondary role. At higher platy particle/flock content, as shown in *Figure 4-11(b)*, the rotund particles will be dispersed in a matrix of platy particles and flocks similar to that observed in the pond samples. The behaviour of the sample will be dominated by the platy particle/flock matrix with the rotund particles playing a supporting role.
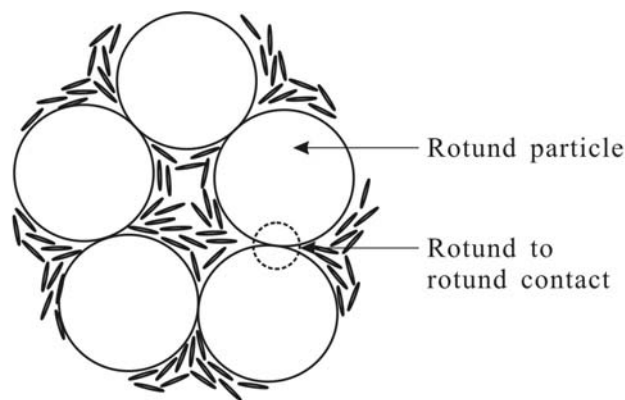
a) Low platy particle content
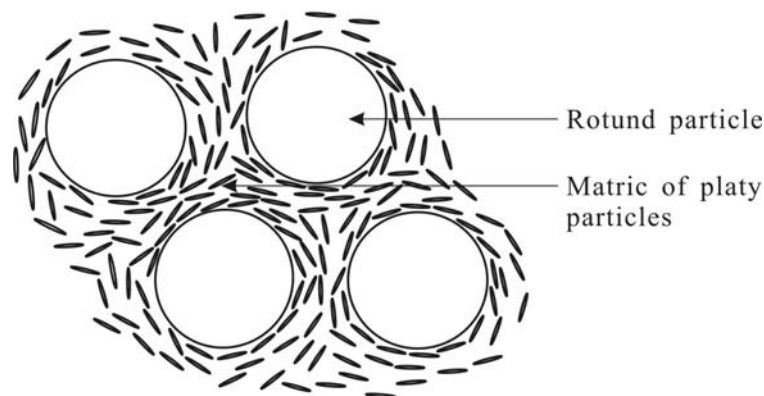
b) High platy particle content

Figure 4-11. Idealized particle interaction in non-aggregated gold tailings.

The postulated models indicate significantly different modes of particle contact in aggregated and non-aggregated gold tailings. The behaviour of cohesionless soils such as gold tailings is dominated by mechanical particulate interaction, and thus it can be expected that some difference in behaviour will be observed in the test samples. Aggregation has been shown to affect the behaviour of natural and artificial soils and this is discussed in the following section.

4.3.3 The effect of aggregation on the behaviour of soils

An aggregated fabric can affect the mechanical behaviour of a soil. Engineering behaviour of cohesionless soils is dominated by mechanical interaction between the particles. In the case of gold tailings, this includes the rolling or sliding of rotund particles and the bending or sliding of platy particles. The possible effects of aggregation on the engineering behaviour of gold tailings will be discussed on a particulate level in this section.

Hydraulic conductivity

Aggregated soils consist of inter-aggregate pores (pores between aggregates) and intra-aggregate pores (pores between particles within aggregates). The inter-aggregate pores are larger and more continuous, while the intra-aggregate pore system is smaller and less continuous (Horn et al., 1995). The large inter-aggregate pores facilitate the movement of water through the soil, resulting in a higher permeability in aggregated soils in comparison with homogeneous soils.

Compressibility

Olsen and Mesri (1970) investigated the compressibility behaviour of ground muscovite and concluded that at high consolidation pressures, compressibility and swelling are governed by the flexure of the nearly parallel platy particles. In gold tailings, however, platy particles are actively or passively located between the rotund particles in a random orientation. Compressibility should thus be controlled by the mechanical sliding of the platy particles relative to each other and also relative to the rotund particles.

Matyas et al. (1984) investigated the compressibility of uranium tailings samples and concluded that the fine tailings appear to be more compressible than the coarse tailings. This was noted by other researchers such as Robertson (1987) and Vermeulen (2001). The compressibility of the undisturbed fine silt sample was also higher than its reconstituted version. It is, however, unclear whether moist tamping was used to prepare the reconstituted samples.

According to Terzaghi (1925), the compressibility of cohesionless materials is determined by the grain size, uniformity, volume of voids and mica content. Aggregation in gold tailings can be viewed as a form of heterogeneity which may affect the compressibility of gold tailings. Particle interaction in moist tamped samples may be similar to that of sand-mica mixtures. Moore (1971) showed that the compressibility of sand could be increased with the addition of mica. It seems that the introduction of mica between the sand particles increases the compressibility of the mixture. The mica-sand mixture is analogous to gold tailings, which is essentially a mixture of platy and rotund particles. Mica is generally significantly larger than typical tailings platy particles, and is less affected by surface forces. The analogy of mica-sand mixtures to gold tailings would then be invalid, as surface forces between platy particles may yield a stiffer sample with lower compressibility.

Stiffness

The small strain shear stiffness G_{max} of undisturbed and moist tamped silty sand tailings and natural silt samples at similar void ratios was investigated by Høeg et al. (2000). They concluded that G_{max} obtained for moist tamped samples is generally 20 to 30% lower than that obtained for the undisturbed samples. As no evidence of cementation was found, the effect was ascribed to differences in the fabric.

The stiffness of a soil is a measure of the deformation response to a given stress increment. A sample with high compressibility also has a lower stiffness. It is expected that undisturbed and slurry samples which have more uniform fabric will have higher small strain stiffness than moist tamped samples which are dominated by platy contacts. At medium and large strains the stiffness

should converge to a unique value which is material dependent, as all fabric is progressively destroyed upon continued shear.

Shear behaviour

It has been shown by researchers such as Zlatovic and Ishihara (1997) that the effective angle of friction is independent of the fabric, as all fabric is destroyed when the sample reaches the ultimate condition.

According to Horn et al. (1995), undisturbed, aggregated soils have higher strength than homogenized soils, but both are significantly lower than that observed for a single aggregate. The stress-strain curve for the aggregate also shows a clear peak corresponding to the strength of the aggregate where after the strength decreases drastically upon continued straining.

According to the postulated particle contact model, moist tamped samples will demonstrate strain-softening behaviour when the platy contacts between the aggregates disintegrate.

4.4   SUMMARY

The chapter presented the fabric of gold tailings observed from SEM images of samples tested as part of the experimental programme. The SEM images showed that some visible differences could be observed in the fabric of gold tailings. According to the fabric observed, modes of particle interaction were postulated. In the next chapter, the observed behaviour will be explained in accordance with the postulated particle contact model.

Chapter 5

Analysis and Discussions

5.1   BACKGROUND

The purpose of this chapter is to analyse and interpret the data obtained from the experimental work. The hypothesis for this research states that **accurate simulation of the behaviour of gold tailings under laboratory conditions requires appropriate replication of the material fabric.** All tools and methods required for the analysis are discussed. Results from the preliminary testing are also included in this chapter.

5.2   PRELIMINARY TESTING RESULTS

Preliminary tests were included to classify the material and to aid in the sample preparation for the main tests. In situ conditions were determined from undisturbed triaxial samples and are summarized in *Table 5-1*.

	In situ moisture content	Void ratio	Deg. of saturation
Upper beach	12.73	0.61	0.57
Middle beach	17.32	1.09	0.43
Pond	48.69	1.42	0.94

Table 5-1. In situ conditions for the three sampled positions.

The in situ conditions are in agreement with those presented in the literature. The moisture content and void ratio of tailings in general increase down the

beach of a tailings impoundment due to an increase in the amount of fine particles. The degree of saturation, however, may seem high for a dam which has been decommissioned for 10 years. The high degree of saturation is substantiated by the high rainfall in the summer season and periodic watering for dust prevention purposes. It was reported that watering occurred every three months.

5.2.1 Particle density

Particle density or specific gravity was determined using the density bottle method according to BS 1377: Part 2:1990:8.3. According to Vermeulen (2001), gold tailings have a typical specific gravity of 2.74Mg/m³, irrespective of sampling location or sample size and shape. *Gs* results from the density bottle test are given in *table 5-2*.

	Gs (Mg/m³)				
	Individual results				Average
Pond	2.739	2.745	2.754		2.75
Middle beach	2.687	2.692	2.691	2.685	2.69
Upper beach	2.709	2.728	2.723	2.727	2.72

Table 5-2. Specific gravity results from density bottle test.

The *Gs* results are consistent with those indicated by Vermeulen (2001) in that tailings samples from different positions have similar *Gs* values. This may be explained if the tailings are derived from the same parent rock.

5.2.2 Particle size distribution

Grading of the pond, MB and UB material was determined using the wet-sieving procedure followed by hydrometer sedimentation. Sedimentation makes use of Stoke's law, which assumes spherical particles, and according to

Vermeulen (2001), the method may yield slightly finer grading results due to the elongated or flattened shape of gold tailings particles.

Figure 5-1 shows that the middle and upper beach samples have very similar grading curves, despite the middle beach samples being positioned much lower down the beach. This is typical of open-ended discharge impoundments, where the slurry flows in channels down the beach, resulting in pockets of coarse material alone the beach. The pond sample was, however, significantly finer. It is interesting to note that, despite the MB and UB samples having similar grading, the MB samples have a significantly higher void ratio of 1.09 compared with a void ratio of 0.61 for UB samples. It is speculated that the in situ void ratio is less dependent upon the grading and more sensitive to the depositional environment.
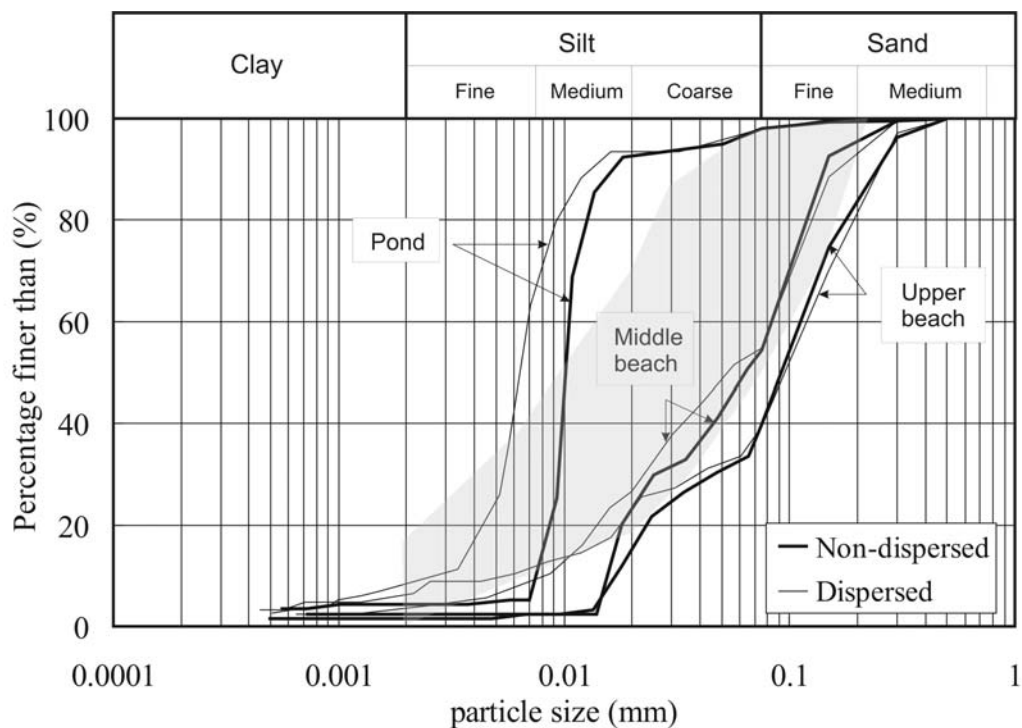
Figure 5-1. Grading of the pond, middle and upper beach material.

The grading curve can generally be described by properties such as fines content *FC* (< 0.075mm), clay content *CC* (<0.002mm), coefficient of uniformity C_u, coefficient of curvature C_Z and D_{50}. For references purposes, grading curve properties have been included in *Table 5-3*.

	Pond		Middle beach		Upper beach	
	Non-Disp.	Disp.	Non-Disp.	Disp.	Non-Disp.	Disp.
FC (%)	98	98	54	55	40	40
CC (%)	4	8	2	3	2	6
C_u	1.5	2.6	5.3	10.5	6.7	24.1
C_Z	1.0	1.6	0.5	0.8	0.9	2.2
D_{50} (mm)	0.010	0.006	0.064	0.053	0.091	0.095

Table 5-3. Grading curve properties for the three test materials.

Grading curves for the fine (pond) and the coarse (middle and upper beach) material approximately coincide with the grading envelope of typical South African gold tailings (Blight and Steffen, 1979) shown in the shaded area in *Figure 5-1*. The material tested in this thesis is thus a good representation of typical South African gold tailings.

Values of coefficient of uniformity for all materials tested are generally smaller than 36, which is the value for the 'ideal' Fuller Curve (Fuller and Thompson, 1907). The Fuller Curve describes the uniformity properties of spherical particles for the densest possible state of packing. A sample of spherical particles with a C_u of less than 36 has an abundance of fines that hold the coarse particles apart. The sample will also be less dense than the maximum density. If C_u is greater than 36, then the voids between the coarse particles are not completely filled with fines. In the case of the gold tailings tested, C_u values are significantly smaller than 36, indicating that the coarse particles are not all in contact with each other, and may be held apart by the finer particles. This is also confirmed by the SEMs presented in the previous chapter. It is also consistent with the results that C_u decreases down the beach as the material becomes finer. The Fuller Curve is, however, based on the arrangement of spherical particles, while tailings fines are predominantly platy. It is unclear how particle shape will influence the Fuller Curve, but it is

suspected that an increase in the proportion of platy particles may result in increased difficulty for samples to reach the densest state.

A well-graded soil has a coefficient of curvature C_Z between 1 and 3 (Craig, 1997). C_Z values for the gold tailings material used in this thesis range between 0.5 to 2.2 and can therefore be considered well-graded.

5.2.3 Atterberg limits

For the purpose of the project, only the liquid and plastic limits were determined. The plastic limit for the MB and UB materials could not be determined as the material crumbled before a three millimetre diameter 'worm' could be obtained. Liquid and plastic limits for the three test materials are summarized in *Table 5-4*.

	Pond	Middle beach	Upper beach
Liquid limit (LL)	51	30	25
Plastic limit (PL)	39	NA	NA
Plasticity index (PI)	12	NA	NA

Table 5-4. Summary of Liquid and plastic limits for the three test materials.

The Atterberg limits shown in *Table 5-4* correspond to the grading observed in *Figure 5-1*. The middle and upper beach samples have similar grading and therefore similar liquid limits. The coarseness of these two material types prevents the formation of a 3mm 'worm' and thus any estimates of plasticity. The pond material, however, has a significantly higher *LL* and some plasticity.

According to the Unified Soil Classification System, the pond material can be classified as ML-MH while the MB and UB materials are classified as SM.

5.2.4 Limiting density

Limiting density tests were done at various moisture content to estimate the range of void ratios that can be expected for the material. It was also assumed that the closer the target (in situ) void ratio is to the minimum void ratio, the less the volumetric collapse would be during flushing. In this way, the damage to the initial fabric of the sample could be minimized. Results for the maximum and minimum density tests are shown in *Figure 5-2*. It should be noted that the limiting densities determined in this thesis can only be used as a guideline, and not for reference purposes, as standard BS and ASTM methods specify the use of dry material while the minimum and maximum densities of gold tailings were determined at various moisture content (as described in section 3.4.4). Furthermore, the maximum density of dry samples could not be determined as material was blown out between the weight and the mould by pore air pressure during compaction. The moisture content used for moist tamped samples is also plotted against the target (in situ) void ratios for each material. These are shown in full circles.
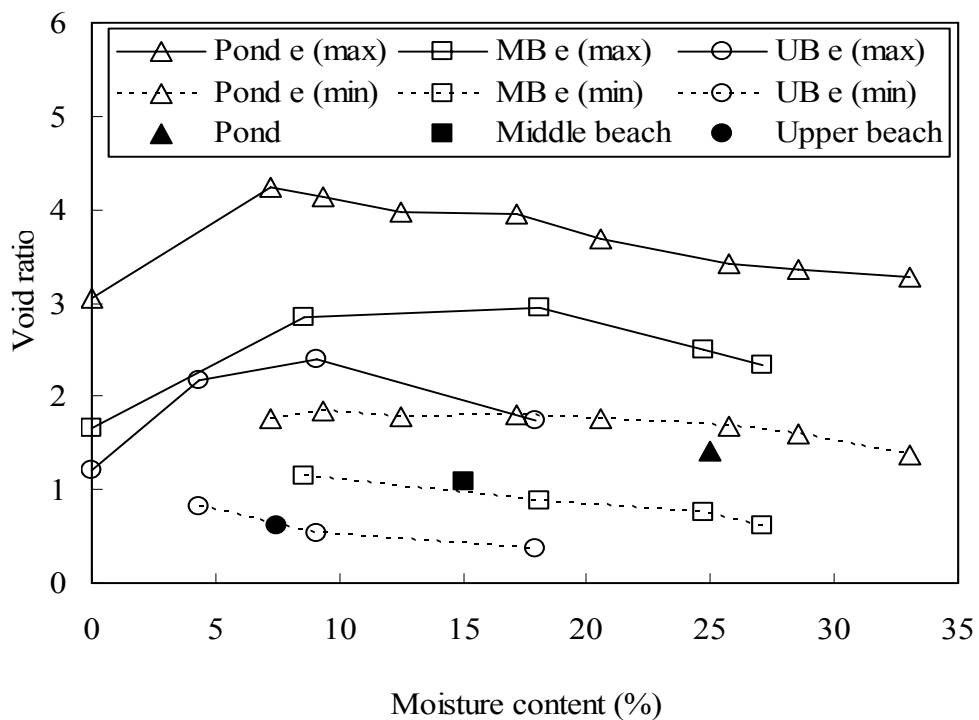
Figure 5-2. Limiting density tests for the three materials.

The void ratio of a soil, relative to the maximum and minimum obtainable void ratios can be expressed as the density index, I_D:

$$I_D = \frac{e_{max} - e}{e_{max} - e_{min}}$$ *Equation 5-1*

where e_{max} and e_{min} are the maximum and minimum void ratios respectively and e is the in situ or target void ratio. The density indices at preparation moisture content are 1.17, 0.95 and 1.03 for pond, middle and upper beach material respectively. It should be noted that these values cannot be compared with those derived from standard maximum and minimum density tests as the standard tests only involve the use of dry material.

The results show that the maximum void ratio increases drastically when the moisture content is increased by a few percent from the dry condition. A peak is reached after which further addition of moisture results in a decrease in the maximum void ratio. It is interesting to note that the peaks for all three material types were found in a relatively narrow range of 7% to 9% moisture, despite the differences in the material type.

The minimum void ratio for all three material types appears flat with a gradual decrease with increasing moisture content. This implies that the in situ void ratio would lie close to or below the minimum void ratio line for almost the entire range of moisture content tested. It was initially decided that the choice of preparation moisture content for moist tamped samples would be based on the relative position of the in situ void ratio and the minimum void ratio at specific moisture content. As changes in minimum void ratio were small with increasing moisture content, it was decided that the preparation moisture content for moist tamped samples would be based on the appearance of the sample (to prevent the formation of visible lumps) and the strength (during handling) as described in section 3.6.2.

The target (in situ) void ratio for the pond material is below the minimum void ratio obtained for the same material at the preparation moisture content (25%

for pond material). This implies that significant preparation energy, such as using the hydraulic jack, is required to construct the moist tamped samples at the target void ratio. The force required decreased as the target void ratio increased in comparison with the minimum void ratio, as seen with the middle and upper beach samples at the preparation moisture content (15 and 7.5% for middle and upper beach samples respectively).

It is interesting to note that the target void ratios for all three material types were close to the minimum void ratio curve shown in *Figure 5-2*. It appears that the in situ depositional environment has similar compaction effort as the vibratory table method described in 3.4.4 for the determination of minimum void ratio. As all samples were surface samples with little or no surcharge load, it is reasonable to assume that this reduction in void ratio is a direct result of suction pressures between the particles during desiccation. As estimated by Westraad (2004), suction pressures on the beach may be of the order of 150kPa.

5.2.5 Sedimentation tests

Sedimentation tests were done using dispersant and flocculent to increase the void ratio obtainable for slurry samples. During the testing programme, it was discovered that the MB and UB slurry samples cannot be constructed at the target void ratio using tap water alone. UB slurry samples needed to be at a void ratio of 0.6, but could only be prepared at a maximum void ratio of 0.5. The target void ratio of MB material was approximately 1.1, but slurry samples could only be prepared at a maximum void ratio of 0.8. Slurry samples for pond material could be prepared at the target void ratio of 1.4 with relative ease. As slurry samples for the middle and upper beach material could not be prepared at the target (in situ) void ratio, dispersant and flocculent were used to increase the initial void ratio of the slurry samples.

The effect of various concentrations of dispersant and flocculent on void ratio was thus investigated in sedimentation tests. The effect of dispersant or flocculent content can be seen in *Appendix E figures E-1* to *E-6* which plots

void ratio against time. Void ratio was calculated from the height of the soil column in the cylinder. The final void ratios (recorded after 5000 minutes) of the three materials are shown in *Figure 5-3*.

Results of the sedimentation tests showed that the addition of dispersant had a varied effect on the final void ratios obtained. Pond material showed an initial decrease followed by an increase in final void ratio with the increase in dispersant content. For middle and upper beach material, an initial increase is observed followed by a decrease in the final void ratio with increasing dispersant content. No consistent explanation was reached for the observed behaviour.
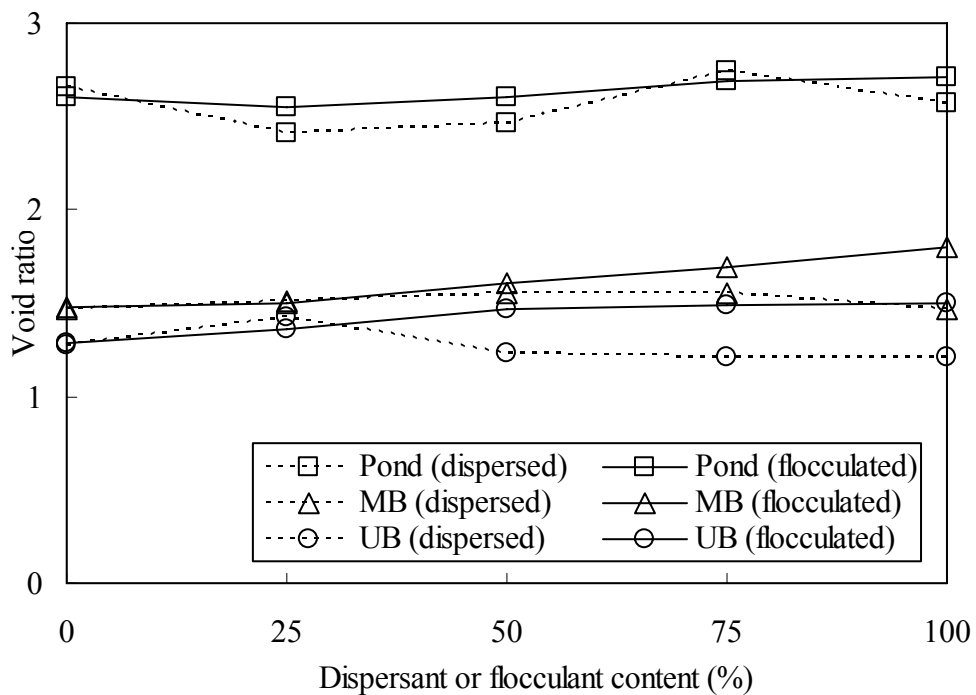
Figure 5-3. Final void ratio of the sedimentation test.

Although no conclusion could be made with regard to the final void ratio, something interesting can be observed from the plots of void ratio with time attached in *Appendix E*. For both pond and middle beach dispersed, a gradual reduction in void ratio with time is observed. For upper beach material, however, there seems to be a limiting dispersant concentration before which the samples become effectively dispersed. The void ratio of a well dispersed sample appears to increase with time due to the settlement of the platy fines.

The void ratio of samples not fully dispersed decrease with time, similar to that observed in pond and MB samples.

The addition of flocculent, however, results in an increase in the final void ratio for all materials. There also seems to be a limiting flocculent content where after further addition of flocculent will have no effect on the final void ratio. This limiting flocculent content seems to vary with material type, but appears to be in the range of 75-100%. The addition of flocculent also has the effect of increased rate of settlement for all materials.

The target void ratio for middle beach slurry samples was obtained with the addition of flocculent and target void ratio for upper beach slurry samples was achieved with the addition of dispersant.

5.3   VOLUME CHANGE BEHAVIOUR

Volume change during undrained triaxial testing includes volume changes during flushing, consolidation and creep. All volume changes were calculated in terms of axial deformation measured from the local LVDT outputs under isotropic conditions from *Equation 5-2*.

$$\varepsilon_v = (1 - \varepsilon_a)^3 \hspace{4cm} Equation\ 5\text{-}2$$

where ε_v and ε_a are volumetric and axial strains respectively.

5.3.1   Volume change during flushing

Collapse during flushing occurs when water is introduced into a soil with a metastable fabric. On the other hand, swell is initiated by the reduction of effective stress by unloading and/or the adding of water. Volume changes were monitored for all test samples and are summarized in *Tables E-1, E-2* and *E-3* in *Appendix E* for pond, middle beach and upper beach materials respectively. The volume changes in the samples cannot be compared directly,

as the initial target void ratio varied to accommodate the difference in consolidation behaviour. Some observations can, however, be made with regards to the volume change behaviour during flushing.

For all three material types, the undisturbed consolidation and shear samples showed volumetric collapse in the order of 2% during flushing.

Moist tamped samples may be constructed to void ratios well above the standard maximum value due to capillary effects between the grains (Zlatovic and Ishihara, 1997). Yi (1991) demonstrated that silty soils prepared at a loose state may display a considerable decrease in volume due to loss of the capillary forces upon wetting. This is observed to some extent in the volumetric behaviour of gold tailings during flushing. The volume change can be related directly to the effort of sample preparation for moist tamped samples. The amount of collapse is indirectly proportional to the effort required for sample preparation. The samples may even swell, as seen in the pond samples, when high preparation effort is required. Preparation of moist tamped samples involves the compaction of aggregates with some strength. For the pond material, a significant amount of effort was required, resulting in an increasingly stable fabric with significant stresses being locked in the sample. The stress is released with the addition of water during flushing, resulting in the volumetric swell observed. Middle and upper beach samples, however, require far less preparation effort. The result is a metastable fabric which collapses during flushing.

No significant volume change was expected for slurry samples, as the samples were prepared in water. There was, however, a significant decrease in volume observed in the middle beach slurry samples prepared at very high void ratios with the addition of flocculent. The addition of flocculent creates an aggregated fabric at high void ratio which cannot sustain the initial cell pressure. Volume changes in slurry samples can thus not be classified as collapse or swell, as the samples were prepared to near full saturation.

5.3.2   Consolidation behaviour

Consolidation was analysed for the shear-200 samples as well as the consolidation samples. It should be noted that as the consolidation behaviours differ, the initial void ratio before consolidation for the shear-200 samples was not constant for each material type. They, however, arrived at the same void ratio after the consolidation and creep, and could thus be sheared at the same state.

Consolidation characteristics for the three materials could be estimated from the shear-200 samples, which underwent standard isotropic triaxial consolidation. The coefficient of consolidation, C_v, can be determined using Taylor's well-known root time method:

$$C_v = \frac{0.848d^2}{t_{90}}$$

Equation 5-3

where d is the drainage path length and t_{90} is the time to 90% consolidation. *Equation 5-3* is based on Terzaghi's theory of one-dimensional consolidation, and application to isotropic triaxial consolidation is questionable. The issue is complex and is not discussed in this thesis. Readers can refer to the work of Biot (1941) for generalization of Terzaghi's one-dimensional consolidation theory to three dimensions. The coefficients of consolidation values for all shear-200 samples are summarized in *Table 5-5*. C_v values are expressed in m^2/year.

	Coefficient of consolidation, C_v (m^2/year)		
	Pond	Middle beach	Upper beach
Undisturbed	96	697	2862
Slurry	228	2222	9402
Moist tamped	180	1367	3339

Table 5-5. Coefficient of consolidation for shear-200 samples.

Upon first inspection of the results in *Table 5-5*, it appears that the C_v values are high. Although high C_v values can be expected for coarse materials such as the middle and upper beach, the validity of Darcy's law in Terzaghi's one-dimensional consolidation theory may be questionable. At high hydraulic gradients, flow may be turbulent if pore sizes and flow rates are sufficiently great, and Darcy's law (which assumes laminar flow) may not apply. Grading results in *Figure 5-1* and *Table 5-3* indicate that the test material is generally silt or clay-sized, with few sand-sized particles. The SEM images also showed that pore size may be a maximum of 100μm. The combination of small particle and pore size for gold tailings suggests that turbulent flow is not present and Darcy's law is still valid.

A practical aspect with regard to triaxial consolidation of highly permeable materials with high C_v values is that as consolidation occurs quickly, the accuracy of volume gauge reading is reduced. Estimation of C_v values from consolidation data may also be difficult and more subjective.

The high hydraulic gradient may, however, affect the fabric of the samples observed from the SEM images. As discussed in section 4.3.2, platy particles or flocks which exist in the voids between the rotund particles (*Figure 4-8*) are passive and non-load-bearing. Under high hydraulic gradients, these passive particles may migrate to create a non-uniform fabric. Migration of fine particles within a soil matrix may also block or unblock interconnected voids and affect the result of consolidation (Mitchell and Soga, 2005).

Table 5-5 indicates that the C_v values were in the same range as those summarized in *Table 2-7* for gold tailings. It can also be seen that C_v increases up the beach as would be expected as the material becomes coarser.

The coefficient of consolidation is of the same order of magnitude for the pond samples. This is validated by the similar fabric observed for pond material. As no side drains were used, the only drainage path in all the triaxial samples was vertical, and the horizontal particle orientation observed in the P-I-200 sample may have caused a slightly lower C_v value.

The aggregated fabric observed may have contributed to the high C_v values in moist tamped samples of middle and upper beach material. Aggregation results in a high connectivity inter-aggregate pore system to facilitate drainage. High permeability coupled with the unstable R-P-R particle contact resulted in the observed high coefficient of consolidation.

Cell pressure for the consolidation tests was ramped at a rate of 10s/kPa. Consolidation was limited to 1000 or 900kPa effective stress (depending on back pressure used) due to the cell capacity of 1300kPa. Reconstituted samples were prepared to the same void ratio as the undisturbed sample after saturation. In this way consolidation samples could be consolidated at the same initial void ratio and the effect of fabric on consolidation could then be investigated. Void ratios for all consolidation samples before consolidation are summarized in *Table 5-6*. The difference is defined, in percentage, as the difference between the reconstituted (moist tamped and slurry) samples and the undisturbed samples. As mentioned in section 3.2, consolidation samples were prepared to a target void ratio difference, Δ, of two percent.

	Pond		Middle beach		Upper beach	
	Void ratio	Δ (%)	Void ratio	Δ (%)	Void ratio	Δ (%)
Undisturbed	1.374		1.097		0.628	
Slurry	1.377	0.4	1.105	0.7	0.636	1.2
Moist tamped	1.376	0.3	1.076	1.9	0.633	0.7

Table 5-6. Void ratios before consolidation of all consolidation samples.

Consolidation results for the three materials with different fabrics are shown in *Figure 5-4*. A distinct change of slope can be observed in the compression curve for the undisturbed pond sample, clearly defining the pre-consolidation pressure. The compression curves of undisturbed middle and upper beach samples show gentle curvature over the test pressure range. This is characteristic of sand behaviour where the transition from elastic to plastic

deformation is gradual, and relatively high confining stresses are required to locate the normal consolidation line.
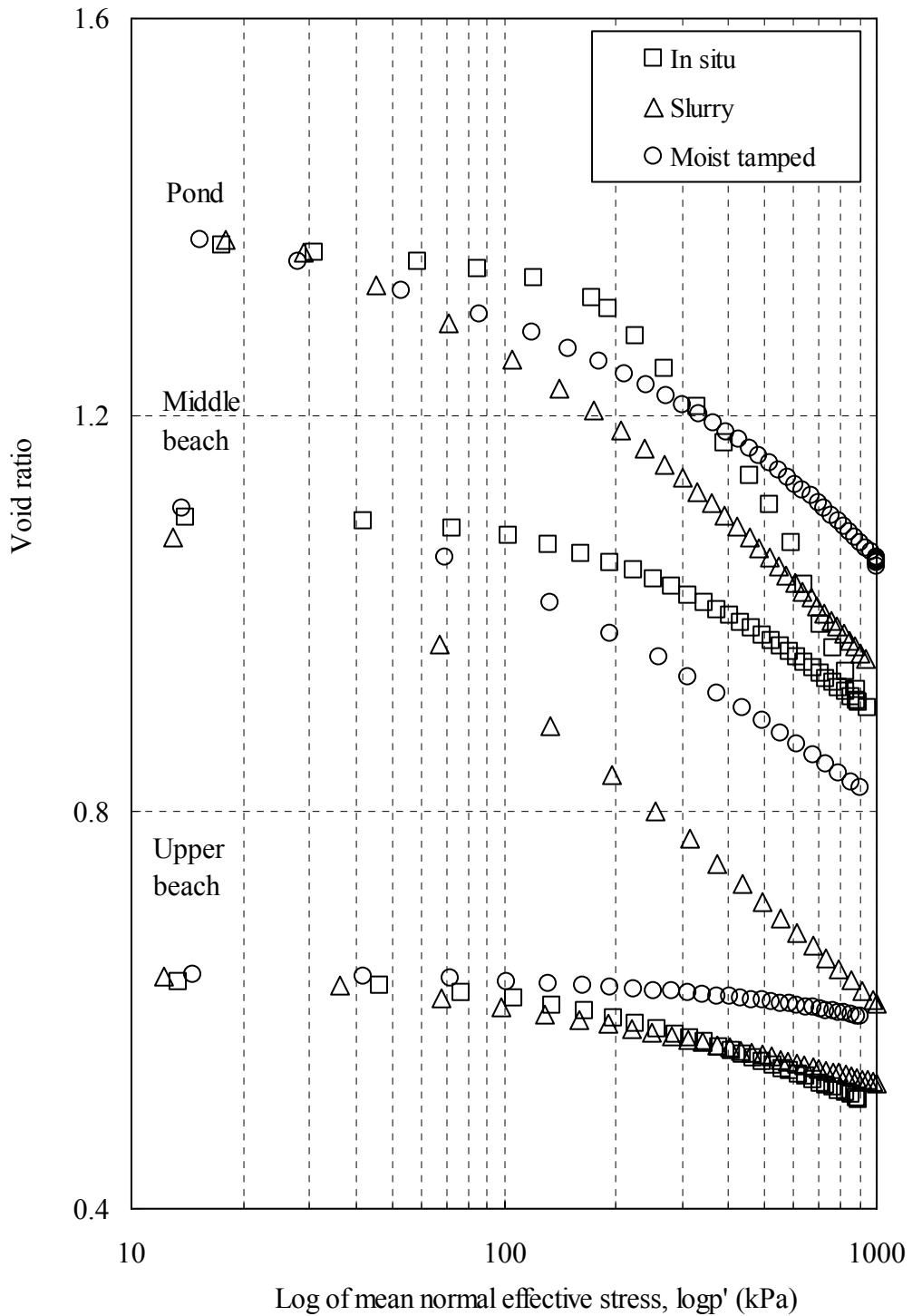
Figure 5-4. Consolidation results for the three materials.

Two parameters were used to quantify and compare the consolidation behaviour of gold tailings: the 'initial' slope and the compression index, *Cc*. The 'initial' slope was estimated from the first 5 data points on the consolidation curve and is an indication of the initial behaviour of the samples. *Cc* was estimated from last 5 data points of the consolidation curve, and is the best estimation of the linear slope of the normal consolidation line from the available data. The 'initial' slopes and the *Cc* values of the test samples are summarized in *Table 5-7*.

	Pond		Middle beach		Upper beach	
	Initial	*Cc*	Initial	*Cc*	Initial	*Cc*
Undisturbed	0.040	0.656	0.028	0.279	0.023	0.157
Slurry	0.155	0.429	0.187	0.268	0.036	0.070
Moist tamped	0.104	0.370	0.095	0.342	0.010	0.099

Table 5-7. 'Initial' slope and Cc of the consolidation samples.

A consistent trend can be observed in the 'initial' slope of the gold tailings samples. Slurry samples showed the highest 'initial' slope while the undisturbed samples generally had the lowest 'initial' slope, with the exception of the UB-I-400. This implies that both the slurry and moist tamped samples have lower initial bulk stiffness in comparison with the undisturbed samples. Bulk and shear stiffness is discussed in section 5.4.

Isotropic compression of a soil can also be expressed in terms of critical state soil mechanics. The normal compression line can be defined in terms of critical state parameters λ and N in the *Equation 5-4:*

$$v = N - \lambda \ln p' \hspace{4cm} Equation\ 5\text{-}4$$

where λ defines the slope of the normal consolidation line NCL in the compression (v-lnp') plane and N defines the NCL at $p' = 1$kPa. Although from *Figure 5-4* it appears that the normal consolidation line was reached,

values of λ were nevertheless estimated from the consolidation data available. Values of λ (obtained from the last 5 data points) are summarized in *Table 5-8*. The difference in C_c and λ values at the end of the test is in agreement with the findings from the SEM images that the fabric was not destroyed at large isotropic stresses and strains.

	Pond	Middle beach	Upper beach
Undisturbed	0.281	0.121	0.068
Moist tamped	0.154	0.116	0.031
Slurry	0.186	0.144	0.043

Table 5-8. Critical state parameters λ for gold tailings.

Vermeulen (2001) reported λ values for fine gold tailings to be in the range of 0.1 to 0.17 and for coarse and whole tailings to be in the range of 0.04 to 0.07. The λ values for pond and upper beach samples are consistent with those presented by Vermeulen (2001) for fine and coarse gold tailings.

The consolidation results indicate that the pond samples have the highest compression and the upper beach exhibits the lowest C_c and λ values. It can be expected that the pond samples, having a behaviour dominated by platy particles which can bend and slide, will yield the higher C_c and λ values than middle or upper beach samples. The behaviour of middle and upper beach samples are dominated by the rotund particle and thus yield a lower slope during isotropic consolidation.

Values from *Table 5-7* and *Table 5-8* show that on average, reconstituted samples exhibit 40% lower C_c and λ values than undisturbed counterparts, with the exception of the higher slope for the middle beach slurry sample (which may be the result of the flocculated fabric). Although the block samples appeared uniform, undisturbed samples may nevertheless contain some fissures or cracks which would significantly lower the bulk stiffness of these samples and result in a higher slope during consolidation. Moist tamped

samples show slightly lower C_c and λ values than the slurry deposited counterparts. This may be as a result of the isotropic compression forces being normal to the orientation of the platy particles as suggested in section 4.3.2. C_c and λ values of the moist tamped samples were on average 25% lower than those of the slurry samples.

5.3.3 Secondary compression

The terms creep and secondary compression are often used interchangeably to describe the time-dependent strain at constant stress that develops in soils. According to Mitchell and Soga (2005), however, creep is associated with the time-dependent shear and/or volumetric strains while secondary compression refers to a special case of constrained creep which follows primary consolidation. For this thesis, both terms are used to describe the same time-dependent volumetric strains that occur after primary consolidation. Secondary compression in shear samples was monitored to ensure that the rate was small when compared with the subsequent shear rate. Jardine (1995) suggested a creep rate to shear strain rate ratio of less than 1% before shear could begin, to avoid measurement errors during shear. All shear samples were rested for approximately 24 hours before shearing. Volume changes were monitored for 10 minutes prior to shear to ensure that the creep rate to shear strain rate ratio was within the recommended one percent. Creep rate for all samples, except MB-S-400, were well within the recommended range after 24 hours. Creep rate *CR* for all tests are summarized in *Table 5-9*.

SR refers to the shear rate at the beginning of shear, calculated from the machine rate of 0.103mm/min and the height of the sample at the beginning of shear. It should be noted that shear-200 samples underwent standard consolidation procedures while the shear-400 samples were ramped at 10s/kPa. Consolidation and creep data for the two should thus not be compared directly.

200 samples	Creep rate	*CR/SR*	400 samples	Creep rate	*CR/SR*
	(%/min)	(%)		(%/min)	(%)
P-I-200	0.0005	0.46	P-I-400	0.0004	0.34
P-MT-200	0.0004	0.35	P-MT-400	0.0001	0.11
P-S-200	0.0003	0.29	P-S-400	0.0004	0.41
MB-I-200	0.0005	0.47	MB-I-400	0.0010	0.97
MB-MT-200	0.0006	0.59	MB-MT-400	0.0008	0.78
MB-S-200	0.0010	0.91	MB-S-400	0.0016	1.43
UB-I-200	0.0004	0.42	UB-I-400	0.0002	0.16
UB-MT-200	0.0000	0.03	UB-MT-400	0.0001	0.08
UB-S-200	0.0002	0.23	UB-S-400	0.0003	0.31

Table 5-9. Summary of creep rates before shear for shear-200 and shear-400 samples.

The creep of soils can also be expressed in terms of the secondary compression index, C_α, defined as the slope of the creep line on the *e*-log*t'* graph. Secondary compression index for the shear-200 and shear-400 samples are summarized in *Table 5-10*.

Pond		Middle beach		Upper beach	
I-200	0.0068	I-200	0.0079	I-200	0.0033
MT-200	0.0044	MT-200	0.0056	MT-200	0.0003
S-200	0.0040	S-200	0.0125	S-200	0.0024
I-400	0.0075	I-400	0.0094	I-400	0.0010
MT-400	0.0050	MT-400	0.0054	MT-400	0.0005
S-400	0.0012	S-400	0.0147	S-400	0.0023

Table 5-10. Secondary compression indexes for shear-200 and shear-400 samples.

Graphs for the creep data of individual samples are attached in *Appendix E*. It should be noted that the consolidation process for the shear-200 and shear-400

samples were different. Shear-200 samples were consolidated using standard consolidation while the shear-400 samples were ramp consolidated. The effect of the consolidation process on the consequential C_α values is unclear.

To the knowledge of the author, very little work on creep of gold tailings is available in the literature. Values for the coefficient of secondary compression have, however, been reported by various authors in the literature for natural soils, and may be used as reference. Leroueil and Marques (1996) reported values of between 0.029 and 0.059 for inorganic clays. As seen in *Table 5-10*, values of C_α for gold tailings range between 0.0003 and 0.0147 with an average of 0.005. This is significantly lower than values presented for natural soils.

Furthermore, the ratio of C_α/C_c has also been reported in the literature. Mesri and Godlewski (1977) reported C_α/C_c in the range of 0.025 to 0.075 for inorganic clays and silts, and values between 0.035 and 0.1 for organic clays and silts. Mesri et al. (1990) suggested that for all practical purposes, the ratio C_α/C_c for sands can be considered constant and equal to 0.02. The values for the ratio C_α/C_c for gold tailings ranged between 0.004 and 0.037 with an average value of 0.018. This is consistent with the C_α/C_c value of 0.02 suggested by Mesri et al. (1990). The values are also on the low side of the values reported by Mesri and Godlewski (1977) for inorganic clays and silts. This indicates that creep behaviour of tailings is similar to that of sands, showing low C_α values. The platy particles seem more stable than natural clays in terms of time-dependent straining due to particle rearrangement.

From the results, it seems that the coefficient of secondary compression is dependent upon the particle shape as well as on the void ratio in relation to the minimum void ratio of the sample. Although middle and upper beach material have similar particle characteristics, the C_α for middle beach samples is higher in comparison with that of the upper beach samples, probably due to the fact that the upper beach samples are at a lower relative density than the middle beach samples. Comparison of the pond and upper beach samples, which are at similar relative densities, show that a higher C_α is observed in the pond

material, probably due to the slippage and realignment of platy particles. It also appears that creep for moist tamped samples may be lower than for undisturbed and slurry samples, but this is not always the case. Assuming a consistent C_α/C_c ratio, moist tamped samples which show lower C_c values should in theory also yield lower C_α values.

5.4 STIFFNESS

The stiffness of the samples was determined from the two local LVDTs. Both the bulk stiffness and the shear stiffness were investigated. The bulk stiffness was determined from the consolidation results of the consolidation samples (samples isotropically consolidated to 1000kPa), while the shear stiffness was determined from the shear samples. Both the bulk and shear modulus were determined as the secant value as demonstrated in *Figure 5-5*. Bulk modulus K was determined as the secant value shown by the slope of the secant line on the p'- ε_v plot as shown in *Figure 5-5a* at various mean normal effective stress increments. The secant Young's modulus E was defined as the slope of the secant line on the $q' - \varepsilon_a$ graph as shown in *Figure 5-5b*.
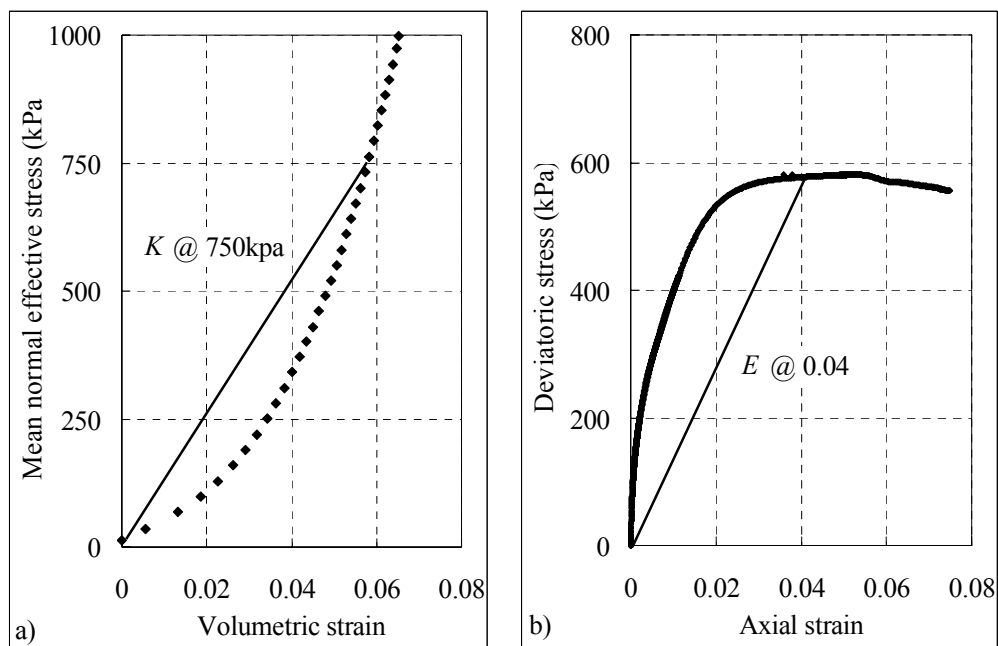
Figure 5-5. Graphic illustration of secant K and E interpretations.

5.4.1 Bulk modulus

As mentioned in section 2.5.6, the bulk stiffness is a measure of the soil's ability to resist volumetric strains under an applied pressure. The bulk modulus determined from *Equation 2-3* for all consolidation samples at effective confining stresses of 250, 500 and 750kPa are shown in *Table 5-11*.

		Bulk modulus at various confining stresses (MPa)		
p_o' (kPa)		250	500	750
Pond	Undisturbed	5.08	4.51	4.33
	Slurry	2.55	3.64	4.56
	Moist tamped	3.73	5.21	6.33
	Average	3.79	4.45	5.07
Middle beach	Undisturbed	8.02	8.49	9.34
	Slurry	1.81	2.74	3.59
	Moist tamped	3.41	4.75	5.97
	Average	4.41	5.33	6.30
Upper beach	Undisturbed	8.44	9.84	11.38
	Slurry	6.96	10.10	12.73
	Moist tamped	24.34	29.70	33.01
	Average	13.25	16.55	19.04

Table 5-11.Bulk stiffness of gold tailings at various confining stresses.

Significant variations in bulk stiffness behaviour can be observed at low confining stresses of up to 100kPa, where after the bulk modulus increases with increasing confining stress. Initial variations in behaviour may be a result of several factors such as over-consolidation ratio and specimen uniformity. Cracks and fissures may also result in a constant bulk modulus as demonstrated by the undisturbed pond sample. In homogeneous samples pores close up as consolidation progresses resulting in a denser configuration and an increase in the bulk stiffness. In cracked or fissured samples, however, consolidation results in the closing of cracks and fissures and constant bulk

stiffness are observed. Once the cracks and fissures are closed the homogeneous sample then displays an increase in bulk stiffness upon further consolidation.

Comparison of the bulk modulus values shown in *Table 5-11* and those obtained by Vermeulen (2001) indicate that the pond samples which have similar initial void ratios (of around 1.4) have similar bulk modulus. Middle beach samples also have similar initial void ratios (of around 0.8) and bulk modulus when compared with Vermeulen's results for coarse tailings (2001). The upper beach samples are however significantly stiffer than those obtained by Vermeulen for coarse tailings. This may be explained by the upper beach samples having a lower initial void ratio (around 0.5) than a void ratio of 0.8 for Vermeulen's coarse tailings.

With regard to sample preparation/fabric effects on bulk modulus, it appears that pond undisturbed, moist tamped and slurry samples exhibit similar values of K for the stress range investigated. This further validates the similar fabric observed from the SEM images of the pond samples. The bulk stiffness of middle beach samples was, however, significantly affected by the fabric. K values for the slurry samples were in the range of 25% to 30% of the undisturbed counterparts. It is speculated that the flocculated fabric may have significantly lowered the stiffness of the slurry samples. Bulk stiffness of the moist tamped samples was approximately half that of the undisturbed counterpart. The bulk stiffness of the undisturbed and slurry upper beach samples was similar, but significantly lower than that of the moist tamped samples. It is unclear why the moist tamped upper beach samples showed significantly higher bulk stiffness than the undisturbed and slurry samples, but it is speculated that the moist tamped sample was constructed at a lower void ratio or that larger rotund particles were included in the sample.

5.4.2 Young's modulus

According to Heymann (1998), stiffness may be plotted against the logarithm of strain to give equal prominence to stiffness at all strain levels. Consider a

typical force time plot for the sample P-I-400 shown in *Figure 5-6.* After the creep rate had been checked, the ram was lowered to a height slightly above the sample, and the machine was started. Due to the limited flow rate of the digital pressure controller, it was important to lower the ram slowly enough to prevent an increase in cell pressure. Data logging was initiated at time zero before the ram touched the top cap. The start of shear was identified by observing lift-off of the measurement as shown in the *Figure 5-6*.
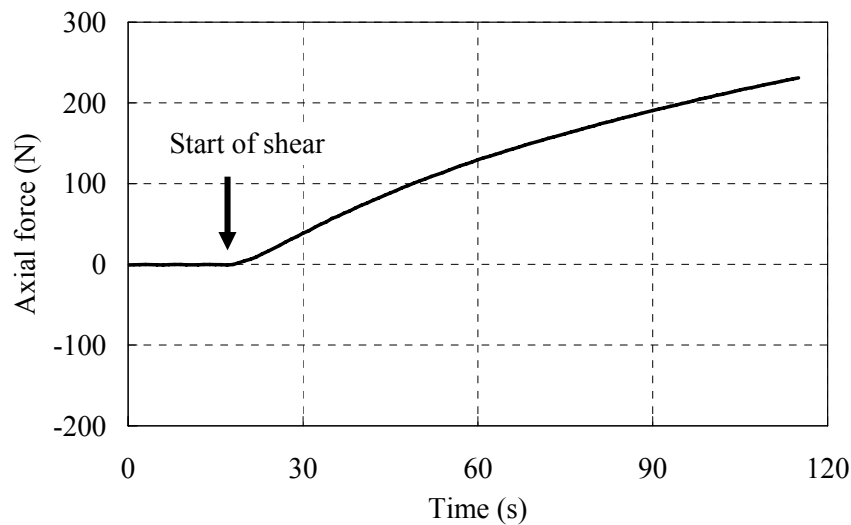
Figure 5-6. Force time plot used to identify the start of shear.

The secant Young's modulus is defined in *Figure 5-5b* and is determined using *Equation 5-5*:

$$E = \frac{q'-q'_0}{\varepsilon_a - \varepsilon_{a0}}$$ *Equation 5-5*

where E is the stiffness, q' the deviatoric stress and ε_a the axial strain. q'_0 and ε_{a0} are points defining the origin.

Small strain stiffness

The small strain stiffness is a measure of soil stiffness in the elastic range. Stiffness of soils in the elastic range is constant and using high accuracy interferometers for local strain measurements, Heymann (1998) was able to

demonstrate that the linear plateau of stiffness for soils and weak rocks is in the range of 0.002% strain. The results show that there is significant below the 0.001% range, indicating that the LVDTs used may not be capable of accurately identifying the linear plateau. The small strain stiffness for gold tailings can, nevertheless, be estimated. It was decided that the small strain stiffness would be taken as the average value of the stiffness values in the range of 0.0001% to 0.001% strain. The scatter of values below 0.0001% strain may be extremely large (positive or negative) and may influence the average value considerably. Values above 0.001% strain may be out of the linear plateau and are thus not included. An example for P-U-200 is shown in *Figure 5-7*.
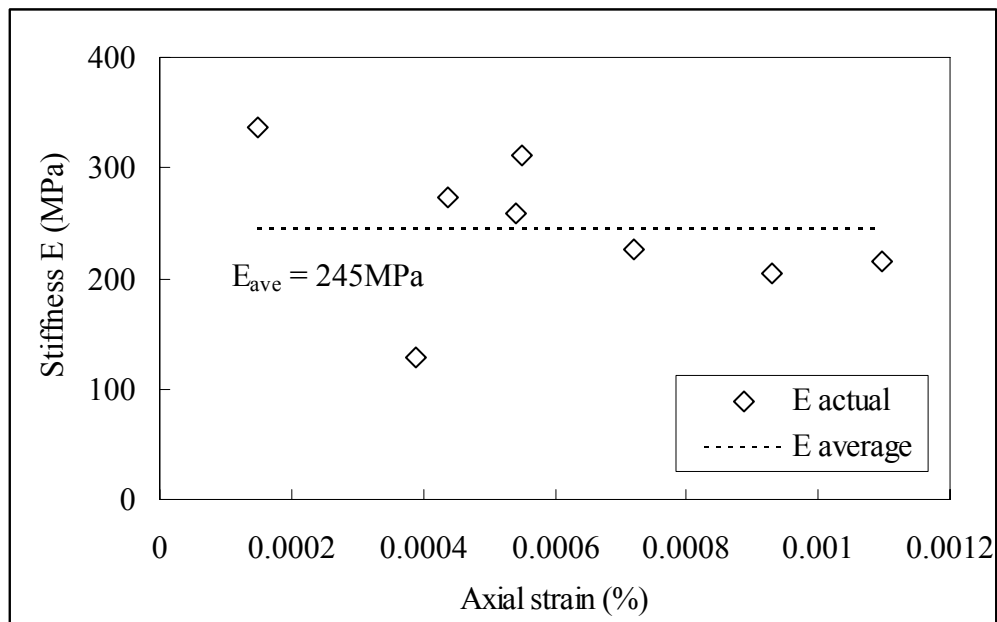
Figure 5-7. Example of small strain stiffness derivation (P-U-200)

The small strain stiffness values for the samples tested are summarized in *Table 5-12*. Theron, Heymann and Clayton (2004) presented small strain shear stiffness data of slurry prepared gold tailings based on bender element measurements. Small strain stiffness of gold tailings is in the order of 100MPa and 175MPa for confining stresses of 200 and 400kPa respectively. G_{max} of moist tamped gold tailings samples determined from shear wave velocities obtained using bender elements (Chang, 2004) were in the order of 60MPa and 100MPa for samples consolidated to 200kPa and 400kPa respectively.

Small strain Young's modulus, E (MPa)						
	Pond		Middle beach		Upper beach	
p_o' (kPa)	200	400	200	400	200	400
Undisturbed	245	336	237	451	174	470
Moist tamped	226	332	135	280	234	374
Slurry	301	383	251	460	180	447

Table 5-12. Small strain Young's modulus values for gold tailings.

Under isotropic conditions, the Young's modulus E can be related to the shear modulus G via *Equation 5-6:*

$$G = \frac{E}{2(1+v)} \qquad\qquad \textit{Equation 5-6}$$

where v is the Poisson's ratio. Under undrained conditions, v equals 0.5 and the equation can be simplified to:

$$E_u = 3G. \qquad\qquad \textit{Equation 5-7}$$

The undrained Young's modulus from Theron, Heymann and Clayton's results for gold tailings can then be approximated to 300MPa and 525MPa for confining stresses of 200kPa and 400kPa respectively. Results of Chang's bender element tests yield a Young's modulus of 180MPa and 300MPa for confining stresses of 200kPa and 400kPa respectively. This is consistent with the results of this section, as Theron, Heymann and Clayton (2004) tested slurry samples and the samples of Chang (2004) were moist tamped.

It appears that the small strain stiffness results shown in *Table 5-12* are in between those obtained by Theron, Heymann and Clayton (2004) and Chang (2004). The difference between the results of Theron, Heymann and Clayton (2004) and Chang (2004) may partly be a result of the preparation method and thus the fabric.

From *Table 5-12*, it can be seen that fabric may have a significant effect on the small strain stiffness of gold tailings. All but one slurry sample show higher small strain stiffness when compared with the undisturbed counterparts. With the exception of UB-MT-200, all moist tamped samples show lower small strain stiffness than the undisturbed samples. The difference may be minimal, as in the case of the pond samples, or significant, as in the case of middle beach samples. Comparison of small strain stiffness of undisturbed and reconstituted samples is summarized in *Table 5-13*. Differences are shown as percentages and negative values indicate a value lower than the undisturbed stiffness.

	Pond		Middle beach		Upper beach	
p_o' (kPa)	200	400	200	400	200	400
Moist tamped	-7.8%	-1.2%	-43%	-37.9%	34.5%	-20.4%
Slurry	24.8%	14.2%	10.4%	3.2%	2.6%	-6.1%

Table 5-13. Differences in E values between undisturbed and reconstituted gold tailings.

The small strain stiffness of soils is significantly affected by the homogeneity of the sample. Triaxial tests conducted on reconstituted Laval and Sherbrooke samples indicate that stiffness increases as the material becomes more homogeneous (Clayton et al., 1992). This is consistent with the small strain stiffness results observed for gold tailings. Slurry samples represent samples with the highest degree of homogeneity and thus exhibited the highest small strain stiffness values. Undisturbed samples generally contain small cracks and fissures which can significantly lower the homogeneity and thus the small strain stiffness of the sample. According to the particle contact model postulated in section 4.3.2, shear force transfer through the aggregates is accomplished through the parallel orientated platy particles, and this may significantly reduce the initial stiffness of the sample in the small strain range.

Stiffness degradation

It is generally recognized that soils stiffness decreases with increasing strain (e.g. Simpson, 1979; Jardine et al., 1984; Clayton and Khatrush, 1986; Tatsuoka, 1988). An idealized stiffness degradation curve such as the one shown in *Figure 5-8* includes an initial linear plateau at small (<0.002%) strains followed by continued degradation at intermediate and large strains.
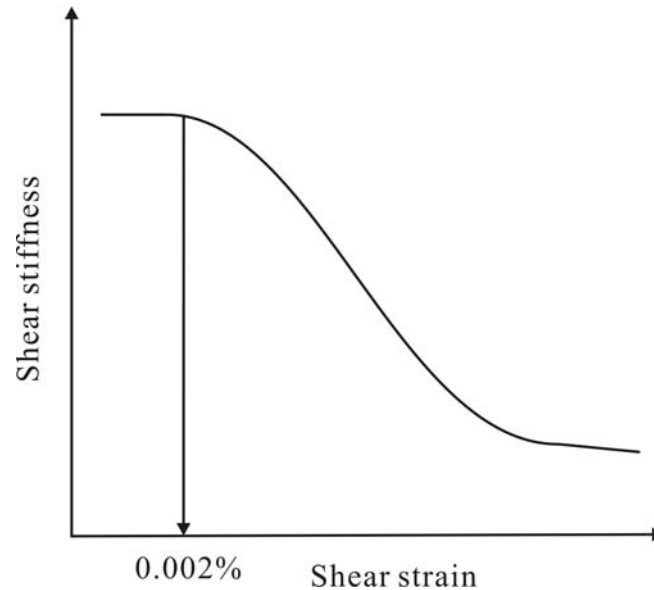
Figure 5-8. Idealized stiffness degradation for soils.

The stiffness of the pond, middle and upper beach samples are attached in *Figures E-10, E-11* and *E-12* respectively in *Appendix E*. The entire stiffness degradation curve can generally be described by values of stiffness at various strain levels and the ratios of these stiffness values. Stiffness of gold tailings at strain levels of 0.001, 0.01 and 0.1 and 1% strain and the stiffness ratios are summarized in *Table E-4*.

From the figures, it can be seen that there is convergence of the data points at higher strain levels. For pond and upper beach samples, no significant differences can be observed in the stiffness of the shear samples at the same effective stress. It is expected that pond material will have similar stiffness values, as the behaviour is dominated by the matrix of platy particles and flocks. The aggregated fabric observed in the middle and upper beach moist

tamped samples implies that moist tamped samples should have a lower stiffness than the undisturbed and slurry counterparts.

For the middle beach samples, the stiffness for moist tamped 200 and 400 samples are considerably lower than those for the undisturbed and slurry counterparts, as expected from the aggregated fabric. Contrary to the author's expectations, the stiffness values of upper beach samples are similar. It may be that the higher relative density has suppressed the instability of the unstable contacts in the aggregated fabric.

The shape of the stiffness degradation curves, described by the ratio of the stiffness at various strain levels seems to be similar for all samples. Average values for these ratios for gold tailings are summarized in *Table 5-14*.

Stiffness ratio	Pond	Middle beach	Upper beach
$E_{0.01}/E_{0.001}$	0.78	0.84	0.80
$E_{0.1}/E_{0.001}$	0.34	0.35	0.30
$E_{1.0}/E_{0.001}$	0.06	0.07	0.05

Table 5-14. Average stiffness ratios gold tailing of varying material type.

Stiffness ratios shown in *Table 5-14* indicate that the rate of degradation is not significantly affected by the material type. These ratios are, however, lower than values presented by Heymann (1998) for natural geomaterials. The effect of sample preparation method (fabric) on the stiffness degradation of gold tailings is demonstrated in *Figure 5-9*.

Average stiffness degradation compared on the basis of preparation method shows that moist tamped samples display lower rates of degradation than the undisturbed and slurry samples. It should be noted that a higher stiffness ratio indicates a lower rate of degradation, suggesting that moist tamped samples degrade at a slower rate than the undisturbed and slurry samples. The effect of fabric on stiffness of gold tailings decreases as the sample straining is

continued. It seems that the stiffness tends to a unique value dependent on the material type only. As stiffness tends to a constant value, the higher stiffness ratio (lower rate of stiffness degradation) of moist tamped samples may be a function of the lower small strain stiffness observed in the moist tamped samples.
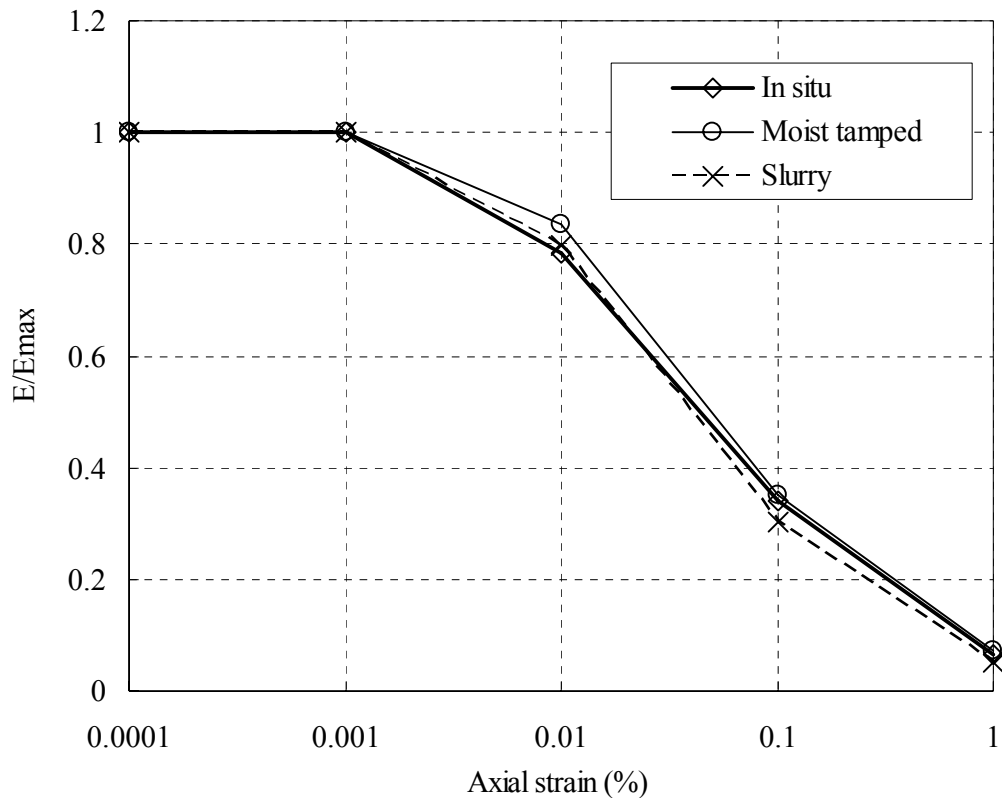
Figure 5-9. Average stiffness ratios gold tailing for varying preparation method.

Normalized stiffness

The stiffness may also be normalized against the current mean effective stress *p'* to eliminate the effects of *p'*. The normalization by division by *p'* is strictly only applicable for large strains and it is generally more conventional to divide by $(p')^n$ where *n* is a function of, among other things, the strain level (Porovic, 1995). As the value of *n* for gold tailings is unclear, it is assumed to be unity. The normalized stiffness of gold tailings is shown in *Figure 5-10*.
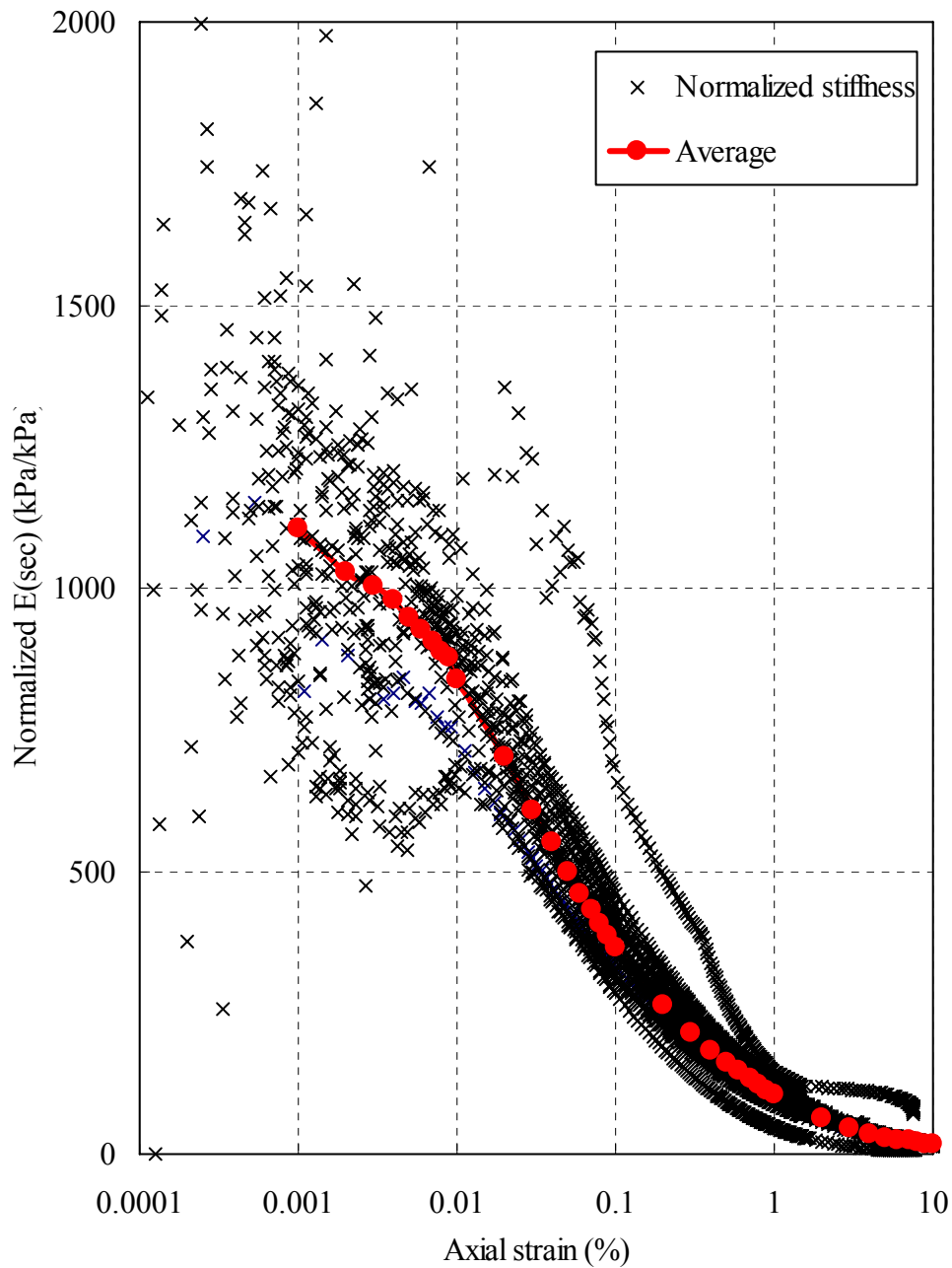
Figure 5-10. Normalized (against current p') stiffness of gold tailings.

The figure shows that there is considerable scatter in the normalized stiffness values, particularly in the small to medium strain range. There is, however, increasing convergence at larger strains. From the figure, is can be concluded that the normalized small strain stiffness (against p') of gold tailings is generally in the range of 1000 to 1500kPa/kPa, with the exception of the two moist tamped samples which show significantly lower values (in the order of

750kPa/kPa). Average values have been plotted as red points. The average was determined for every log scale increment from 0.001 to 10. The two moist tamped samples were also included in the calculation for completeness. The trend for the average curve shows that gold tailings has a normalized small strain stiffness of around 1200kPa/kPa and appears to tend to a linear plateau below the 0.001% strain level.

The figure also shows that the fabric has no significant effect on the stiffness of gold tailings, again with the exception of the two moist tamped samples. It seems that the effect of fabric on small strain stiffness is also a function of the relative density state of the sample.

5.4.3 Stiffness anisotropy

Sample stiffness anisotropy can also be investigated from the stress paths in *p'-q'* space. According to Graham and Houlsby (1983), stiffness anisotropy, can be expressed by the initial slope of the stress path in *p'-q'* space. A soil which is stiffer horizontally will display an initial decrease in *p'* while the stress paths of a soil which is stiffer vertically will move initially to the right displaying an initial increase in the mean effective stress. An isotropic soil will display a near vertical initial stress path. The initial slope of the stress path in *p'-q'* space has been summarized in *Table 5-15* in terms of the initial slope angle *θ* at 0.05% axial strain following *Equation5-8*:

$$\theta = \tan^{-1}(\frac{\delta p_{0.05}}{\delta q_{0.05}}) \qquad\qquad Equation\ 5\text{-}8$$

Assuming 0° at the vertical, a positive *θ* indicates a positive slope (initially to the right, stiffer vertically) and a negative *θ* suggests a negative slope (initially to the left, stiffer horizontally).

	Pond		Middle beach		Upper beach	
p_o' (kPa)	200	400	200	400	200	400
Undisturbed	-4.6	-1.9	-2.6	-2.0	0.2	2.9
Moist tamped	1.1	4.5	-3.6	0.3	3.2	4.6
Slurry	4.2	3.9	-3.6	-0.4	11.3	2.4

Table 5-15. Initial stress path slope θ of gold tailings.

From the stress paths, it can be seen that most of the samples show a near vertical initial stress path, with the exception of UB-S-200 which displays strong anisotropy in the vertical direction, probably as a result of the initial one-dimensional consolidation of the slurry sample which resulted in a higher vertical stiffness. It is surprising, however, that the other slurry samples did not show some anisotropy. Moist tamped samples are expected to be isotopic and this is confirmed by the near vertical initial stress paths. It is also surprising that the undisturbed samples were also isotropic. Horizontal layering seen in tailings generally yields a sample which is stiffer in the horizontal direction, and would display an initial decrease in the mean normal stress p'. The isotropy observed in the undisturbed sample indicates that layered blocks were avoided during block sampling.

5.5 SHEAR BEHAVIOUR

Gold tailings have generally been regarded as material which shows phase transfer dilation upon undrained shear (Vermeulen, 2001). To the author's knowledge, there has been limited evidence, besides the Merriespruit samples (Wagener et al., 1998), that undisturbed gold tailing samples actually contract and strain-soften during static loading in a triaxial test. This fact has been confirmed to some degree by the outcome of the shear tests. The results of the undrained shear tests are attached in *Appendix E* and are presented in the form of stress-strain relationships of mean normal effective stress p' (*Figures E16-E18*), deviatoric stress q'(*Figures E13-E15*) and excess pore pressure u_e

(*Figures E19-E21*). Stress paths plotted in *s'-t'* and *p'-q'* space for all three material types have also been attached in *Appendix E* (*Figures E22-E27*).

5.5.1 Available shear strength

The shear behaviour of the undisturbed samples is generally characterized by an increase in deviatoric stress and the generation of excess pore pressure. This is accompanied by a decrease of mean normal effective stress to constant values. Stress paths of undisturbed gold tailings samples indicated initial contraction followed by dilation after phase transfer. Failure generally occurred close to the point of phase transformation without significant dilation occurring. Sample UB-U-400, however, showed a significant increase in deviatoric stress accompanied by a decrease in excess pore pressure and an increase in mean normal effective stress, indicative of strong dilative behaviour.

The shear behaviour of slurry samples is generally similar to the undisturbed counterparts, exhibiting initial contraction followed by phase transfer dilation. Slurry samples, however, showed stronger dilative response than the undisturbed samples. This can be observed by the increase in both deviator stress and mean normal effective stress accompanied by a decrease in excess pore pressure in the pond and upper beach samples. This strong dilative behaviour can also be seen in the stress paths where, following the point of phase transformation, dilation continues substantially before failure occurs.

The shear behaviour of some moist tamped samples was significantly different from that observed for the undisturbed and slurry deposited samples. Moist tamped pond samples showed almost identical behaviour to the undisturbed and slurry deposited counterparts, with initial contraction followed by phase transfer dilation. The shear behaviour of the moist tamped middle and upper beach samples was, however, significantly different to that of the undisturbed and slurry deposited samples. The moist tamped samples demonstrated contractive and strain-softening behaviour as suggested by a decrease in deviatoric stress to a residual value.

Difference in the stress path of undisturbed, moist tamped and slurry samples have significant implications in terms of the available shear strength in the gold tailings samples. The difference in available shear strength is not only between the strain-hardening undisturbed and slurry samples and the strain-softening moist tamped samples, but also between the strain-hardening undisturbed and slurry samples. This is exemplified by the stress paths of middle beach shear-400 samples shown in *Figure 5-11*.
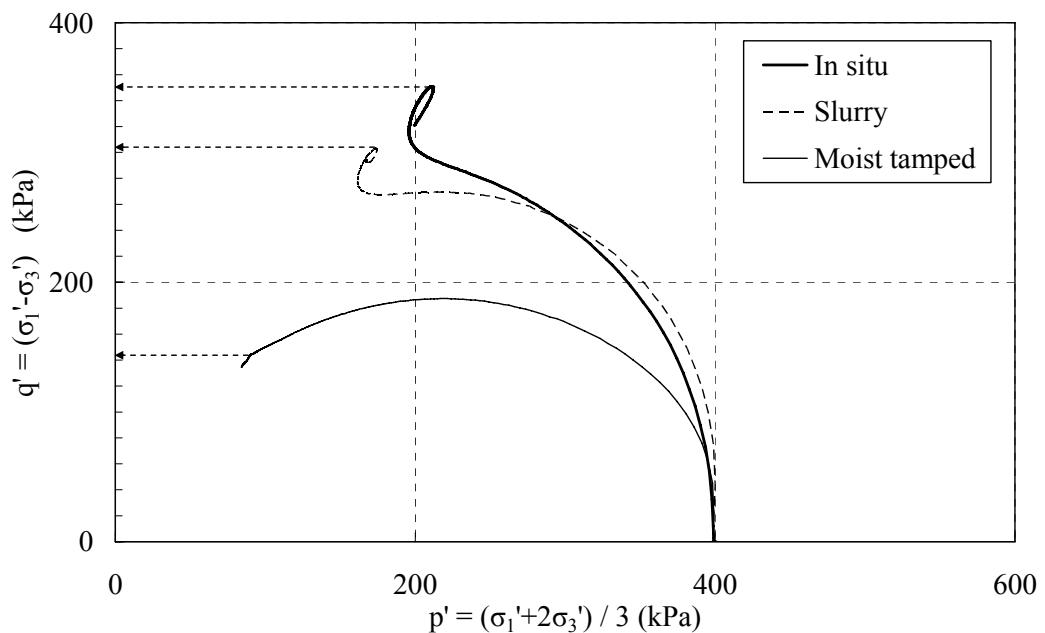
Figure 5-11. Difference in available shear strength between middle beach shear-400 samples.

It can be observed that, although both undisturbed and slurry samples exhibit phase transfer dilation behaviour, the available shear strength between the two samples is still different. The strain-softening moist tamped sample, however, had significantly lower shear strength than the undisturbed and slurry counterparts. The strain-softening behaviour of the moist tamped samples may have been caused by a tendency of the aggregates to move into a denser configuration during shear, resulting in an increase in excess pore pressure and a decrease in effective stress.

The available shear strength of gold tailings samples are summarized in *Table 5-16.*

Available shear strength (kPa)						
	Pond		Middle beach		Upper beach	
p_o' (kPa)	200	400	200	400	200	400
Undisturbed	248.2	365.8	187.8	386.0	142.2	1021.2
Moist tamped	197.5	595.4	82.5	160.9	113.4	542.2
Slurry	313.2	589.7	161.4	354.5	270.9	686.8

Table 5-16. Available shear strength of gold tailings samples.

From these values, it is clear that although the moist tamped pond samples demonstrated strain-hardening behaviour, the available shear strength of moist tamped samples was in general lower (approximately 25%) than those of the undisturbed samples. Comparison between the undisturbed and slurry samples was indecisive, as in some cases the undisturbed sample had higher shear strength and in other cases the slurry sample had higher strength.

5.5.2 Liquefaction behaviour

The difference in stress paths between gold tailings samples can also have significant implications in terms of the liquefaction behaviour of the sample. Liquefaction is a combined effect of contractive behaviour and strain-softening behaviour and this was observed in some of the moist tamped samples. As described in section 2.5.8, cohesionless soils may exhibit three types of behaviour, namely contractive (C), dilative (D) and limited liquefaction (*LL*). The behaviour types observed for gold tailings are summarized in *Table 5-17.*

From these results, it can be seen that none of the undisturbed or slurry samples strain-softened during shear. For these samples the deviatoric stress and excess pore pressure generally increases to a constant value. For the stress

paths, q' or t' increased until failure while p' or s' first show a decrease and then an increase. It can further be observed that, with the exception of UB-U-400 and UB-S-400, the stress paths of undisturbed and slurry samples are almost identical. Although both UB-U-400 and UB-S-400 samples show different degrees of dilation, the general behaviour is the same.

	Pond		Middle beach		Upper beach	
p_o' (kPa)	200	400	200	400	200	400
Undisturbed	D	D	D	D	D	D
Moist tamped	D	D	C	C	C	D
Slurry	D	D	D	D	D	D

Table 5-17. Liquefaction behaviour type for gold tailings.

From the results, it can also be seen that moist tamped samples may strain-soften during undrained shear, as in the case of MB-MT-200, MB-MT-400 and UB-MT-200 samples. Brittleness index values I_B described in section 2.5.8 for the contractive samples are summarized in *Table 5-18*.

p_o' (kPa)	Middle beach	Upper beach
200	0.26	0.45
400	0.28	NA

Table 5-18. Brittleness index for strain-softening moist tamped samples.

Middle beach samples yielded a similar brittleness index irrespective of confining stress. Upper beach samples, however, displayed a brittleness index of approximately half. No conclusions can be reached with regard to brittleness index as only limited data is available. It can, however, be said that moist tamped samples may lose up to half their peak strength due to strain-softening.

The reason for the observed strain-softening behaviour may be the aggregated fabric described in chapter 4. During shearing, platy particles at the contact points tend to slide relative to each other and the result is a disintegration of the platy contacts between existing aggregates. This causes a tendency of the rotund particles to move into a denser configuration, resulting in an increase in pore-water pressure accompanied by a decrease in deviatoric stress (strength of the sample). This strain-softening behaviour was not visible in all aggregated samples. UB-MT-400 exhibited strong dilative response and this may be a result of dilation due to the sample being in a state of high relative density.

5.5.3   Shear strength

The shear strength of soils is generally described by a cohesion c' and a friction angle, φ'. The values of c' and φ' may be obtained from the stress paths in s'-t' space, as demonstrated in *Figure 5-12* for P-U-400.
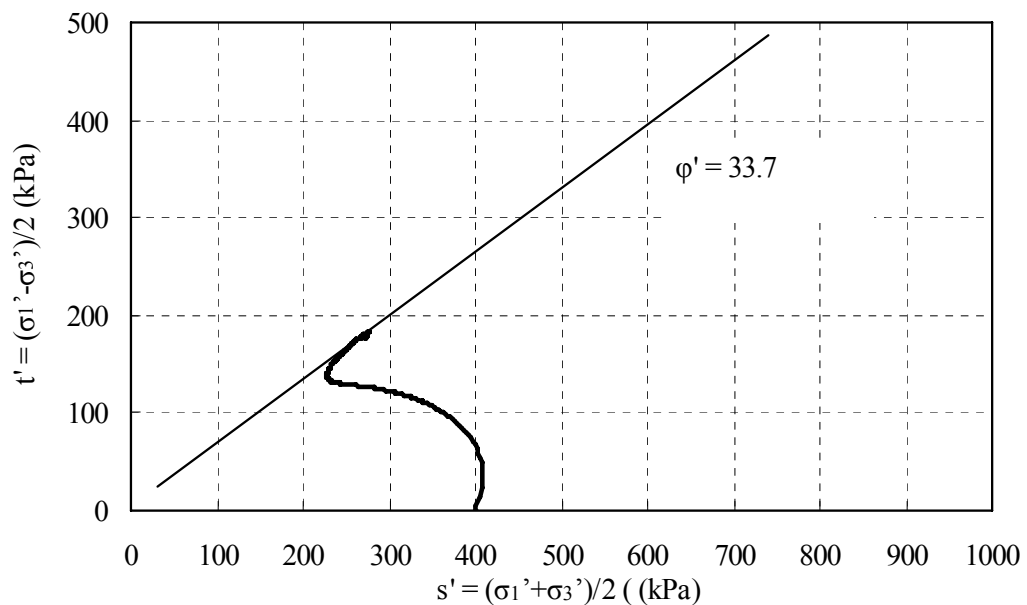
Figure 5-12. Friction angle of P-I-400 sample.

Since gold tailings are generally considered cohesionless, values for the friction angle have been determined based on the assumption that the material

has no cohesion. Each sample was determined individually. The friction angles for the moist tamped middle beach samples were not determined as the sample strain-softened and the stress paths did not reach a constant slope at the end of the test. Values of the friction angle for all gold tailings samples are summarized in *Table 5-19*.

	Pond		Middle beach		Upper beach	
p_o' (kPa)	200	400	200	400	200	400
Undisturbed	31.6°	33.7°	32.6°	33.3°	30.9°	31.5°
Moist tamped	30.4°	30.2°	NA	NA	30.9°	30.5°
Slurry	31.6°	31.5°	34.3°	34.3°	31.5°	31.2°
Average	31.5°		33.6°		31.1°	

Table 5-19. Angles of internal friction for gold tailings.

From the results, it is apparent that the angle of friction is independent of the fabric of the sample as a similar trend can be observed for the same material type. It should be noted that visual determination of samples which failed before dilation or strained-softened is difficult and may cause some scatter in the results.

A better indication of the frictional strength is the critical state parameter *M* defining the slope of the stress path in *p'-q'* space. The value of *M* is defined as the constant to which the stress ratio (*q'/p'*) approaches at increasing axial strain. Plots of stress ratio against axial strain for all samples are attached in *Figure E-28, E-29* and *E-30*. Values of *M* are given in *Table 5-20*. It should be noted that the tests were generally terminated at 20% axial strain or when further straining could damage the LVDTs or the triaxial loading ram. Most samples reached the critical state, with stabilizing of the deviatoric stress q' and effective confining stress p' but some samples were terminated close to the critical state. As a result, the position of the critical state line for some samples could not be accurately identified.

	Pond		Middle beach		Upper beach	
p_o' (kPa)	200	400	200	400	200	400
Undisturbed	1.66	1.71	1.73	1.73	1.61	1.61
Moist tamped	1.54	1.48	1.76	1.69	1.61	1.44
Slurry	1.69	1.66	1.88	1.86	1.53	1.58
Average	1.62		1.78		1.56	

Table 5-20. Critical state parameter M for gold tailings.

The friction angle shown in *Table 5-19* is in the same range as those obtained by Vermeulen (2001). Critical state parameter *M,* however, is somewhat higher than Vermeulen's results.

From the stress ratio plots, it can be seen that all samples yield similar values for *M*. For the same material type, values of *M* also seem to be in a similar range despite some scatter. This is consistent with the findings of Zlatovic and Ishihara (1997) which suggested that the shear strength of soils is only governed by the particle characteristics and is independent of the initial fabric.

Values of friction angle and *M* for middle beach slurry material seem slightly higher than other samples in general. This may be a result of the addition of flocculent in the slurry samples. According to Horn and Deere (1962), the absorption of pore fluid may alter the coefficient of surface friction of the particle. This anti-lubricating effect is especially noticeable on quartz and less on muscovite.

An interesting fact was also visible for pond and upper beach samples. The materials have similar values for friction angle or *M* despite the significant difference in the particle properties. Similar results were published by Vermeulen (2001). As observed in the SEM images, pond material consists predominantly of fine platy particles while particles constituting upper beach material are mainly coarse and rotund.

5.6 THE EFFECT OF FLOCCULENT AND DISPERSANT

The addition of flocculent and dispersant was necessary to prepare slurry samples to the required void ratio. This however, changes the pore fluid chemistry and may result in a change in behaviour of the tailings. The effects of pore fluid chemistry will be both mechanical and physico-chemical, with one dominant mechanism (Olson and Mesri, 1970). Mechanical effects occur when the pore fluid absorbs into the particle surface, resulting in a change in the particle's coefficient of surface friction. This was substantiated by the slightly higher friction angle and M values observed for the middle beach slurry samples.

The physico-chemical effect of pore fluid chemistry was visible during sample preparation of the slurry samples. Sedimentation tests showed that the addition of flocculent to the slurry increased the rate of settlement, but also the final settled void ratio. This confirms the observations of Olson and Mesri (1970), who suggested that physico-chemical effects in the slurry influence the original soil structure.

5.7 SUMMARY

The results of the experimental programme have been presented and discussed in terms of the observed fabric of undisturbed and laboratory prepared gold tailings samples. The differences in behaviour have been explained in terms of the particle contact model proposed in Chapter 4. The model, is however, inadequate to explain the observed behaviour fully.

The results also indicate that a limit in density or relative density may exist for samples of different fabric to behave differently. Compaction above that density or relative density limit may destroy any significant fabric, and results in similar fabric and behaviour. Verification of this, however, will require a systematic experimental programme which is beyond the scope of this thesis.

Chapter 6

Conclusions

6.1   BACKGROUND

The fabric and behaviour of undisturbed and laboratory prepared gold tailings have been investigated. The hypothesis states that **accurate simulation of the behaviour of gold tailings under laboratory conditions requires appropriate replication of the material fabric.** An experimental programme was set up to investigate the difference in the fabric of undisturbed and laboratory prepared gold tailings samples and the subsequent fabric effects on the behaviour of gold tailings. Conclusions based on the results and discussions are presented in this chapter.

6.2   CONCLUSIONS FROM EXPERIMENTAL PROGRAMME

- A method of preparing slurry samples was proposed. Traditional methods result in an hourglass shaped sample. The proposed method allows some vertical settlement and one-dimensional consolidation to take place under low suctions. This method, however, may result in some anisotropy in the sample.

- Middle and upper beach slurry samples could not be prepared to the target (in situ) void ratio using tap water alone. Flocculent and dispersant were required to increase the initial void ratio of the slurry samples.

- The addition of dispersant and flocculent affects the amount of settlement for gold tailings in a sedimentation test. The effect of increased dispersant concentration on the settlement rate and amount of settlement is not clear. Increased flocculent concentration increases the rate of settlement, but also decreases the amount of settlement (i.e. settles to a higher void ratio).

- The fabric of gold tailings can be classified into four levels:

  Level 1: non-aggregated and non-orientated.

  Level 2: aggregated but non-orientated.

  Level 3: orientated but non-aggregated.

  Level 4: aggregated and orientated.

  These four levels were used to describe the differences in the fabric of gold tailings, but may be inadequate to describe soils in general. According to the proposed classification system, difference in the fabric can be observed in undisturbed and laboratory prepared gold tailings samples.

- The initial fabric observed before consolidation is not destroyed at large isotropic stresses and strains.

- A particle contact model was postulated based on the observed fabric of gold tailings. According to the model, isotropic compression forces normal to the parallel alignment of the platy particles of the aggregate contact point results in a higher bulk modulus in aggregated gold tailings samples. The transfer of shear forces through the aggregated fabric during initial stages of shear is dampened by the ineffectiveness of the parallel orientated platy particles to transfer forces tangential to the platy particle orientation. At large strains, the platy contact is destroyed. This results in a tendency of the aggregates to collapse into a denser configuration which causes an increase in excess pore pressure accompanied by strain-softening behaviour.

- Volume changes occurred during sample flushing. All undisturbed samples show collapse of the order of 2%, irrespective of material type. Collapse of

moist tamped samples is dependent on the relative density state. Samples may show collapse up to 10% at low relative density and may even swell at high relative density.

- The coefficient of consolidation, C_v is a function of the material type as well as the fabric. C_v decreases down the beach, due to a decrease in particle size or a change in particle shape from predominantly rotund to predominantly platy. C_v is significantly increased due to aggregation. Undisturbed C_v values are approximately a third that of moist tamped samples and half that obtained for slurry samples.

- Compression index C_c and critical state parameter λ estimated from the last five data points of consolidation data is dependent on both particle characteristics and fabric. C_c and λ both increases down the beach with a decrease in particle size and an increase in platy particle content. C_c and λ values for the reconstituted moist tamped and slurry samples were on average 40% lower than those for the undisturbed samples. The fabric was not destroyed at large isotropic stresses and strains.

- Coefficient of secondary compression, C_α, for gold tailings ranges between 0.0003 and 0.147 with an average of 0.005. C_α is a function of relative density and particle shape. The value increases with decreasing relative density and increasing platy content. C_α is also lower for moist tamped samples.

- The bulk modulus of gold tailings is dependent on the sample fabric. At low confining stresses, undisturbed samples exhibit higher bulk modulus values than the reconstituted samples and at higher confining stresses the moist tamped samples produce the highest K values. Slurry samples generally produce similar or conservative K values compared with the undisturbed counterparts.

- The small strain stiffness, E_{max}, of gold tailings is a function of the fabric. Slurry samples show higher E_{max} values (approximately 10%) than the

undisturbed samples while moist tamped sampled yield lower E_{max} values (approximately 15%) than the undisturbed counterparts. Both laboratory preparation methods may yield erroneous results, but moist tamped samples yield conservative results.

- Moist tamped samples show a lower rate of stiffness degradation at small strains as a result of the lower small strain stiffness values. The samples, however, tend to the same stiffness value upon continued shearing to strains in excess of 10%.

- Gold tailings have normalized (against the current mean normal effective stress) small strain stiffness in the range of 1000 to 1500kPa/kPa with an average value of around 1200kPa/kPa and tend to a linear plateau below the 0.001% strain level.

- Undisturbed and slurry samples at the target (in situ) void ratio only show dilating behaviour. Moist tamped samples at the same state may exhibit contractive and strain-softening behaviour. The available shear strength of slurry samples are in general 20% higher than those for the undisturbed samples while the available shear strength of moist tamped samples are on average 25% lower in comparison with the undisturbed counterpart.

- The angle of friction and M are independent of the fabric. The friction angle and M may however be influenced by changes in pore fluid chemistry.

- *Table 6-1* shows the recommended laboratory sample preparation method for testing of gold tailings specimens based on the behaviours in comparison with undisturbed samples.

Behaviour type or engineering parameter	Moist tamped	Slurry
Collapse/Swell	👎	NA
Coefficient of consolidation, C_v	👎	👎
Compression Index C_c and λ	👎	👎
Coefficient of secondary compression, C_α	👎	👎
Bulk modulus, K	👎	👍
Small strain stiffness	👎	👎
Medium to large strain stiffness	👍	👍
Friction angle and M	👍	👍
Liquefaction potential	👎	👍
Total	2/9	4/8

👍 Reconstitution method yields similar results in comparison with undisturbed samples

👎 Reconstitution method yields different results in comparison with undisturbed samples

Table 6-1. Recommended laboratory preparation method for triaxial testing of gold tailings.

In conclusion, it appears that neither moist tamping nor slurry deposition can fully replicate the behaviour of undisturbed samples. It is recommended that moist tamping be used when the friction angle of gold tailings is required. The method may also be used for small strain stiffness determinations as the results are conservative. Slurry samples generally replicate the behaviour of undisturbed samples better than moist tamped samples do, but may yield higher C_v, and small strain stiffness values which may be un-conservative. It should be emphasized that the recommendations shown in the table are based on general application and may not be applicable to special cases.

Based on the conclusions presented in this chapter, the hypothesis: **Accurate simulation of the behaviour of gold tailings under laboratory conditions requires appropriate replication of the material fabric,** is accepted.

6.3   RECOMMENDATIONS

Recommendations are made based on the findings of this thesis.

- The effect of additives (dispersant and flocculent) on the behaviour of gold tailings requires further investigation. The assumption was made that the influence of additives on the general behaviour of gold tailings will be minimal, but this assumption needs to be validated.

- During the course of this research, it has become increasingly apparent that the effect of fabric is significantly dependent on the relative density of the samples. For this research the in situ density (or void ratio) was used as a benchmark against which all samples were compared. Research may be required to quantify the correlation between relative density and fabric and its effects on the behaviour of gold tailings.

- This research provides a first step in validating that the observed differences in behaviour is in fact due to a difference in fabric. A more comprehensive method for quantifying or classifying soil fabric may need to be developed in order to investigate the relationship between soil fabric and soil behaviour in more detail.

- The proposed particle contact model needs to be validated or refined. The model may provide explanation for some of the observed similarities or differences in behaviour, but is inadequate to model comprehensively the behaviour of gold tailings.

BLIGHT, G.E. (1969) Shear stability of dumps and dams of gold mining waste, *Transactions of the South African Institute of Civil Engineers,* 11(3), 49-54.

BLIGHT, G.E. (1976) Mitigation of subgrade salts damages thin pavements, *ASCE Transportation Engineering Journal,* 102(TE4), 779-791.

BLIGHT, G.E. (1980) Properties of pumped tailings fill, *Journal of the South African Institute of Mining and Metallurgy,* 79(15), 446-453.

BLIGHT, G.E. (1981) Assessment for environmentally acceptable disposal of mine waste, *The Civil Engineer in South Africa,* 23(10), 480-499.

BLIGHT, G.E. (1997) Destructive mudflows as a consequence of tailings dyke failures, *Proceedings of the Institute of Civil Engineers: Geotechnical Engineering,* 125(1), 9-18.

BLIGHT, G.E. and STEFFEN, K.H. (1979) Geotechnics of gold mine waste disposal, *Current Geotechnical Practice in Mine Waste Disposal,* New York: ASCE, 1-53.

BLIGHT, G.E., VORSTER, K. and THOMPSON, R.R. (1985) Profiles of hydraulic-fill tailings beaches, and seepage through hydraulically sorted tailings, *Journal of the South African Institute of mining and Metallurgy,* 85(5), 157-161.

BLIGHT, G.E. and DU PREEZ, J. (1997) The escape of salt pollution from decommissioned gold residue deposits in South Africa, *Journal of the South African Institute of mining and Metallurgy,* July/August, 201-204.

BREWER, R. and SLEEMAN, J.R. (1988) *Soil Structure and Fabric,* Adelaide: CSIRO.

BURLAND, J.B. (1990) On the compressibility and shear strength of natural clays, *Géotechnique*, 40(3), 329-378.

CAFARO, F. and COTECCHIA, F. (2001) Structural degradation and changes in the mechanical behaviour of a stiff clay due to weathering, *Géotechnique*, 51(5), 441-453.

CASTRO, G. and POULOS, S.J. (1977) Factors affecting liquefaction and cyclic mobility, *ASCE Journal of the Geotechnical Engineering Division*, 103(GT6), 501-516.

CETIN, H. (2004) Soil-particle and pore orientations during consolidation of cohesive soil, *Engineering Geology*, 73, 1-11.

CHANG, H.N. (2004) *The Relationship between Shear Wave Velocity and Void Ratio of Gold Tailings*, Thesis (Meng), University of Pretoria.

CHEN, H.W. and VAN ZYL, D.J.A. (1988) Shear strength and volume change behaviour of copper tailings under saturated condition, *In*: D.J.A. VAN ZYL and S.G. VICK (ed.) *Hydraulic Fill Structures*, New York: ASCE, 430-451.

CHILLARIGE, A.R.V., MORGENSTERN, N.R., ROBERTSON, P.K. and CHRISTIAN, H. (1997) Seabed instability due to flow liquefaction in the Fraser River delta, *Canadian Geotechnical Journal*, 34, 520-533.

CLAYTON, C.R.I. and KHATRUSH, S.A. (1986) A new device for measuring local axial strains on triaxial specimens, *Géotechnique*, 36(4), 593-597.

CLAYTON, C.R.I., HIGHT, D.W. and HOPPER, R.J. (1992) Progressive destructuring of Bothkennar clay: Implications for sampling and reconsolidation procedures, *Géotechnique*, 42(2), 219-240.

CLAYTON, C.R.I., MATTHEWS, C. and SIMONS, N.E. (1995) *Site Investigation, 2ⁿᵈ edition,* Oxford: Blackwell Science.

COLLETT, C.V. and HOPE, A.D. (1983) *Engineering Measurements,* Bath: Pitman Books.

COLLINS, K. and MCGOWN, A. (1974) The form and function of microfabric features in a variety of natural soils, *Géotechnique,* 24(2), 223-254.

COTECCHIA, F. and CHANDLER, R.J. (1997). The influence of structure on the pre-failure behaviour of a natural clay, *Géotechnique*, 47(3), 523-544.
CRAIG, R.F. (1997) *Soil Mechanic, 6ᵗʰ edition,* New York: E&FN Spon.

DEWHURST, D.N., CLENNELL, M.B., BROWN, K.M. and WESTBROOK, G.K. (1996) Fabric and hydraulic conductivity of sheared clay, *Géotechnique,* 46(4), 761-768.

DOEBELIN, E.O. (1990) *Measurement systems- Application and Design, 4ᵗʰ edition*, New York: McGraw-Hill.

DYVIK, R. and HØEG, K. (1999) Comparison of tests on undisturbed and reconstituted silt and silty sand, *In* P.V. LADE AND J.A. YAMAMURO (ed.) *Physics and Mechanics of Soil Liquefaction,* Rotterdam: AA Balkema, 159-168.

EAST, D.R., RANSONE, J.W. and CINCILLA, W.A., 1988. The use of the electric piezocone for mine tailings deposits, *In:* J.DE RUITER (ed.) *Penetration Testing 1988,Vol 2,* Rotterdam: AA Balkema, 2, 745-750.

FEARON, R.E. and COOP, M.R. (2000) Reconstitution: What makes an appropriate reference material? *Géotechnique,* 50(4), 471-477.

FEDA, J. (1982) *Mechanics of Particulate Materials,* Amsterdam: Elsevier.

FREDRICH, J.T., MENENDEZ, B. and WANG, T.F. (1995) Imaging the pore structure of geomaterials, *Science,* 268, 276-279.

FROST, J.D., JANG, D-J., CHEN, C-C. and PARK, J-Y. (1998) Quantitative characterization of microstructure evolution, *In*: P.V. LADE and J.A. YAMAMURO (ed.) *Physics and Mechanics of Liquefaction,* Rotterdam: AA Balkema, 169-178.

FULLER, W.B. and THOMPSON, S.E. (1907) The laws of proportioning concrete, *Transactions of the American Society of Civil Engineers, paper no. 1053,* 67-172.

GARGA, V.K. and MCKAY, L.D. (1984) Cyclic triaxial strength of mine tailings, *ASCE Journal of Geotechnical Engineering,* 110(8), 1091-1105.

GARGA, V.K. and ZHANG, H. (1997) Volume change in undrained triaxial tests on sands, *Canadian Geotechnical Journal,* 34, 763-772.

GOWEN, M.J. and WILLIAMSON, J.R.G. (1987) A review of tailings deposition techniques in South Africa and appropriate selection of application, *In:* J.A. WATES and D. BRINK (ed.) *Mining and Industrial Waste Management,* Johannesburg: SAICE, 81-87.

GRAHAM, J. and HOULSBY, G.T. (1983) Elastic anisotropy of a natural clay, *Géotechnique,* 33(2), 165-180.

HAMEL, J.V. and GUNDERSON, J.W. (1973) Shear strength of Homestake slimes tailings, *ASCE Journal of the Soil Mechanics and Foundation Division,* 99, 427-431.

HARTGE, H. and RATHE, I. (1983) Schrumpf- und Scherrisse-Labormessungen, *Geoderma,* 31, 325-336.

HEYMANN, G. (1998) *The Stiffness of Soils and Weak Rocks at Very Small Strains,* Thesis (PhD), University of Surrey.

HEYMANN, G. and CLAYTON, C.R.I. (1999) Block sampling of soils: some practical considerations, *In:* G.R. WARDLE, G.E. BLIGHT and A.B. FOURIE (ed.) *Geotechnics of Developing Africa,* Rotterdam: AA Balkema, 331-339.

HØEG, K., DYVIK, R. and SANDBAEKKEN, G. (2000) Strength of undisturbed versus reconstituted silt and silty sand specimens, *Journal of Geotechnical and Geoenvironmental Engineering,* 126(7), 606-616.

HORN, R., BAUMGARTL, T., KAYSER, R. and BAASCH, S. (1995) Effect of aggregate strength on strength and stress distribution in structured soils, *In:* K.H. HARTGE and B.A. STEWART (ed.) *Soil Structure, its Development and Function,* Florida: CRC Press, 31-52.

IMAI, G. (1981) Experimental studies on sedimentation mechanisms and sediment formation of clay materials, *Soils and Foundations,* 21(1), 7-20.

INGLES, O.G. and LAFEBER, D. (1966) The influence of volume defects on the strength and strength isotropy of stabilized clays, *Engineering Geology,* 305-310.

ISHIHARA, K. (1993) Liquefaction and flow failure during earthquakes, *Géotechnique,* 43(3), 351-415.

JARDINE, R.J. (1995) One perspective of the pre-failure deformation characteristics of some geomaterials, *In:* M. B. JAMIOLKOWSKI, R. LANCELLOTTA AND D. LO PRESTI (ed.) *Prefailure deformation of Geomaterials,* Rotterdam: AA Balkema, 885-886.

JARDINE, R.J., SYMES, N.J. and BURLAND, J.B. (1984) The measurement of soil stiffness in the triaxial apparatus, *Géotechnique,* 34(3), 323-340.

JOHNS, R.A., STEUDE, J.S., CASTANIER, L.M. and ROBERTS, P.V. (1993) Nondestructive measurements of fracture aperture in crystalline rock cores using X-ray computed tomography, *Journal of Geophysical Research,* 98(B2), 1889-1900.

KEALY, C.D. and BUSCH, R. (1979) Evaluation of mine tailings disposal, *In:* ASCE Committee on Embankment Dams and Slopes of the Geotechnical Engineering Division (ed.) *Current Geotechnical Practice in Mine Waste Disposal,* New York: ASCE, 181-201.

KUERBIS, R. (1989) *The drained loading response of sands,* Thesis (Msc), University of British Columbia.

KUERBIS, R. and VAID, Y.P. (1988) Sand sample preparation- the slurry deposition method, *Soils and Foundations,* 28(4), 107-118.

KUERBIS, R., NEGUSSEY, D. and VAID Y.P. (1988) Effect of gradation and fines content on the undrained response of sands, *In*: D.J.A. VAN ZYL AND S.G. VICK (ed.) *Hydraulic Fill Structures,* New York: ASCE, 330-345.

LADD, R.S. (1974) Specimen preparation and liquefaction of sands, *ASCE Journal of the Geotechnical Engineering Division,* 100(GT10), 1180-1184.

LADD, R.S. (1977) Specimen preparation and cyclic stability of sands, *ASCE Journal of the Geotechnical Engineering Division,* 103(GT6), 535-547.

LADE, P.V. and YAMAMURO, J.A. (1997) Effects of non-plastic fines on the static liquefaction of sands, *Canadian Geotechnical Journal,* 34(6), 918-928.

LAMBE, T.W. and WHITMAN, R.V. (1969) *Soil Mechanics*, Ney York: Wiley, 71.

LAWRENCE, G.P. (1978) Stability of soil pores during mercury intrusion pososimetry, *Journal of Soil Science,* 29, 299-304.

LEFEBVRE, G. and DELAGE, P. (1986) The use of mercury intrusion porosimetry for the analysis of soft clay microstructure, *In:* A.S. BALASUBRAMANIAM, S. CHANDRA, and D.T. BERGADO (ed.) *Recent Developments in Laboratory and Field Tests and Analysis of Geotechnical Problems,* Rotterdam: AA Balkema, 31-42.

LEROUEIL, S. and MARQUES, M.E.S. (1996) Importance of strain rate and temperature effects in geotechnical engineering, *In:* T.C. SHEAHAN and V.N. KALIAKIN (ed.) *Measuring and Modeling Time Dependent Soil Behaviour,* New York: ASCE, 1-60.

LUCIA, P.C., DUNCAN, J.M. and SEED, H.B. (1981) Summary of research on case histories of flow failures of mine tailings impoundments, *Mine Waste Disposal Technology,* Washington, DC: US Department of Interior, Bureau of Mines, 46-53.

LUPINI, J.F., SKINNER, A.E. and VAUGHAN, P.R. (1981) The drained residual strength of cohesive soils, *Géotechnique,* 31(2), 181-213.

MAHMOOD, A. and MITCHELL, J.K. (1974) Fabric-property relationships in fine granular materials, *Clays and Clay Minerals,* 22, 397-408.

MAO, X. and FAHEY, M (1999) A method of reconstituting aragonite soil using a synthetic flocculant, *Géotechnique,* 49(1), 15-32.

MATYAS, E.L., READES, D.W. and WESCH, D.E. (1984) Geotechnical parameters and behaviour of uranium tailings, *Canadian Geotechnical Journal,* 21(3), 489-504.

MCPHAIL, G.I. and WAGNER, J.C. (1989) Disposal of residues, *In:* G.G. STANLEY (ed.) *The Extractive Metallurgy of Gold in South Africa, volume 2,* Johannesburg: The Chamber of Mines of South Africa, 655-707.

MESRI, G. and GODLEWSKI, P.M. (1977) Time and stress-compressibility interrelationship, *ASCE Journal of the Geotechnical Engineering Division,* 105(1), 106-113.

MESRI, G., FENG, T.W. and BENAK, J.M. (1990) Post densification penetration resistance of clean densified sands, *ASCE Journal of Geotechnical Engineering,* 116(7), 1095-1115.

MITCHELL, J.K. (1956) The fabric of natural clays and its relation to engineering properties, *Proceedings of the Highway Research Board*, 35, 693-713.

MITCHELL, J.K. (1976) *Fundamentals of Soil Behaviour*, New York: Wiley.

MITCHELL, J.K. (1993) *Fundamentals of Soil Behaviour*, 2nd *edition,* New York Wiley.

MITCHELL, J.K. and SOGA, K. (2005) *Fundamentals of Soil Behaviour, 3rd edition,* New York: Wiley.

MITCHELL, J.K., CHATOIAN, J.M. and CARPENTER, G.C. (1976) *The influence of sand fabric on liquefaction behaviour, Report No. TE 76-1*, Vicksburg, MS: Department of Civil Engineering, University of California, Berkley.

MITTEL, H.K. and MORGENSTERN, N.R. (1975) Parameters for the design of tailings dams, *Canadian Geotechnical Journal,* 12, 277-293.

MIURA, S. and TOKI, S. (1982) A sample preparation method and its effect on static and cyclic deformation-strength properties of sand, *Soils and Foundations,* 22(1), 61-77.

MOORE, C.A. (1971) Effect of mica on k_o compressibility of two soils, *Journal of Soil Mechanics and Foundation Division,* ASCE 97(SM9), 1275-1291.

MORGENSTERN, N.R. and TCHALENKO, J.S. (1967) Microscopic structures in kaolin subjected to direct shear, *Géotechnique,* 17, 309-328.

MULILIS, J.P., SEED, H.B., CHAN, C.K., MITCHELL, J.K. and ARULANANDAN, K. (1977) Effects of sample preparation on sand liquefaction, *ASCE Journal of the Geotechnical Engineering Division,* 103(GT2), 91-108.

ODA, M. (1972) Deformation mechanism of sands in triaxial compression tests, *Soils and Foundations,* 12(4), 45-63.

ODA, M. and KAZAMA, H. (1998) Microstructure of shear band and its relation to the mechanics of dilatency and failure of granular soils, *Géotechnique,* 48(4), 465-481.

ODA, M., KOISHIKAWA, I. and HIGUCHI, T. (1978) Experimental study of anisotropic shear strength of sands by plane strain test, *Soils and Foundations,* 18(1), 25-38.

ODA, M., TAKEMURA, T. and TAKAHASHI, M. (2004) Microstructure in shear band observed by microfocus X-ray computed tomography, *Géotechnique,* 54(8): 539-542.

OLSEN, R.E. and MESRI, G. (1970) Mechanisms controlling compressibility of clays, *ASCE Journal of the Soil Mechanics and Foundation Division,* 96, 1853-1878.

PAN, Y-W. and DONG, J-J. (1999) A micromechanics-based methodology for evaluating the fabric of granular material, *Géotechnique,* 49(6), 761-775.

PAPAGEORGIOU, G. (2004) *Liquefaction Assessment and Flume Modelling of the Merriespruit Gold and Bafokeng Platinum Tailings,* Thesis (PhD), University of Witwatersrand.

PENMAN, A.D.M. (1994) Tailings dams, some aspects of their design and construction, *In:* K.R.SAXENA (ed.) *Geotechnical Engineering: Emerging Trends in Design and Practice,* Rotterdam: AA Balkema, 247-277.

PETTIBONE, H. and KEALY, D. (1971) Engineering properties of mine tailings, *ASCE Journal of the Soil Mechanics and Foundation Division,* 97, 1207-1225.

POROVIC, E. (1995) *Investigations of soil behaviour using a resonant column torsional shear hollow cylinder apparatus*, Thesis (PhD), Imperial College of Science, Technology and Medicine, University of London.

QIU, Y. and SEGO, D.C. (2001) Laboratory properties of mine tailings, *Canadian Geotechnical Journal,* 38(1), 183-190.

RAD, N.S. and TUMAY, M.T. (1987) Factors affecting sand specimen preparation by raining, *ASTM Geotechnical Testing Journal,* 10(1), 31-57.

RIPLEY, E.A., REDMANN, R.E. and MAXWELL, J. (1982) Environmental impact of mining in Canada, *The National Impact of Mining Series,* Kingston: Center for Resource Studies.

RIPPA, F. and PICARELLI, L. (1977) Some considerations on index properties of southern Italian shales, *Proceedings, International Symposium on the Geotechnics of Structurally Complex Formations,* 19- 21 September, 1977, Capri, 401-406.

RITCEY, G.M. (1989) *Tailings Management, Problems and solutions in the mining industry,* Excerpts: Elsevier.

ROBERTSON, A.M. (1987) Alternative acid mine drainage abatement measures, *Proceedings, Mine Land Reclamation Confrence,* Campbell River, British Columbia.

ROBRINSKI, E.I. (1975) Thickened discharge- A new approach to tailings disposal, *The Canadian Institute of Mining and Metallurgy Bullitin,* 68, 47-59.

ROWE, P.W. (1972) The relevance of soil fabric to site investigation practice, *Géotechnique,* 22(2), 195-300.

RUEHRWEIN, W.A. and WARD, D.W. (1952) Mechanism of clay aggregation by polyelectrolytes, *Soil Science,* 73, 485-492.

SANTAMARINA, J.C. and CASCANTE, G. (1996) Stress anisotropy and wave propagation: a micromechanical view, *Canadian Geotechnical Journal,* 33(5), 770-782.

SCHIFFMEN, R.L., VICKS, S.G. and GIBSON, R.E. (1988) Behaviour and properties of hydraulic fills, *In*: D.J.A. VAN ZYL AND S.G. VICK (ed.) *Hydraulic Fill Structures,* New York: ASCE, 166-202.

SEED, H.B. and DE ALBA, P. (1986) Use of SPT and CPT tests for evaluating the liquefaction resistance of sands, *In:* S.P. CLEMENCE (ed.) *Use of in situ tests in geotechnical engineering,* Philadelphia: ASTM, 281-302.

SEED, H.B., MITCHELL, J.K. and CHAN C.K. (1962) Swell and swell pressure characteristics of compacted clays, *Highway Research Board Bullitin,* 313, 12-39.

SHERARD, J.L., DUNNIGAN, L.P. and TALBOT, J.R. (1984) Basic properties of sand and gravel filters, *ASCE Journal of Geotechnical Engineering,* 110(6), 700-718.

SHERWOOD, P.T. and RYLEY, D.M. (1968) *An examination of cone-penetrometer methods for determining the liquid limit of soils*, *TRRL Report LR 233*, Crowthorne: Transport and Road Research Laboratory.

SIMPSON, B., O'RIORDAN, N.J. and CROFT, D.D. (1979) A computer model for the analysis of ground movements in London Clay, *Géotechnique,* 29(2), 149-175.

SLADEN, J.A., D'HOLLANDER, R.D. and KRAHN, J. (1985) The liquefaction of sands: a collapse surface approach, *Canadian Geotechnical Journal,* 22(4), 564-578.

SMITH, E.S. (1972) Tailings disposal- Failures and lessons, *In:* C.L. APLIN and G.O. ARGALL (ed.) *Tailings Disposal Today,* Arizona, Miller Freeman, 356-376.

STANLEY, G.G. (ed.) (1987) The Extractive Metallurgy of Gold in South Africa, *The S.A. Institute of Mining and Metallurgy Monograph Series M7,* Johahannesberg: The Chamber of Mines.

STONE, K.J.L., RANDOLPH, M.F. TOH, S. and SALES, A.A. (1994) Evaluation of consolidation behaviour of mine tailings, *ASCE Journal of Geotechnical Engineering,* 120(3), 473-490.

SULLY, J.P. (1985) Geotechnical aspects of remedial design for a gold tailings dam, *International Journal for Numerical and Analytical Methods in Geomechanics,* 9(6), 589-598.

SYDENHAM, P.H. (1982) *Standardization of Measurements: Fundamentals and Practice,* Chichester: John Wiley and Sons.

TATSUOKA, F. (1988) Some recent developments in triaxial testing systems for cohesionless soils, *Advanced Triaxial Testing of Soils and Rocks,* Philadelphia: ASTM, 7-67.

TATSUOKA, F., OCHI, K., FUJII, S. and OKAMATO, M. (1986) Cyclic undrained triaxial and torsional shear strength of sands for different sample preparation methods, *Soils and Foundations,* 6(3), 23-41.

TERZAGHI, K. (1925) Zur charakteristik der bausande, *Zeitschrift des Oesterreichischen Ingenieur und Architekten Vereines*, 33-34.

TERZAGHI, K. and PECK, R.B. (1948) *Soil Mechanics in Engineering Practice, 2nd edition*, New York: John Wiley and Sons.

THEVANAYAGAM, S., SHENTHAN, T., MOHANS, S. and LIANG, J. (2002) Undrained fragility of clean sands, silty sands and sandy silts, *Journal of Geotechnical and Geoenvironmental Engineering,* 128, 849-859.

THERON, M. (2004) *The Influence of Fine Platy Particles on the Behaviour of a Rotund Sand,* Thesis (PhD), University of Southampton.

THERON, M., HEYMANN, G. and CLAYTON, C.R.I. (2004) The small strain stiffness of gold tailings, *In:* A.V. DA FONSECA and P.W. MAYNE (ed.) *Geotechnical and Geophysical Site Characterization, volume 1,* Rotterdam: Millpress, 575-580.

VAID, Y.P. and NEGUSSEY, D. (1984) Relative density of air and water pluviated sand, *Soils and Foundations,* 24(2): 101-105.

VAID, Y.P. and NEGUSSEY, D. (1988) Preparation of reconstituted sand specimens, *Advanced Triaxial Testing of Soils and Rocks,* Phiadelphia: ASTM, 405-417.

VAID, Y.P. and PILLAI, V.S. (1992) Critical state of sands, *Géotechnique,* 42(4), 655-663.

VAID, Y.P. and SIVATHAYALAN, S. (1996) Static and cyclic liquefaction potential of Fraser Delta sand in simple shear and triaxial tests, *Canadian Geotechnical Journal*, 33, 281-289.

VAID, Y.P. and SIVATHAYALAN, S. (2000) Fundamental factors affecting liquefaction susceptibility of sands, *Canadian Geotechnical Journal,* 37: 592-606.

VAID, Y.P., CHUNG, E.K.F. and KUERBIS, R.H. (1990) Stress path and steady state, *Canadian Geotechnical Journal,* 27: 1-7.

VAID, Y.P., SIVATHAYALAN, S. and STEDMAN, D. (1999) Influence of specimen reconstituting method on the undrained response of sands, *Geotechnical Testing Journal,* 22(3): 187-195.

VAN ZYL, D. (1993) Mine waste disposal, *In*: D.E. DANIEL (ed.) *Geotechnical Practice for Waste Disposal,* London: Chapman Hall, 269-286.

VAUGHAN, P.R. (1985) Mechanical and hydraulic properties of in situ residual soils, *Proceedings, 1st International Conference on Geomechanics in Tropical, Lateritic and Saprolitic Soils,* February, 1985, Brazil, 231-263.

VAUGHAN, P.R. (1997) Panel discussions: Sedimentation of tailings, *Proceedings, 14th International Conference on Soil Mechanics and Foundation Engineering,* September, 1997, Hamburg, Germany, 2561-2562.

VAUGHAN, P.R., MACCARINI, M. and MOKHTAR, S.M. (1988) Indexing the engineering properties of residual soils, *Quarterly Journal of Engineering Geology,* 21(1): 69-84.

VERMEULEN, N.J. (2001) *The Composition and State of Gold Tailings*, Thesis (Ph.D), University of Pretoria.

VICKS, S.G. (1983) *Planning, Design and Analysis of Tailings Dams,* New York, Wiley.

VICKS, S.G. (1990) *Planning, Design and Analysis of Tailings Dams,2nd edition,* New York, Wiley.

WAGENER, F.M., CRAIG, H.J., BLIGHT, G.E., MCPHAIL, G., WILLIAMS, A.A.B. and STRYDOM, J.H. (1998) The Merriespruit tailings dam failure- A review, *Proceedings of the 5th International Conference on Tailings and Mine Waste,* Fort Collins, USA, 925-952.

WAGENER, F. and JACOBSZ, S.W. (1999) Penstock failure on gold tailings dams in South Africa, *Proceedings, 12th Regional Conference for Africa on Soil Mechanics and Geotechnical Engineering,* October, 1999, Durban, South Africa, 95-100.

WESTRAAD, D. (2004) *Suction induced shear strength of gold mine tailings*, Thesis (Meng.), University of Pretoria.

WOOD, F.M. (1999) *Influence of Specimen Reconstitution Method on the Undrained Response and Microstructure of Silty Sands,* Thesis (Meng.), Clarkson University.

WOOD, F.M. and YAMAMURO, J.A. (1999) The effect of depositional method on the liquefaction behaviour of silty sands, *Proceedings, 13th ASCE Engineering Mechanics Conference,* June, 1999, Baltimore,

YAMAMURO, J.A. and LADE, P.V. (1997) Static liquefaction of very loose sands, *Canadian Geotechnical Journal,* 34: 905-917.

Chapter 7

References

AKERS, R.J. (1975) *Flocculation,* London: The Institute of Chemical Engineers.

ANANDARAJAH, A. and KUGANENTHIRA, N. (1995) Some aspects of fabric anisotropy of soils, *Géotechnique,* 45(1), 69-81.

ANANDARAJAH, A. and ZHAO, D. (2000) Triaxial behaviour of kaolinite in different pore fluids, *Journal of Geotechnical and Geoenvoironmental Engineering*, 126(2), 148-156.

ARCH, J. and MALTMAN, A.J. (1990) Anisotropic permeability and tortuosity in deformed wet sediments, *Journal of Geophysical Research,* 95(B6), 9035-9047.

BABEL, U., BENECKE, P., HARTGE, K.H., HORN, R. and WEICHMANN, H. (1995) Determination of soil structure at various scales, *In*: K.H. HARTGE AND B.A. STEWART (ed.) *Soil Structure, its Development and Function,* Florida: CRC Press, 1-10.

BIOT, M.A. (1941) General theory of three-dimensional consolidation, *Journal of Applied Physics,* 12, 155-164.

BISHOP, A.W. (1967) Progressive Failure- with special reference to machanism causing it, *In: Proceedings of the Geotechnical Conference, Oslo, Norway,* 2, 142-150.

YI, F. (1991) Behaviour of compacted collapsible soils subjected to water infiltration, Thesis (Dr. Eng.), University of Tokyo.

YOSHIMI, Y. TOKIMATSU, K. and HOSAKA, Y. (1989) Evaluation of liquefaction resistance of clean sands based on high quality undisturbed samples, *Soils and Foundations,* 29(1): 3-104.

ZLATOVIC, S. and ISHIHARA, K. (1997) Normalized behaviour of very loose non-plastic soils: effects of fabric, *Soils and Foundations,* 37(4): 47-56.

ZLATOVIC, S. and ISHIHARA, K. (1998) Flow failure- Some data on onset conditions, *In:* B. MARIC, Z. LISAC and A. SZAVITS-NOSSAN (ed.) *Geotechnical Hazards, Proceedings, 11th Danube-European Conference on Soil Mechanics and Foundation Engineering,* May, 1998, Croatia.

Appendix A
Preliminary SEMs

SEM images of various gold tailings samples were taken as a preliminary investigation on the observable fabric and the possibilities with regards to using SEM images. These include SEM images of moist tamped, slurry and in situ gold tailings samples. Backscattered SEM images were also taken of the same samples prepared in a polished section. Images obtained from the SEM are three-dimensional, while Backscattered images are two-dimensional. The use of 2D (backscattered SEM) or 3D (conventional SEM) images will thus need to be decided and evaluated from these preliminary images.
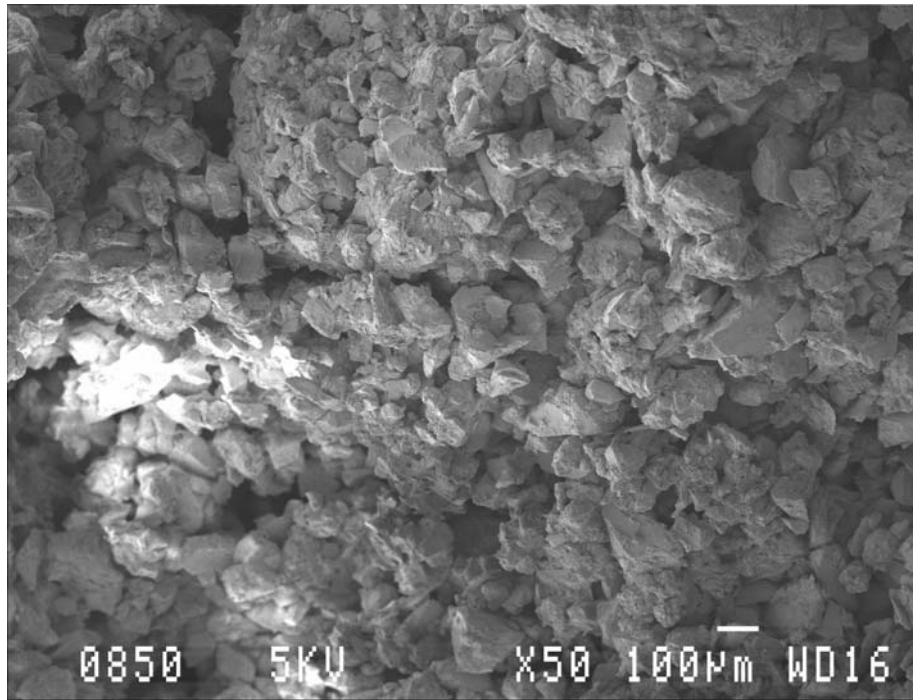
Figure A-1. SEM image of a moist tamped sample at an arbitrary void ratio (50X magnification).
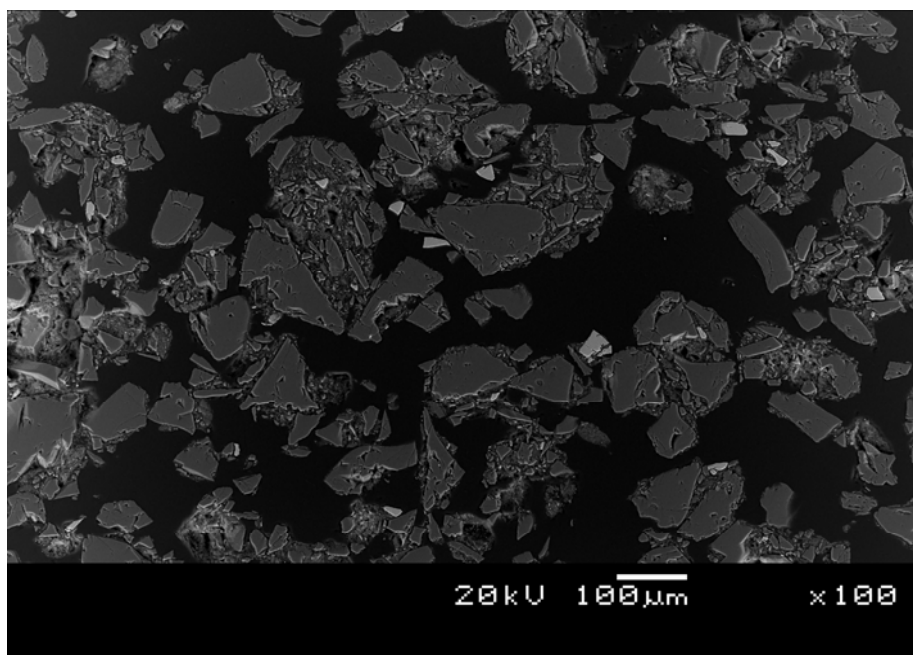
Figure A-2. Backscattered SEM image of a moist tamped sample polished section at an arbitrary void ratio (50X magnification).
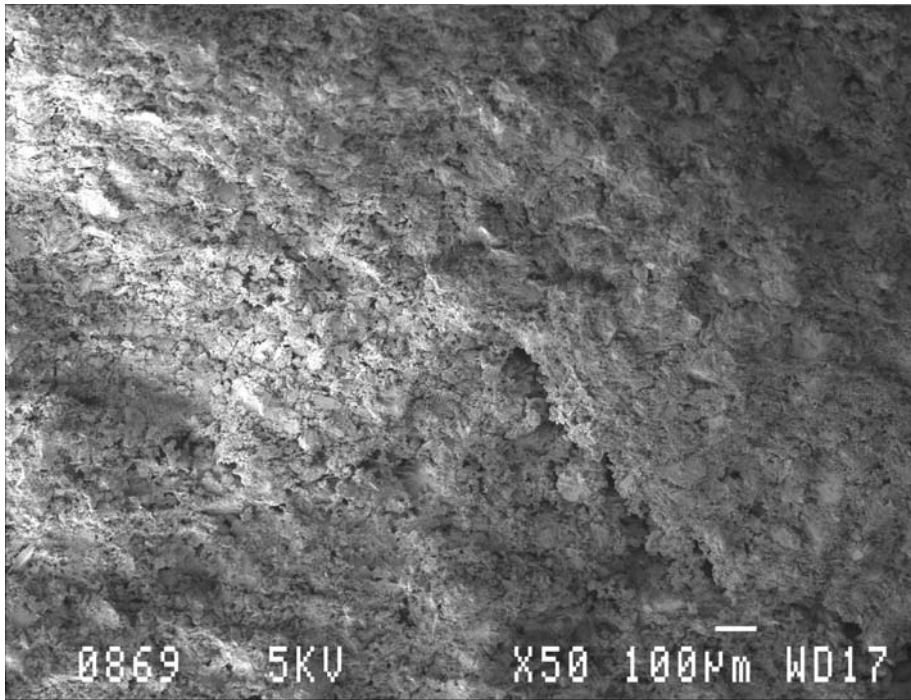
Figure A-3. SEM image of a slurry sample at an arbitrary void ratio (50X magnification).
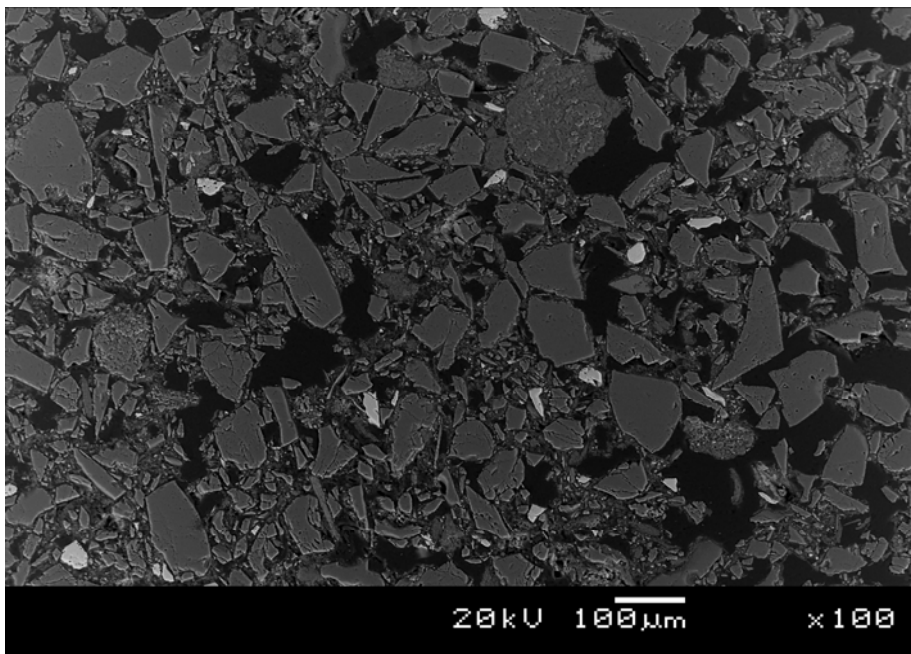
Figure A-4.Backscattered SEM image of a slurry sample polished section at an arbitrary void ratio (50X magnification).
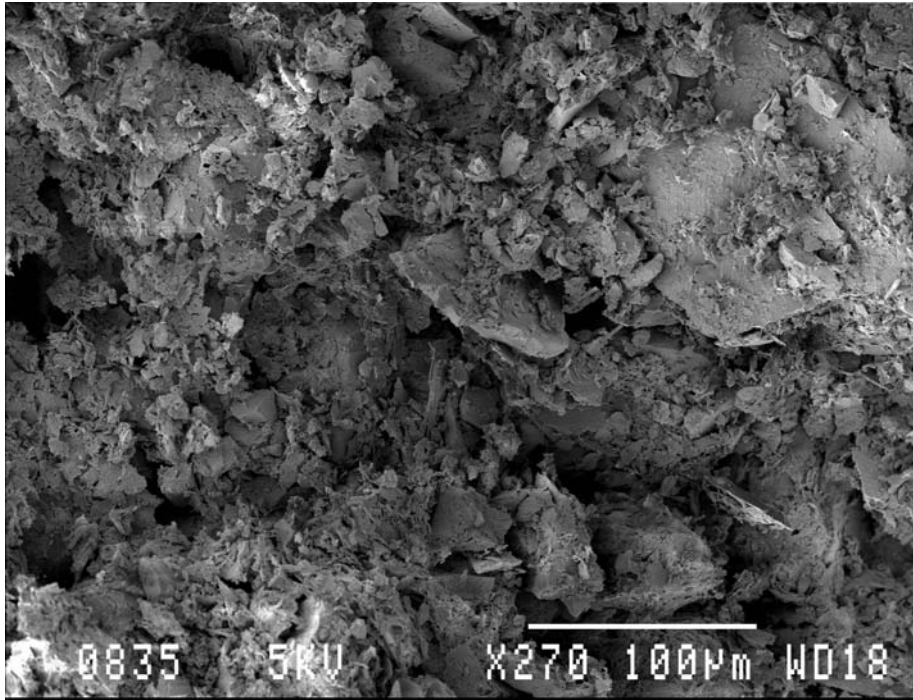
Figure A-5. SEM image of in situ gold tailings (270X magnification).
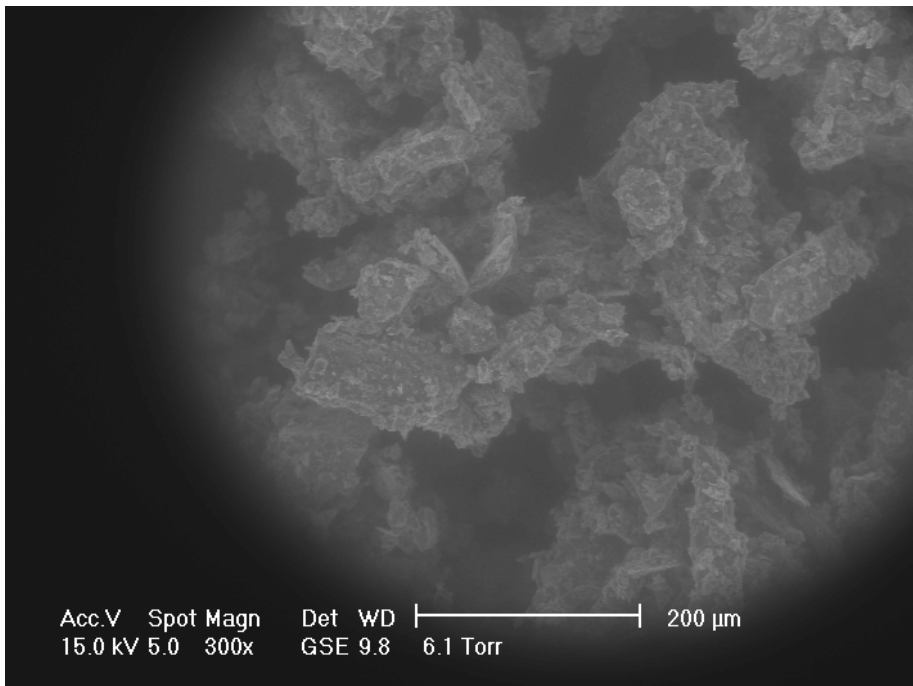
Figure A-6. Environmental SEM image of moist tamped sample (300X magnification).

Appendix B

Instrumentation and Calibration

The calibration methodology used in this thesis has been described in Chapter 3. Appendix B includes the specifications for the instrumentation used, the calibration devices as well as the calibration, error and hysteresis graphs for all instrumentation. An additional armature position test was also included for both LVDTs to investigate the linear range of the apparatus.

Internal LVDT 1

Calibrated Instrument	RDP 6385 D5/200WRA submissible LVDT/RDP Transducer Amplifier Type S7AC
Department	Civil engineering, University of Pretoria
Instrument no.	6385

Calibration device 1	YGP Tungsten Carbide Gauge Blocks
Department	National Metrology, CSIR
Instrument no.	80112
Certificate no.	DM/1177
Accuracy	±30 nm @ 20°C

Calibration device 2	Mitutoyo ID-F150 Micrometer
Department	Civil Engineering, University of Pretoria
Instrument no.	6049
Accuracy	±1.5 μm

Data acquisition card	National Instruments PCI-6014
Department	Civil Engineering, University of Pretoria
Instrument no.	1044CB9
Certificate no.	70772
Resolution	65536 bit
Absolute accuracy	1 day 0.0154 % of reading
	90 days 0.0174 % of reading
	1 year 0.0196 % of reading

DAQ card settings	
Sensor range	-10V to +10V
Input method	Differential
Channel	0

Figure B-1. Armature position test for LVDT1 at gain level 5.
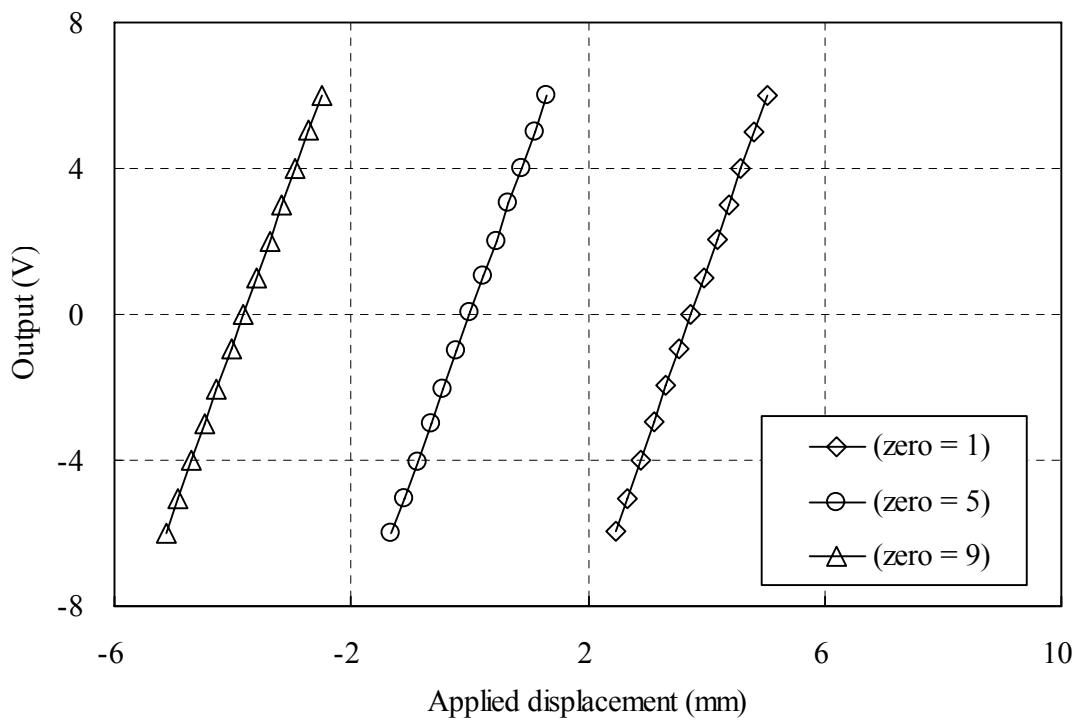
Figure B-2. Armature position test for LVDT1 at gain level 6.
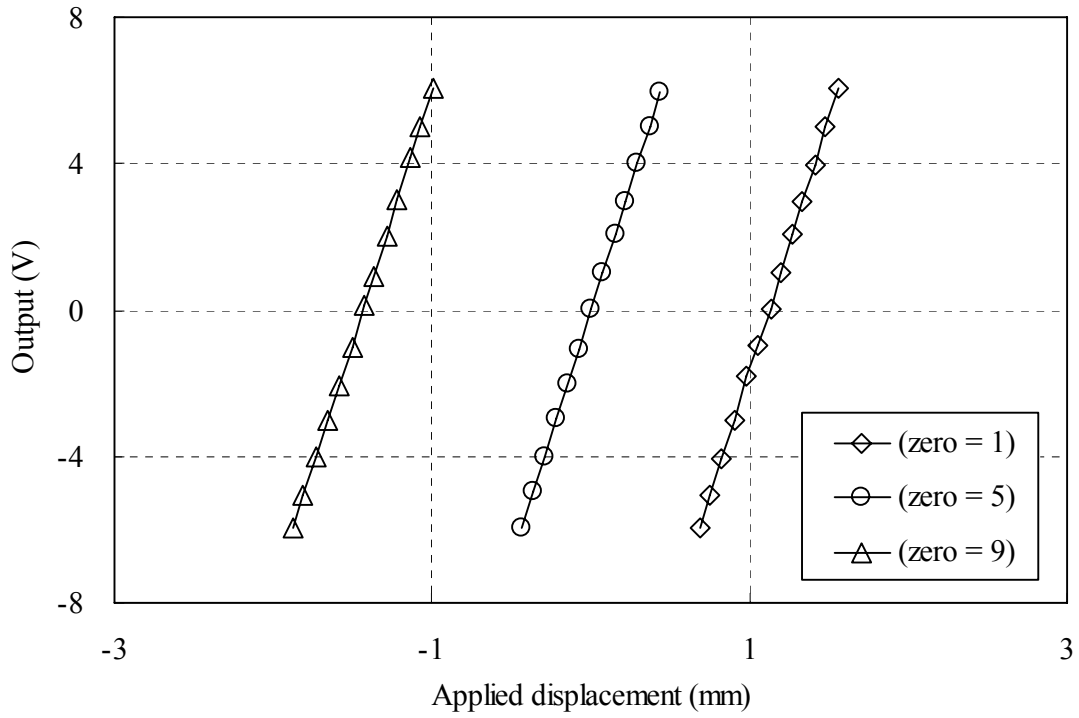
Figure B-3. Armature position test for LVDT1 at gain level 7.
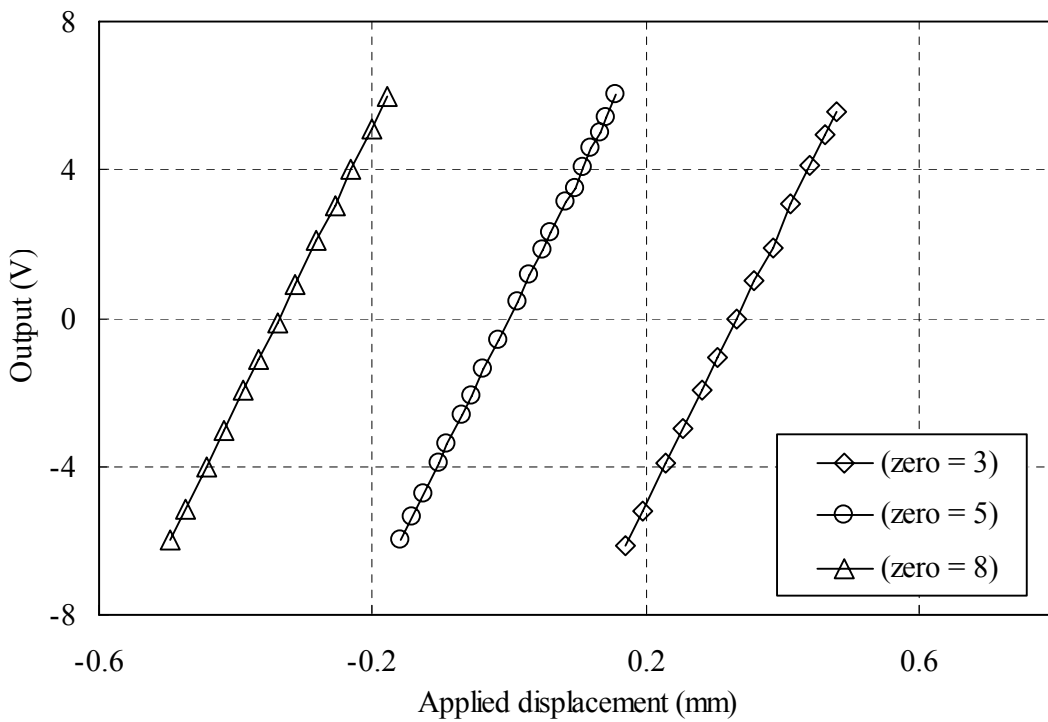
Figure B-4. Armature position test for LVDT1 at gain level 8.
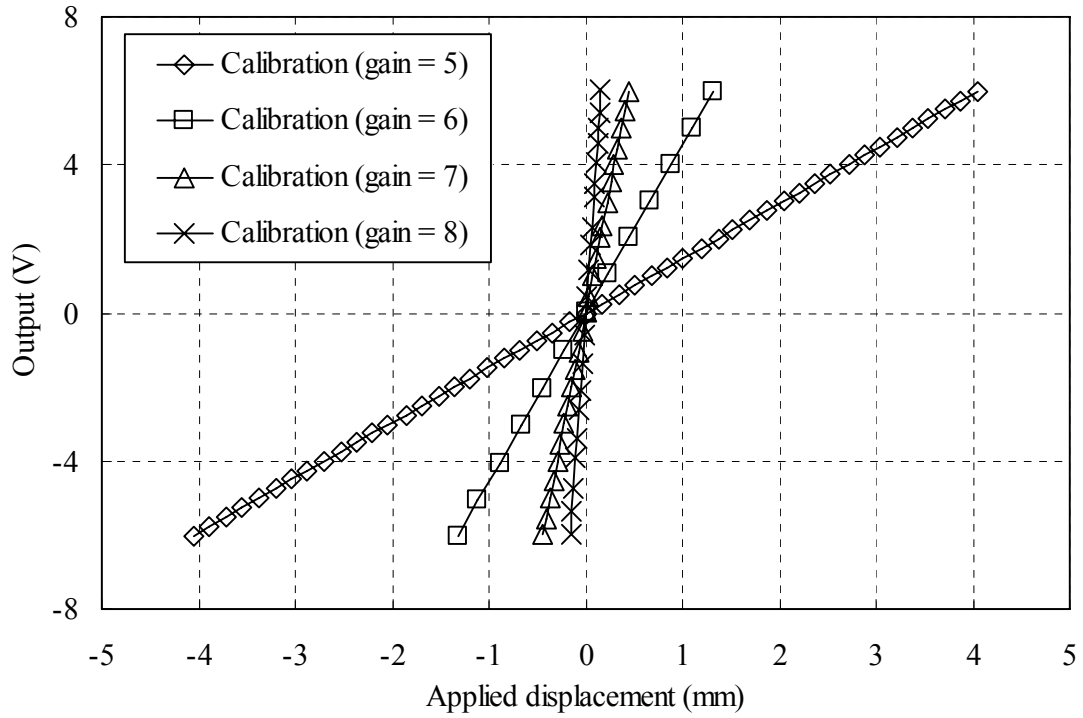
Figure B-5. Calibration graph for LVDT1 at gain levels 5, 6, 7 and 8.
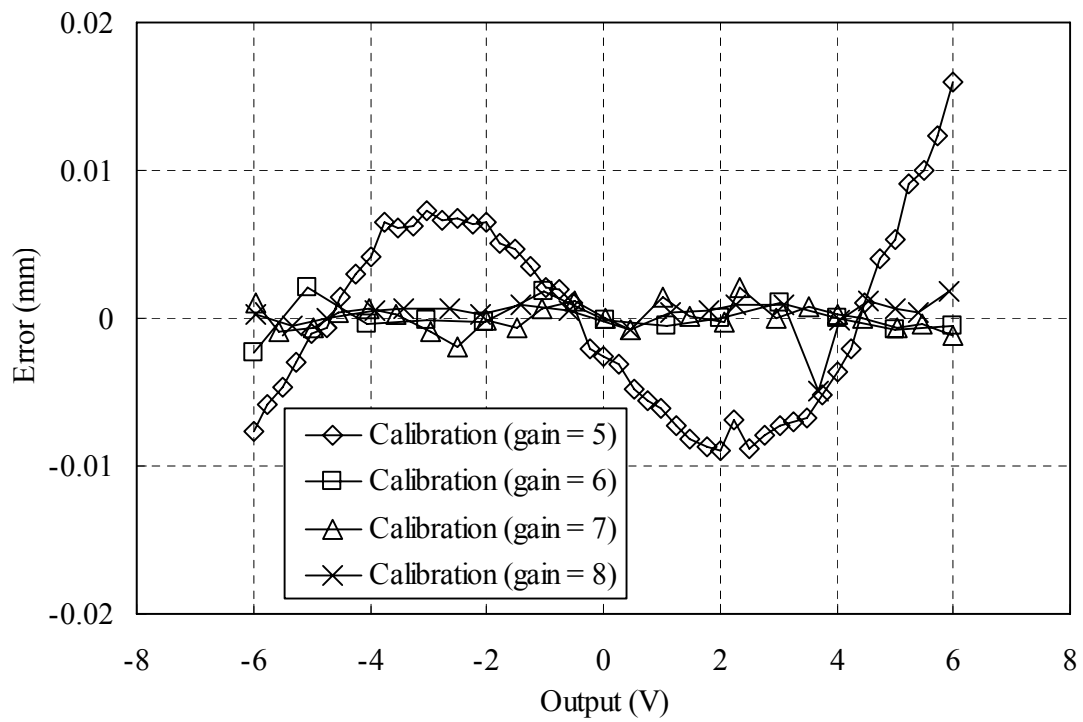
Figure B-6. Error graph for LVDT1 at gain levels 5, 6, 7 and 8.
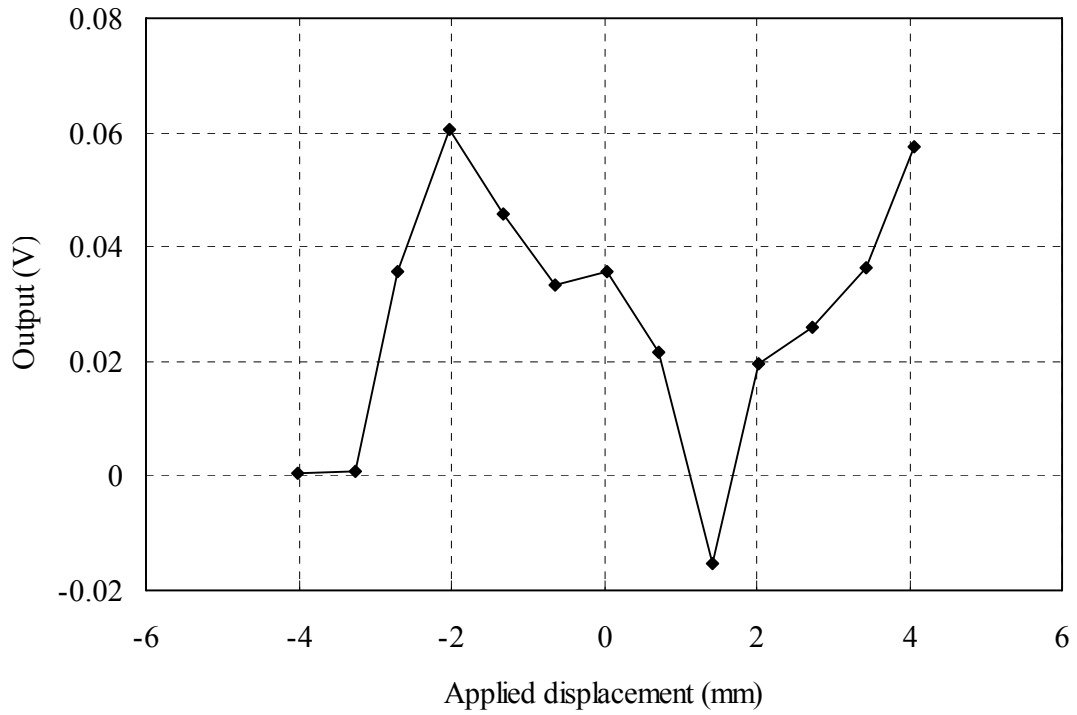
Figure B-7. Hysteresis graph for LVDT1 at gain level 5.
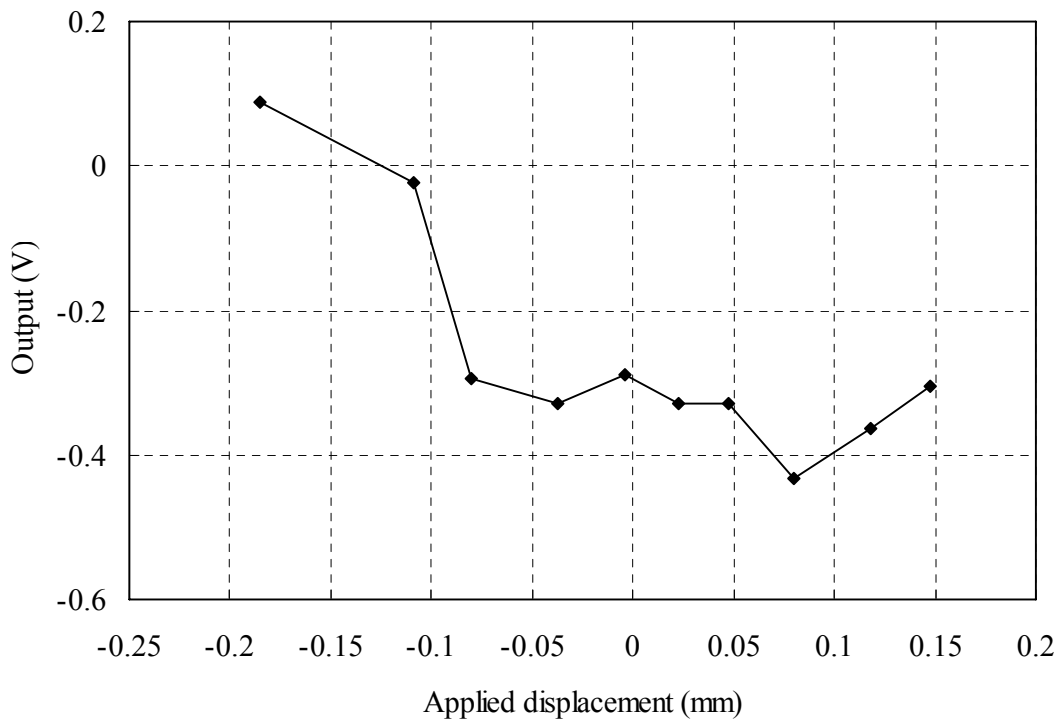
Figure B-8. Hysteresis graph for LVDT1 at gain level 8.

Internal LVDT 2

Calibrated Instrument	RDP 6385 D5/200WRA submissible LVDT/RDP Transducer Amplifier Type S7AC
Department	Civil engineering, University of Pretoria
Instrument no.	6385

Calibration device 1	YGP Tungsten Carbide Gauge Blocks
Department	National Metrology, CSIR
Instrument no.	80112
Certificate no.	DM/1177
Accuracy	±30 nm @ 20°C

Calibration device 2	Mitutoyo ID-F150 Micrometer
Department	Civil Engineering, University of Pretoria
Instrument no.	6049
Accuracy	±1.5 μm

Data acquisition card	National Instruments PCI-6014
Department	Civil Engineering, University of Pretoria
Instrument no.	1044CB9
Certificate no.	70772
Resolution	65536 bit
Absolute accuracy	1 day 0.0154 % of reading
	90 days 0.0174 % of reading
	1 year 0.0196 % of reading

DAQ card settings	
Sensor range	-10V to +10V
Input method	Differential
Channel	1

Figure B-9. Armature position test for LVDT2 at gain level 5.

Figure B-10. Armature position test for LVDT2 at gain level 6.

Figure B-11. Armature position test for LVDT2 at gain level 7.
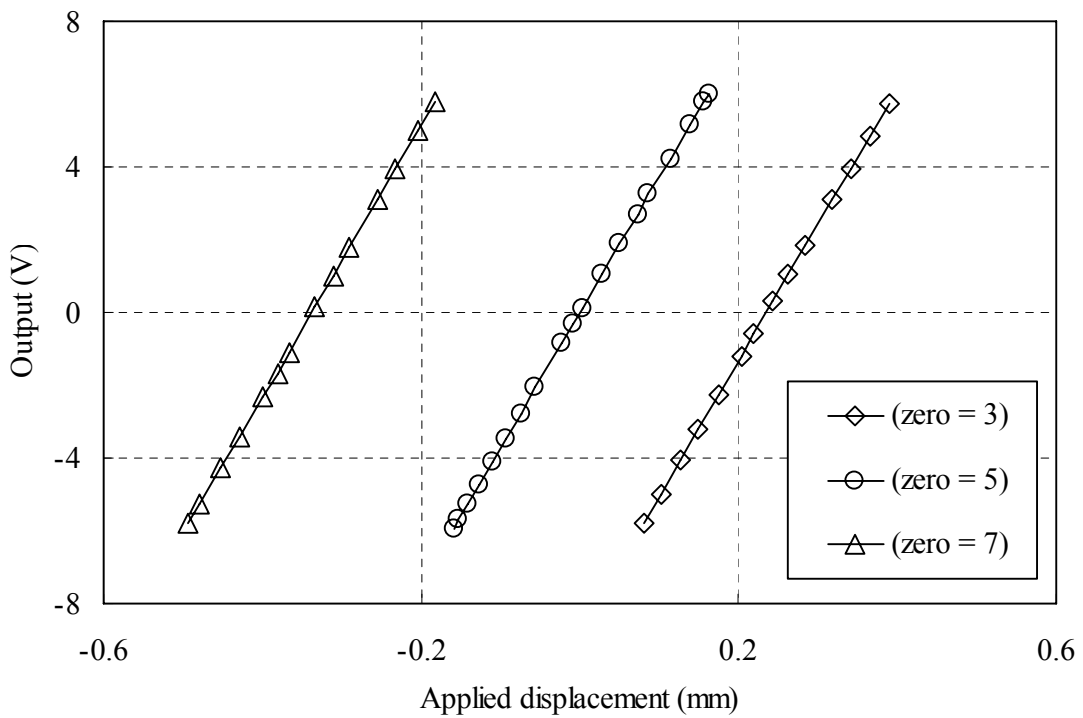
Figure B-12. Armature position test for LVDT2 at gain level 8.
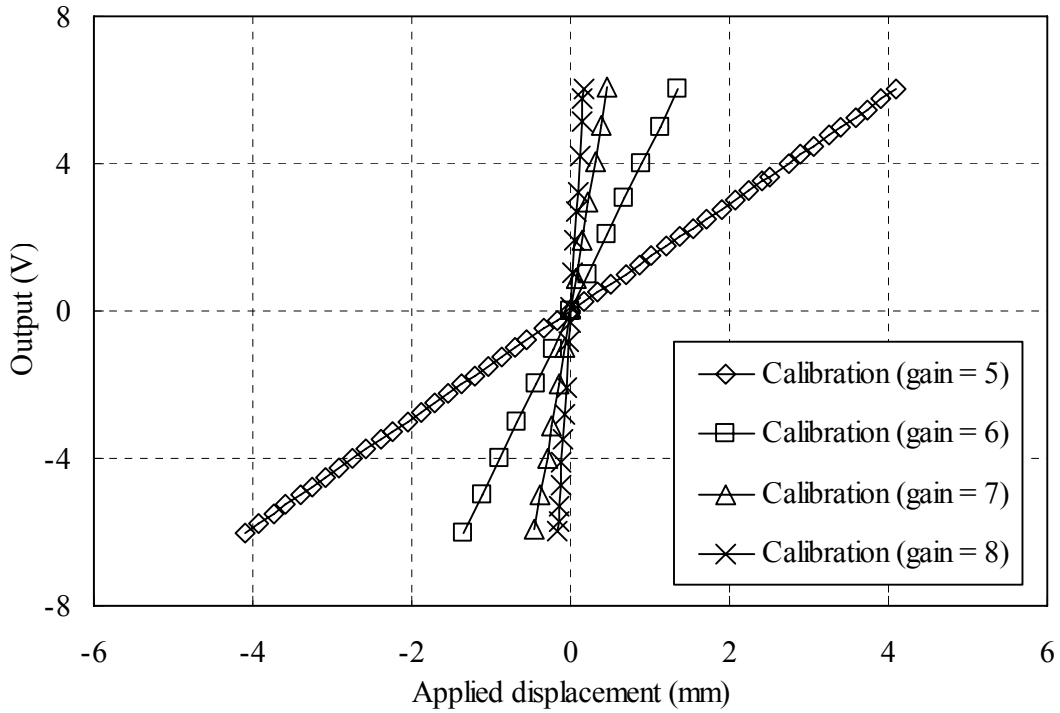
Figure B-13. Calibration graph for LVDT2 at gain levels 5, 6, 7 and 8.
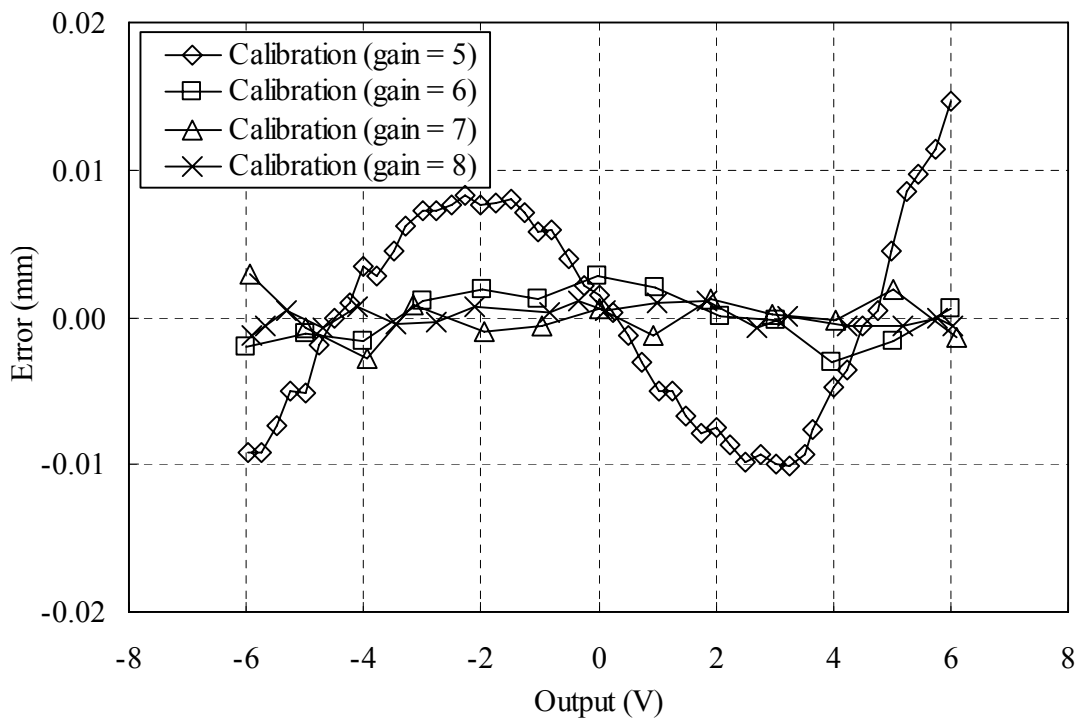
Figure B-14. Error graph for LVDT2 at gain levels 5, 6, 7 and 8.
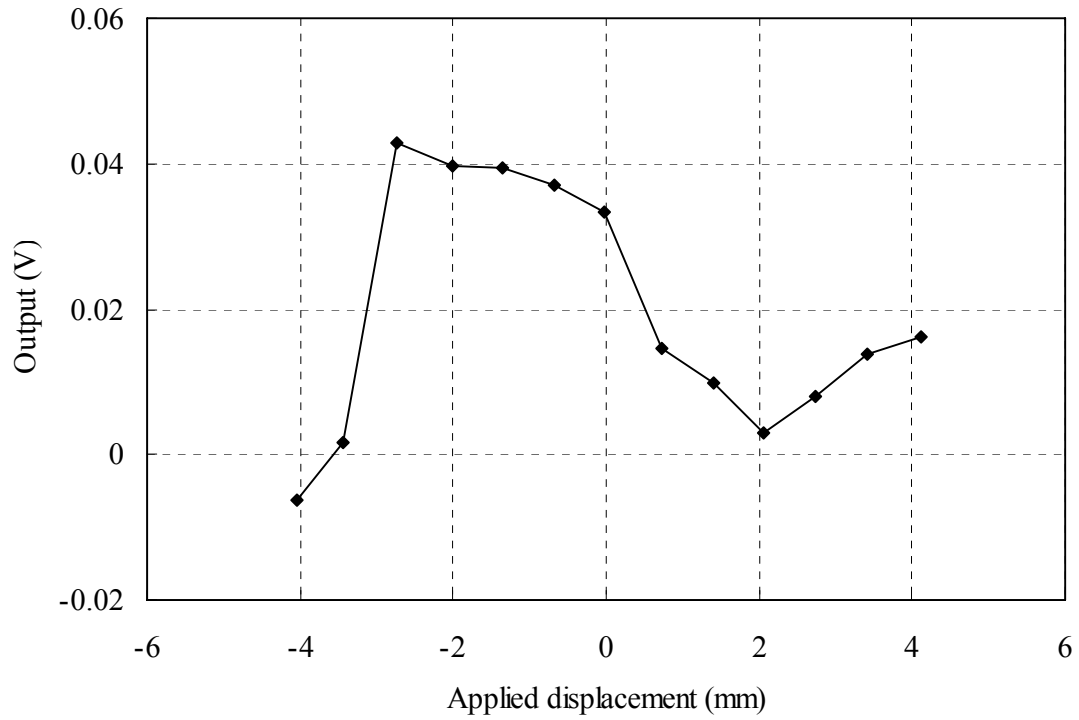
Figure B-15. Hysteresis graph for LVDT2 at gain level 5.
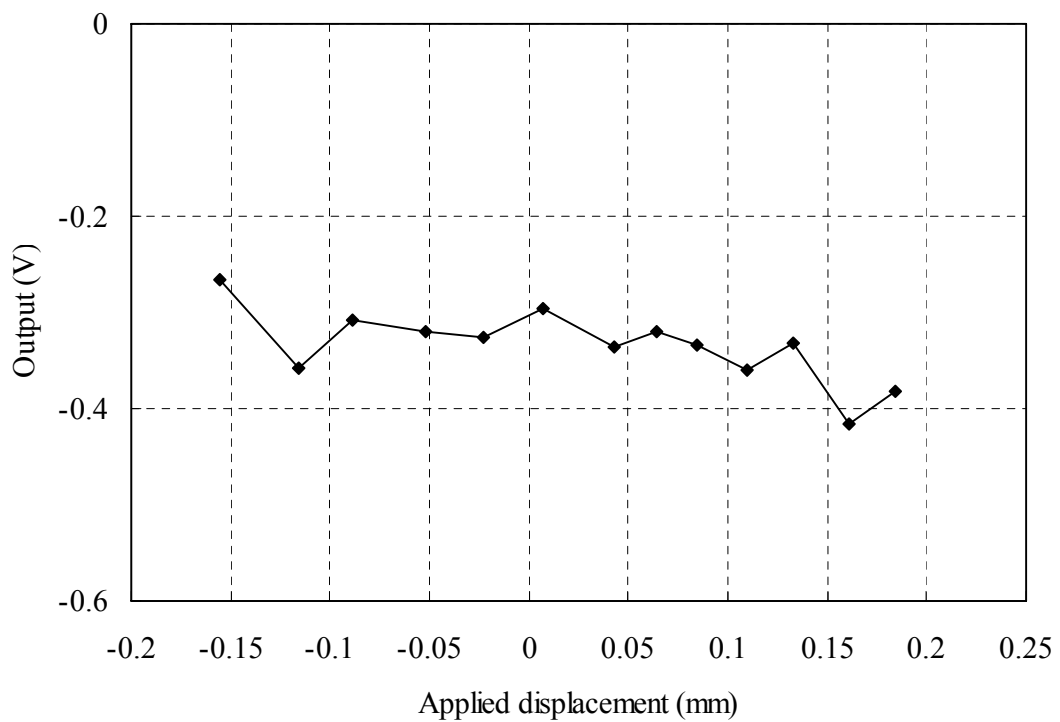
Figure B-16. Hysteresis graph for LVDT2 at gain level 8.

Linear displacement transducer

Calibrated Instrument	Kyowa linear displacement transducer
Department	Civil engineering, University of Pretoria
Instrument no.	DT-20-D
Serial no.	YB-6279

Calibration device 1	YGP Tungsten Carbide Gauge Blocks
Department	National Metrology, CSIR
Instrument no.	80112
Certificate no.	DM/1177
Accuracy	±30 nm @ 20°C

Calibration device 2	Mitutoyo ID-F150 Micrometer
Department	Civil Engineering, University of Pretoria
Instrument no.	6049
Accuracy	±1.5 μm

Data acquisition card	National Instruments PCI-6014
Department	Civil Engineering, University of Pretoria
Instrument no.	1044CB9
Certificate no.	70772
Resolution	65536 bit
Absolute accuracy	1 day 0.0154 % of reading
	90 days 0.0174 % of reading
	1 year 0.0196 % of reading

DAQ card settings	
Sensor range	-10V to +10V
Input method	Differential
Channel	2

Amplifier	HBM KWS 3073
Kal. Signal @ 2mV/V	4983
Measurements @	1mV/V
Channel	1
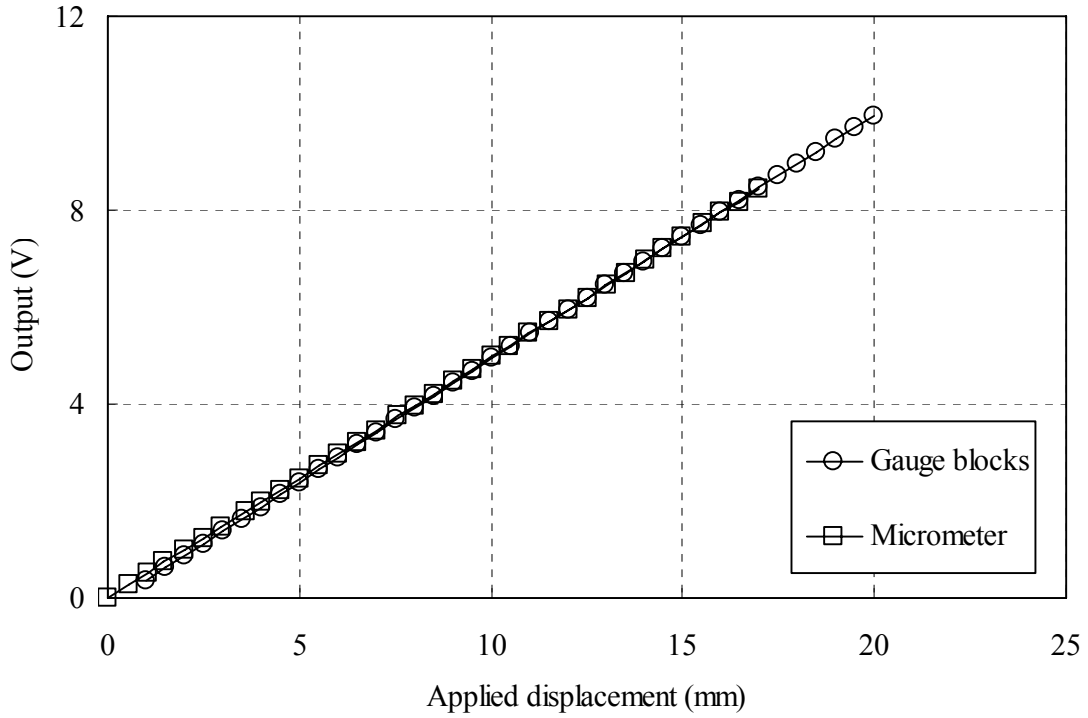
Figure B-17. Calibration graph for external displacement transducer using gauge blocks and micrometer.
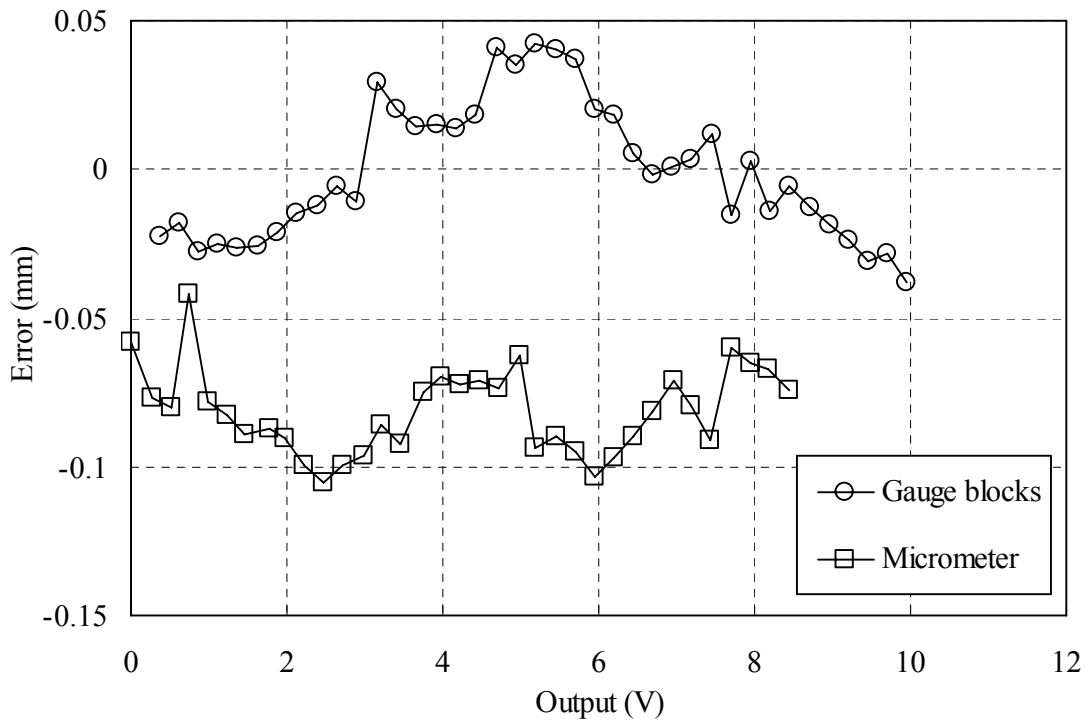
Figure B-18. Error graph for external displacement transducer using gauge blocks and micrometer.
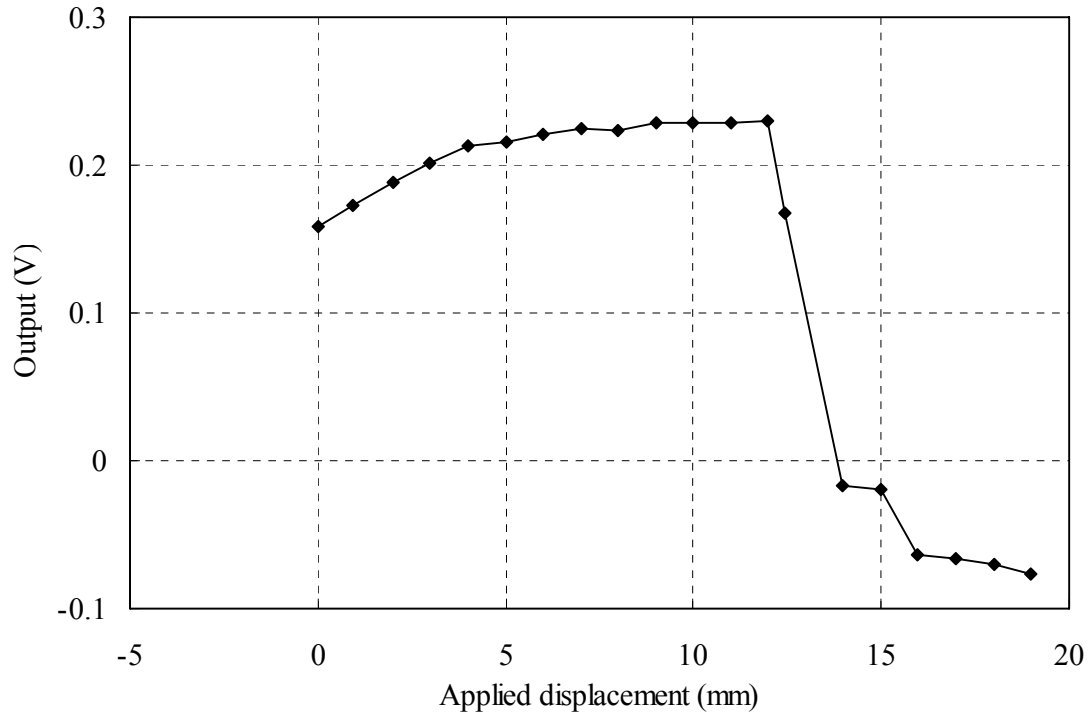
Figure B-19. Hysteresis graph for external displacement transducer using gauge blocks and micrometer.

Internal submersible load cell

Calibrated Instrument	Imperial College type submersible load cell
Department	Civil engineering, University of Pretoria
Calibration device	Lloyds LRX Plus single column test system
Department	Civil engineering, University of Pretoria
Instrument no.	UNIV VAN PTA 633195
Certificate no.	UP19222B
Accuracy	0.5% FS @ 20°C with 95% confidence
Data acquisition card	National Instruments PCI-6014
Department	Civil Engineering, University of Pretoria
Instrument no.	1044CB9
Certificate no.	70772
Resolution	65536 bit
Absolute accuracy	1 day 0.0154 % of reading
	90 days 0.0174 % of reading
	1 year 0.0196 % of reading
DAQ card settings	
Sensor range	-10V to +10V
Input method	Differential
Channel	3
Amplifier	HBM KWS 3073
Kal. Signal @ 2mV/V	5008
Measurements @	0.5mV/V
Channel	2
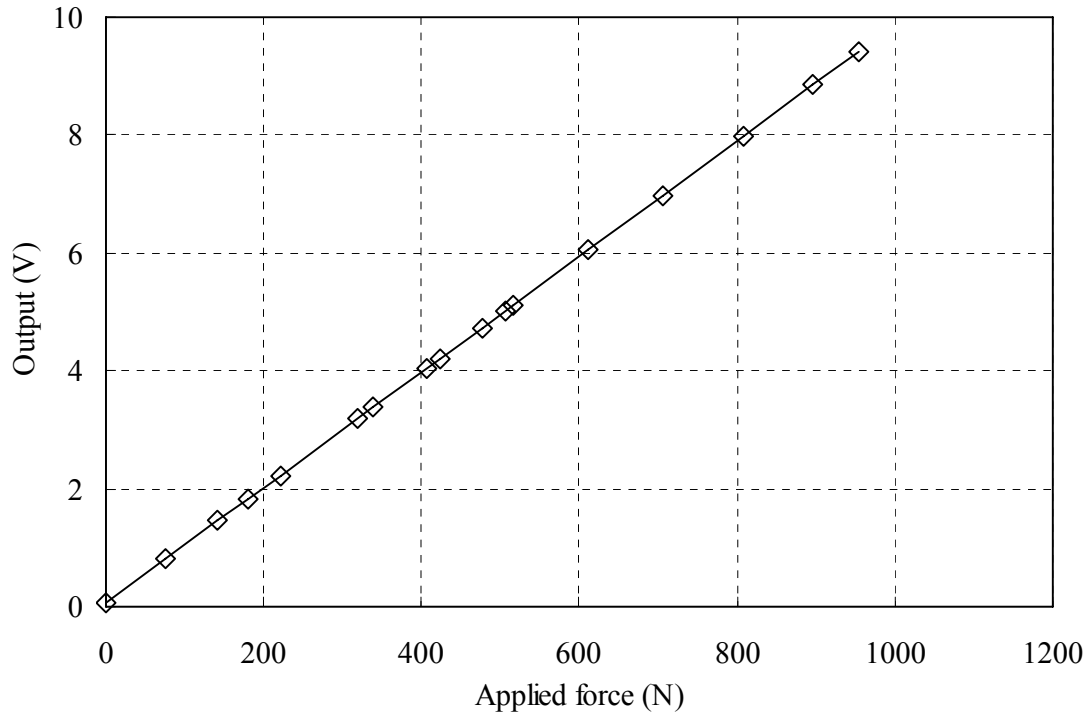
Figure B-20. Calibration graph for submersible load cell.
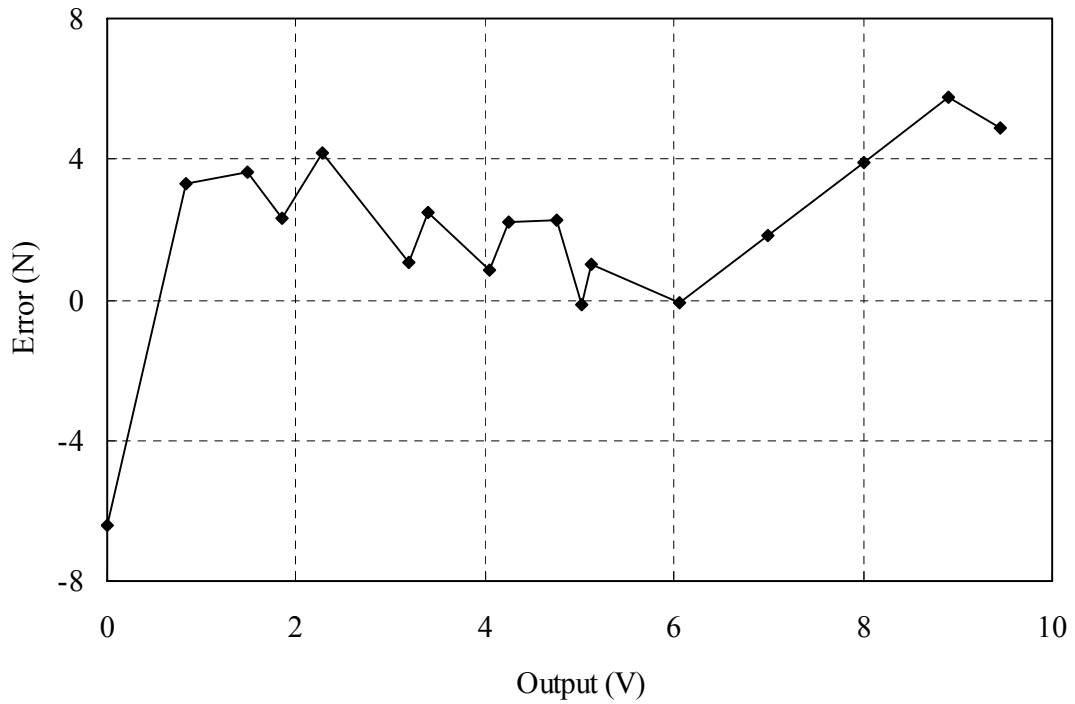
Figure B-21. Error graph for submersible load cell.

Pressure transducers and gauges

Calibrated Instrument 1	Genspec GS4200 pressure transducer
Department	Civil engineering, University of Pretoria
Calibrated Instrument 2	Standard GDS pressure controller
Department	Civil engineering, University of Pretoria
Calibrated Instrument 3	Budenberg standard test gauge
Department	Civil engineering, University of Pretoria
Calibration device	Budenberg 3/500 dead weight system
Department	Civil engineering, University of Pretoria
Instrument no.	UNIV VAN PTA 0473573
Certificate no.	UP19222L
Accuracy	0.02% between 6 and 2600 bars @ 24°C with 95% confidence
Data acquisition card	National Instruments PCI-6014
Department	Civil Engineering, University of Pretoria
Instrument no.	1044CB9
Certificate no.	70772
Resolution	65536 bit
Absolute accuracy	1 day 0.0154 % of reading
	90 days 0.0174 % of reading
	1 year 0.0196 % of reading
DAQ card settings	
Sensor range	-10V to +10V
Input method	Differential
Channel	4

Figure B-22. Calibration graph for pressure transducer.
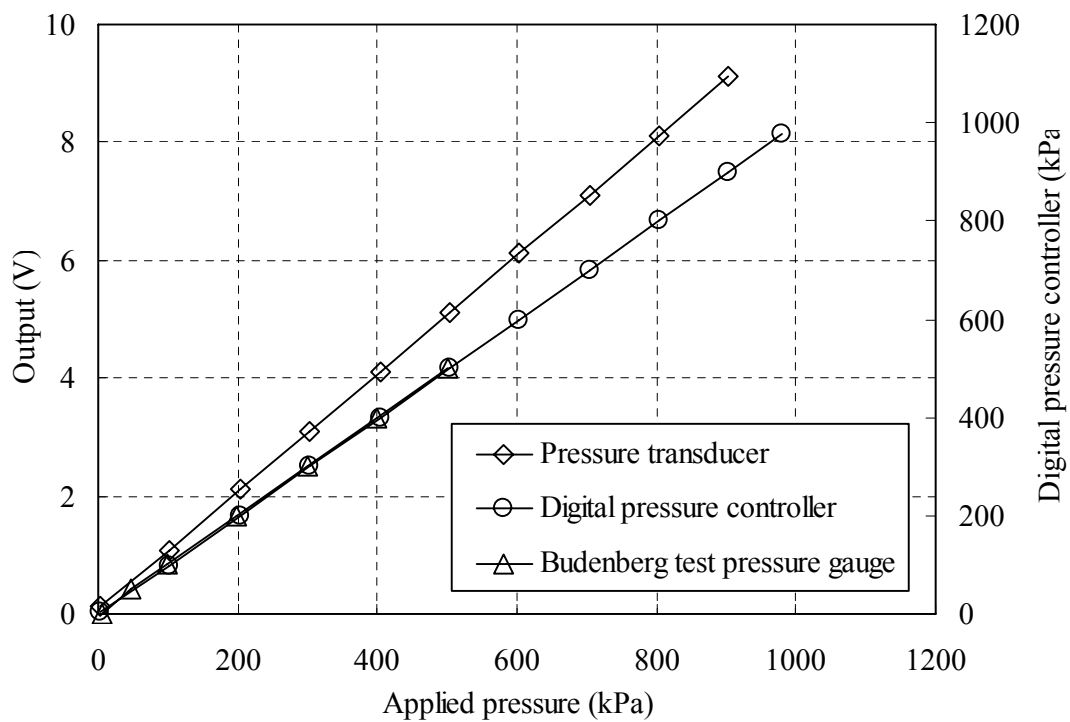
Figure B-23. Calibration graph for pressure transducer, digital pressure controller and Budenberg test pressure gauge.
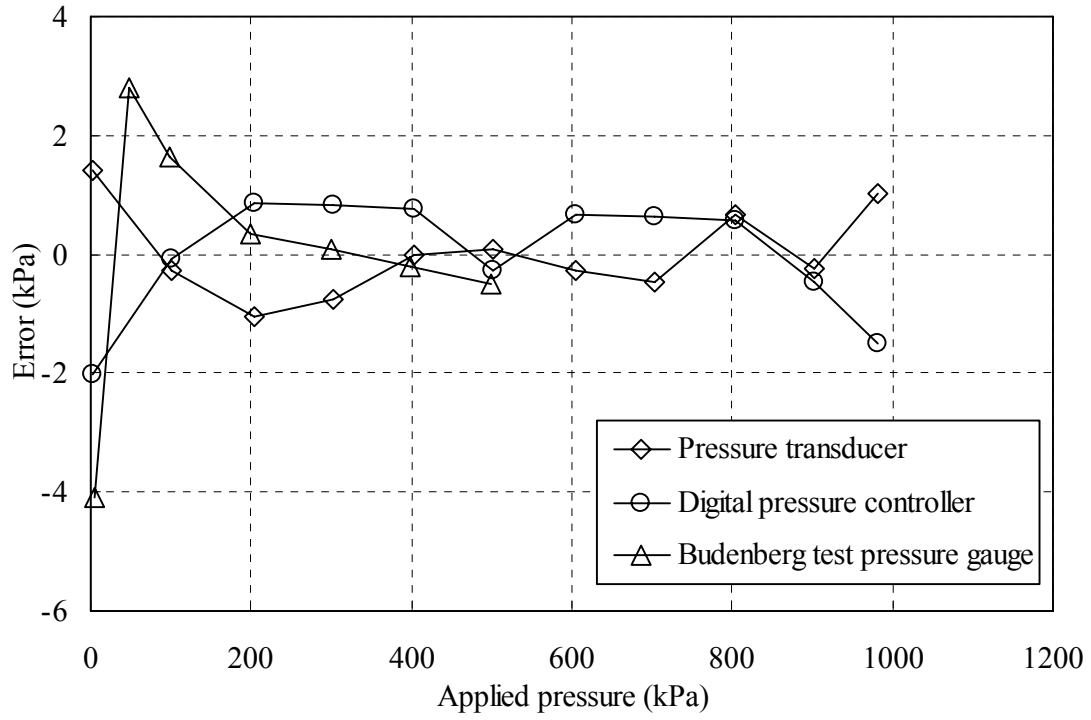
Figure B-24. Error graph for pressure transducer, digital pressure transducer and Budenberg test pressure gauge.

Volume gauge

Calibrated Instrument	Wykeham Ferrance volume gauge
Department	Civil engineering, University of Pretoria

Calibration method	Weight of water expelled at 21 °C
Density of water	0.997968 Mg/m³
Resolution	0.1g
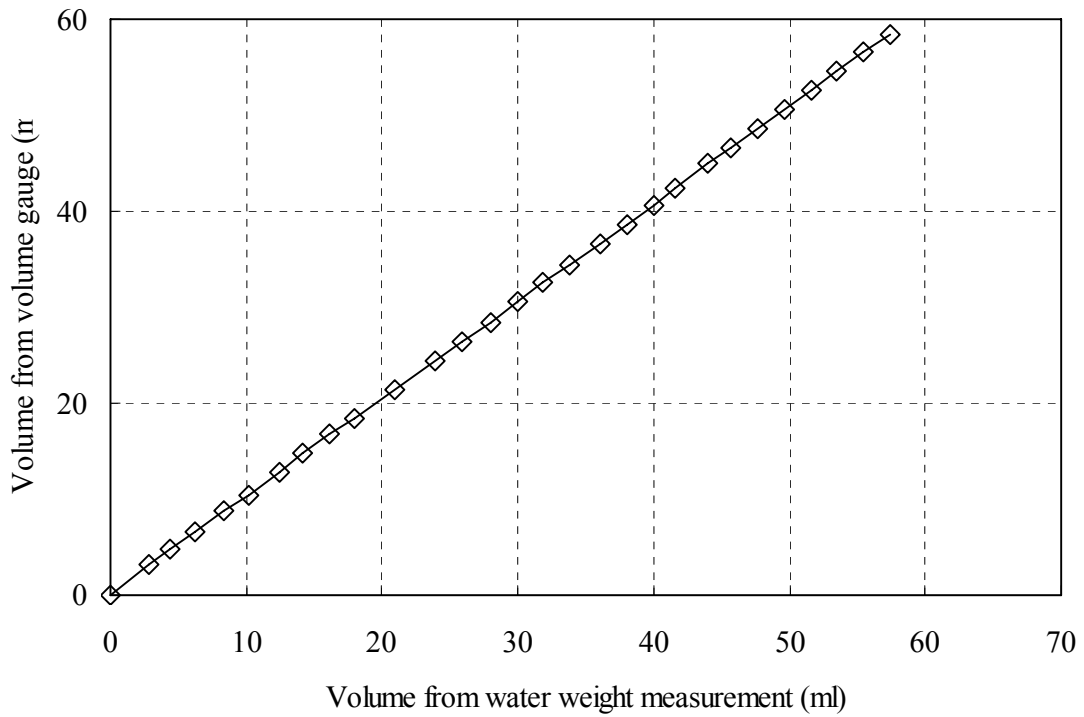
Figure B-25. Calibration graph for the volume gauge.
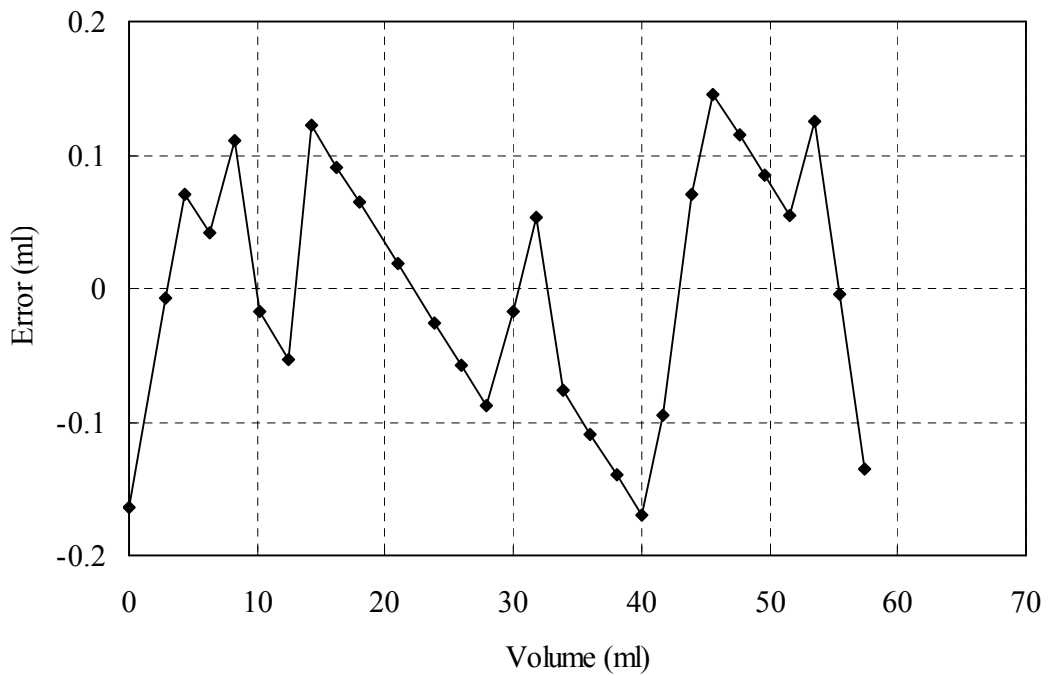
Figure B-26. Error graph for volume gauge.

Appendix C
Sample Preparation

This appendix discusses sample preparation for all samples tested for this research. This includes undisturbed and laboratory prepared samples. Laboratory sample preparation methods include moist tamping and slurry deposition. Both methods were modified to facilitate the preparation process. Photographs are used to aid the description.

Preparation of undisturbed samples
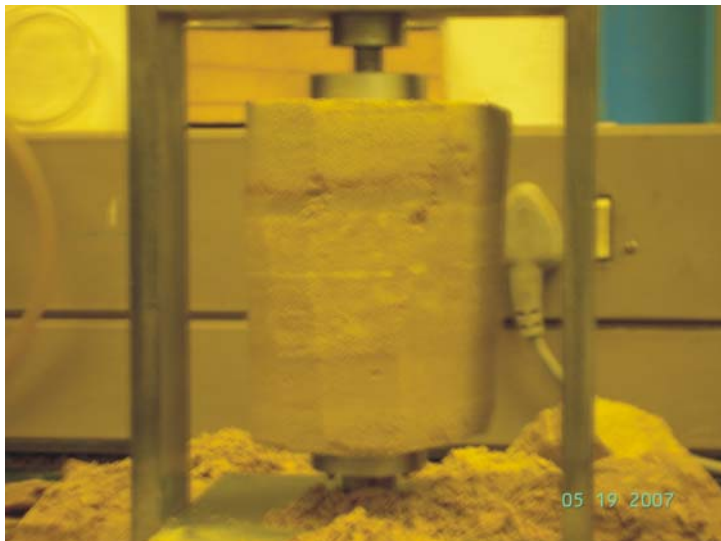
Undisturbed samples were cut from the in situ blocks. Samples were first cut to the required height and size to fit into the soil lathe, and then shaped using a spatula to the required size (50mm diameter). The sample was then removed from the soil lathe and shaped to the required height.

A porous disk was placed on the base pedestal, followed by the undisturbed sample. It was important that the openings under the porous disk were properly flushed to prevent any airlock. A second porous disk was placed on top of the sample. The membrane was stretched over a membrane stretcher and over the sample. Bottom o-rings were stretched over the membrane on the base pedestal. The top cap was then positioned above the top porous disk. The membrane was pulled over the top cap and secured via two o-rings. Procedures for the installation of LVDTS are described later in the Appendix.

Preparation of moist tamped samples

The split mould used for preparing moist tamped samples was modified to include a top ring and a base to hold the mould together. The top ring and the base were held together using threaded rods and bolts. The modified mould assembly was placed on the hydraulic jack. Material was prepared to the required moisture content 24 hours before preparation to allow the moisture to equalize throughout the material. The sample mass was determined from the target void ratio, the volume of the mould and the moisture content of the material. Material was compacted in five 20mm layers to yield a uniform sample. The sample mass was divided by 5 to obtain the mass of material required per layer. Material was placed in the mould as shown in the figure. Before compaction, the material was stirred to prevent excess compaction on one side.

The compaction rod was inserted into the mould and a stopper was placed on top of the compaction rod. Compaction was done by raising the mould into the compaction rod as shown in the figure. Grading marks on the compaction rod indicate when the layer has reached the required height. The first 3 layers were under-compacted to lesser extents to prevent over-compaction due to compaction of the subsequent layers. A moist cloth was placed on the mould in between compactions to prevent loss of moisture. The compacted layer was scratched before the material for the subsequent layer was added to minimize layering. The process was continued until the entire sample was constructed.

After the sample was completed, the bolts were unscrewed and the base of the mould was removed. The mould and sample assembly was placed on the compaction rod as shown in the figure. The sample was extruded by raising the compaction rod. The use of a hydraulic jack was required to prepare samples at high density, such as the pond material. Preparation of MB and UB moist tamped samples was probably possible with the mould, but for consistency all moist tamped samples were prepared using the

hydraulic jack. The extrusion also prevented cracking of the sample when the mould was removed, as is often seen in samples compacted to high densities. Samples were then placed on the pedestal in the same manner as with undisturbed samples.

Preparation of slurry samples

The preparation of slurry samples involved preparation on the triaxial pedestal. After preparation to the required moisture content, the slurry was de-aired for 30 minutes in a desiccator. Preparation of the mould involved first stretching the membrane over the pedestal and securing it with two o-rings as shown in the figure. A customized seal was made to seal the suction applied by the vacuum pump. This vacuum seal was also stretched over the membrane, as seen above the o-rings in the figure. A circular clamp used to clamp the mould was also put in place in advance.

A mould stand was used to raise the split mould to the required height to be clamped against the vacuum seal. The two halves of the split mould were brought together and clamped as shown in the figure. The clamp was tightened around the two spacers. A second, temporary clamp was used to clamp the top of the mould. Caution was exercised so the two split moulds did not to pinch the membrane when clamped, as this will cause leakage. It was also important to ensure that the mould clamps the vacuum seal and that vacuum could be maintained in the chamber between the mould and the membrane.
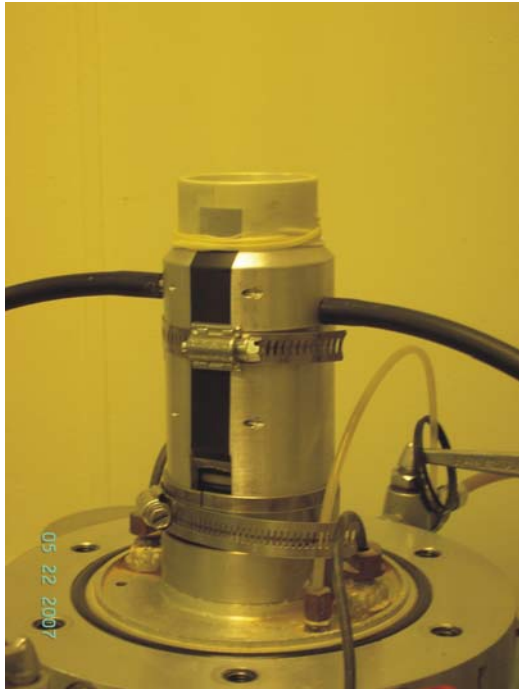
Insulation tape was used to seal the contact between the two halves of the split mould. Once the tape is in place, a third clamp was used to clamp the mould at mid-height as shown in the figure. The second clamp was removed to make room for the membrane. The membrane was pulled over the top of the mould to create an air-tight chamber between the mould and the membrane. It was important that the membrane was vertical and tight to prevent deformations of the sample.

Once the setup was complete, vacuum was switched on. The vacuum pulled the membrane against the inside of the split mould within which material was deposited. It was important at this stage to ensure the drainage leads were properly flushed, as any air trapped under the porous disk would cause an airlock. A 50mm porous disk was first placed, followed by a 50mm diameter filter paper to prevent material entering the pores of the porous disk. Deposition of slurry

involved spooning in layers. Each layer was stirred before the following layer was placed to prevent segregation. Segregation was not observed, as the material was either in a near plastic state (in the case of pond and upper beach samples) or in a flocculated state (in the case of middle beach samples). Stirring also allowed trapped air bubbles to escape. Slurry was deposited to the brim, where after a second filter

206
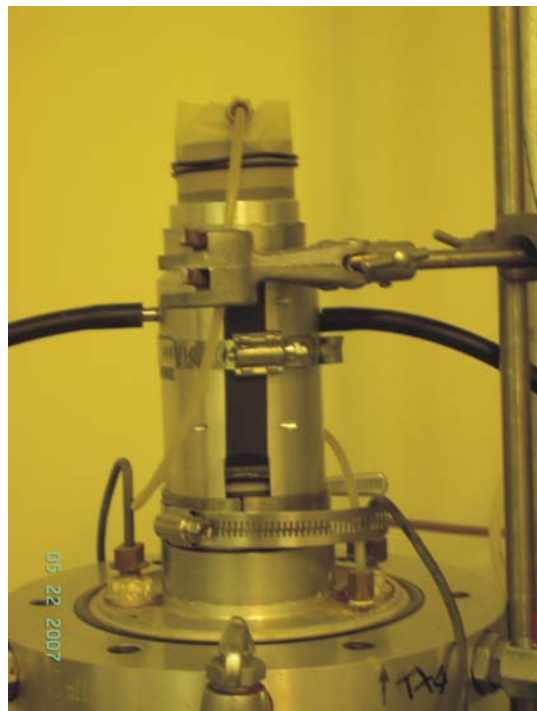
paper followed by the top porous disk was placed on top of the deposited slurry. The top cap was positioned in place and the membrane was pulled over the top cap and secured via two o-rings. A 10kPa suction was then applied through the top valve, whilst keeping the surrounding suction on. It was also important that the gap between the membrane and the top of the mould was not sealed. This allowed some one-dimensional consolidation to take place. The tube connecting the top cap and the base pedestal was supported to keep the top cap in an upright position. The suction was applied until the 10kpa suction was registered by the pore pressure transducer.

Removal of the mould was done in steps, as some suction drop was encountered during each step. After the entire mould setup was removed, the suction was maintained until a -10kPa was again registered by the pore pressure transducer. The sample was now ready and LVDTs could be installed. During installation of the LVDTs, any slight disturbance caused a drop in the suction in the sample, and it was important that the suction was maintained. If the suction drops below -3kPa, all processes were halted to allow the suction to recover.

Installation of LVDTs

LVDTs were mounted onto clamps and secured onto the membrane using superglue on opposite ends of the sample. Clamps used were similar to that used by Heymann (1998). Clamps were installed at distance of 50mm in the middle half of the sample. The position for the LVDTs were first measured and marked on the membrane. The LVDTs were first mounted on to the top clamp and glued to the sample. The LVDT pins were then held in place while the bottom clamp

was glued in place. The pins rested on a flat-headed screw in the bottom clamp. The screws could be used to adjust the initial position of the armature and therefore the initial output of the LVDTs. This was required to accommodate for volume changes before shear so that shearing could start in the range of the highest gain (8). Installation of LVDTs was done in this manner for all samples tested.

Appendix D

SEM IMAGES

Appendix D includes all SEM images of consolidation and shear samples before the test. These images were used as the basis of the image analysis. Images were taken for each sample with a vertical orientation at magnifications of 50, 200, 500, 1000 and 2000 times. Only magnifications of 50, 200 and 1000 times are attached in the appendix. Sample coding follows that as described in section 3.2. Preparation of SEM samples is described in section 3.8. The testing procedures of all SEM samples are described here and summarized in the table below.

- Flushing/saturation: were used on all triaxial samples. Consolidation samples (-con) used for the SEM were removed after this process.
- Consolidation/creep: isotropic consolidation for all triaxial shear samples. Shear samples (-200 or -400) used for the fabric analysis were removed after consolidation and creep has taken place. Creep was allowed for at least 24 hours.
- Desiccation- all samples were desiccated before entering the SEM.

Sample	Material	Flushing/ saturation	Consolidation/ creep	Desiccation
Pond undisturbed	Pond			√
P-U-con	Pond	√		√
P-MT-con	Pond	√		√
P-S-con	Pond	√		√
P-U-200	Pond	√	√ (200kPa)	√
P-MT-200	Pond	√	√ (200kPa)	√
P-S-200	Pond	√	√ (200kPa)	√
P-U-400	Pond	√	√ (400kPa)	√
P-MT-400	Pond	√	√ (400kPa)	√
P-S-400	Pond	√	√ (400kPa)	√
MB undisturbed	Middle beach			√
MB -U-con	Middle beach	√		√
MB -MT-con	Middle beach	√		√
MB -S-con	Middle beach	√		√
MB -U-200	Middle beach	√	√ (200kPa)	√
MB -MT-200	Middle beach	√	√ (200kPa)	√
MB -S-200	Middle beach	√	√ (200kPa)	√
MB -U-400	Middle beach	√	√ (400kPa)	√
MB -MT-400	Middle beach	√	√ (400kPa)	√
MB -S-400	Middle beach	√	√ (400kPa)	√
UB undisturbed	Upper beach			√
UB -U-con	Upper beach	√		√
UB -MT-con	Upper beach	√		√
UB -S-con	Upper beach	√		√
UB -U-200	Upper beach	√	√ (200kPa)	√
UB -MT-200	Upper beach	√	√ (200kPa)	√
UB -S-200	Upper beach	√	√ (200kPa)	√
UB -U-400	Upper beach	√	√ (400kPa)	√
UB -MT-400	Upper beach	√	√ (400kPa)	√
UB –S-400	Upper beach	√	√ (400kPa)	√

Pond in situ   P-U-con

a)

d)
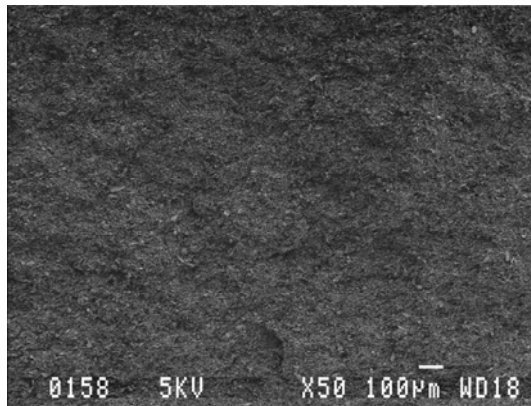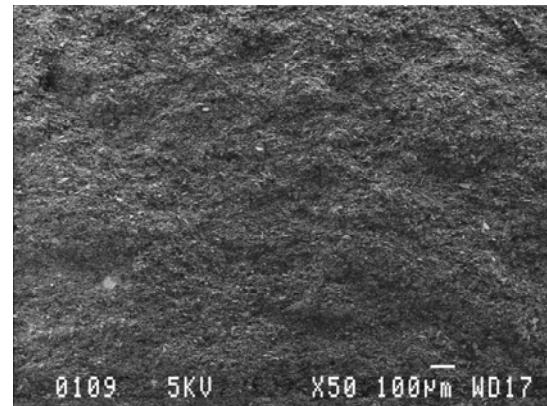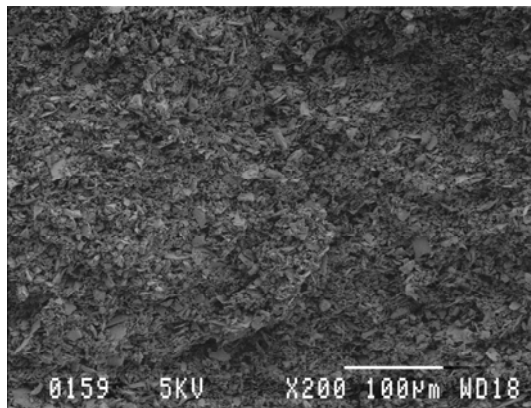
b)
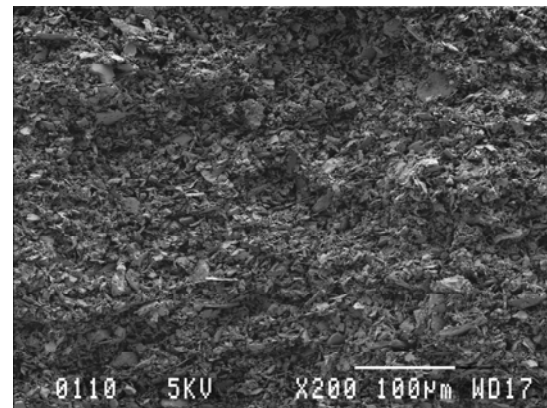
e)
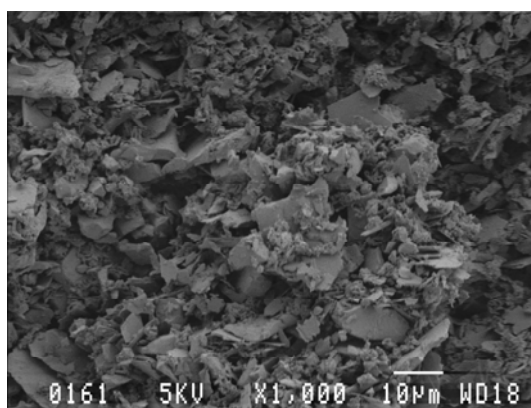
c)
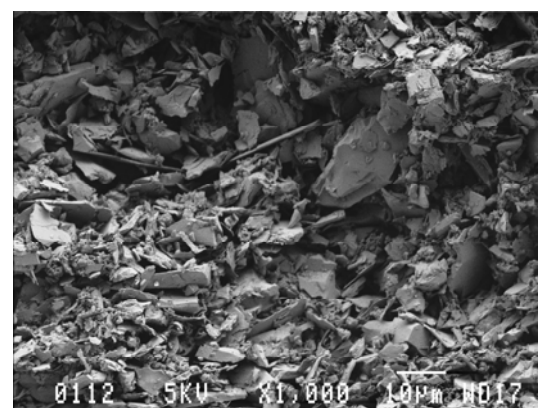
f)

P-MT-con   P-S-con

a)

d)

b)

e)

c)

f)

P-MT-con   P-S-con
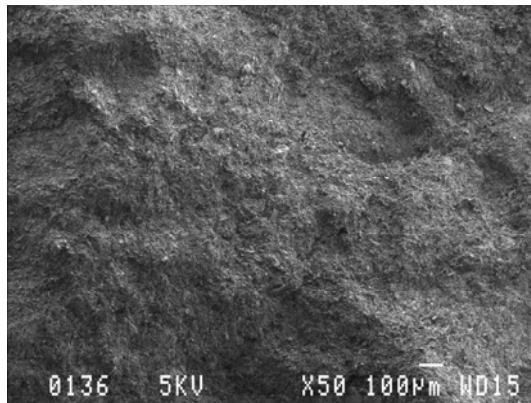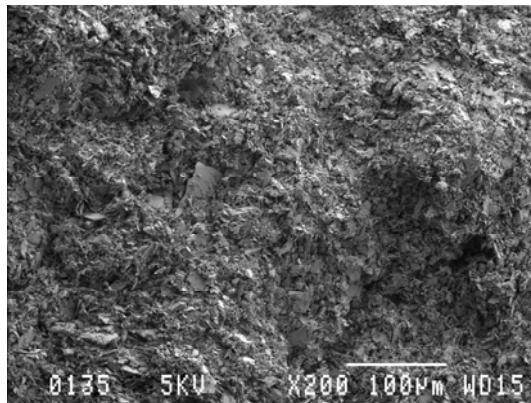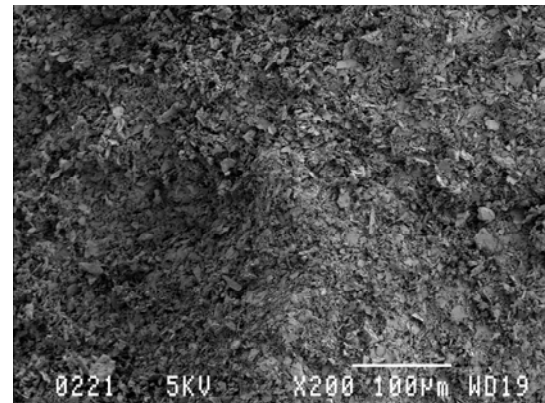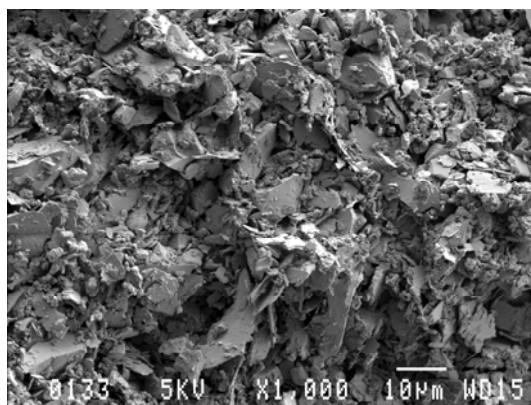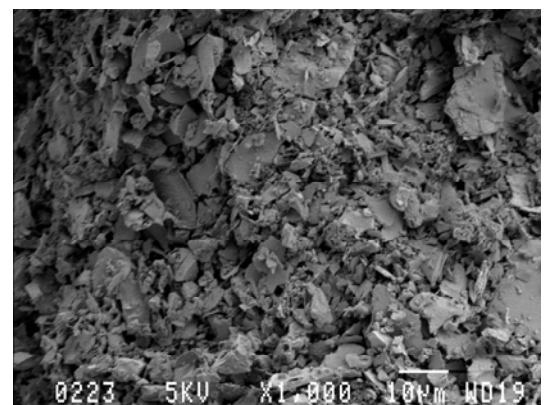
P-U-200   P-MT-200

a)

d)

b)

e)

c)

f)

P-U-200   P-MT-200
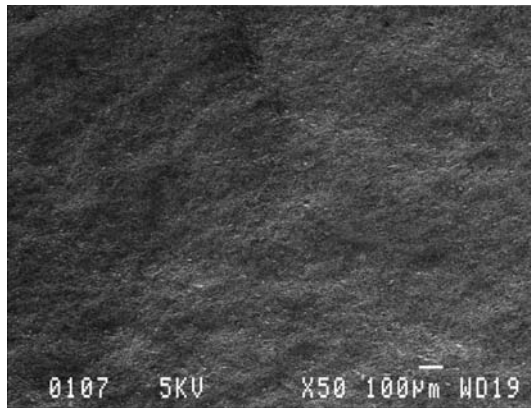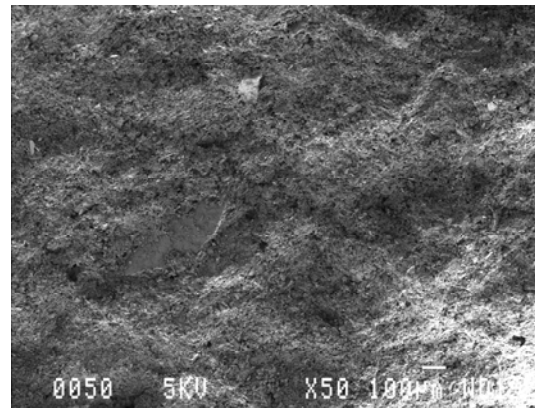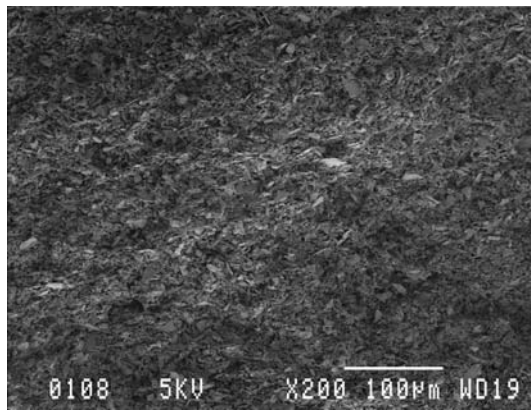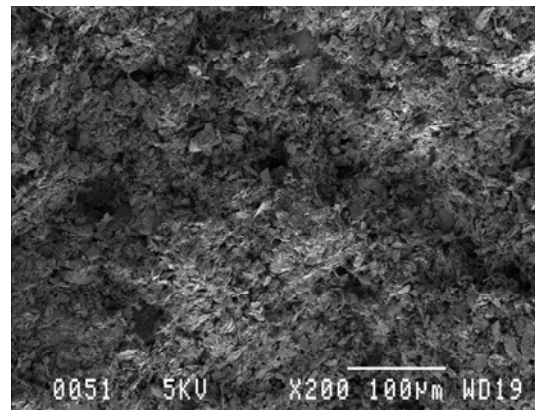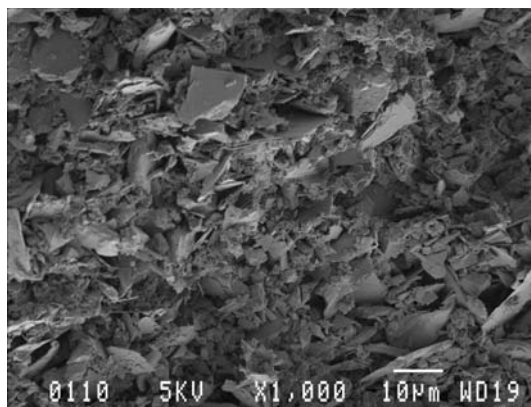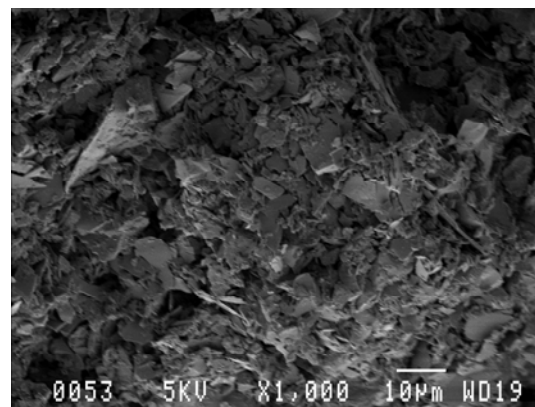
P-S-200   P-U-400

a)

d)
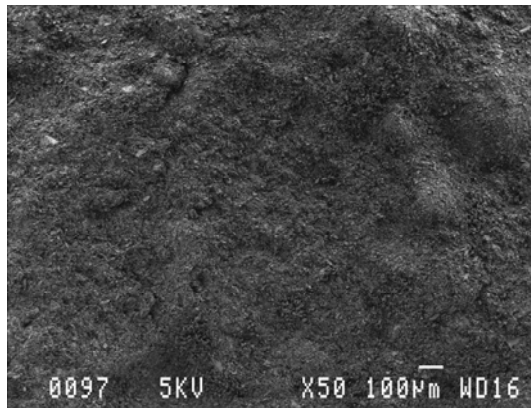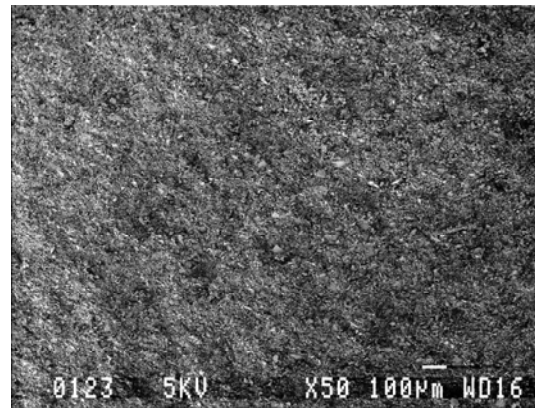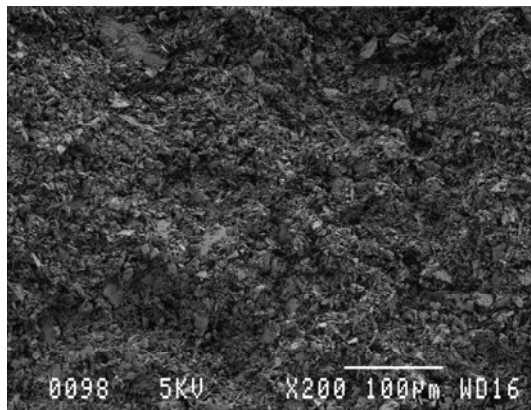
b)
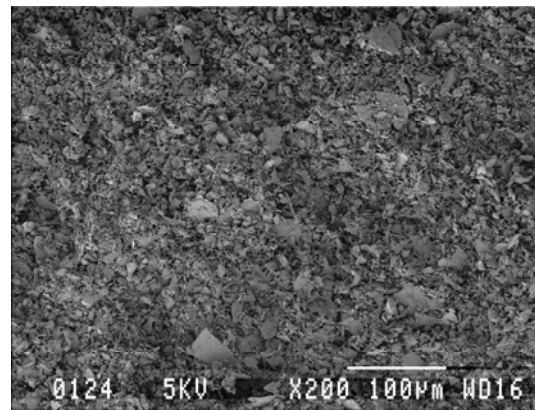
e)
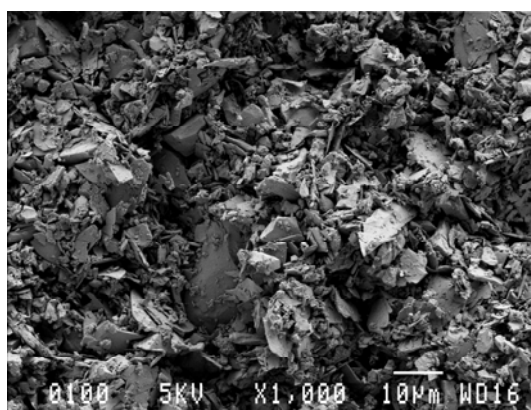
c)
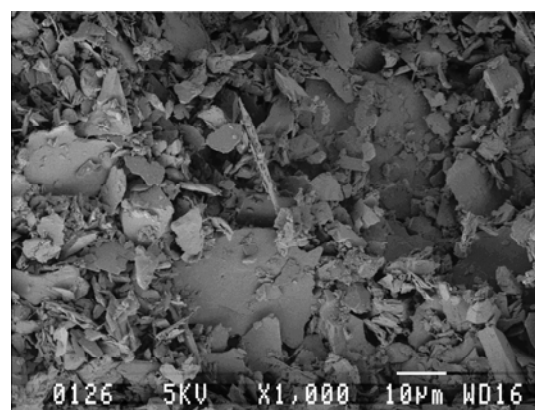
f)

P-MT-400   P-S-400

a)   d)

b)   e)

c)   f)

P-MT-400   P-S-400
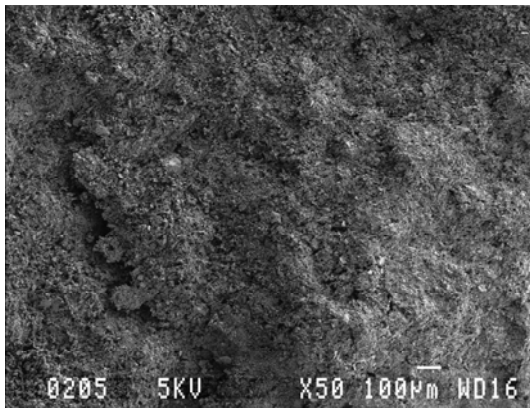
MB in situ   MB-U-con

a)
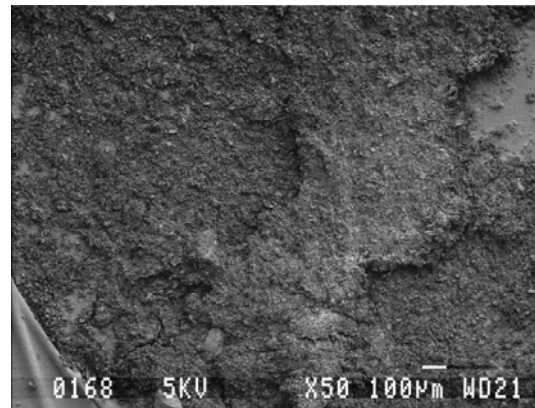
d)
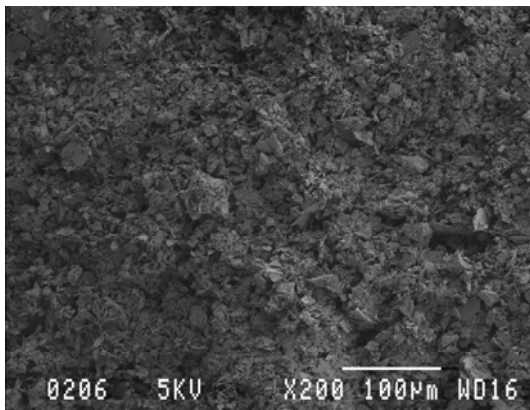
b)
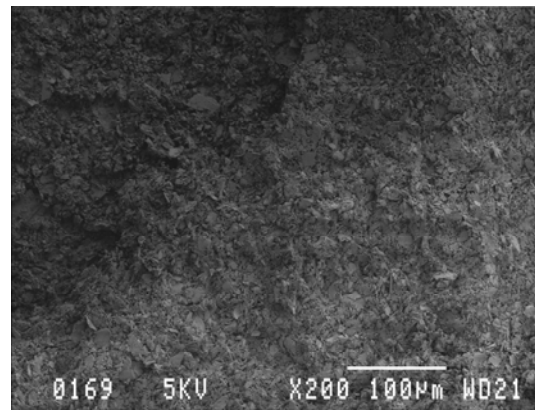
e)
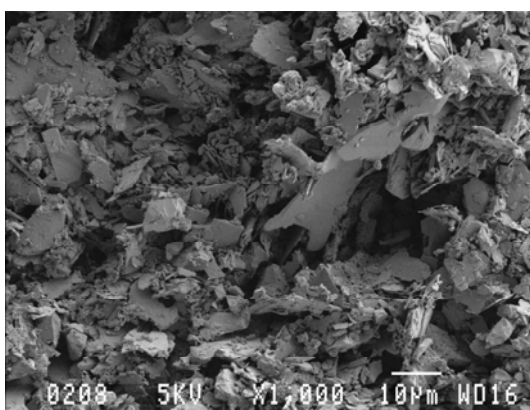
c)

f)

MB in situ   MB-U-con
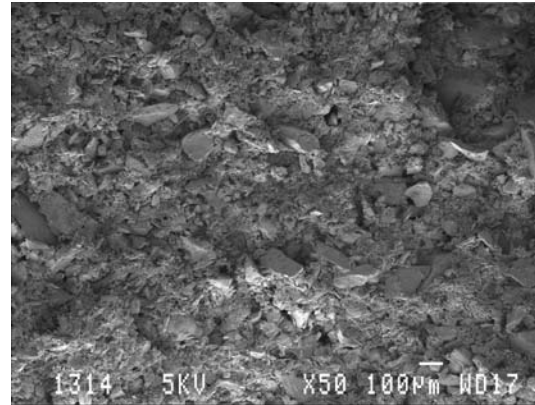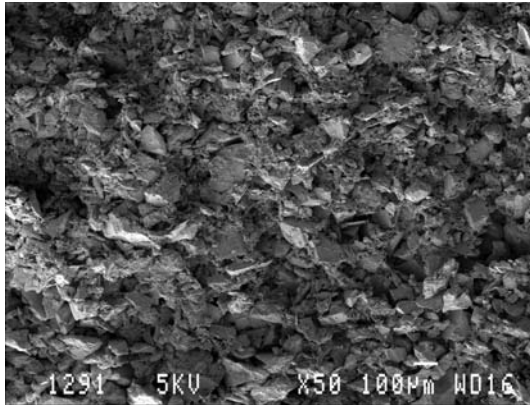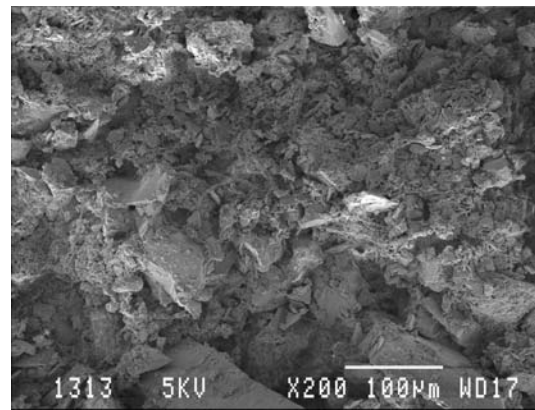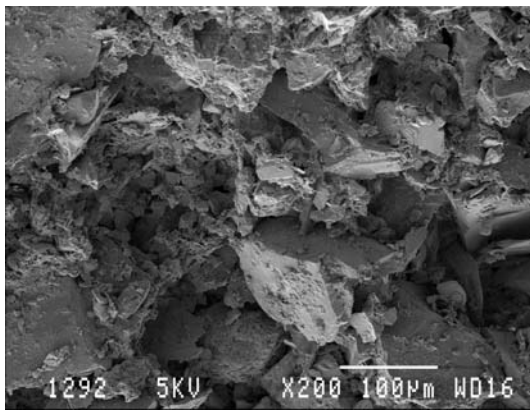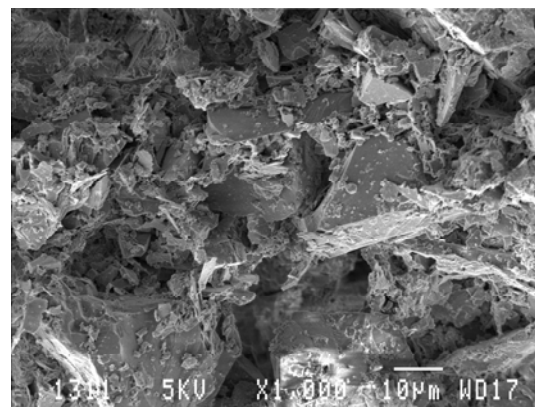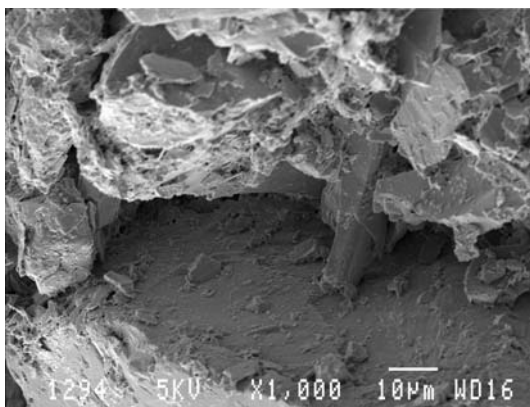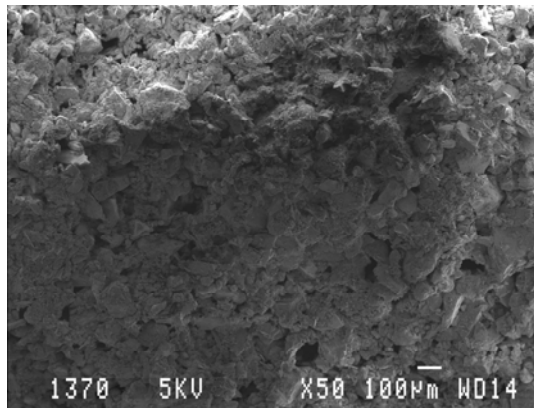
MB-MT-con   MB-S-con

a)
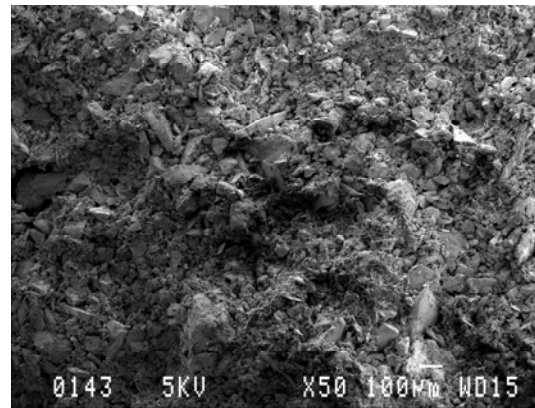
d)
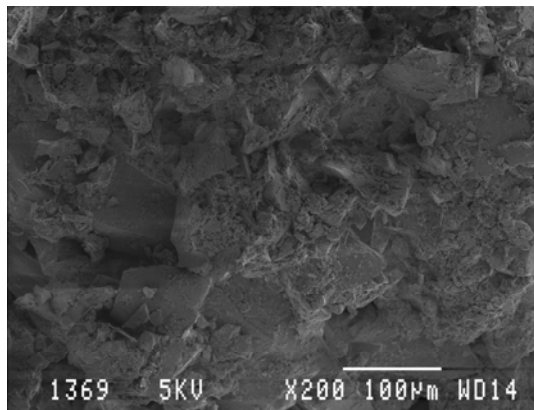
b)
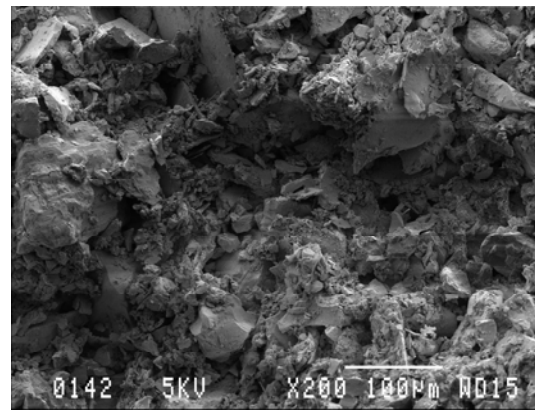
e)
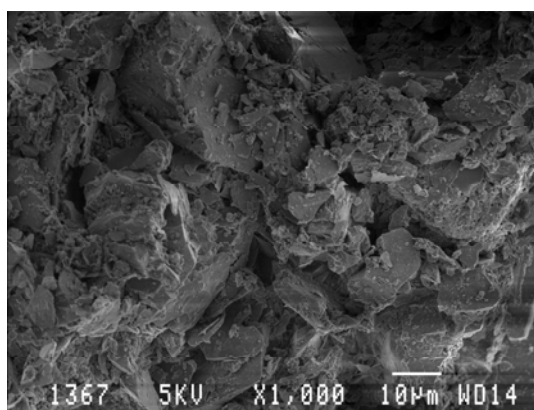
c)
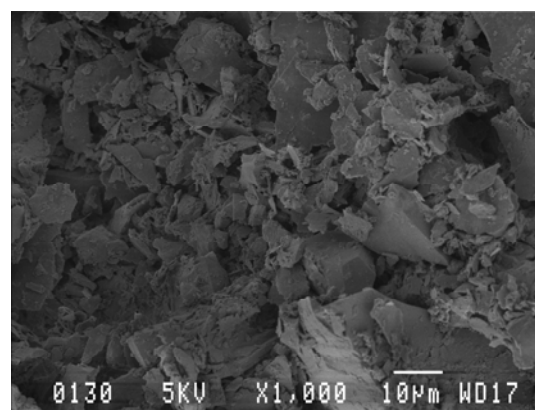
f)

MB-U-200   MB-MT-200
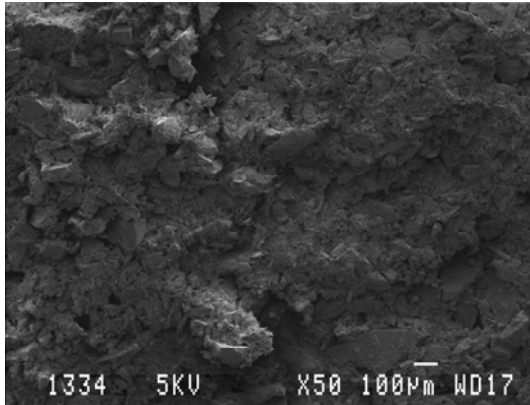
a)
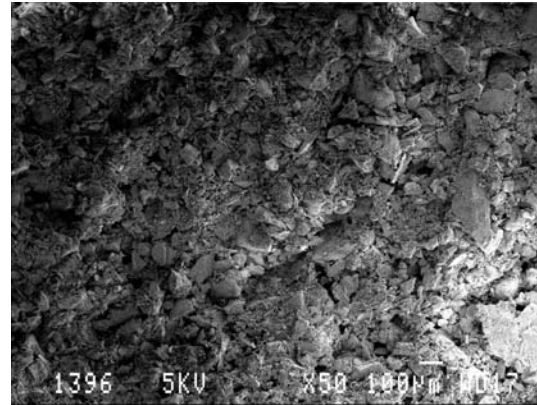
d)
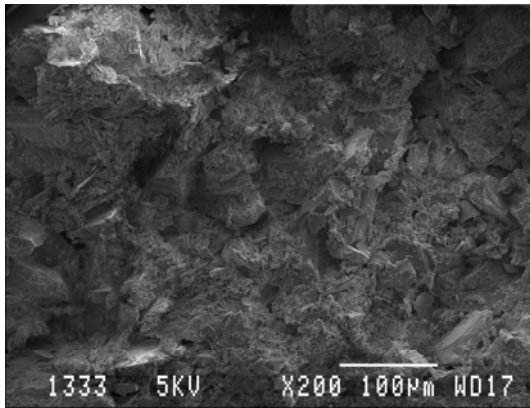
b)
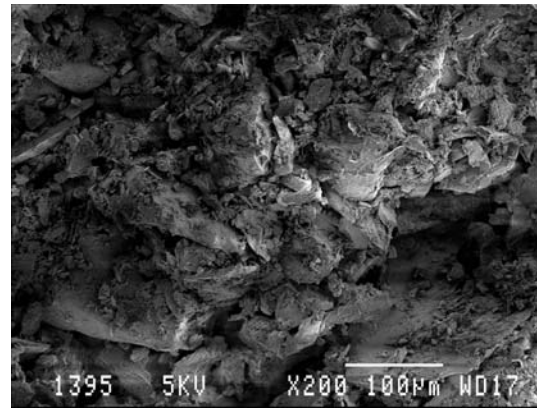
e)
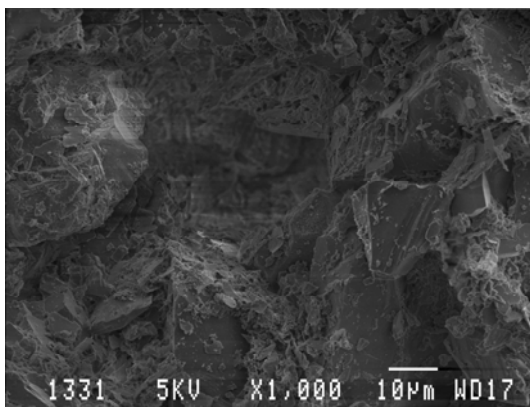
c)
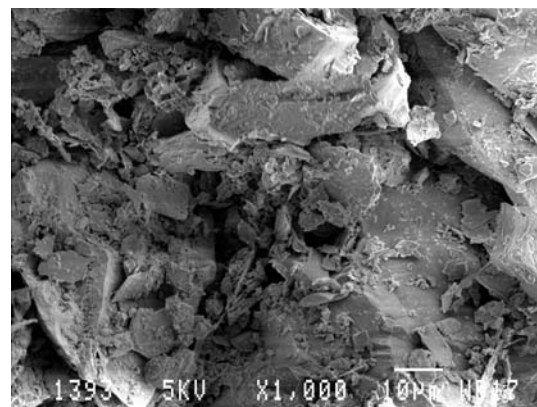
f)

MB-S-200   MB-U-400
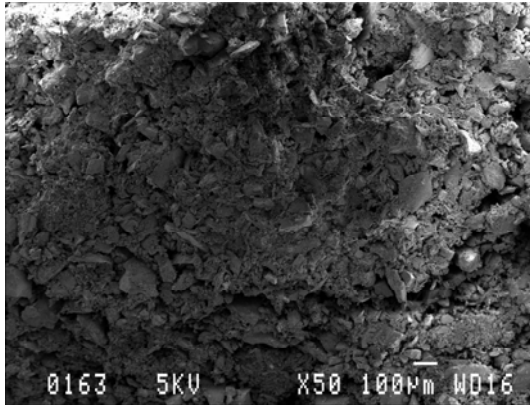
a)
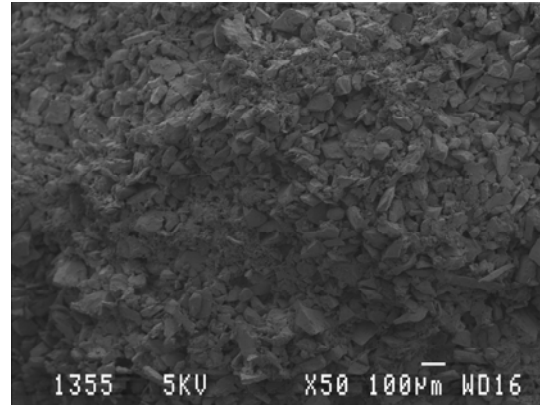
d)
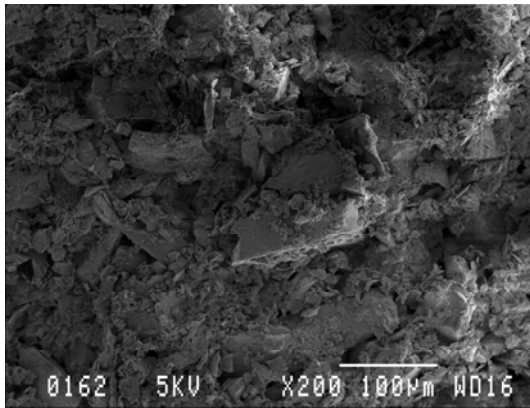
b)
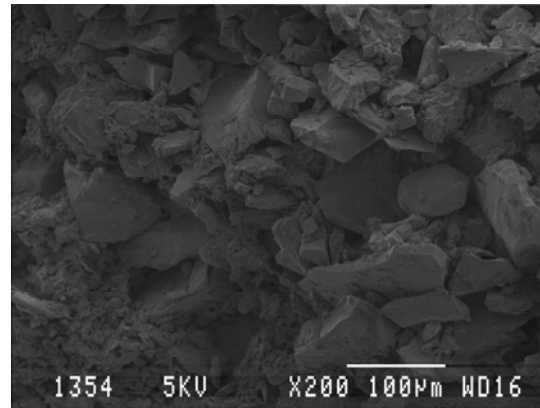
e)
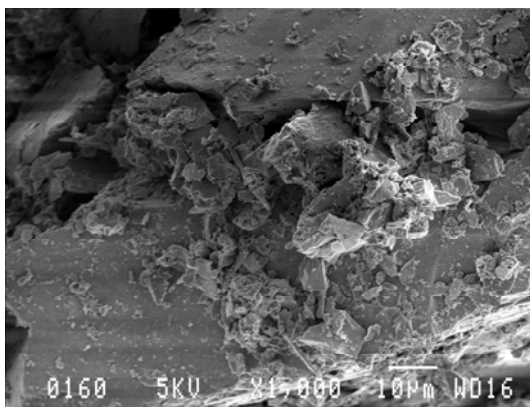
c)

f)

MB-MT-400   MB-S-400

a)

b)

c)

d)

e)
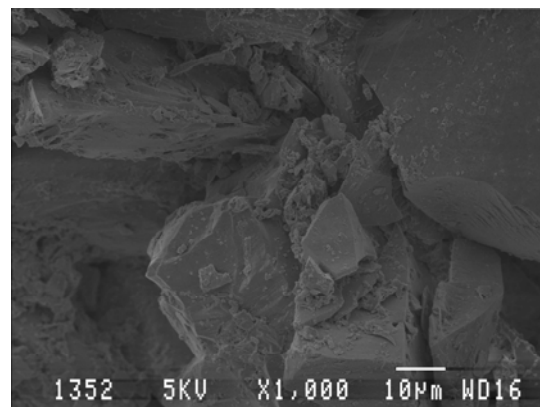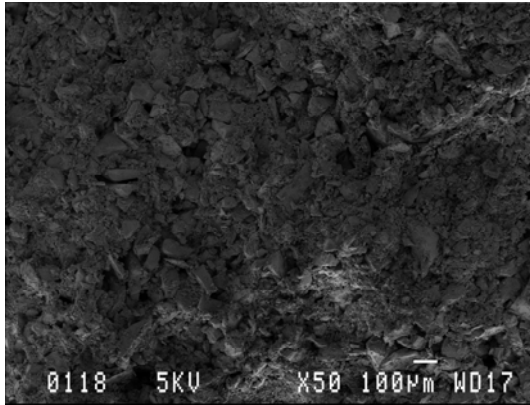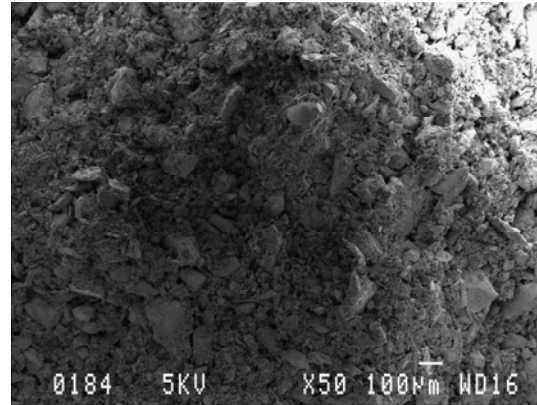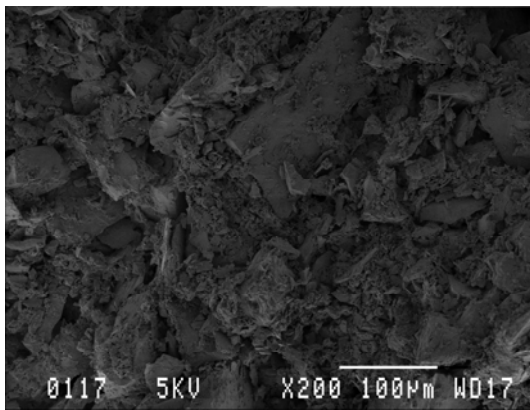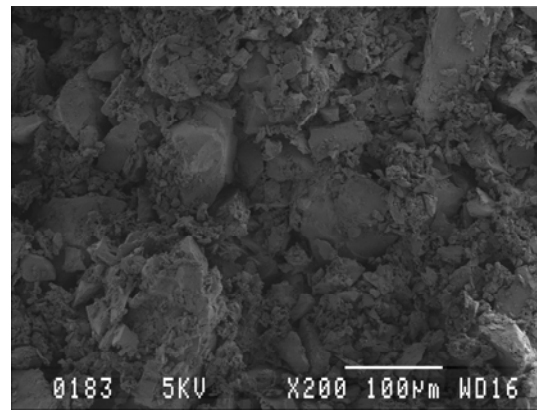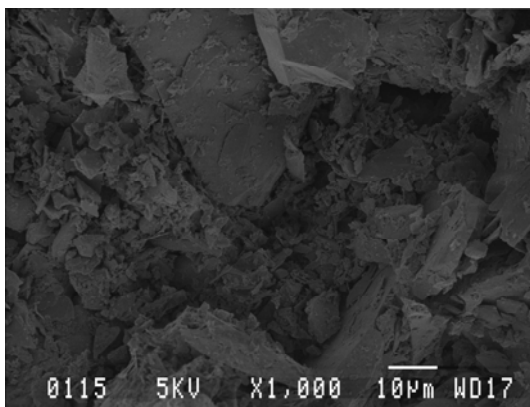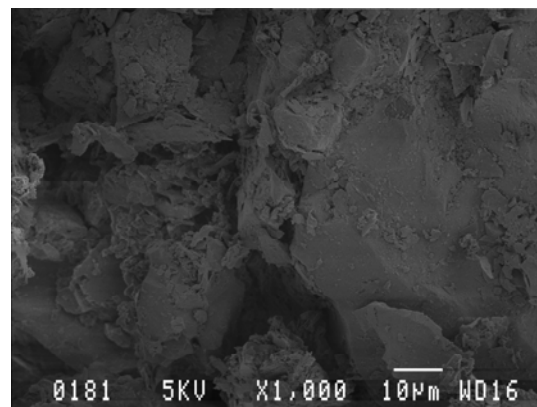
f)

UB in situ   UB-U-con
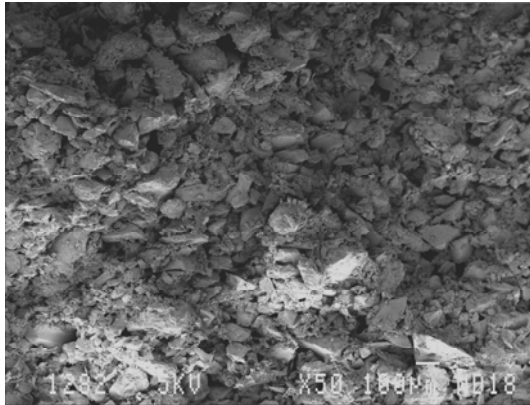
a)
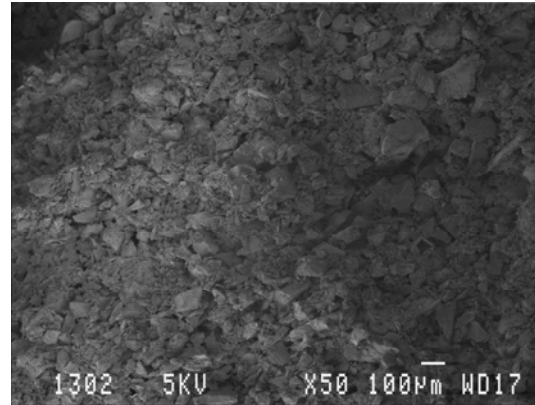
d)
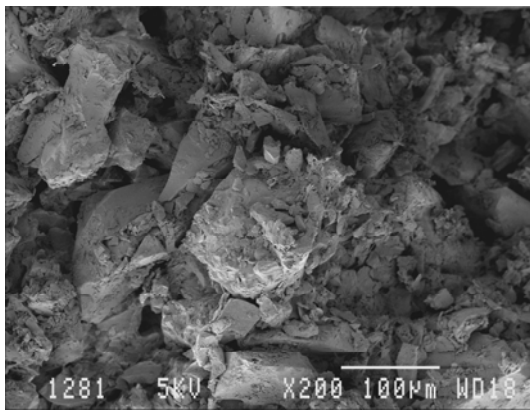
b)
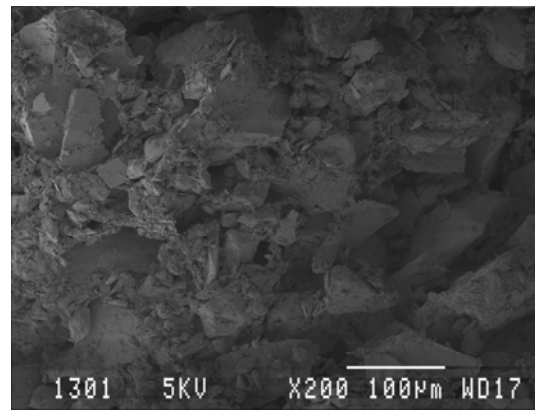
e)
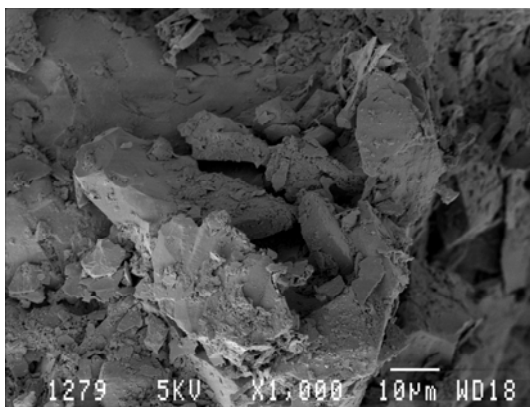
c)
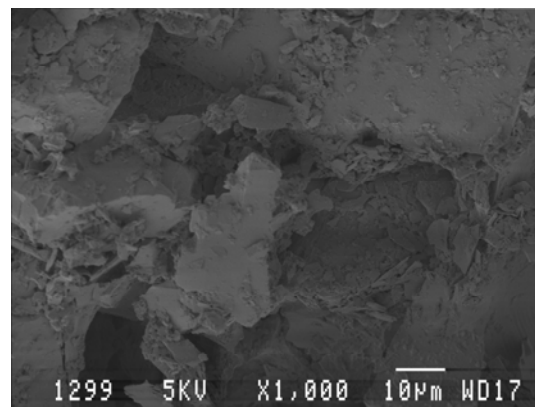
f)

UB-MT-con   UB-S-con
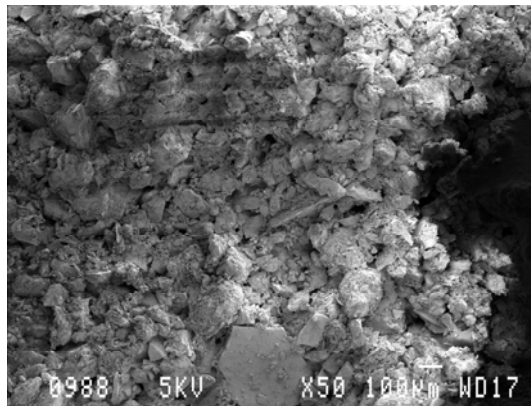
a)
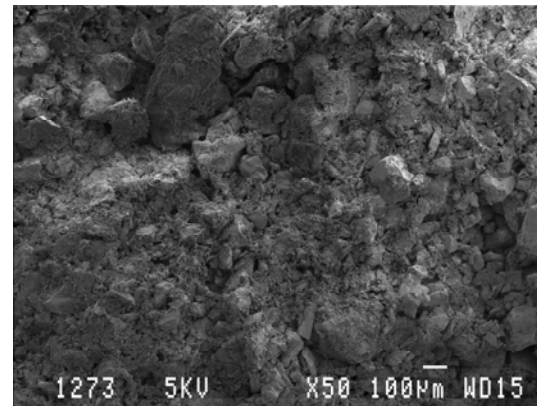
d)
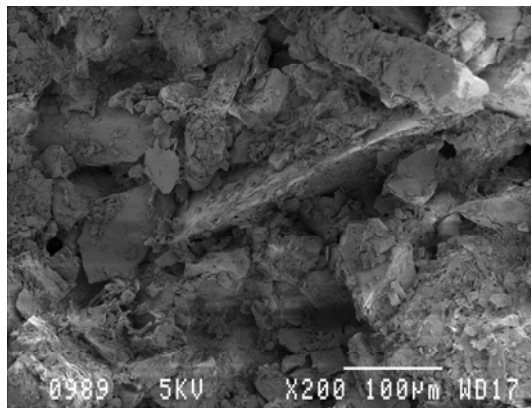
b)
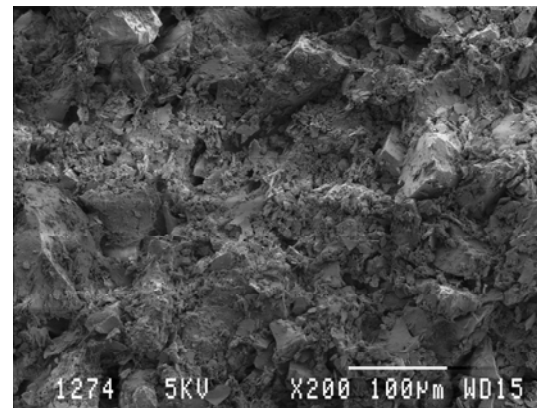
e)
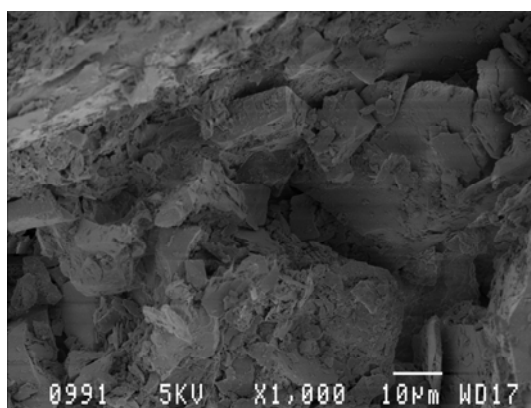
c)
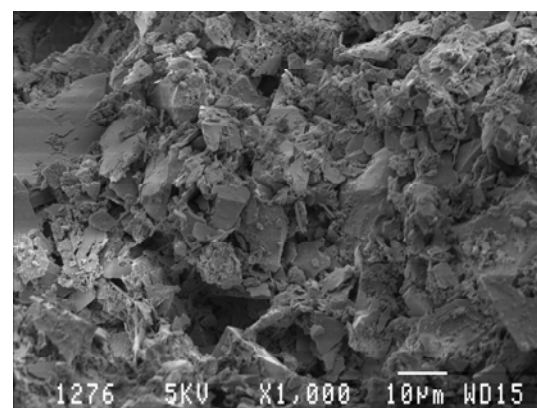
f)

UB-U-200   UB-MT-200

a)   d)

b)   e)

c)   f)

223
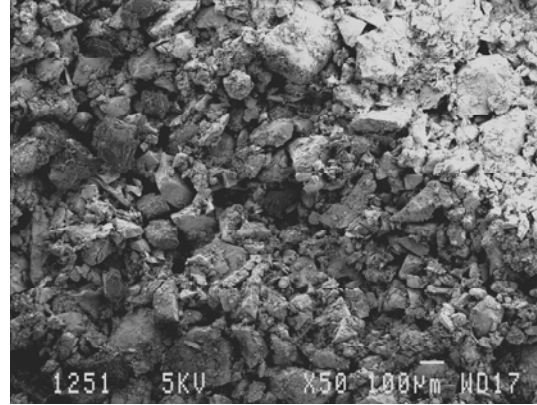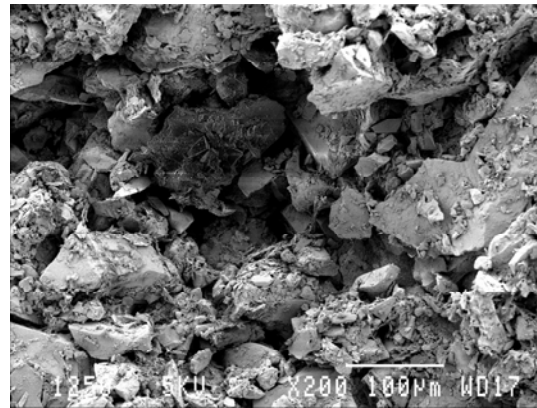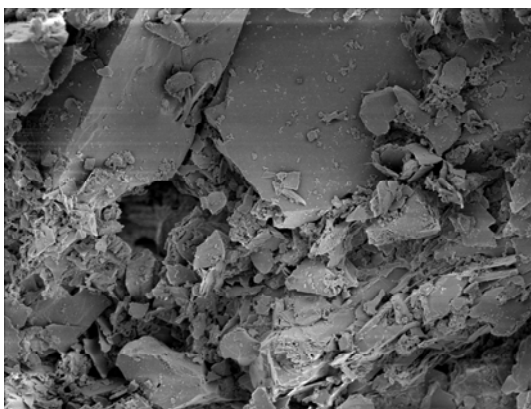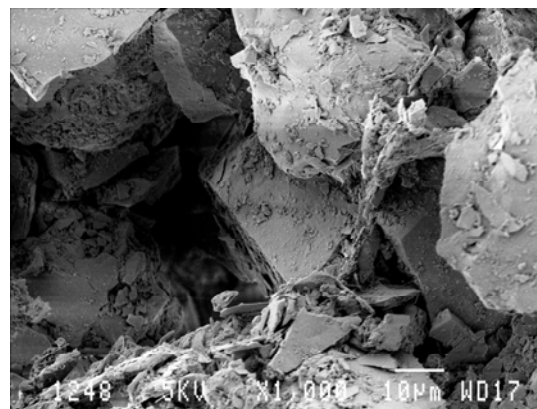
UB-S-200   UB-U-400

a)   d)

b)   e)

c)   f)

UB-S-200   UB-U-400
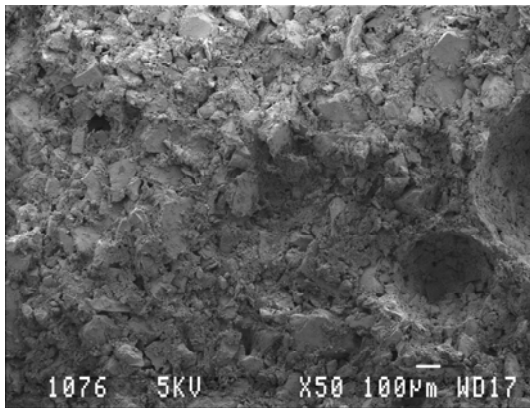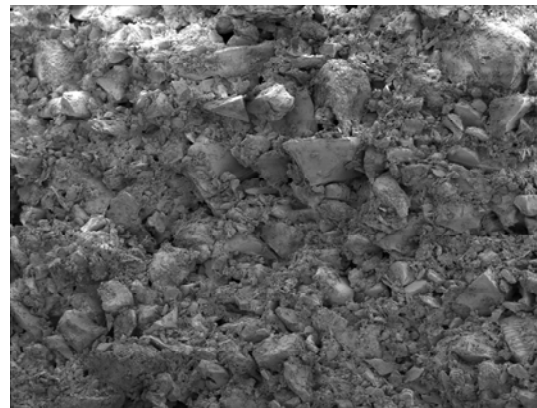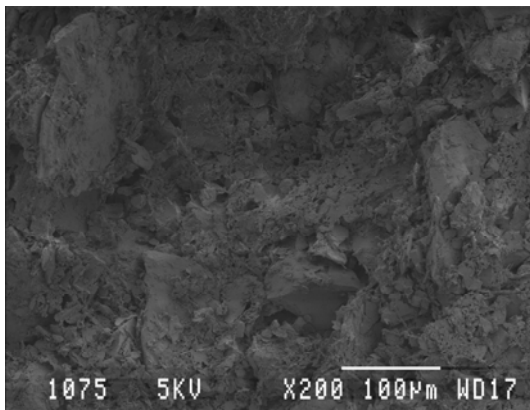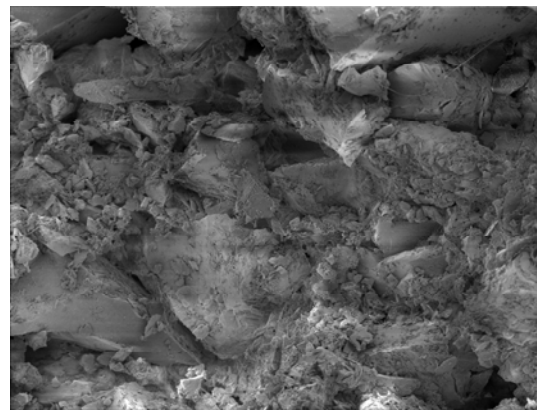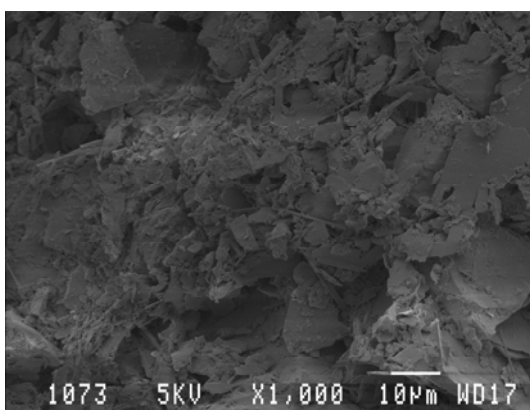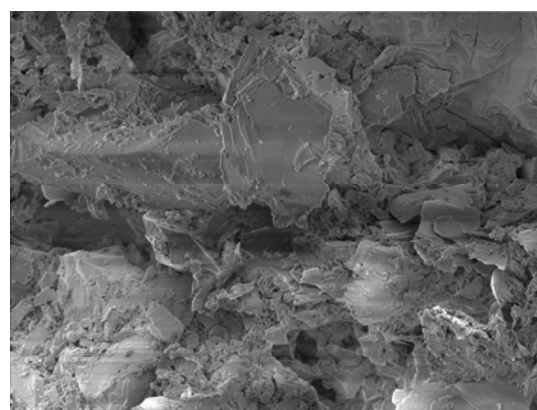
UB-MT-400   UB-S-400
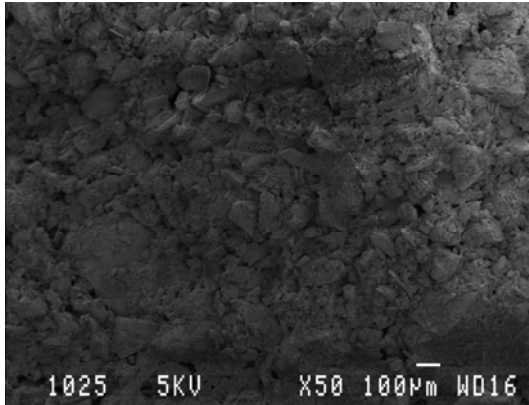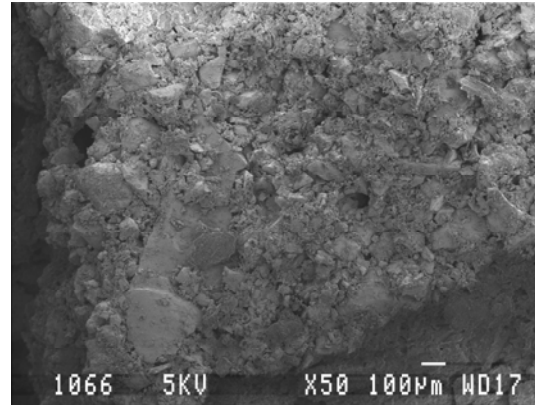
a)   d)
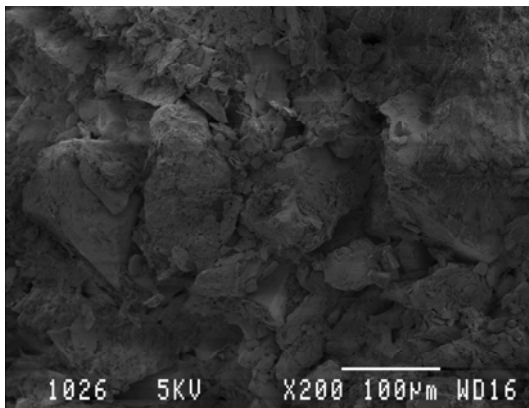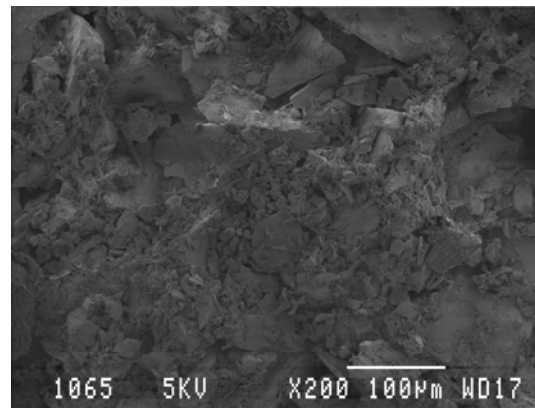
b)   e)
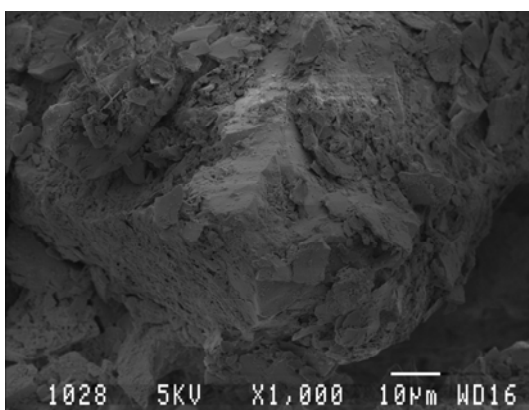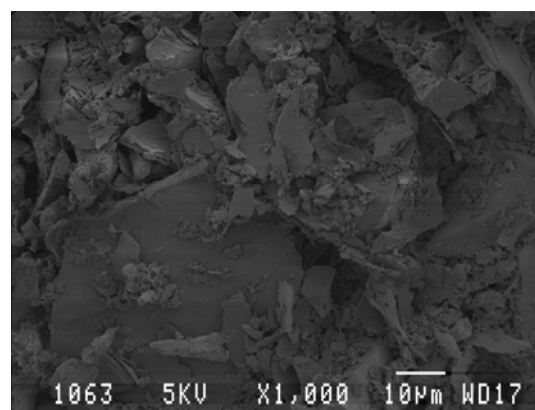
c)   f)

Appendix E
Test Results

To assist the reader in the flow of the thesis, test results are summarized in the main body of the thesis. All test results and graphs from the experimental program are attached in Appendix E. This includes the preliminary testing and the main experimental work. Descriptions of the figures and tables attached in this appendix are summarized in the table below

| Table	Description
E-1	Volume change behaviour for pond material during flushing
E-2	Volume change behaviour for middle beach material during flushing
E-3	Volume change behaviour for upper beach material during flushing
E-4	Stiffness degradation curve properties for gold tailings
Figure	Description
E-1	Sedimentation result for pond material dispersed
E-2	Sedimentation result for middle beach material dispersed
E-3	Sedimentation result for upper beach material dispersed
E-4	Sedimentation result for pond material flocculated
E-5	Sedimentation result for middle beach material flocculated
E-6	Sedimentation result for upper beach material flocculated
E-7	Creep data for pond shear 200 and 400 samples
E-8	Creep data for middle beach shear 200 and 400 samples
E-9	Creep data for upper beach shear 200 and 400 samples
E-10	Stiffness of pond samples

E-11	Stiffness of middle beach samples
E-12	Stiffness of upper beach samples
E-13	q'-ε_a graph for pond samples
E-14	q'-ε_a graph for middle beach samples
E-15	q'-ε_a graph for upper beach samples
E-16	p'-ε_a graph for pond samples
E-17	p'-ε_a graph for middle beach samples
E-18	p'-ε_a graph for upper beach samples
E-19	U_e- ε_a graph for pond samples
E-20	U_e- ε_a graph for middle beach samples
E-21	U_e- ε_a graph for upper beach samples
E-22	Stress path of pond samples (s'-t' space).
E-23	Stress path of middle beach samples (s'-t' space).
E-24	Stress path of upper beach samples (s'-t' space).
E-25	Stress path of pond samples (p'-q' space).
E-26	Stress path of middle beach samples (p'-q' space).
E-27	Stress path of upper beach samples (p'-q' space).
E-28	Stress ratio against axial strain for pond samples
E-29	Stress ratio against axial strain for middle beach samples
E-30	Stress ratio against axial strain for upper beach samples
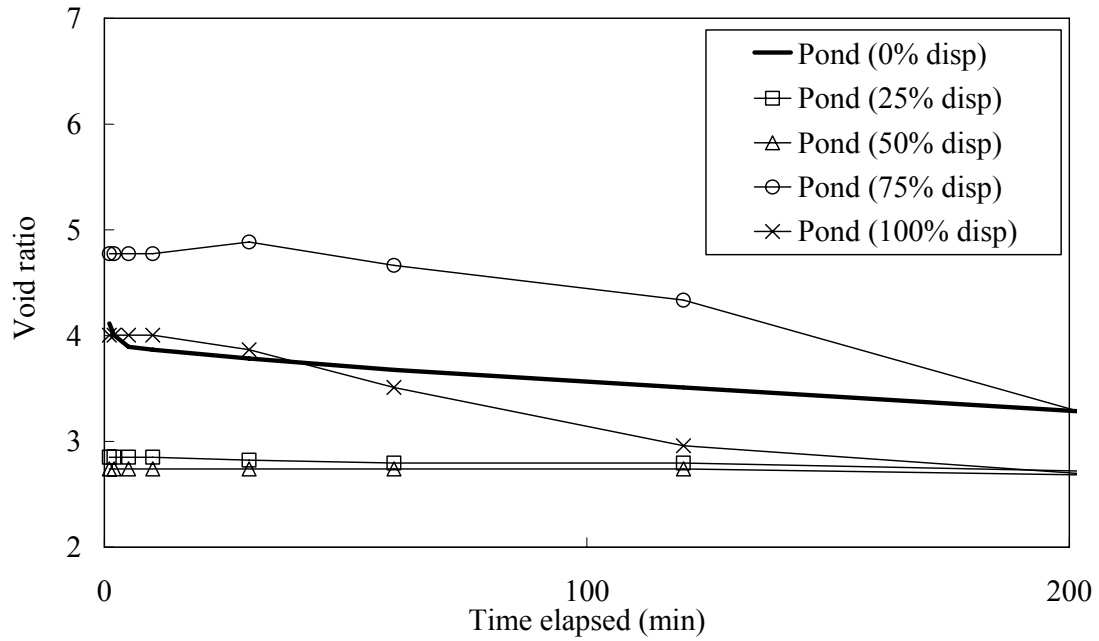
Figure E-1. Sedimentation result for pond material dispersed

Figure E-1. Sedimentation result for pond material flocculated

228
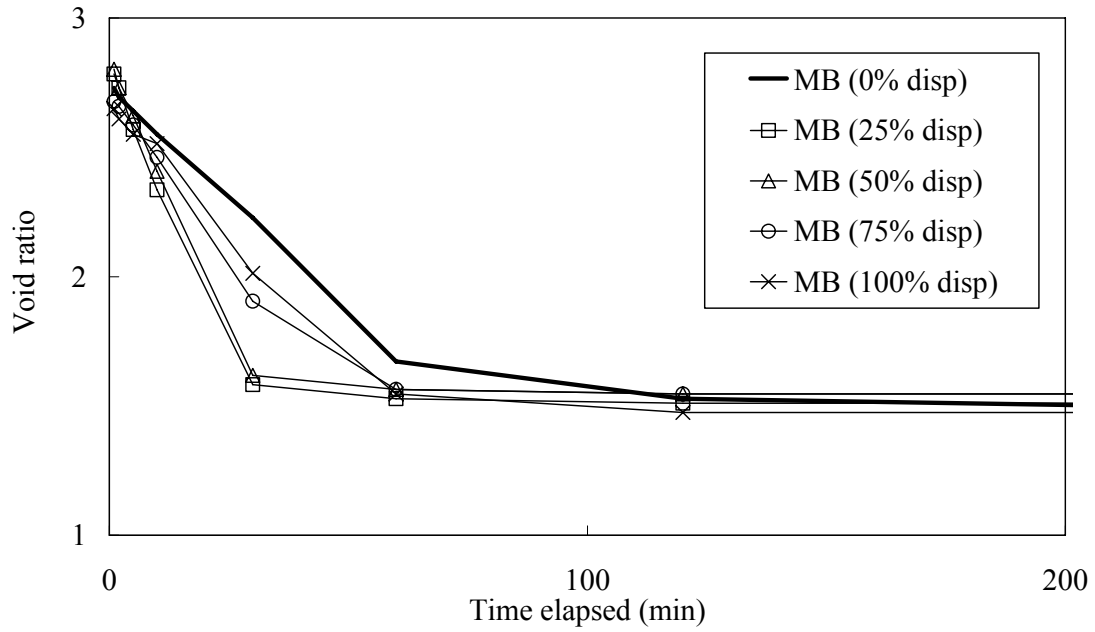
Figure E-3. Sedimentation result for middle beach material dispersed
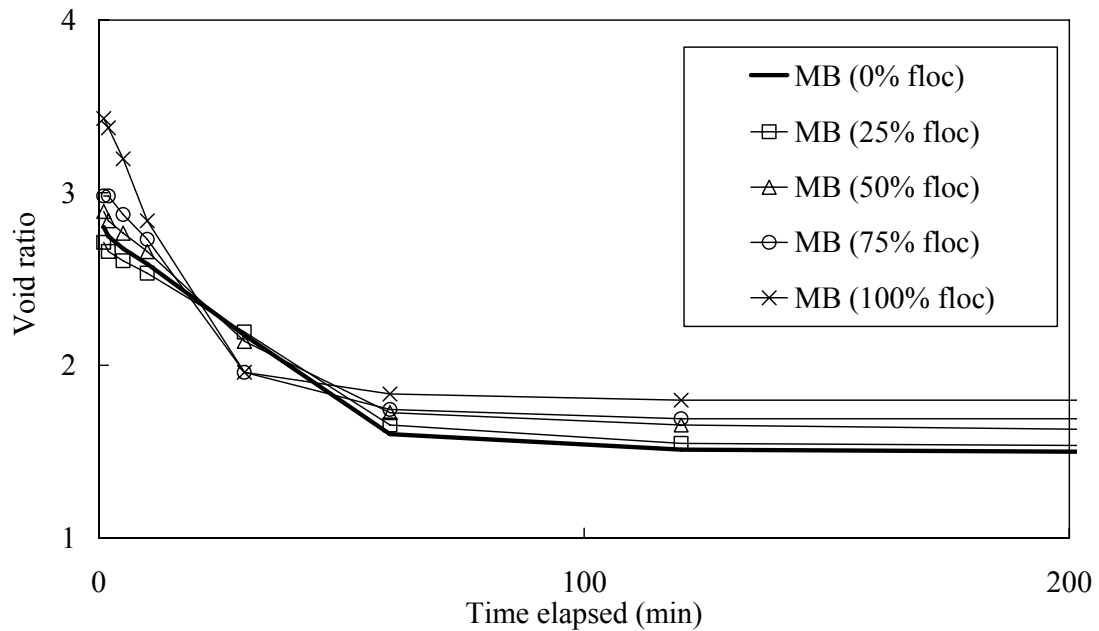
Figure E-4. Sedimentation result for middle beach material flocculated.
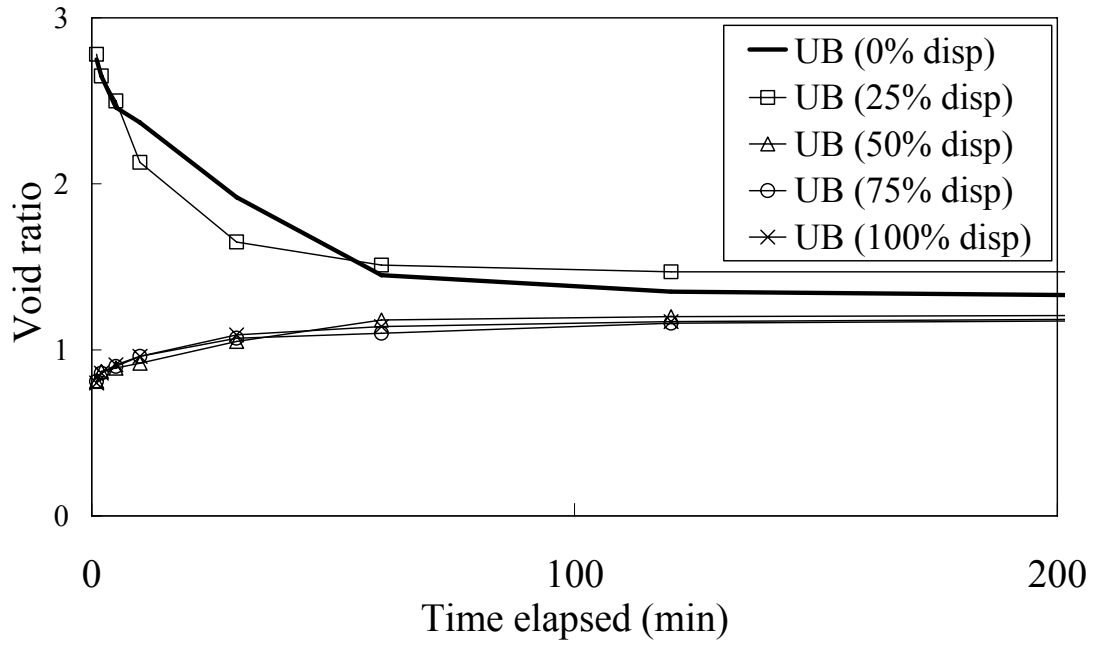
Figure E-5. Sedimentation result for upper beach material dispersed
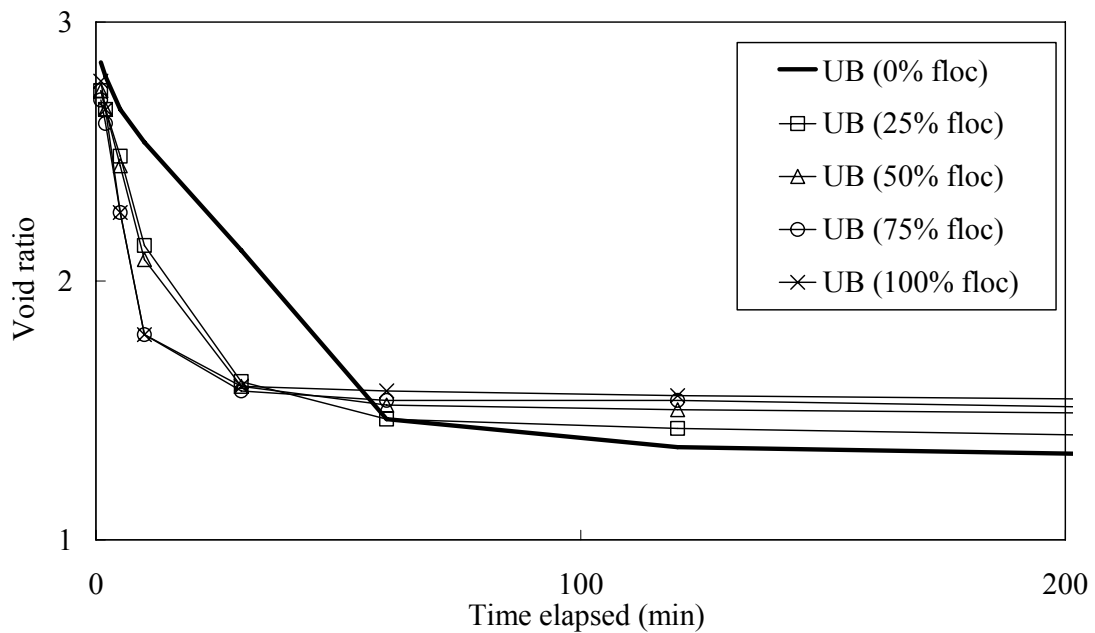
Figure E-6. Sedimentation result for upper beach material flocculated.

Volume change during flushing

Pond sample	Void ratio before flushing	Void ratio after flushing	Volume change (%)
P-U-200	1.37	1.35	1.60
P-U-400	1.41	1.39	1.70
P-U-con	1.39	1.38	1.15
P-MT-200	1.36	1.39	-1.84
P-MT-400	1.16	1.21	-4.48
P-MT-con	1.35	1.38	-2.15
P-S-200	1.50	1.49	1.07
P-S-400	1.40	1.39	0.79
P-S-con	1.43	1.40	1.75

Table E-1. Volume change behaviour for pond material during flushing.

Middle beach sample	Void ratio before flushing	Void ratio after flushing	Volume change (%)
MB-U-200	1.07	1.07	0.00
MB-U-400	1.10	1.11	-0.55
MB-U-con	1.10	1.10	-0.09
MB-MT-200	1.31	1.17	10.62
MB-MT-400	1.37	1.19	12.78
MB-MT-con	1.12	1.12	0.00
MB-S-200	1.56	1.39	10.77
MB-S-400	1.70	1.51	11.29
MB-S-con	1.17	1.16	0.94

Table E-2. Volume change behaviour for middle beach material during flushing.

Upper beach Sample	Void ratio before flushing	Void ratio after flushing	Volume change (%)
UB-U-200	0.65	0.64	0.77
UB-U-400	0.54	0.54	0.37
UB-U-con	0.63	0.63	0.63
UB-MT-200	0.63	0.63	1.26
UB-MT-400	0.55	0.55	0.55
UB-MT-con	0.64	0.64	0.47
UB-S-200	0.64	0.64	0.31
UB-S-400	0.59	0.59	1.02
UB-S-con	0.64	0.64	0.47

Table E-3. Volume change behaviour for upper beach material during flushing.
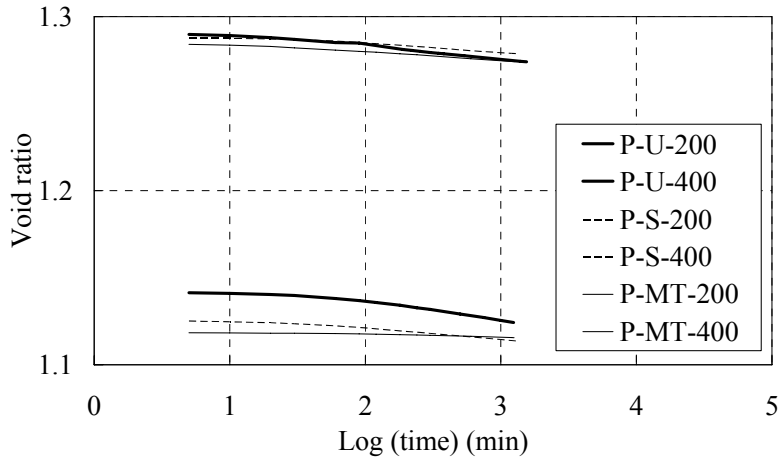
Figure E-7. Creep data for pond shear 200 and 400 samples.
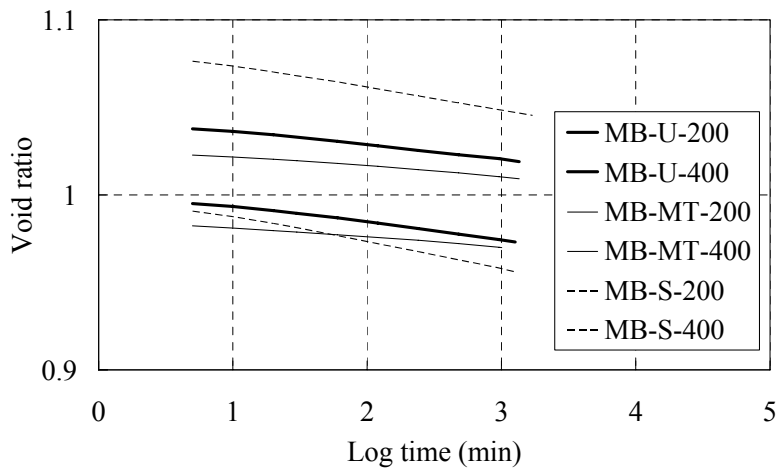
Figure E-8. Creep data for middle beach shear 200 and 400 samples
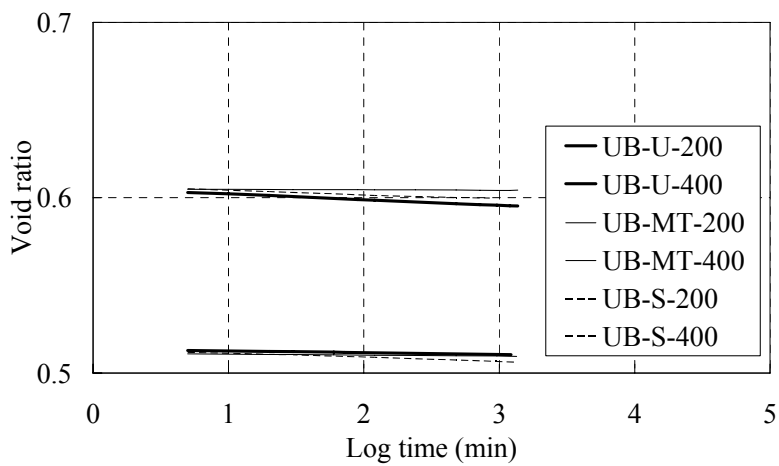
Figure E-9. Creep data for upper beach shear 200 and 400 samples.

233
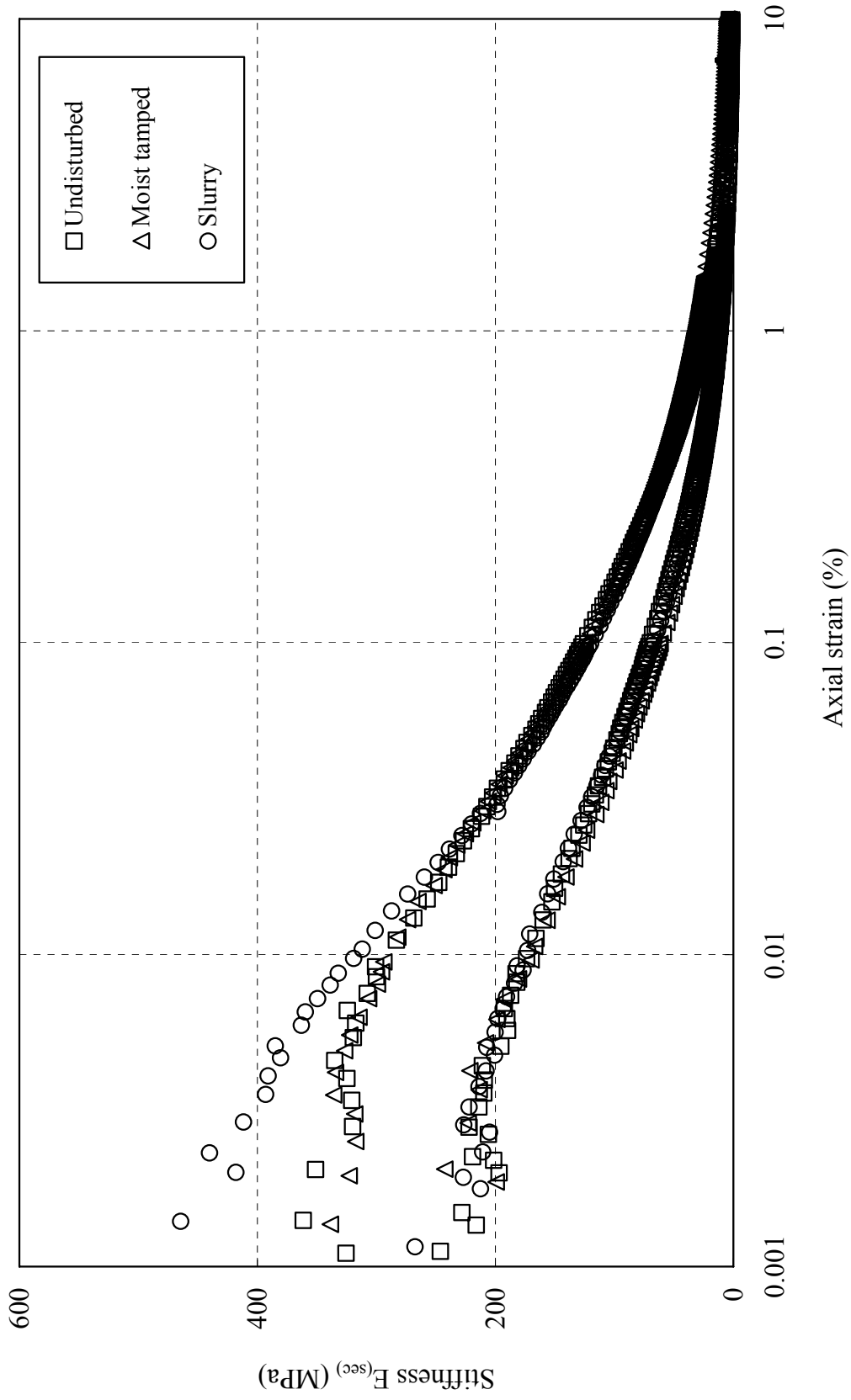
Figure E-10. Stiffness of pond samples
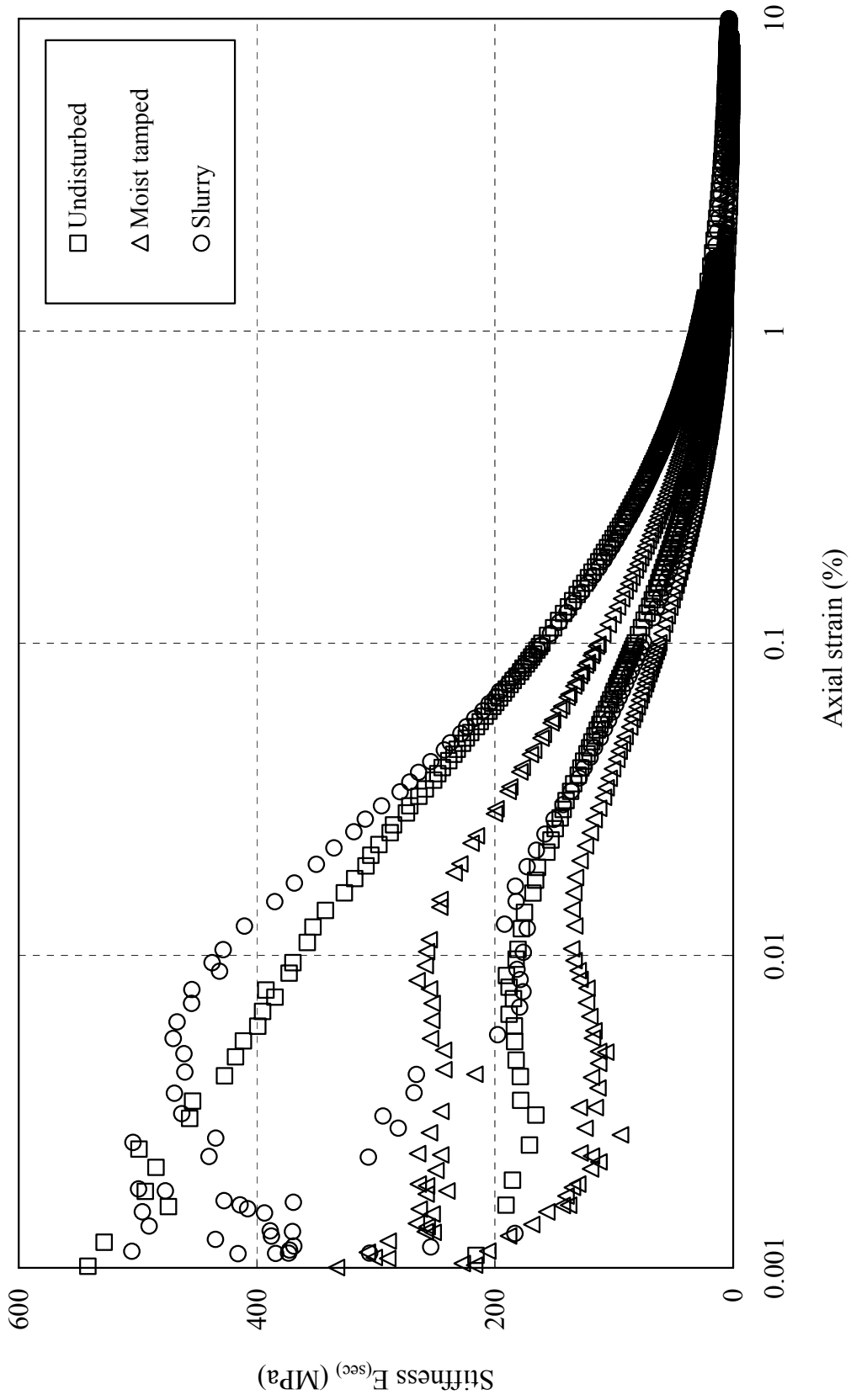
Figure E-11. Stiffness of middle beach samples
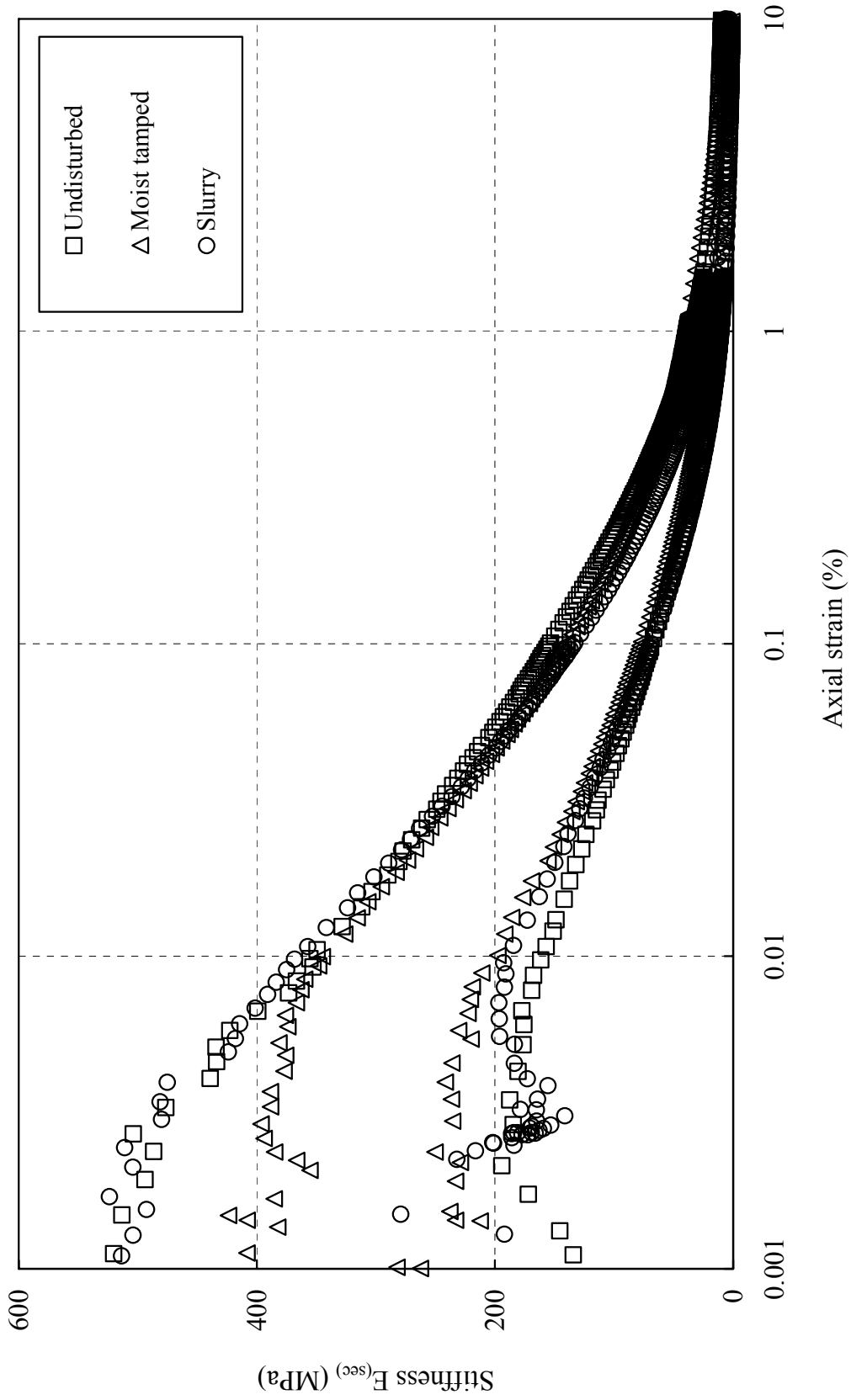
Figure E-12. Stiffness of upper beach samples

Sample	$E_{0.001}$	$E_{0.01}$	$E_{0.1}$	$E_{1.0}$	$E_{0.01}/E_{0.001}$	$E_{0.1}/E_{0.001}$	$E_{1.0}/E_{0.001}$
	(MPa)	(MPa)	(MPa)	(MPa)			
P-U-200	240	173	70	13	0.72	0.29	0.05
P-MT-200	240	168	61	12	0.70	0.25	0.05
P-S-200	240	178	67	12	0.74	0.28	0.05
P-U-400	335	285	125	25	0.85	0.37	0.07
P-MT-400	335	288	125	32	0.86	0.37	0.10
P-S-400	460	315	119	26	0.68	0.26	0.06
MB-U-200	200	181	82	14	0.91	0.41	0.07
MB-MT-200	140	134	62	9	0.96	0.44	0.06
MB-S-200	200	176	76	12	0.88	0.38	0.06
MB-U-400	480	365	160	29	0.76	0.33	0.06
MB-MT-400	280	258	113	19	0.92	0.40	0.07
MB-S-400	475	428	159	27	0.90	0.33	0.06
UB-U-200	200	158	69	13	0.79	0.35	0.07
UB-MT-200	260	198	78	17	0.76	0.30	0.07
UB-S-200	220	193	69	10	0.88	0.31	0.05
UB-U-400	520	355	154	34	0.68	0.30	0.07
UB-MT-400	420	345	140	40	0.82	0.33	0.10
UB-S-400	520	368	134	22	0.71	0.26	0.04

Table E-4. Stiffness degradation curve properties for gold tailings.
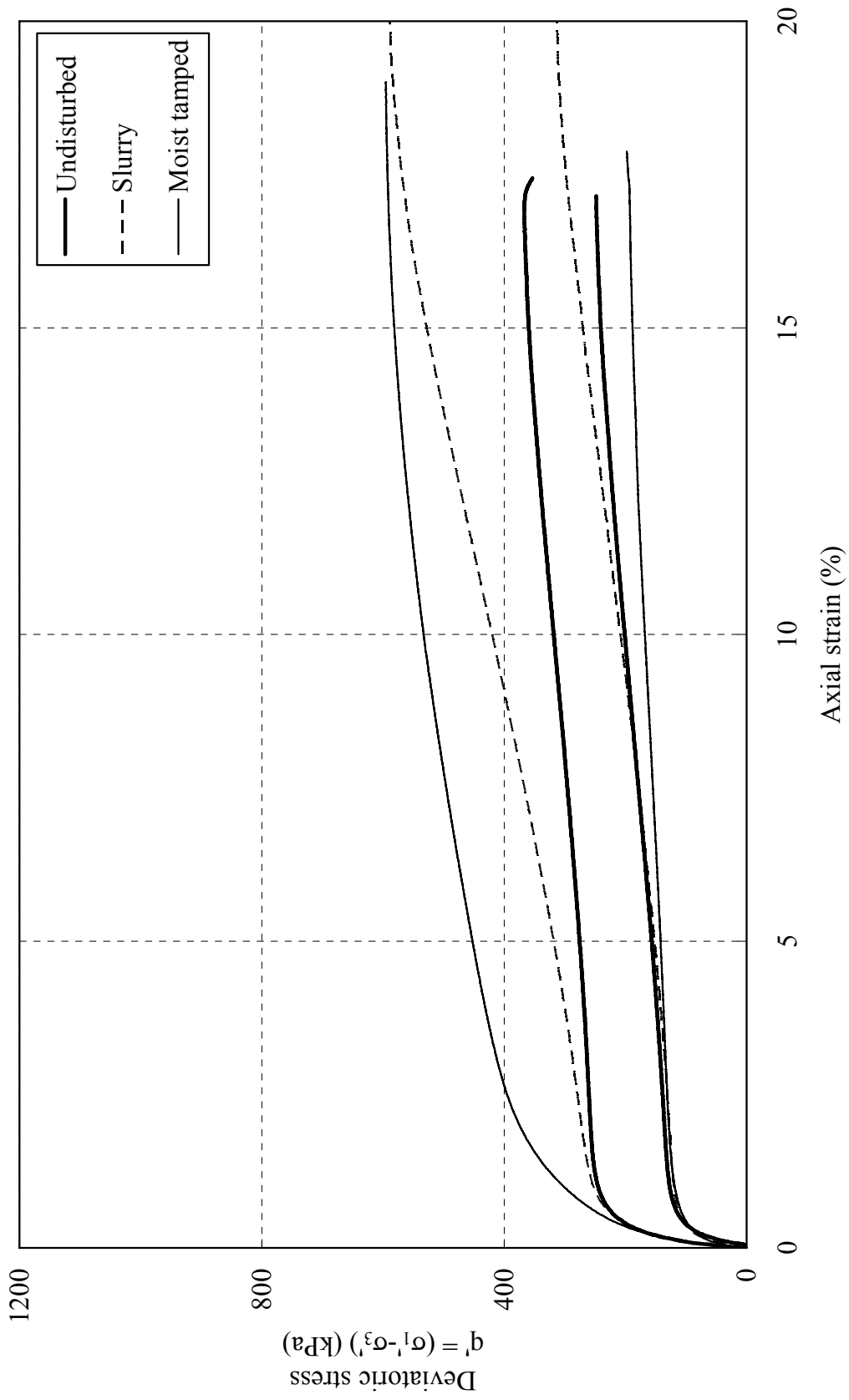
Figure E-13. q'-ε_a graph for pond samples
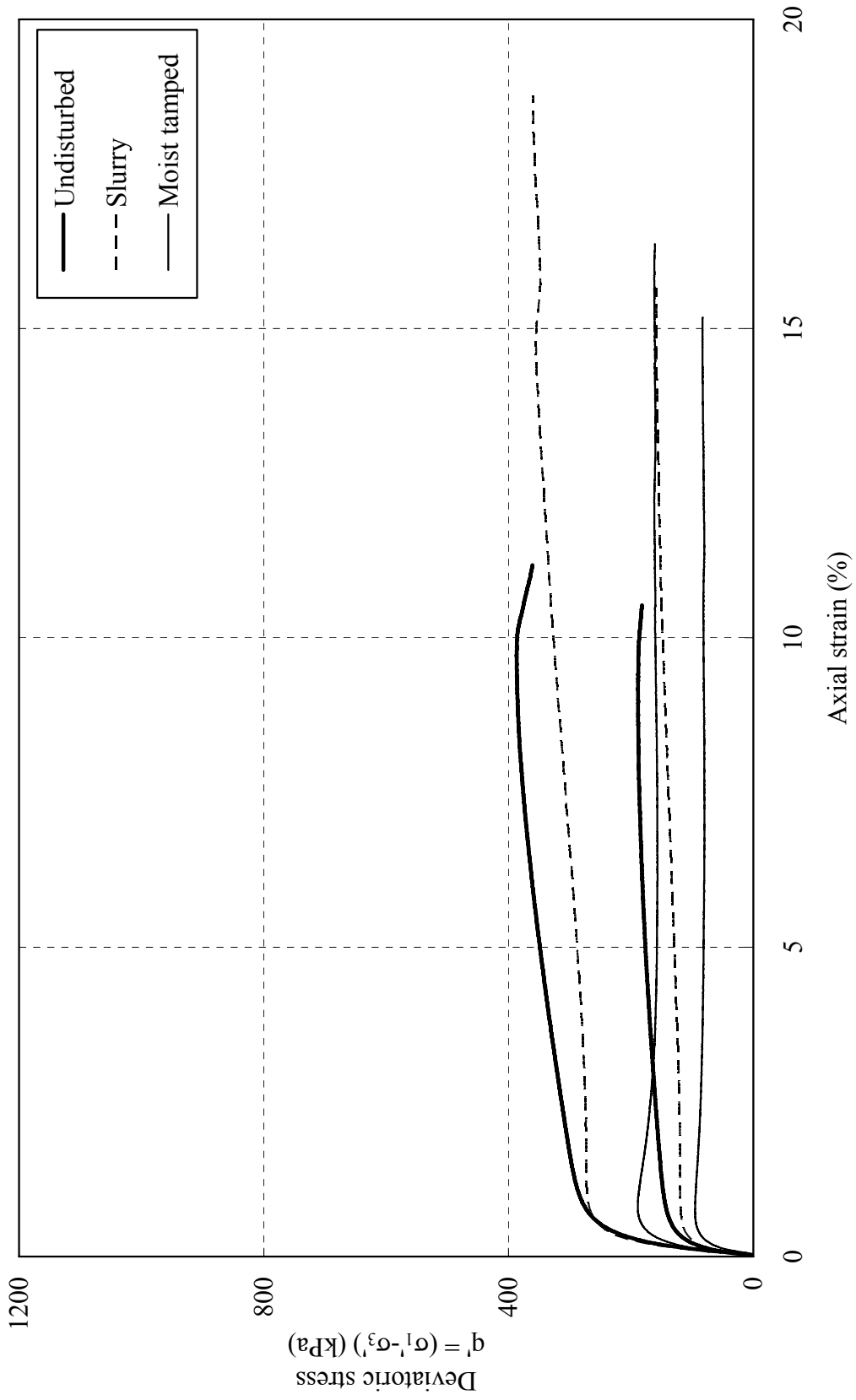
Figure E-14. q'-ε_a graph for middle beach samples
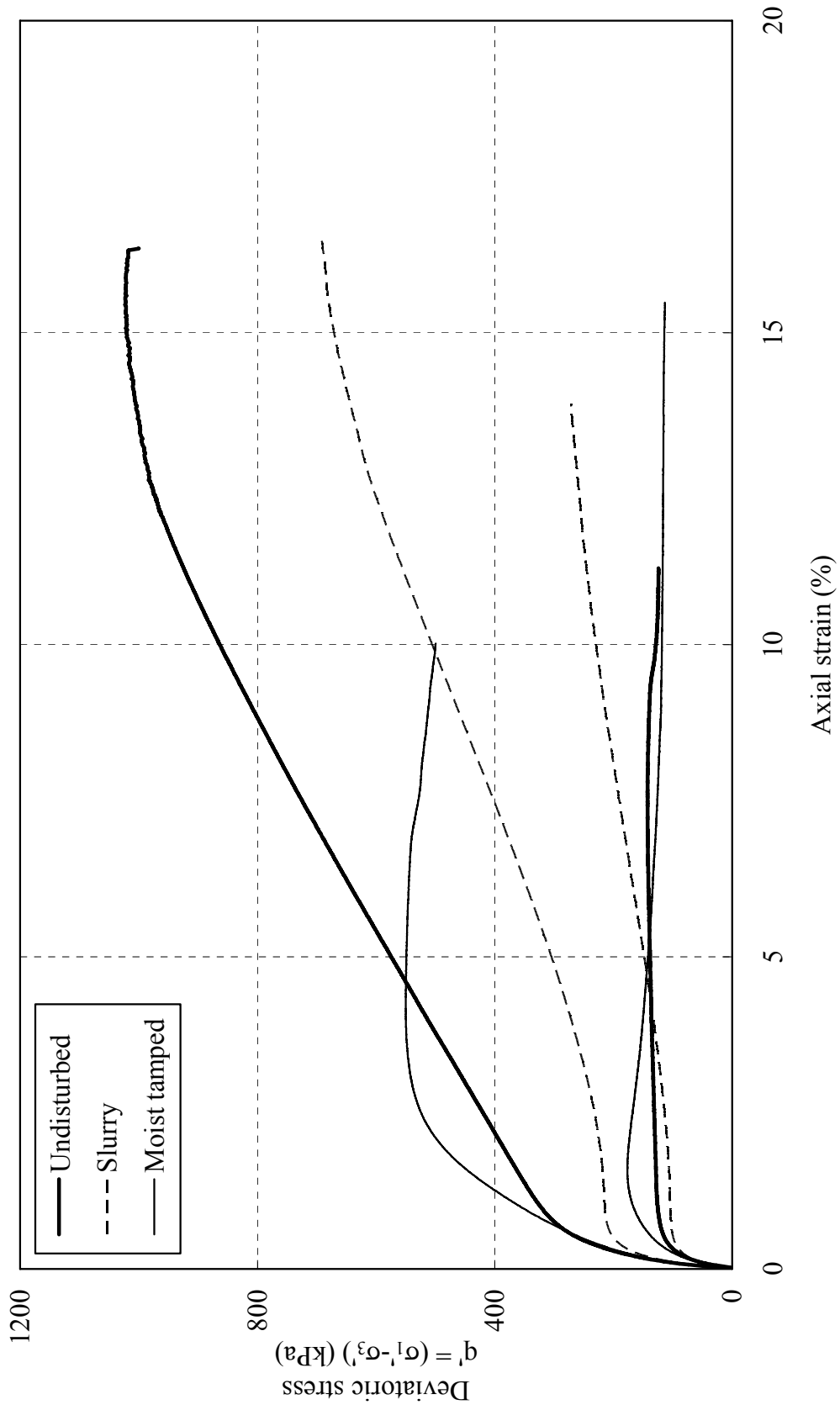
Figure E-15. p'-ε_a graph for pond samples
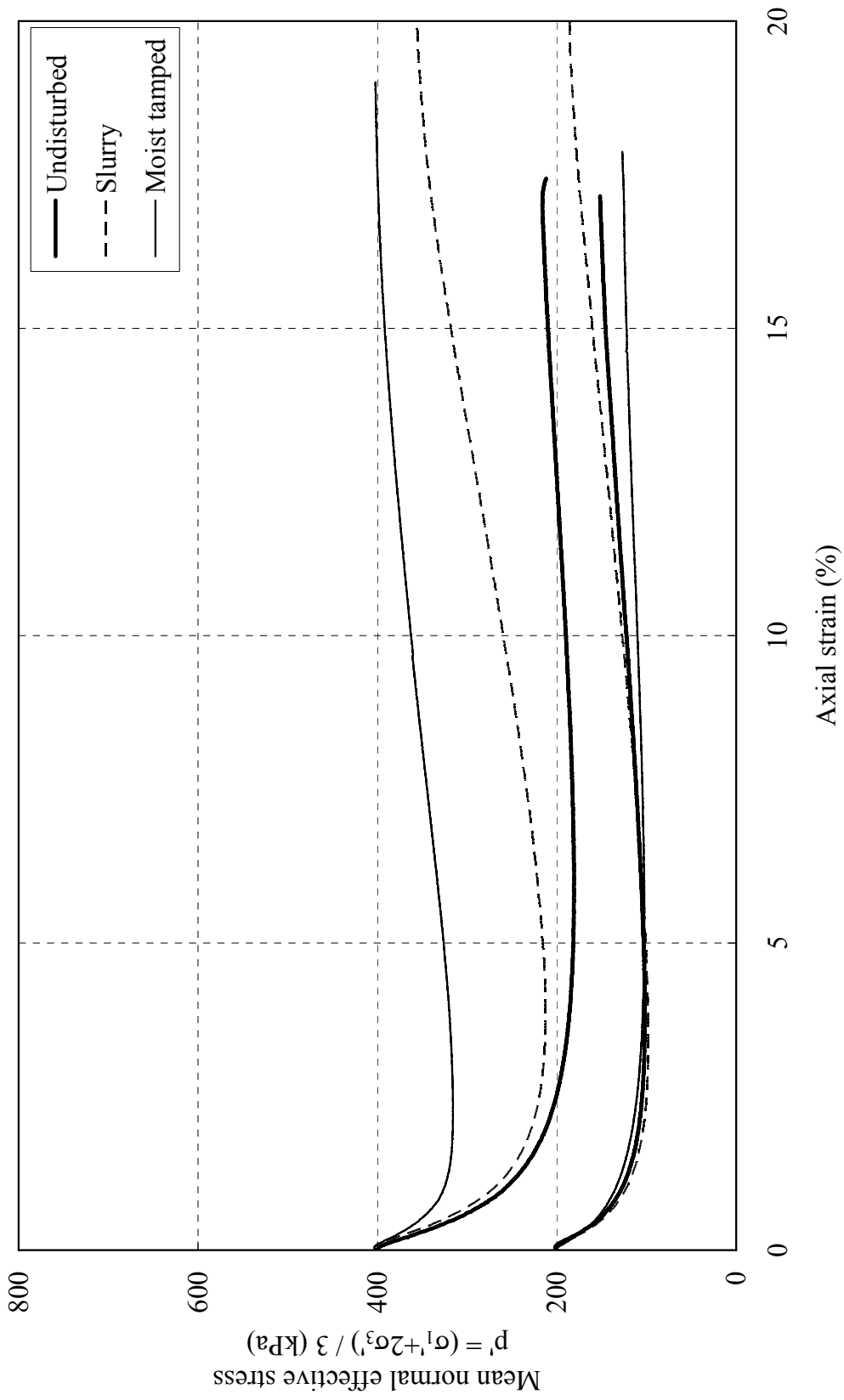
Figure E-16. p'-ε_a graph for pond samples
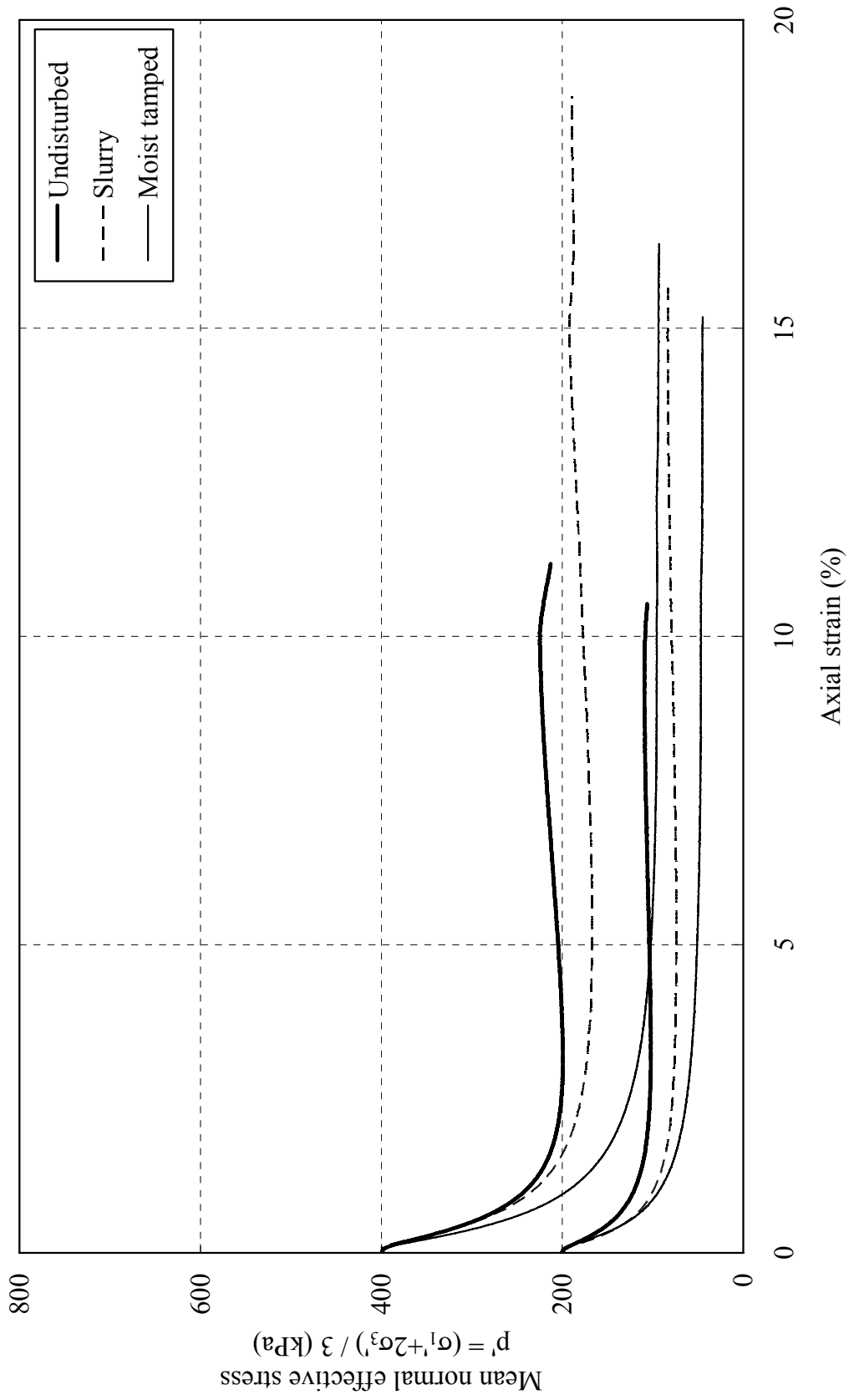
241

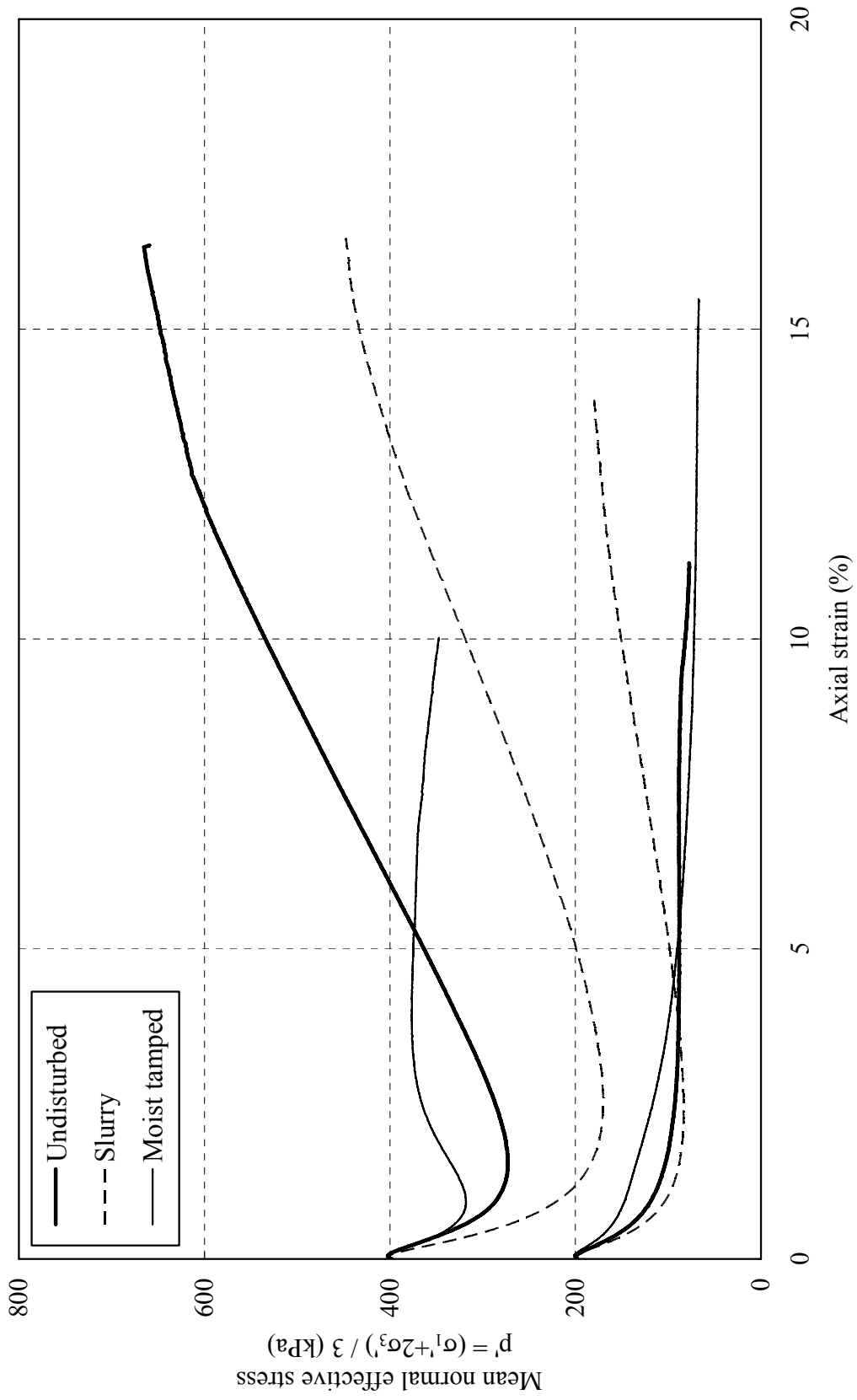*Figure E-17. p'-ε_a graph for middle beach samples*

242

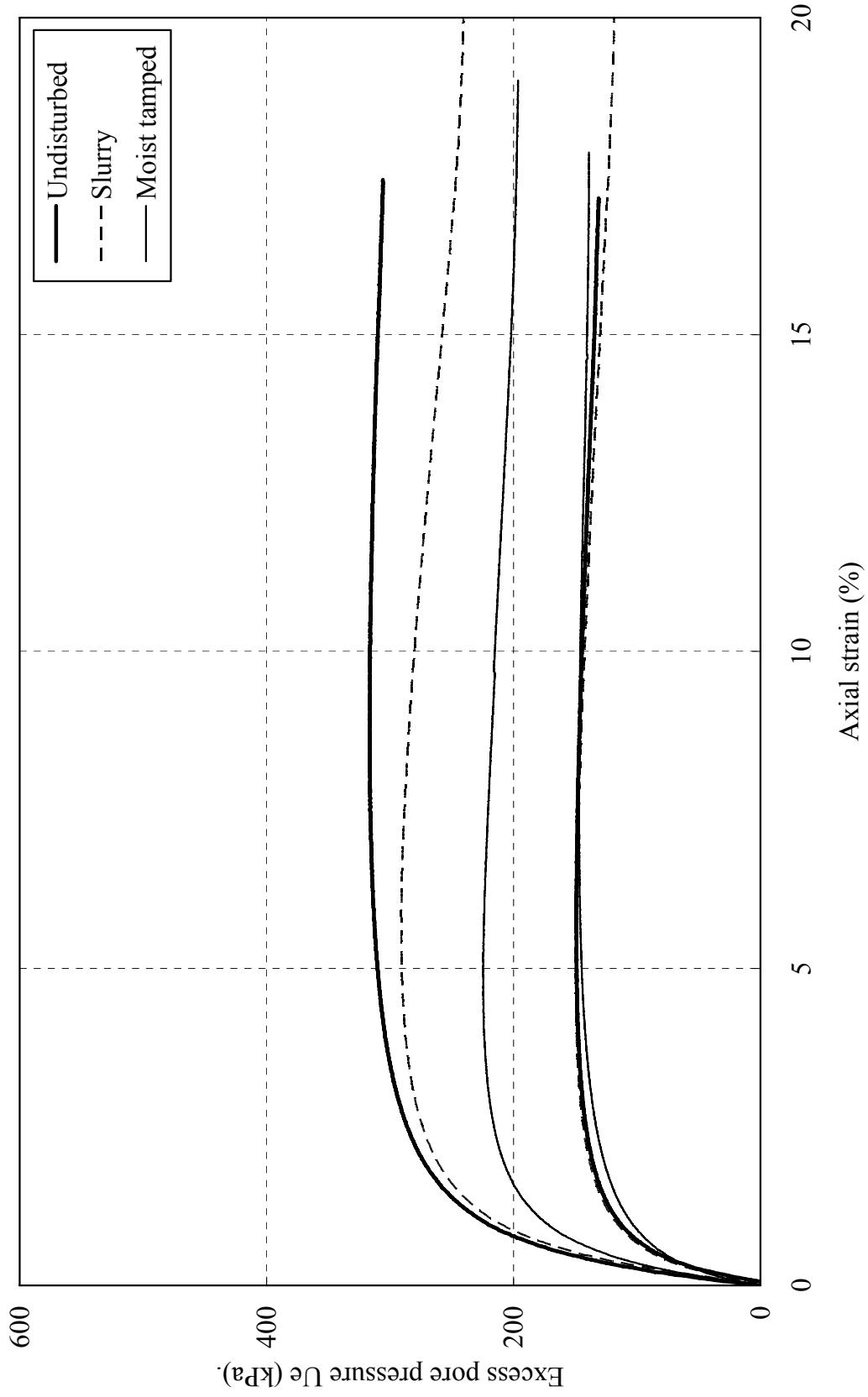*Figure E-18. p'-ε_a graph for upper beach samples*

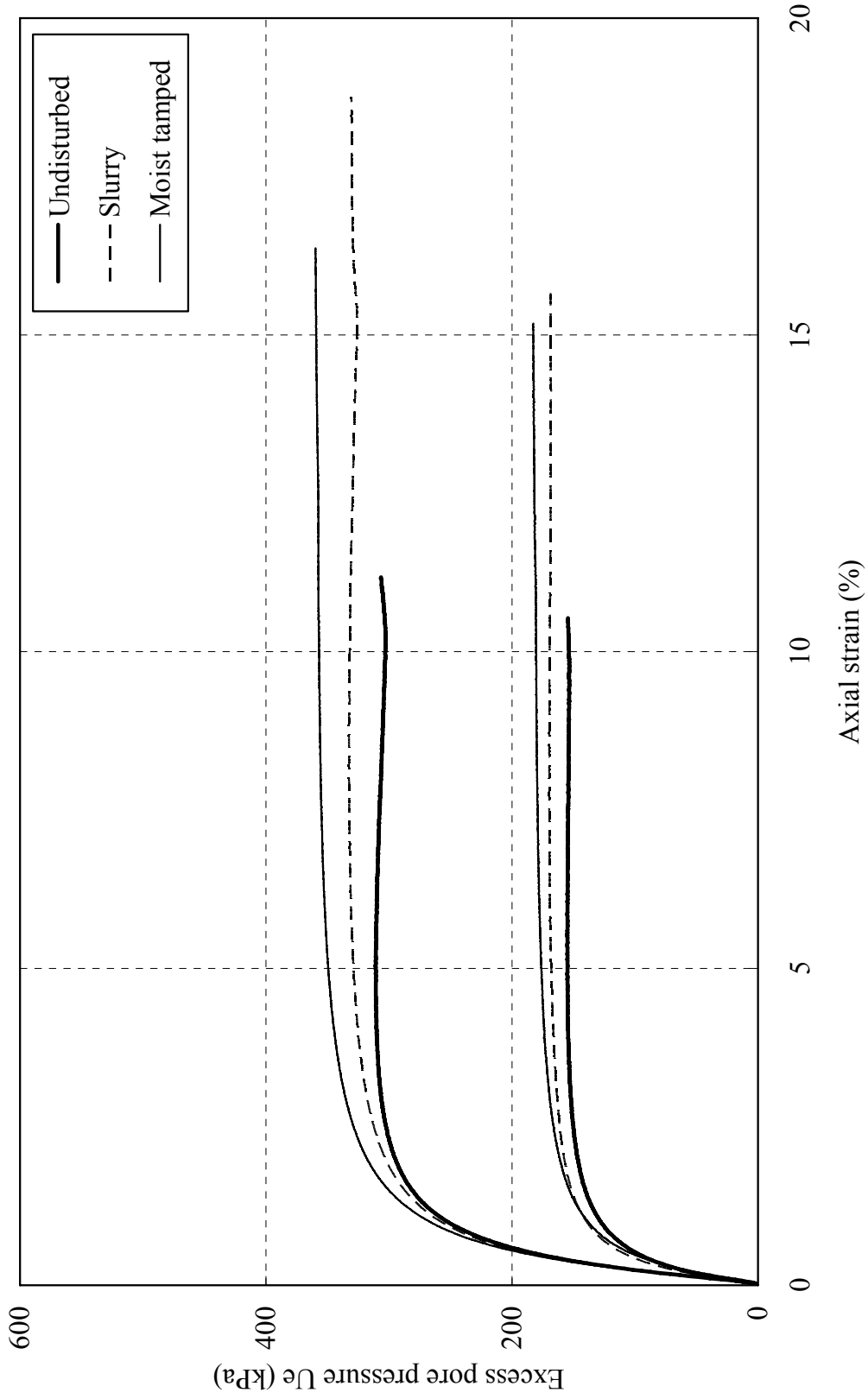*Figure E-19. U_e- ε_a graph for pond samples*
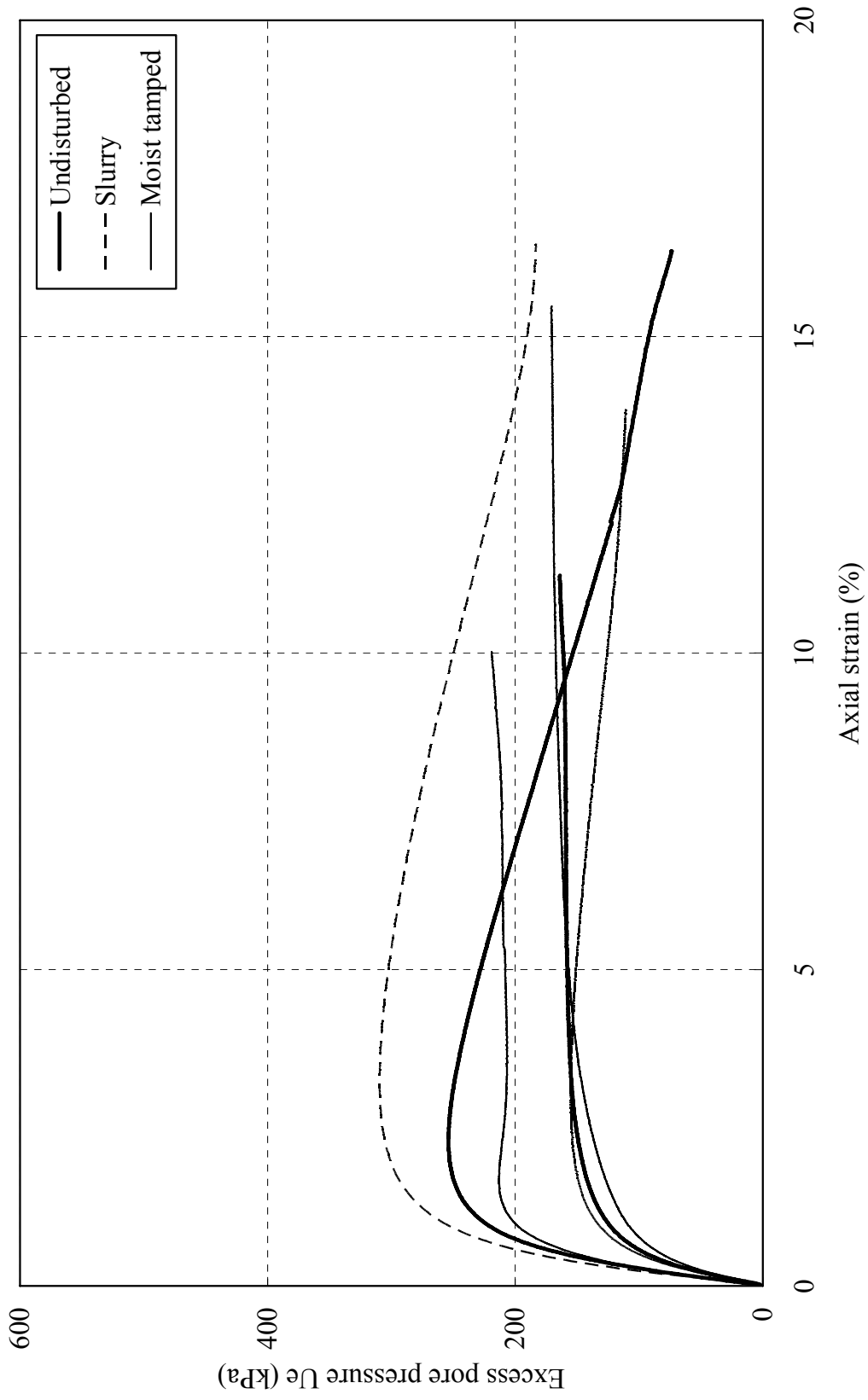
Figure E-20. U_e- ε_a graph for middle beach samples

Figure E-21. U_e- ε_a graph for upper beach samples
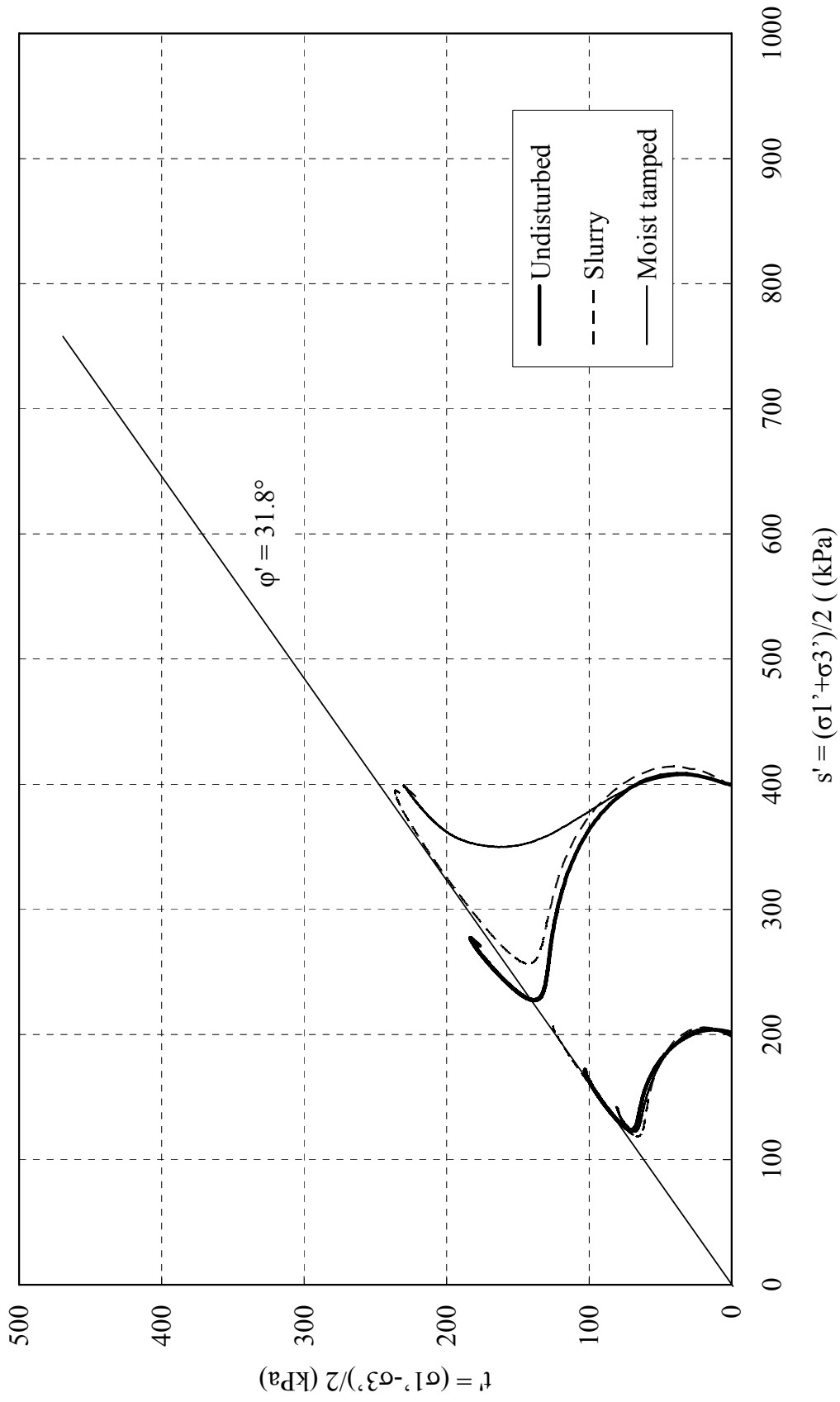
Figure E-22. Stress path of pond samples (s'-t' space)
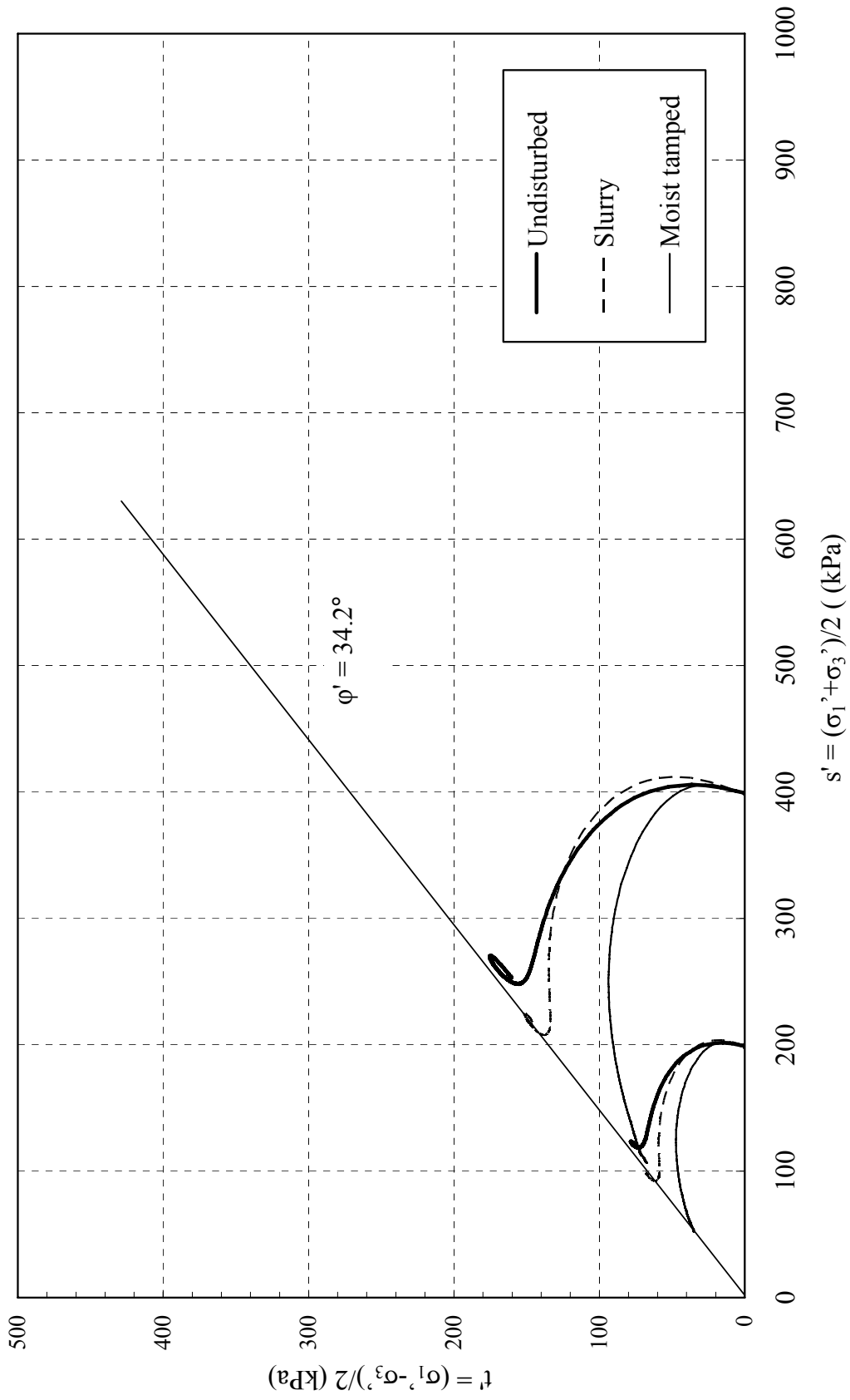
Figure E-23. Stress path of middle beach samples (s'-t' space)
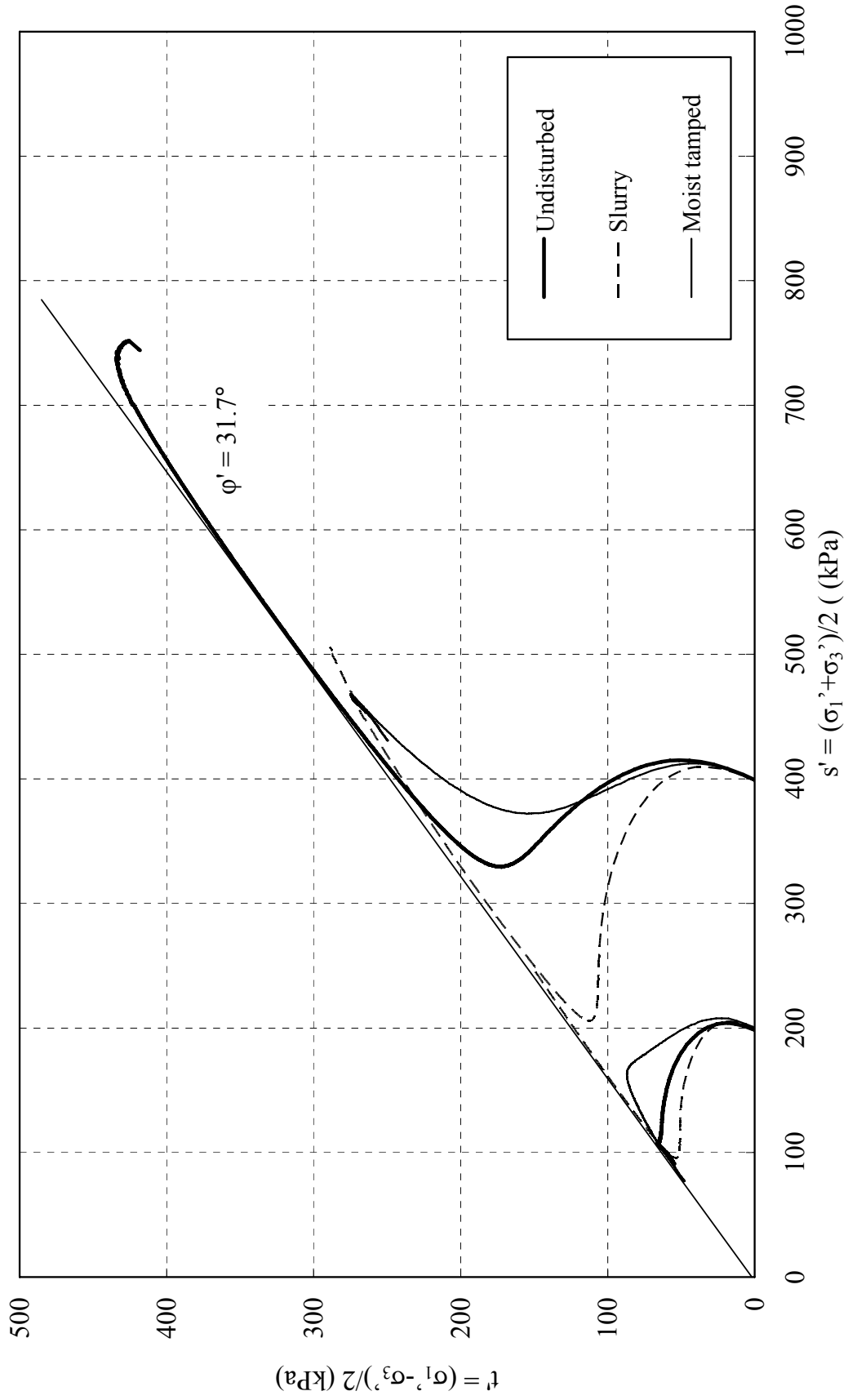
Figure E-24. Stress path of upper beach samples (s'-t' space)
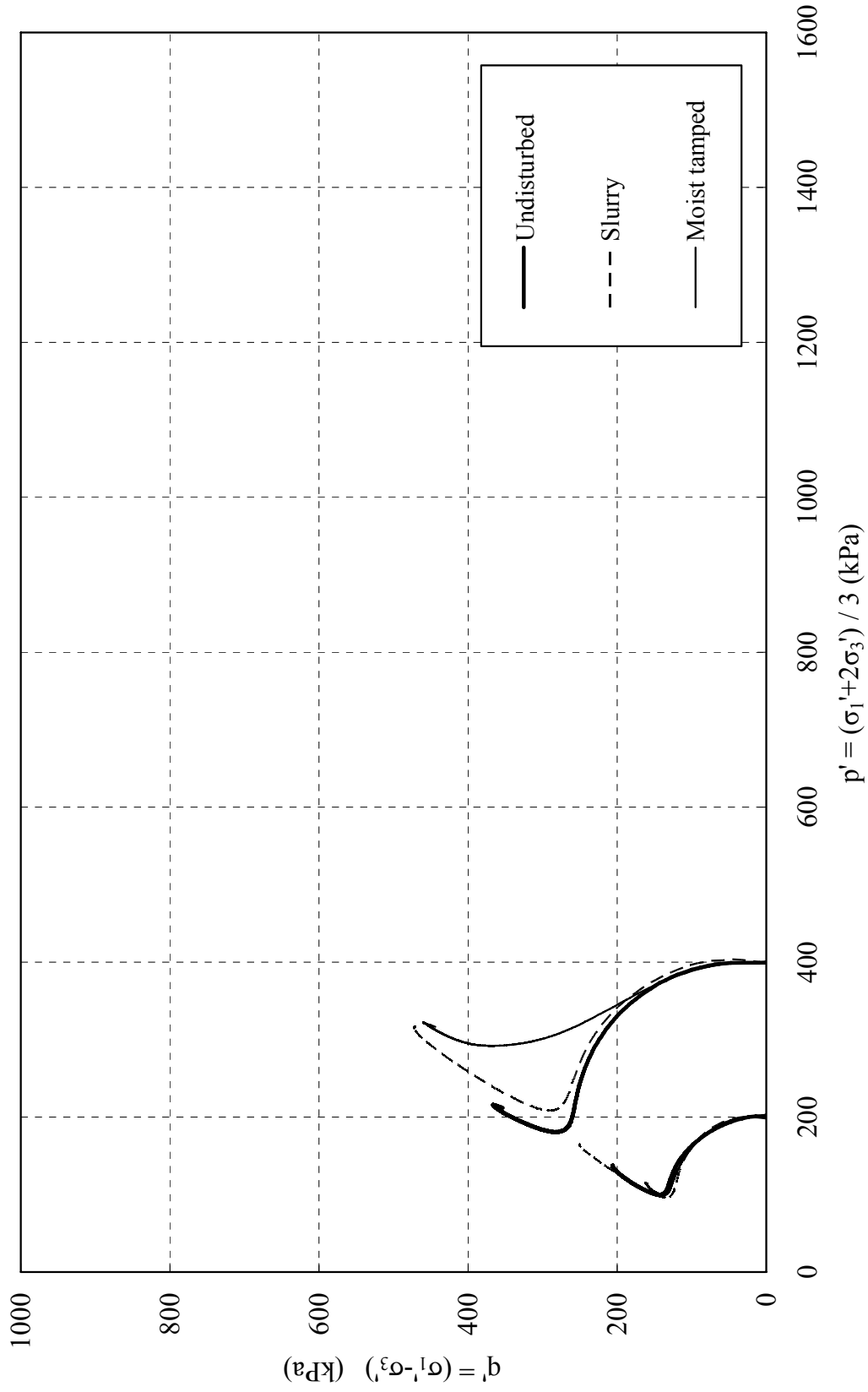
Figure E-25. Stress path of pond samples (p'-q' space)
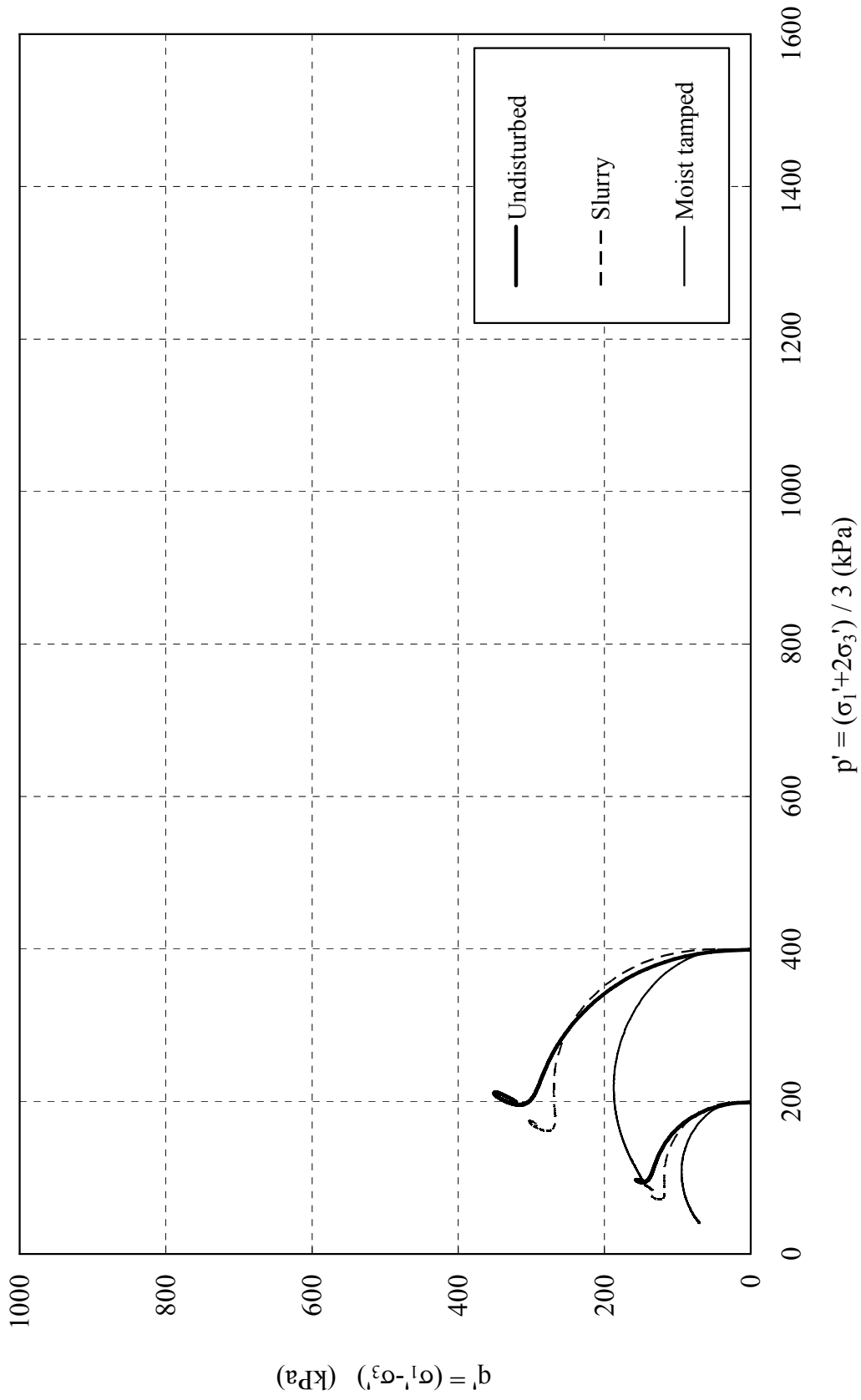
Figure E-26. Stress path of middle beach samples (p'-q' space)
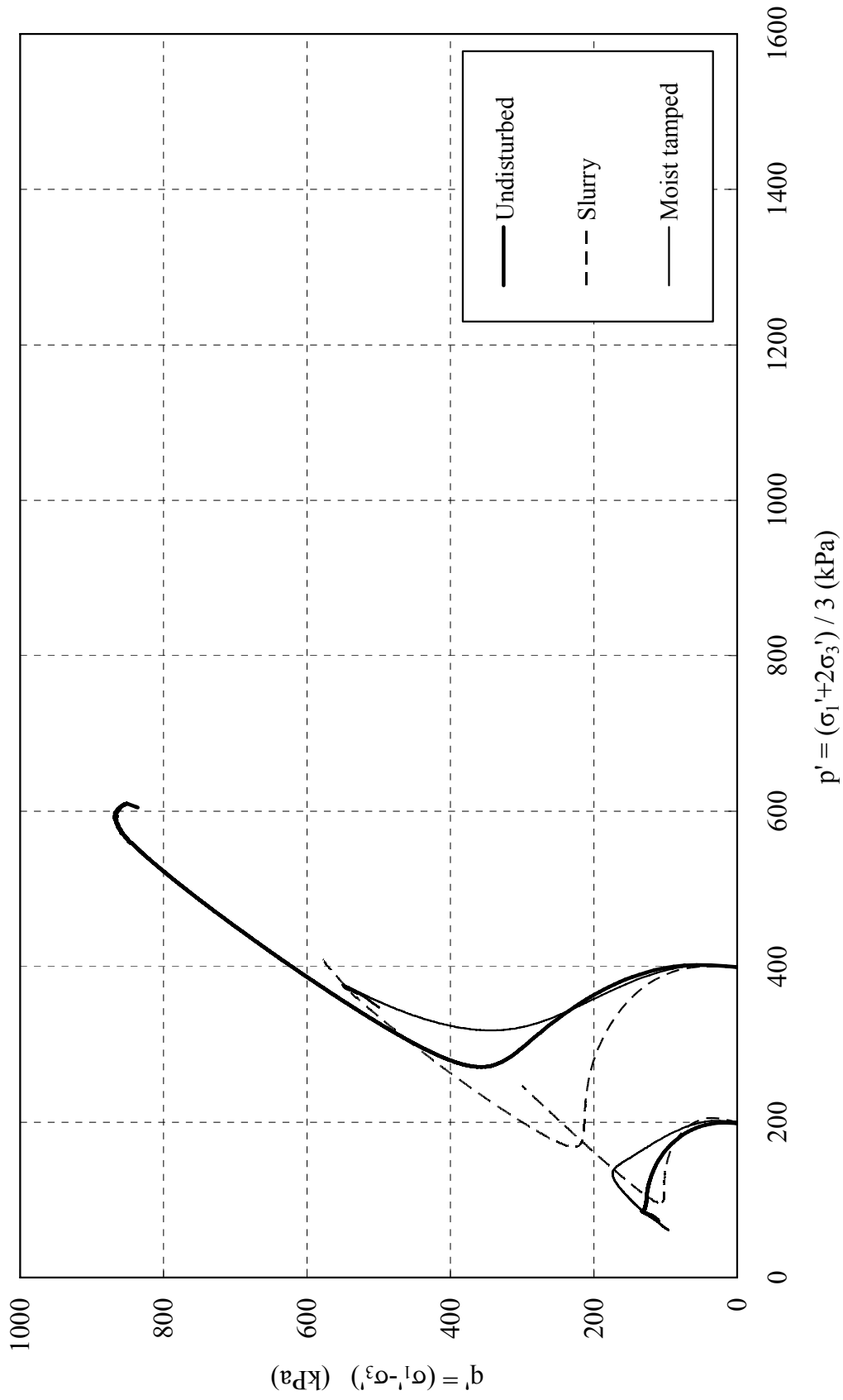
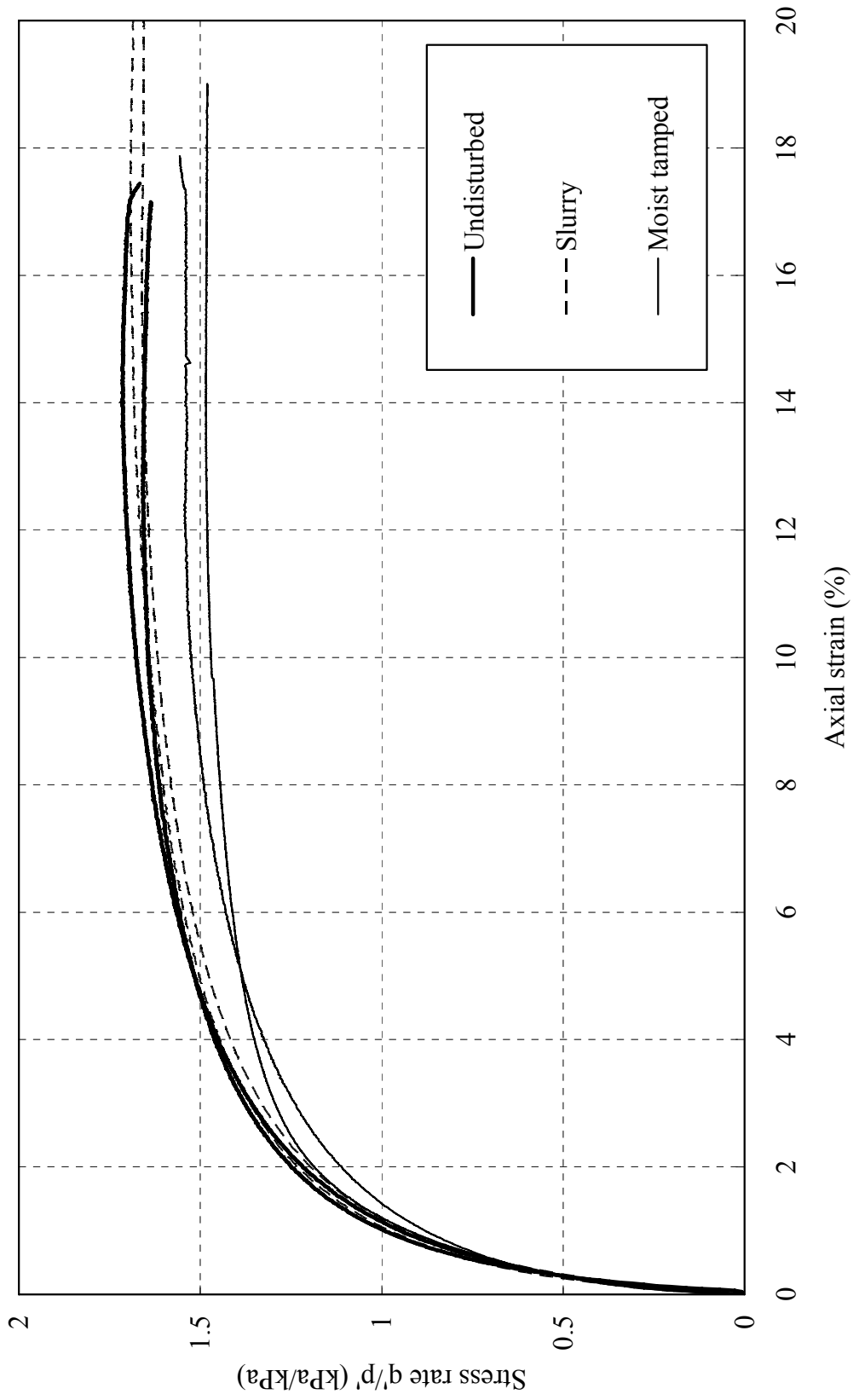*Figure E-27. Stress path of upper beach samples (p'-q' space)*

Figure E-28. Stress ratio against axial strain for pond samples
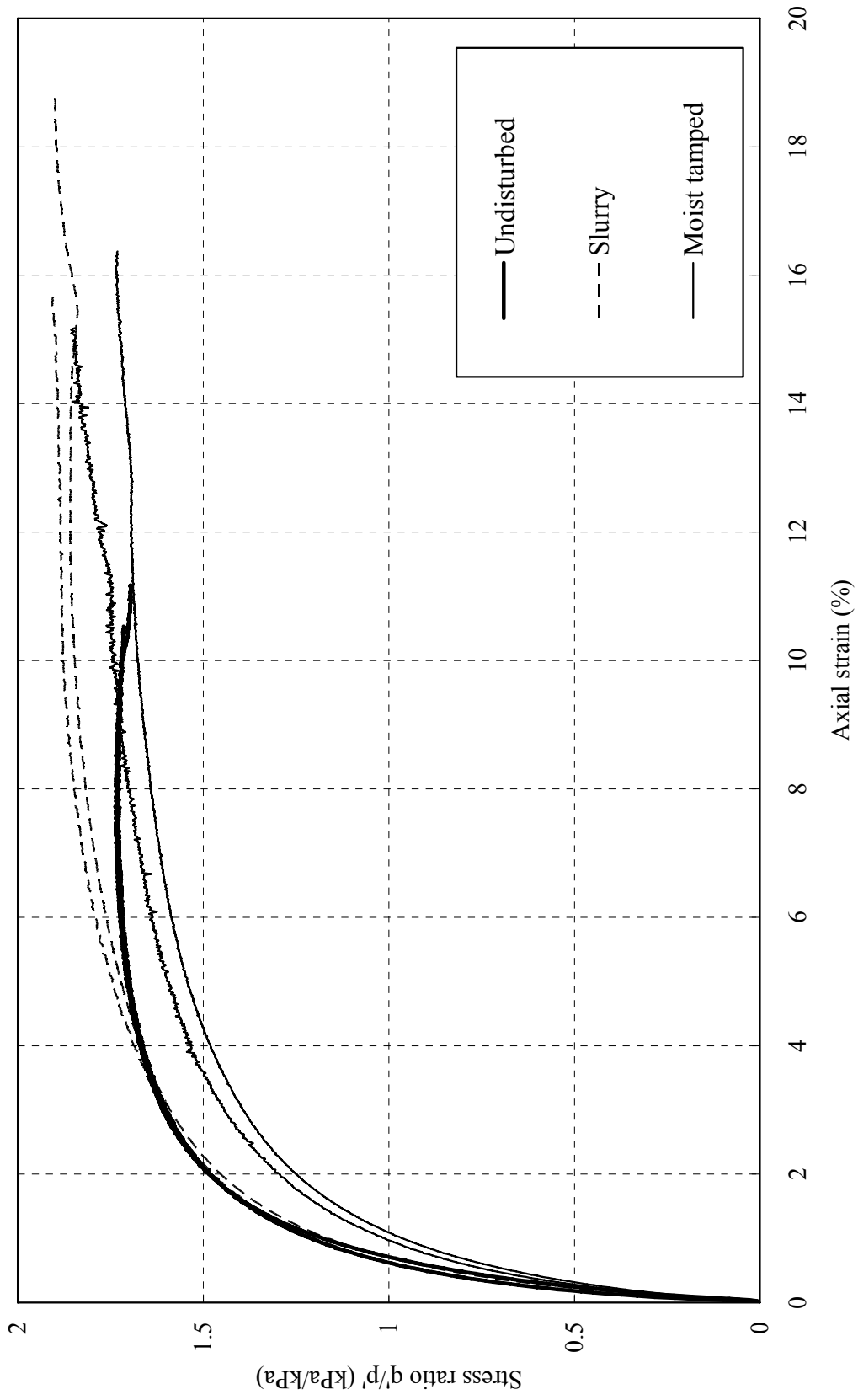
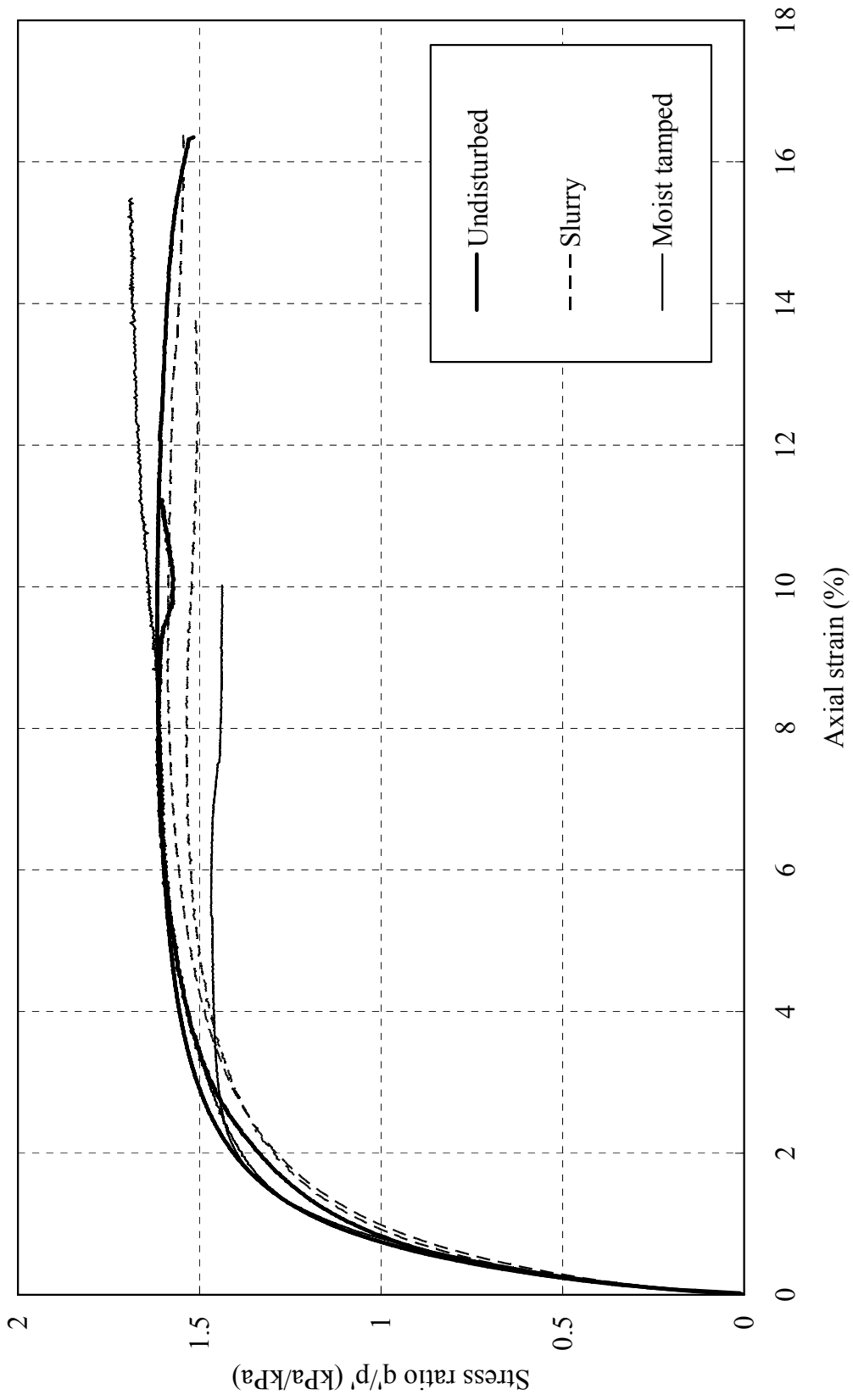*Figure E-29. Stress ratio against axial strain for middle beach samples*

Figure E-30. Stress ratio against axial strain for upper beach samples